October 2018

Performance and economic analysis of hybrid microhydro systems

Ram Poudel

PERFORMANCE AND ECONOMIC ANALYSIS OF HYBRID MICROHYDRO SYSTEMS

A Dissertation Presented

by

RAM C. POUDEL

Submitted to the Graduate School of the

University of Massachusetts Amherst in partial fulfillment

of the requirements for the degree of

DOCTOR OF PHILOSOPHY

September 2018

Mechanical and Industrial Engineering

PERFORMANCE AND ECONOMIC ANALYSIS OF HYBRID MICROHYDRO SYSTEMS

A Dissertation Presented

By

RAM C. POUDEL

Approved as to style and content by:

Jon G. McGowan, Chair

James F. Manwell, Member

John E. Tobiason, Member

Sundar Krishnamurty, Department Head
Mechanical and Industrial Engineering

DEDICATION

To my father

ACKNOWLEDGMENTS

This research would not be possible without the support of mentors and colleagues. First and foremost, I would like to extend my sincere thanks to supervisor Prof. Jon G. McGowan. I would never be able to finish this work without his inspiration and guidance. Prof. McGowan has been an exceptional mentor, at the same time, a local guardian here in the USA. I am indebted to Prof. James F. Manwell for all his encouragement and support. Prof. Manwell has been a great source of knowledge in many technical matters. I got an opportunity to join UMass because of his confidence in me.

I am grateful to Prof. John E. Tobiason for the overall support extended to me to comprehend downscaling of water resource. His timely advice and suggestion have greatly improved this cross-disciplinary effort as well as my writing. Kapil Gnawali supported me on questions related to local hydrology in Nepal. I also benefited from interaction with Prof. Colin Gleason (Civil Engineering), Prof. Ashish Sharma (University of New South Wales), and Pravin Karki (World Bank).

In my effort to understand economic science better, Professors Erin Baker, Michael Ash, and J. Mohan Rao have been very supportive. Thanks also due to Dylan Chase, Tulsi Vembu, Luis Pagan-Quinones and Manager Jodi Lally at Wind Energy Center.

I am obliged to the MIE Department for the support above and beyond. Jane Knapp entrusted me for various TA positions in Physics Department over the years. I would like to acknowledge The William Heronemus Fellowship (Fall 2014), and support from Prof. Hongkun Zhang (Mathematics) toward stochastic modeling (Winter 2016). It was a pleasure to discuss Chapter 4 with Prof. Luc Rey-Bellet (Mathematics).

Above all, I would never pursue PhD without encouragement from my late father. Unconditional love and support from my spouse during challenging times been a great inspiration. I know Sajan (11) and Sagun (3) have missed a lot during this endeavor.

ABSTRACT

PERFORMANCE AND ECONOMIC ANALYSIS OF HYBRID MICROHYDRO SYSTEMS

SEPTEMBER 2018

RAM C. POUDEL, B.E., TRIBHUVAN UNIVERSITY
RAM C. POUDEL, MSREE., TRIBHUVAN UNIVERSITY
RAM C. POUDEL, M.E., NORTHERN ARIZONA UNIVERSITY
Ph.D., UNIVERSITY OF MASSACHUSETTS AMHERST
Directed by: Professor Jon G. McGowan

Microhydro (MHP) systems usually employ unregulated turbines and an electronic load controller, a demand-side control device. Existing analytical models for such systems are lacking details, especially supply-side flow control, for performance simulation at hourly or sub-hourly scales. This work developed stochastic models for downscaling of streamflow and an empirical model of MHP systems. We integrated these models within the framework of Hybrid2 tool to simulate the long-term performance of a tri-hybrid system consisting of hydropower, solar PV and wind turbine.

Based on an additive model of time series decomposition, we develop a Multiple Input Single Output (MISO) model in order to synthesize an hourly time series of streamflow. The MISO model takes into account daily precipitation dataset as well as regional hydrological characteristics. The model employs a constrained Monte-Carlo Markov

Chain (MCMC) algorithm which is validated against an hourly time series of flow data at Blue River at Blue, Oklahoma. A non-dimensional performance model of MHP systems is developed based on empirical data from Nepal.

Three design configurations are presented for a case study. The results show that, along with a small pond that can store water for an hour at the rated capacity of MHP system, a hybrid system with half the size of the battery bank can supply the load year around at Thingan Project in Nepal. This system meets the availability requirements of the Multi-Tier Framework for measuring energy access for household supply. The new proposed system is marginal in the economic sense as well. This project can never recover the initial capital cost at a current rate of the tariff which is about 7 cents/kWh. Other O&M risks aside, the sensitivity analysis suggests that the system may barely recover the initial capital cost, excluding the subsidy, at twice the existing rate of tariff and half the interest rate.

This study aspires to come up with better techniques to simulate hybrid microhydro systems and enhance their design and operation through more effective utilization of resources. Future use of this model will enable designers and developers of MHP systems to enhance their performance and cost-effectiveness. The models of MHP system we developed in this research could be integrated with Hybrid2 to come up with an updated version for general public use.

TABLE OF CONTENTS

Page

LIST OF TABLES

Table Page

LIST OF FIGURES

Figure Page

LIST OF ABBREVIATION

ADB	-	Asian Development Bank
AEPC	-	Alternative Energy Promotion Center, Nepal
AFDC	-	annual flow duration curve
ANN	-	artificial neural networks
ARMAX	-	autoregressive–moving-average model with exogenous inputs
ASL	-	above sea level
BYS	-	Balaju Yantra Shala, Nepal
CDF	-	cumulative distribution function
CFD	-	computational fluid dynamics
CMS	-	cubic meter per second
DEM	-	digital elevation model
DHM	-	Department of Hydrology and Metrology, Nepal
DMIP	-	The Distributed Model Intercomparison Project
ELC	-	electronic load controller, microhydro power
FAO	-	The Food and Agriculture Organization, The United Nations
FCD	-	flow control device
FDC	-	flow duration curve
FIT	-	goodness of the fit
GEF	-	Global Environment Facility
GIS	-	Geographic Information System
GPM	-	Global Precipitation Measurement
GTF	-	Multi-Tier Global Tracking Framework
GTI	-	grid-tied inverter
HAWT	-	horizontal axis wind turbine
HES	-	hybrid energy system
HOMER	-	a software, Hybrid Optimization Model for Multiple Energy Resources
Hybrid2	-	a software, Hybrid2 developed at Umass Amherst
IEC	-	The International Electrotechnical Commission
IRR	-	internal rate of return
KUKL	-	The Kathmandu Upatyaka Khanepani Limited, Nepal
KUTTL	-	Turbine Testing Lab, Kathmandu University in Nepal
LCOE	-	levelized cost of energy
LEAP	-	Global Lighting and Energy Access Partnership
LED	-	light emitting diode
MCMC	-	Monte-Carlo Markov Chain
MCP	-	measure–correlate–predict, an algorithm
MGSP	-	The Mini Grid Support Program , Nepal
MHP	-	microhydro or microhydro power
MHSP	-	Medium Hydropower Study Project, Nepal Electrical Authority

MIP	-	Medium Irrigation Project, Nepal
MISO	-	multiple input single output
MIT	-	Massachusetts Institute of Technology
MPP	-	maximum power point
NASA	-	The National Aeronautics and Space Administration
NEA	-	Nepal Electrical Authority
NMHDA	-	Nepal Micro Hydropower Development Association
NOCT	-	nominal operating cell temperature
NPC	-	net present cost
NPV	-	net present value
NREL	-	National Renewable Energy Laboratory, USA
NRREP	-	National Rural and Renewable Energy Program (NRREP), Nepal
NWS	-	The National Weather Service, USA
O&M	-	operation and maintenance
PID	-	proportional–integral–derivative, an electronic controller
PDF	-	probability density function
PLC	-	programmable logic controller
POV	-	power output verification
PV	-	Photovoltaic, Solar
QAF	-	quality assurance framework
RCM	-	regional climatological models
RERL	-	Renewable Energy Research Laboratory, University of Massachusetts
RET	-	renewable energy technology
RHS	-	right hand side
RoR	-	Run-of-river, a type of hydroelectric plant
RPM	-	revolution per minute
SAIDI	-	System Average Interruption Duration Index
SAIFI	-	System Average Interruption Frequency Index
SAMS	-	a software, Stochastic Analysis Modeling and Simulation
SDGs	-	Sustainable Development Goals
SE4All	-	Sustainable Energy for All, The United Nations
SHS	-	solar home systems
SOC	-	state of charge in a battery
SOW	-	state of water in a pond
SOW_{max}	-	size of the pond normalized in hours, or in m^3
TMY	-	typical meteorological year
TPM	-	transitional probability matrix
TRMM	-	Tropical Rainfall Measuring Mission
UMass	-	University of Massachusetts Amherst
UN	-	The United Nations
USGS	-	United States Geological Survey

VDC	-	village development committee
ViPOR	-	a software, The Village Power Optimization Model for Renewable
VOC	-	open circuit voltage
WECS	-	Water and Energy Commission Secretariat, Nepal

CHAPTER 1

INTRODUCTION/BACKGROUND

1.1 Introduction

Access to energy services is one of the cornerstones of human development. The Sustainable Development Goals (SDGs), agreed to by the member countries of The United Nations (UN) in September 2015, aim to transform the world's energy services by 2030. The stated aim of Goal 7 of the SDGs [SDG.07] [1] is to: Ensure access to affordable, reliable, sustainable and modern energy for all. The SDGs and national policies in many developing countries have provided an impetus for rural electrification. An option for some remote rural villages could be hybrid energy systems (HES) that include microhydro power (MHP).

HES utilize more than one source to generate electricity and distribute it to end users. Nowadays, rural electrification programs in many developing countries utilize HES to provide electricity to remote villages far away from the national grid. Such programs aim to maximize use of local renewable resources to meet local demand for electric power. HES consists of multiple generators and 'balance-of-system' components to make sure production of electricity from variable renewable resources and consumption are in sync most of the time. Modeling HES is an important step in the design, implementation, and operation and maintenance (O&M) of rural electrification projects. Such modeling is normally done utilizing computer models.

A computer model of a component of HES is a set of mathematical equations that characterizes the subsystem/component in relation to the system. The model normally consists of input and output described in a form of equations that mimic the function of the subsystem or the system as a whole. A hydro/solar/wind hybrid energy system, as the name may suggest, utilizes renewable energy resources available in nature in order to generate electricity locally. The HES consists of three generators, along with many

components that generate and supply electricity set to a standard designated by the country code or a code required by the appliances.

A hydroelectric power station utilizes the energy of flowing water to generate electricity. The class of hydroelectric power stations that are less than 100 kW capacities are known as microhydro power (MHP) plants. Figure 1.1 presents a sketch of a typical MHP. An MHP makes sense for providing provisions of electricity to remote rural areas that are located away from the national grid and where there are adequate local resources along with demand. MHP has become one of the pillars for rural electrification in Nepal. MHP is a local and reliable renewable energy technology that is popular in many countries in the developing regions of the world. Microhydro is more than a scaled-down version of large hydropower, it retains its own benefits and challenges. MHP has not been able to internalize advances in engineering and technology because of various socio-economic reasons.

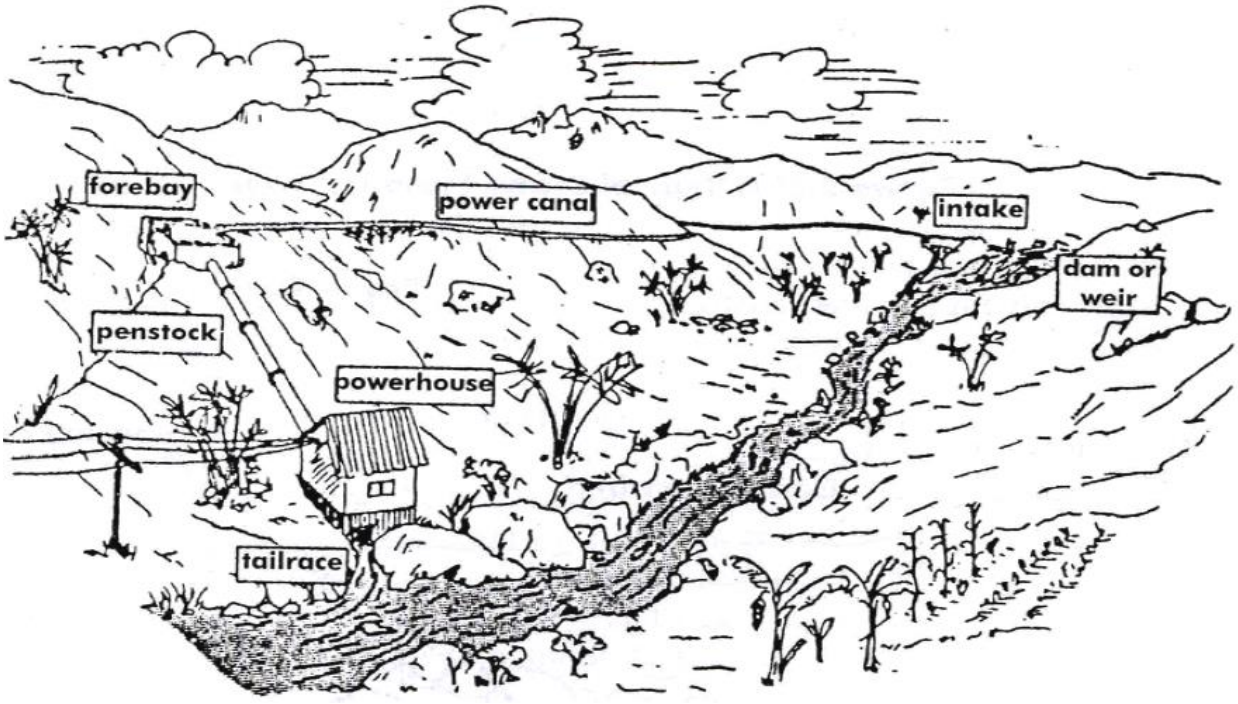

Figure 1.1: A Layout of Microhydro Power Plant [2]

Some villages may not have a perennial stream of water. For example, in one case, the minimum flow is available for only about ten months of the year. For other villages, the renewable resource may not be feasible. Sometimes local resources such as solar and wind may complement each other leading to a better design. In such a situation, it may be a good idea to combine multiple generators to form a HES. What would be an optimal mix of such generators? There are a number of ways to approach this question. Out of various possibilities, this study will focus on a class of computer models known as the performance models in order to find an answer.

There are a number of various software that utilizes performance models in order to evaluate HES for rural electrification. HOMER, RETScreen, and Hybrid2 are some popular examples. HOMER Legacy (a free version) does not characterize MHP systems on a par with the wind turbine or solar PV systems. RETScreen does not resolve seasonal or monthly variations in water flow. The water flow through the turbine may have to be regulated and controlled because the water flow that makes sense for the MHP may not be available throughout the year. In such situations, we will also need to take into account MHP system characteristics at partial load. In some cases, we let water accumulate and operate the MHP for a couple of hours a day, especially during dry season. To reflect such ground reality in modeling, it may be a good idea to study some MHP projects thoroughly, and develop a detailed model of the MHP system.

The aim here is to characterize a microhydro power (MHP) system using a parsimonious model without losing the overall general concept. We conduct a survey of governing mechanisms [3] that may make sense for MHP, especially flow control mechanisms that can conserve water in dry seasons. We expand MHP models within the framework of the Hybrid2 model [4] that was developed at the Renewable Energy Research Laboratory, University of Massachusetts. The models have been used to analyze some hybrid microhydro systems for rural electrification in Nepal.

1.2 Background of the Problem

Hydroelectricity started around the end of 19th century and is one of the most mature forms of electricity generation we have at our disposal today. MHP systems, however, are yet to internalize innovative technical developments in utility scale hydropower for various reasons. The same is the case for the models of MHP. MHP models are lacking details required for a performance analysis of HES to produce the optimal utilization of resources.

Many research and simulation models in the public domain do characterize MHP in some ways, but they use a generic model for simplicity. A generic model of MHP is:

$$P = \eta \rho Q g h; \qquad \text{Equation 1.1}$$

where P is power in W, η is efficiency, ρ is the density of water kg/m^3, Q is flow rate in m^3/s, g is acceleration due to gravity (9.8 m/s^{-2}) and h is net head in meters. HOMER Legacy (a free version) utilizes a version of the generic model of a hydro-turbine. It assumes a constant efficiency around a range of design flow rate (Qdesign). RETscreen has a better way of specifying an MHP system. RETscreen, though, utilizes the same load duration curve each day of the year and makes use of the annual flow duration curve (AFDC). However, it does not resolve temporal variation in flow. Hence RETscreen is recommended more for prefeasibility study of a single technology, not for the overall design/simulation of a hybrid rural electrification project. Hybrid2 [4], developed here at the Renewable Energy Research Laboratory (RERL), University of Massachusetts, provides much more detailed options to simulate a hybrid system consisting of solar/wind/diesel but it is yet to incorporate an option to simulate MHP systems.

In general, MHP systems are characterized based on a value of water-to-wire efficiency. This overall efficiency is calculated as $\eta_O = \eta_p \eta_t \eta_g$, where the subscripts *p* stands for the penstock, *t* for turbine and *g* for the electric generator. Figure 1.2 portrays overall efficiency of some MHP systems in Nepal that utilizes Pelton turbines [5]. The overall

efficiency seems to vary significantly at partial load, Q/Qmax. The generic model with constant efficiency term used in HOMER Legacy, may not capture this ground reality.

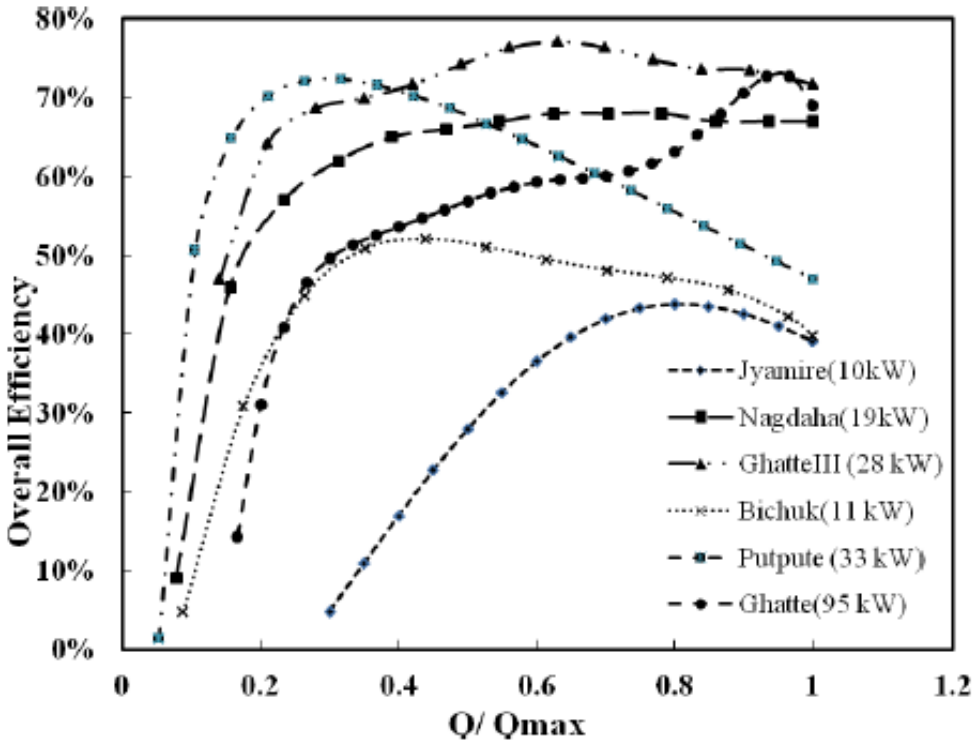

Figure 1.2: Field Performance of some MHP utilizing Pelton Turbine in Nepal [5]

In Nepal, most of the MHP plants are run-of-river (RoR) types and employ unregulated turbines. Even though the flow in the river may vary significantly across seasons, the flow through the turbine (Qturbine) may not change. For normal operation of an MHP, the flow through the turbine is fixed, for example, to the design flow rate (Qdesign). The flow alters, practically, only when there is an external intervention by the operator such as by adjusting a spear valve of the nozzle for the Pelton turbine, Figure 1.3. Many simulation programs in the public domain do not take this reality into account. For simplicity, some of these models use a generic model of MHP represented by Equation 1.1, and alter the flow through the turbine as the mean streamflow changes between

the months. A generic model of the MHP system with a constant efficiency term, as evidence in Figure 1.2 above, may not capture the performance of the MHP at partial load. We may need efficiency curves to capture the actual performance of the MHP system, just as we use a power curve for a given type of wind turbine.

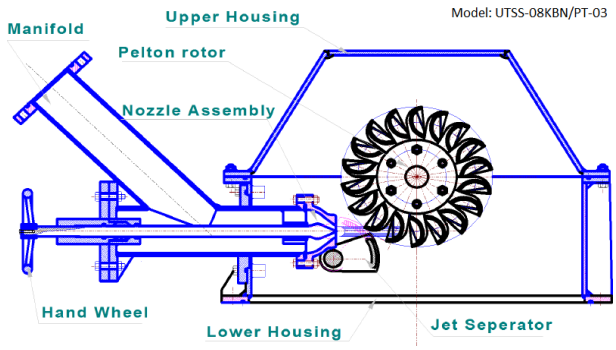

Figure 1.3: Nozzle and Spear valve of Pelton Turbine [2]

Performance analysis of hybrid energy systems (HES) within the framework of Hybrid2 requires an hourly time series of each resource that constitutes the system. Unlike the case for solar and wind resources, streamflow is not measured everywhere in a timescale of an hour or less. Most of the river flows in developing countries are recorded daily, while real-time flows may be available in some areas, such as WaterWatch [6] in the USA. Traditionally, a time series of daily flows recorded in such a manner are reported concisely in the form of a flow duration curve (FDC) by various methods [7]. An MHP project, which may not be bankable, may not afford such a data acquisition campaign of its own. However, hydrologists may be able to estimate the FDC utilizing various techniques such as multiple regression [8] or regionalization within the hydrologically homogeneous regions [9].

Hydrological models set at finer timescales are studied under stochastic/statistical hydrology. Historically, stochastic models of streamflow have focused on monthly and annual timescales. The current trend is, obviously, toward models with resolutions of daily and hourly timescales [10]. None of the popular hydrology software (SAMS 2007,

SPIGOT 2.5) we have come across in extant literature provides a way to synthesize the hourly time series of streamflow required for the performance analysis of hybrid microhydro systems. In addition, MHP sites are on non-gauged basins which further add challenges to estimating the hourly streamflow.

As shown in Figure 1.1 a typical microhydro power plant includes the following components: intake, power canal, forebay, penstock, power house and tailrace. The intake is where the water enters from the adjoining stream. Water flows through the power canal to the forebay, which is at the entrance to the penstock. The forebay usually has trash rack to keep out debris that may entered from the stream as well as a gate to close off the water flow for maintenance. The penstock is pipe that carries the water to the powerhouse, which is where the turbine, generator and various other mechanical and electrical equipment is located. The turbine is the device which converts the power of the water to mechanical power. An output shaft from the turbine is connected to a generator, which converts the mechanical power from the turbine to electricity. Most MHP plants use a synchronous generator with a voltage regulator; the voltage regulator maintains the system voltage. Some MHP systems use an induction generator with additional electronics, but that is less common. Traditionally, mechanical governor would control the flow through a turbine (Qturbine) in response to system load variations so as regulate the power output and keep the grid frequency constant. However, the MHP systems for rural electrification do not employ a governor in order to control the flow of water through a turbine. The cost of a governor is prohibitive for the economic scale of the MHP. In most MHP plants today the generator runs at a fixed output and an electronic load controller (ELC) controls the frequency by diverting surplus generation in excess of the system load to the dump/ballast load.

As indicated above, typical MHP plants today use electronic load control devices rather than mechanical governors. These have many benefits, but they can also waste a substantial amount of water. If we can come up with a robust yet simple mechanism to

regulate flow in some way, even at a coarse level, we may be able to conserve water. This mechanism will be useful especially during dry seasons when the design flow may not be available all the time, and turbines may have to operate only a few hours a day. A given volume of water in the forebay tank (or a pond, if incorporated in the initial design) may be utilized to prolong the supply of electricity.

These issues mentioned above may have to be addressed in order to enhance the performance analysis of HES that include MHP. Current MHP models do not address these problems adequately. The improved MHP models we have developed may lead to the better design and effective operation of hybrid microhydro systems for rural electrification.

1.3 Statement of the Problem

In the rural areas of a developing country, electricity is used mainly for household lighting. Accordingly, the demand for electricity varies widely throughout a day. Figure 1.4 presents a typical diurnal profile of a demand cycle in Nepal. The average load factor is about 52%. This load profile consists of three distinct zones: baseload, morning peak and evening peak. If this load is to be served by an unregulated MHP plant, which usually is the case for an MHP system, about 48 percent of the electricity generated will be dissipated in the dump/ballast load. This matters a lot especially in the dry season when there may not be enough water resources to meet demand. A simple flow control device, along with a pond (or enlarged settling basin/forebay tank) may conserve water and hence enhance the overall performance of an MHP and HES.

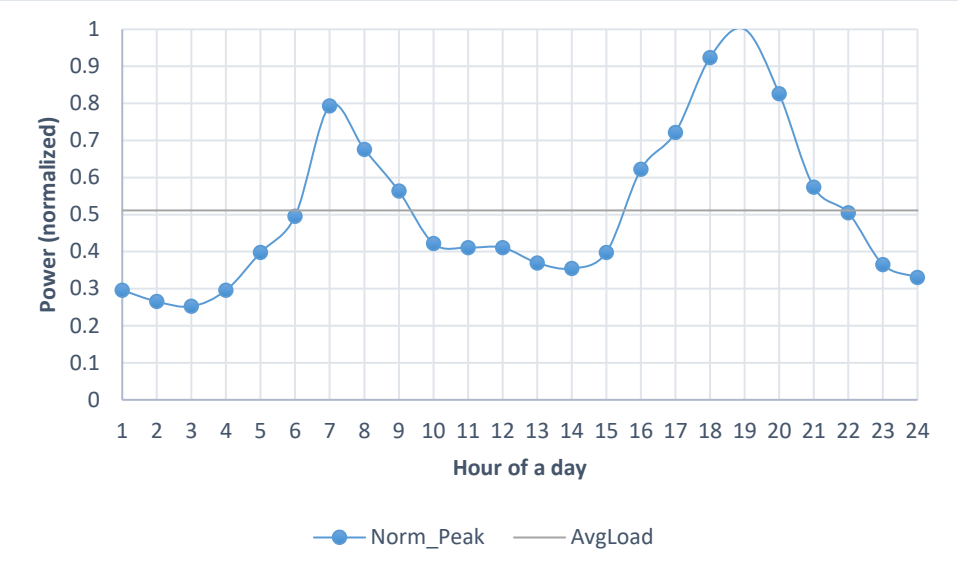

Figure 1.4: Diurnal Profile of Load in typical Nepali village

Some villages may not have perennial streams of water. In such cases, the design flow (Qdesign) of the MHP may not be available throughout a year. Can a hybrid MHP system still be an option for such villages? It depends. We may not always have a general answer to this specific question. The answer may depend on other factors such as the relative abundance of other renewable resources and local know-how about technologies [11]. Suppose that a hybrid MHP may be an option for the village. How do we size the MHP subsystem for an optimal portfolio mix of the HES? The performance simulation of the HES may provide answers to some of these technical questions.

The performance simulation of HES will require, in general, an hourly time series of all resources involved. Such a time series can be measured using an anemometer and a pyranometer in the cases of wind and solar energy resources respectively. Unfortunately, there does not now exist any such convenient common meters/sensors to measure the time series of the hourly streamflow for the MHP application in an ungauged basin. Hence, the design of a hybrid microhydro system bases on data from empirical models/methods that can only estimate monthly averages and the long-term annual flow duration curve (AFDC).

Many design and simulation tools do not characterize the MHP system on a par with other sources of generators of HES, such as solar PV or wind turbine systems. The basic guidelines with applicable procedures are lacking for the design and analysis of MHP system [12]. Even if a few published guidelines may exist [13, 14], they do not delve into the hourly or sub-hourly scales. Hence we may not be able to address the problems discussed in this section utilizing only industry standard models and software. This scenario demands a need to develop better models. We will need a detailed model of MHP to support better design and operation strategies to minimize the excess energy dissipated in the dump/ballast load, and conserve water in order to prolong the supply of electricity during dry seasons.

1.4 Objectives of the Study

This study aims to contribute to the general guidelines for a feasibility study of hybrid energy systems (HES) that includes microhydro power (MHP) and toward the integration of renewable energy based generators for decentralized application. The main objective of this study is to come up with an optimal design and operation strategy of a hybrid MHP system through the performance analysis approach used in the Hybrid2.

The probabilistic/time-series approach used in Hybrid2 (and in many other industry standard software) requires a time-series for hourly generation of electricity from each subsystem of the HES. The MHP models, as indicated in the previous sections, are lacking details required for the performance analysis of the microhydro systems. In an effort to fill this research gap, this study will focus on the following specific objectives:

a) Review contemporary literature on physics and performance studies of MHP and come up with an idea to characterize an MHP better and to improve its operational performance.
b) Develop a detailed model of a regulated MHP system within the framework/structure of Hybrid2.

c) Utilize the MHP model to simulate an existing hybrid MHP system, and design a hybrid energy system having a better technical performance.
d) Conduct an economic analysis of hybrid microhydro systems with reference to the data from case studies in Nepal.

1.5 Scope of the Study

The first hybrid microhydro system in Nepal, The Thingan Project, will be used as a case study for this research. The Thingan Hybrid Energy System Project is located in Ghalegau, Thingan -3 of the Makawanpur district (Latitude: 27°26'35.60"N; Longitude: 85°14'42.20"E, WGS84, 1354 m ASL). Table 1-1 below presents the size of each subsystem that constitutes the HES.

Table 1-1: Size of Systems

Subsystem of HES	System Size
Microhydro Power	20 kW
Solar PV	5 kW
Wind Turbine	3 kW
Battery Bank	48 kWh

Three design options we plan to study for the tri-hybrid project at Thingan are:

a) Existing system – Base case (unregulated microhydro plant),
b) Renewable + battery system (with regulated microhydro plant),
c) Renewable only system (with regulated microhydro plant).

The first option employs unregulated MHP while the second and third options employ regulated MHP system. The second option contains only renewable power generators and batteries. The last one contains only renewable power generators, no batteries.

We use data from the project reported by [15] along with the most recent data (resources and operations) from the Alternative Energy Promotion Center (AEPC),

Nepal. The AEPC/GON, with the help from Asian Development Bank (ADB), is considering retrofitting the Thingan project[1] [16].

The model of MHP is based on the physics of turbine design and the performance data from: a) Turbine testing lab, Kathmandu University in Nepal, (KUTTL) [17] and b) power output verification (POV) test [18] commissioned by Alternative Energy Promotion Center (AEPC), Nepal. The POV test is a type of third-party auditing of the microhydro plant installation to ascertain that the MHP installation meets performance criteria as specified by the AEPC. The Mini Grid Support Program (MGSP), AEPC, has conducted a field test of about 20 MHP systems (Pelton: 8, and Crossflow: 12) using the additional dump load method [5]. Data from these studies can provide key insights into the development of a detailed model of the MHP system for performance analysis.

1.6 Evaluation Framework: Energy Access

The technical performance of a HES is evaluated generally with reference to a local or an international framework for energy access. The Sustainable Energy for All (SE4ALL) Global Tracking Framework (GTF) [19, 20] classifies the access to energy into 5 tiers, with Tier 0 (no access) and Tier 5 being the highest level of access. It utilizes seven energy attributes for household electricity supply. These attributes are (i) Peak capacity, (ii) Availability (iii) reliability, (iv) quality, (v) affordability, (vi) legality, and (vii) health and safety. Table 1-2 presents two relevant attributes of the GTF for this study.

Rural villages differ from one another in terms of socio-economic conditions. Accordingly, the demand for electricity and affordability may vary significantly. Not all villages may require access to electricity around the clock. A typical off-grid rural electrification project in Nepal aims for the Tier 3 level of energy access of the

[1] Email communication on Jan 30, 2017, with Narayan Adhikari, Assistant Director, Head of Technology Division, AEPC/Government of Nepal.

framework. The Alternative Energy Promotion Center (AEPC) in Nepal recommends a power capacity of 125 Watt per household.

Table 1-2: Multi-Tier Framework for Measuring Energy Access for HH supply

Attributes		Metric	Tier 0	Tier 1	Tier 2	**Tier 3**	**Tier 4**	**Tier 5**
1	Peak Capacity	Power Capacity		> 3 W	> 50 W	> 200 W	> 800 W	> 2 kW
		Daily Wh		> 12 Wh	> 200 Wh	> 1000 Wh	> 3.4 kWh	> 8.2 kWh
2	Availability	Hours/day		> 4 hrs	> 4 hrs	> 8 hrs	> 16 hrs	> 23 hrs
		Hours/evening		> 1 hrs	> 2 hrs	> 3 hrs	> 4 hrs	> 4 hrs

The National Renewable Energy Laboratory (NREL) has developed a framework for quality assurance of isolated mini-grids power system [21] under Global Lighting and Energy Access Partnership (LEAP). The framework measures the level of service in the similar fashion to that of the SE4All's framework but with its own metrics. This frameworks proposes two non-dimensional indexes for measuring the power reliability. The System Average Interruption Frequency Index (SAIFI) measures the average number of power outages that an average customer experiences in a year, while the System Average Interruption Duration Index (SAIDI) measures the average number of minutes that an average customer is without power over the defined time period, typically a year. These indexes are defined as follows:

$$SAIFI = \frac{Total\ Number\ of\ Customer\ Interruptions}{Total\ Number\ of\ Customers\ Served} \qquad \text{Equation 1.2}$$

$$SAIDI = \frac{Total\ Minutes\ of\ Customer\ Interruption}{Total\ Number\ of\ Customers\ Served} \qquad \text{Equation 1.3}$$

Table 1-3 presents values of indices for various level of services ranging from the basic to the high level of service. The basic level corresponds to 90% reliability and the high level to the 100% reliability.

Table 1-3: Power reliability and level of service for isolated mini-grid system

Level of Service	Unplanned			Planned	
	SAIFI	SAIDI	Reliability	SAIFI	SAIDI
Basic	< 52 per year	<876 hours	90%	-	-
Standard	<12 per year	<438 hours	95%	-	-
High	<2 per year	<1.5 hours	99.99%	<2 per year	<30 minutes

This NREL Quality Assurance Framework (QAF) echoes a structure that of a mature utility in scale and sophistication. In this study, however, we use the performance metrics stipulated by the SE4ALL's Global Tracking Framework because of its ease of use.

1.7 Definition of Terms

There is not a consensus on the definition of small, mini, and micro hydropower plants. We will follow the definition used by the Alternative Energy Promotion Center (AEPC) in Nepal. Microhydro power plants have nameplate capacities less than or equal to 100 kW.

Annual Flow Duration Curve (AFDC) is a counterpart of the Typical Meteorological Year (TMY) used in the design of solar energy systems [22]. AFDC is collated based on data that spans much longer than a year, a time known as the period of record in the hydrological study. The AFDC bases on the period of record flow duration curve (PoRFDC). AFDC portrays the percentage of time a given flow equals or exceeds its value over a representative year, similar to the velocity duration curves [23] in case of wind energy resource. TMY is a time series whereas AFDC is expressed as a complement of the cumulative probability distribution for the daily streamflow.

Flow rate definitions: In designing the MHP we must deal with various water flow rates. With reference to a layout, see Figure 1.1, of an MHP plant, Figure 1. 5 delineates various flow rates in the context of this thesis.

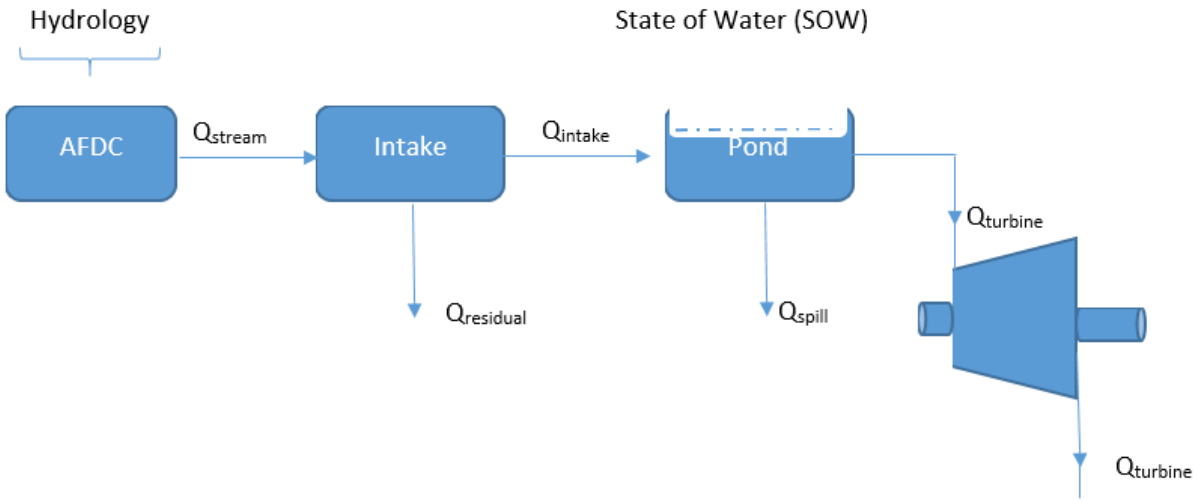

Figure 1.5: Various flow states in MHP systems

Qstream is a flow upstream of the intake. The dam (or weir) diverts a portion of Qstream to the power canal which is denoted by Q_{intake}. For environmental reasons, the MHP may not use up all water in the stream. The minimum flow discharge [24] downstream of the plant is $Q_{residual}$. Based on conservation of mass, we can combine these flows as:

$$Q_{stream} = Q_{turbine} + Q_{spill} + Q_{residual}, \qquad \text{Equation 1.4}$$

In Equation 1.4, $Q_{turbine}$ is a volume of water that runs actually through the water turbine. Q_{spill} is an overflow from the pond that passes without seeing the turbine. All

three streams out in Figure 1.5 join the stream somewhere downstream of the intake to the same end point.

Design flow (Qdesign): It is the flow rate corresponding to the rated capacity of the MHP. If the flow through the turbine (Qturbine) is equal to the Qdesign, the MHP will generate the rated power.

Q(firm, x%): The firm flow is defined as the flow available to the turbine at least x% of the time in a year. In general, 90% < x < 100%. Q95 is the flow available 95% of the time in a year.

State of Water (SOW): This term compares with the State-of-Charge (SOC) for a battery system. In this thesis, we are proposing a method to regulate flow through the turbine and also keep track of how much water is available in a pond of size $(SOW)_{max}$ to use in particular time steps during the simulation. The SOW describes the amount of water available in the pond, which could be integrated with a settling basin or forebay tank. The ponds act as virtual batteries for a regulated MHP system. The unit of SOW is an hour. If SOW = 2hrs, the water available in the pond can operate the MHP system for two hours at the rated capacity. Normally, MHPs are Run-of-River (RoR) type plants that do not employ such pond water by default.

In some simulations, we use this relative unit of SOW which is hours because of the normalization of variables. It is more convenient unit when studying a range of MHP capacity. However, the absolute unit of SOW is m^3. For an MHP plant with the SOW of 2 hours and design flow Qdesign in Liter/s, the same in absolute unit

$$SOW\ (m^3) = SOW(hour) \times Qdesign \times 60 \times 60/1000\ . \qquad \text{Equation 1.5}$$

1.8 Conclusions

Hybrid energy systems (HES) utilize local renewable energy resources for a provision of electricity to a remote rural village located away from the national power grid. Recently, microhydro systems have been integrated with other sources of generators such as the solar PV and wind turbine systems. There are many merits for such integration; however, there are various technical aspects of microhydro systems that can be improved on in order to realize the full potential of hybrid energy systems. We study some of these aspects and improve models of microhydro systems. Using these models, we simulate hybrid microhydro systems within the framework of the Hybrid2 software developed earlier at the University of Massachusetts.

CHAPTER 2

REVIEW OF THE LITERATURE

2.1 Introduction

A Hybrid Energy System (HES) utilizes more than one type of resource in order to meet the demand for electricity. The HES in this study harnesses variable renewable resources for rural electrification. Design and analysis of such a system configuration require a model of each subsystem for simulation and optimization. There are many models for each subsystem plus the whole system for a specific application. The National Renewable Energy Laboratory (NREL) documents a broad range of energy analysis tools [25] that utilize such models. Some analysis tools (Hybrid2, HOMER, ViPOR, etc.) can be used for optimizing renewable energy projects for rural electrification. The PV performance modeling collaborative at the Sandia National Laboratory provides a toolbox (Matlab and Python) for solar calculations and PV models. Some of these tools are equally applicable for utility-scale projects as well as a stand-alone project in remote rural settings.

Hydropower is the longest established source for the generation of electricity. There is not a consensus, however, on the definition of small, mini, and micro hydropower plants. In Nepal, a hydropower project capacity of less than or equal to 100 kW is termed as a microhydro power (MHP) project. An MHP utilizes technology that is accessible to developing regions of the world. It is one of the pillars of rural electrification in Nepal. By the end of the fiscal year 2016, with about 54 MW installations since 1962, MHP provides access to electricity to more than 250,000 households in remote rural villages [26].

As Nepal is moving toward electrifying the last quintiles of its hinterlands, the challenges are mounting in terms of both technology and finance [27, 28]. Many villages are very remote, and resources are sparse - a single resource may not be enough economically in

many cases. We may, therefore, need to combine local renewable energy resources to produce adequate electrification in those places. Recently microhydro plants are being combined with solar PV and/or wind turbines [15] to meet the electricity demands of the villages in Nepal and elsewhere. A hybrid microhydro system may unleash the capabilities of renewable energy based rural electrification project that can deliver a reliable range of supply in order to meet the demands of some rural households [29]. Such hybrid microhydro systems may offer elegant solutions over a HES employing batteries. There are only a few such hybrid MHP projects in Nepal; the trend, however, is on rising in Asia and Africa.

An MHP in Nepal utilizes typically Pelton or Cross-flow turbines and a synchronous generator. A turbine converts the energy of flowing water into mechanical energy. The turbine is coupled with a generator, 3 phase or 1 phase, which in turn converts the mechanical energy into electrical energy. Most of the MHP systems do not regulate flow through the turbine in response to the varying load. A simple flow control device which may mimic the function of a governor, even at a coarse level, may add to the value of hybrid microhydro systems. This value will be more apparent during dry seasons when streamflow could go below the design flow rate. The device will help conserve water and may also aid to the reliability of the HES.

This chapter is organized as follows. In the following section, we present a search description relevant to the research objectives/questions in the previous chapter. We start with a review of HES modeling approaches that are in the extant literature followed on by Section 2.3 where we summarize the MHP models/methods used in the leading software for the performance analysis of hybrid microhydro systems. The state-of-art in resource modeling of the MHP system is documented in Section 2.4. The subsystems of the HES, with an emphasis on microhydro technology, are summarized in Section 2.5. The final section of this chapter presents an overview of flow regulation in MHP systems.

2.2 Search Description and State-of-Art

This research is about design of optimal HES that includes microhydro. The HES is composed of microhydro, solar PV, and wind turbine subsystems. A significant volume of literature is available on performance analysis of HES for rural electrification, especially in the form of case-studies employing solar and wind systems. However, there are only a few studies that deal with all three resources (solar, wind and microhydro) at a site. For solar and wind systems, we will use the state-of-art models utilized in Hybrid2. An emphasis for the microhydro power (MHP) systems will be on performance models that regulate flow in response to the demand fluctuations. We will also review hydrological models there are in the extant literature to synthesize an hourly time series of streamflow.

Naturally, a literature review for this study will focus on the objectives proposed in Chapter 1.4. To reiterate, this literature review presents the state-of-art concisely in the following three related areas:

a) Modeling hybrid microhydro system within the framework of Hybrid2;
b) Resource model for MHP: Hourly Time series of streamflow;
c) Regulation of MHP: Flow control Mechanism.

A hybrid microhydro system offers an interesting site-specific design and optimization questions. Optimization will require a thorough analysis of the AFDC and resource information for the subsystems that constitute the HES. There are various techniques in order to optimize a hydroelectric plant. In general, these techniques use one of the following approaches:

a) Lagrange Multiplier;
b) Numerical Optimization;
c) Analytical Optimization.

The Lagrange approach uses some design parameter (penstock size, # of turbines) of the plant to come up with optimal size. Some authors have also used a multivariate function to optimize a hydroelectric project. The other two approaches, generally, utilize the AFDC. A paper [24] by Basso and Botter presents an analytical framework to optimize the energy production and the economic profitability of small run-of-river power plants. The marginal cost and marginal profit functions help determine the optimum size of the plant. At optimal design flow (Q*design), the marginal revenue due to increase in the plant size equals the corresponding marginal cost. A plant could be optimized separately for energy or other standard economic metrics such as the net present value (NPV) or the internal rate of return (IRR). The optimization approach could be the same for a hybrid energy system consisting of multiple subsystems. Unlike grid-interactive system, decentralized systems are optimized for the load profile. Economics comes later.

For this study, an optimal design is a feasible hybrid microhydro system configuration with minimum net present cost (NPC) after the subsidy, if any. For each feasible configuration, we will also look at the levelized cost of energy (LCOE). To compute LCOE and NPC, we will use equations from [29] and the economics module of the Hybrid2 software.

2.3 Hybrid Energy System Codes

A hybrid energy system for rural electrification requires thorough analysis to make sure it meets design requirements utilizing a best possible combination of generators. There are several software packages to facilitate simulation, optimization and sensitivity analysis of HES. A review paper [30] documents the main features of 19 software tools and compares the output of some of them, mainly HOMER and RETScreen for a PV-Wind-Battery system.

A report [31] presents solar PV models developed and used at the Sandia National Laboratory. This report also documents models developed outside the laboratory to support the design and analysis of hybrid energy system. A study commissioned by the International Energy Agency reviews some design and simulation tools for hybrid PV systems [32]. One of the recommendations of the study is to include other energy sources, such as wind and hydro turbines, into the dimensioning and simulation tools. Another report [33] provides some recommendations for deployment of PV hybrid system for rural electrification.

In this section, various classes of models used for the modeling of HES are reviewed. Three leading performance modeling software, namely RETScreen by the Natural Resource Canada, HOMER by the Homer Energy, and the Hybrid2 developed here at the University of Massachusetts are discussed along with the MHP models they utilize, where applicable. This section concludes with a brief description of the Village Power Optimization Model for Renewable (ViPOR) developed at the National Renewable Energy Laboratory (NREL) for designing a village level electricity distribution system.

2.3.1 Model Types

There are various models of hybrid energy systems (HES). These models may be classified [4] into two broad categories: a) Logistic models and b) Dynamics models. Logistic models are utilized for sizing subsystem or component, and for providing inputs to the economic analysis of the hybrid systems. Dynamic models are utilized primarily for a more detailed analysis such as component design, system stability, and power quality analysis. There are other ways for the classification as well. One report from the International Energy Agency [32] has classified hybrid system analysis models into three categories: a) basic dimensioning, b) system design and c) research and simulation. In Table 2-1 below, we make an attempt to give an example of each category of the classifications discussed above.

Table 2-1: Various types of models of HES

Category	Examples
Logistic models	RETScreen, HOMER, Hybrid2
Dynamic models	PSAT [34]
Basic dimensioning	RETScreen
System design	HOMER
Research and simulation	Hybrid2, HOMER

The logistic models, following the Hybrid2 Theory Manual [4], can be further classified into the following three categories:

- Time series (or quasi-steady state);
- Probabilistic; and
- Time series/probabilistic.

Some scholars also utilize stochastic models for characterizing renewable energy resources and load estimates. Stochastic models are generally based on the Ito calculus that extends methods of calculus to stochastic phenomena. Stochastic models have found a niche mainly in the financial markets where decisions are to be made under uncertainty. The HES we propose for this study utilizes variable renewable energy resources. Hence stochastic models may also make sense for modeling the HES. In fact, we offer a stochastic model for the hydro resources latter in this thesis.

Dynamic models have been classified further based on time-scales for the system simulation. According to Manwell et al. [4], general categories of dynamic models may include:

- Dynamic Mechanical Model;
- Dynamic Mechanical, Steady-State Electrical Model; and
- Dynamic Mechanical and Electrical Model.

An emphasis of this research will be on the logistic models that utilize statistical modeling techniques. Logistic models are sometimes also known as performance models. In the section it follows, we present a short introduction of three leading hybrid energy system analysis tools including the Hybrid2 developed here at the University of Massachusetts. The introduction includes an overview of the models used by each code, with emphasis on the microhydro subsystems where applicable.

2.3.2 RETScreen

RETScreen is a software system for project feasibility analysis as well as ongoing energy performance analysis. This clean energy management software is developed by the Ministry of Natural Resource Canada [35], and its limited functionality version, RETScreen Expert, is available to download free of charge. Its first MS Excel edition was launched in the year 1998. The current version uses Visual Basic and C-language as the working platform. It utilizes five standard steps for a project analysis, namely,

1) Energy Model,
2) Cost Analysis,
3) Greenhouse Gas Analysis (optional),
4) Financial Summary, and
5) Sensitivity and Risk Analysis.

Figure 2.1 displays a schematic diagram of a typical RETScreen model.

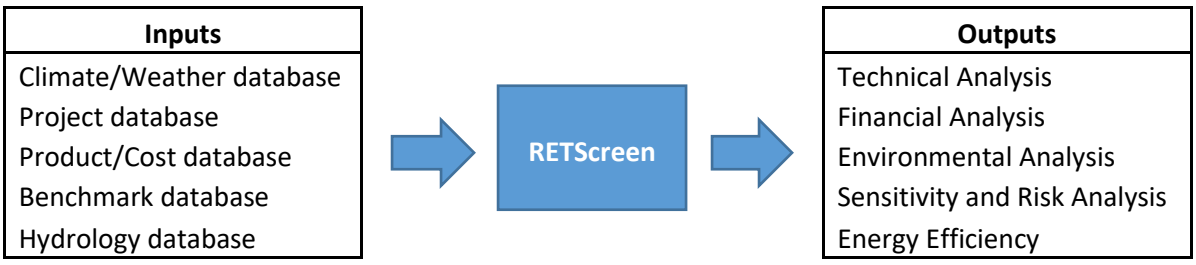

Figure 2.1: Schematic diagram of RETScreen model.

The RETScreen® uses The Small Hydro Model [36] for evaluation of hydroelectric projects. A flow-duration curve represents hydrological data for a typical representative day of the year. The flow-duration curve is specified at 5% increments in time. It does not take into account variations in the head. The variations in the energy demand and available energy are taken into account by changing "Available Flow Adjustment Factor" in the model.

The RETScreen® requires a daily load demand in the form load-duration curve (L) spread over a day, and a power curve (P) corresponding to the AFDC. Figure 2.2 presents some sample curves from the Engineering & Cases Textbook [36].

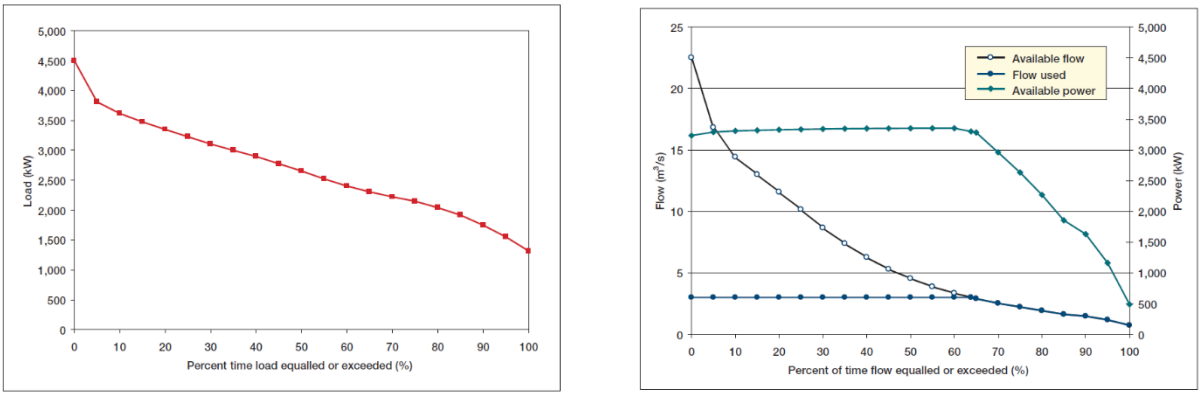

a) Load Duration Curve b) Power – Duration Curve

Figure 2.2: Duration Curves, Small Hydro Project Model, RETScreen®

The RETScreen® uses the same load profile for each day of a year as represented by the load duration curve. The energy demand for a day and energy available for a year are calculated based on those curves by integration using the Trapezoidal rule as follows:

Energy Demand = $\sum_{k=1}^{20} \left(\frac{L_{5(k-1)} + L_{5k}}{2}\right) \frac{5}{100}\ 24$; and

Energy Available = f(Area Under the Power Curve | Flow Duration Curve)

$= \sum_{k=1}^{20} \left(\frac{P_{5(k-1)} + P_{5k}}{2}\right) \frac{5}{100}\ 8760\ (1 - l_{dt})$

where l_{dt} is annual downtime losses.

The RETScreen® does not resolve daily or hourly variations in the demand for electricity nor the generation of electricity.

2.3.3 HOMER

Hybrid Optimization Model for Multiple Energy Resources (HOMER) is a microgrid software for optimization of HES. HOMER can help evaluate HES design options for both off-grid and on-grid rural electrification. This software was developed at the National Renewable Energy Laboratory (NREL), USA, in 1993 and its user-friendly Windows application version came in 1997. The NREL has licensed HOMER to Homer Energy, LLC in 2009. Its free version, HOMER Legacy (v2.68 beta) can still be downloaded with a new or existing account at Homer Energy which maintains the software.

A short description of the methods HOMER utilizes to models loads, resources, components, and dispatch is documented in [37]. A user guide [38]of HOMER Legacy published jointly by the Homer Energy, and NREL describes eleven basic steps ranging from the problem formulation to sensitivity analysis of a HES. HOMER simulates the operation by making energy balance calculations for each of the 8,760 hours in a year. Figure 2.3 presents a schematic diagram of a typical HOMER model.

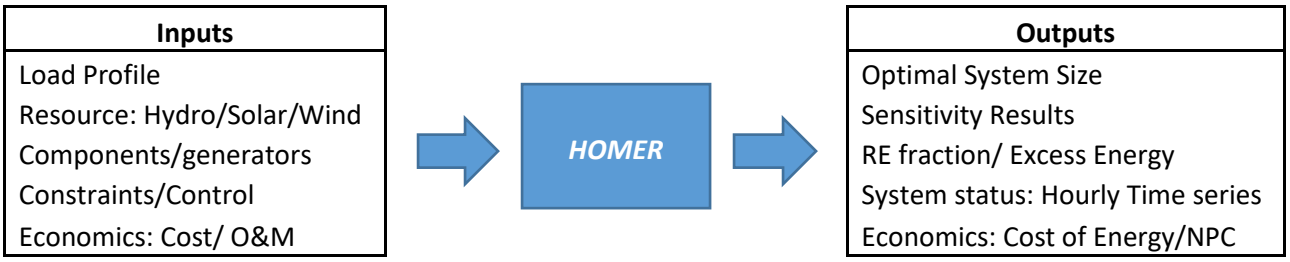

Figure 2.3: Schematic diagram of HOMER model.

HOMER uses the following generic models, Equations (2.1) through (2.4), for performance simulation of MHP systems.

h_{net}= h (1- f_h) ;

Equation 2.1

$$\dot{Q} = \dot{Q}_{stream} - \dot{Q}_{residual}$$

Equation 2.2

$$\dot{Q}_{\text{turbine}} = \begin{cases} \min(\dot{Q}, \quad w_{\max} Q_{\text{desgin}}) & \text{if } \dot{Q} \geq w_{\min} Q_{\text{desgin}} \\ 0 & \text{if } \dot{Q} < w_{\min} Q_{\text{desgin}} \end{cases}$$

Equation 2.3

Power $P = \eta \, \rho_w \, \dot{Q}_{turbine} \, g \, h_{net}$ Equation 2.4

In the Equation (2.1) above, h is the gross head, and f_h is the head loss (%) in the pipe due to friction. The turbine operates within the minimum ($w_{\min}$) and maximum $w_{\max}$ fraction of the design flow rate (Qdesign) governed by the flow available at a given time step. The MHP system runs always at a fixed overall efficiency even though the flow through the turbine may vary within some limits ($w_{\min} = 50\%$; $w_{\max} = 150\%$, the user can specify) of the design flow. These assumptions may be acceptable for an unregulated turbine most of the time but are not internally consistent. It is the governing system of turbine that can control the flow through the turbine, not the opposite. As MHP systems do not employ any active governor, only the operator can alter the water flow through the turbines. This is typical of MHP systems for rural electrification in developing countries.

HOMER is a popular performance analysis software to design HES for rural electrification. It can accept monthly means or an hourly time series of streamflow data. Unfortunately, the time series data are scarce for MHP project. One may claim that a feasible technology for data collection at hourly time scale is not affordable for an MHP project. This performance analysis software uses the monthly average for each hour of the month under an assumption that the flow rate remains constant within each month [37]. It does not consider variations in streamflow within a month, nor does it take into account variations in efficiency of MHP systems at partial load/flow conditions. By not recognizing these variations, HOMER may be missing improved accuracy of modeling

MHP system at an hourly time scale over statistical models that typically evaluate average monthly performance.

HOMER does not yet have a provision of modeling regulated MHP we propose to study in order to enhance operational performance of hybrid microhydro systems. However, wherever applicable, this study uses HOMER Legacy (v2.68 beta, February 8, 2012) for cross-comparison of the design and the economic analysis of hybrid energy systems.

2.3.4 Hybrid2

Hybrid2 is a simulation model designed for a feasibility study and preliminary design of hybrid energy system. The model is the culmination of many years of research at the University of Massachusetts Amherst in the area of wind/diesel and hybrid power systems. It builds on the wind/diesel model [39] developed at the Renewable Energy Research Laboratory, University of Massachusetts Amherst. A rationale for the development of Hybrid2 is documented in [40]. Hybrid2 was developed jointly by the NREL and UMass with funding from the U.S. Department of Energy. This software is written in Microsoft Visual BASIC and uses Microsoft Access database as a back-end. It is available to download freely from the Wind Energy Center at University of Massachusetts [41].

Currently, Hybrid2 can simulate hybrid energy system consisting of wind turbines, solar PV array, and diesel system. It supports a detailed long-term performance and economic analysis on a wide variety of hybrid power systems and includes some data processing tools (gap filler, data synthesis, etc.) to facilitate the overall simulation process. The underlying theories and algorithms are well documented in [4] and a user manual [42] is published by the NREL. Figure 2.4 displays a schematic diagram of a typical Hybrid2 model.

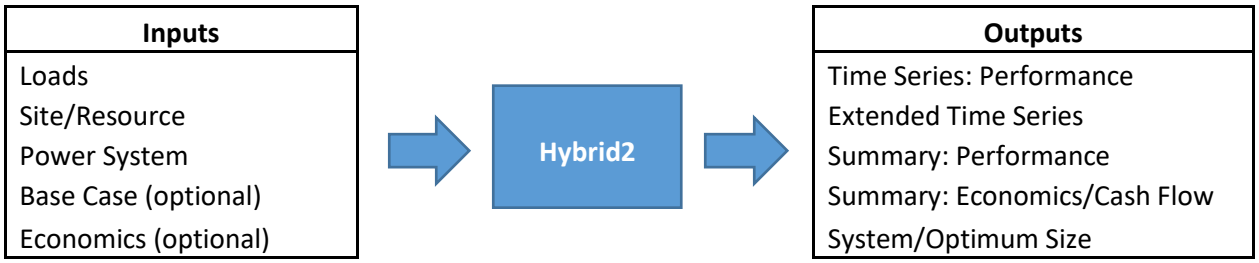

Figure 2.4: Schematic diagram of Hybrid2 model.

Hybrid2 takes a probabilistic/time-series approach for performance analysis of HES. It takes into account variations in wind speed and load within each time step and factors them into the performance predictions using statistical techniques to combine variances.

This in-house research and simulation software incorporates many subcomponents of HES we propose to study except MHP systems. We develop an MHP module within the framework of Hybrid2. Such module may be used for expanding the capabilities of Hybrid2 into Microhydro systems. Hybrid2 (version: 1.3f, April 2011) is used for analysis and comparison wherever applicable.

2.3.5 ViPOR

The Village Power Optimization Model for Renewable (ViPOR) is an optimization model for designing village electrification system, developed by NREL. Given the GIS coordinates of the houses and other features of the village to be electrified by a HES, ViPOR helps identify houses to be included in the centralized distribution grid. The rest of the houses can be electrified using isolated systems such as solar home systems (SHS). ViPOR uses an optimization algorithm called Simulated Annealing or Greedy Algorithm to design the least-cost distribution system. This introduction of ViPOR bases on version 0.9.25 (June 7, 2005).

2.4 Microhydro Power: Resource Model

Performance analysis of HES within the framework of Hybrid2 requires an hourly time series of each resource that constitutes the system. In our case, the HES is composed of microhydro, solar PV, and wind turbine systems. Hence we will require a time series of hourly resources for all three renewable energy sources: hydro, solar and wind resources.

Unlike the case for solar and wind resources, streamflow is not always measured in the timescale of an hour or less. There are advanced technologies that report streamflow in real time such as the one that the U.S. Geological Survey (USGS) utilizes for the WaterWatch [6]. However, such radar/satellite-based advanced technologies are not easily accessible for the developing world. Most gauged rivers in Nepal record daily average flow. Traditionally, a time series of daily flows recorded in this manner are reported concisely in the form of a flow duration curve (FDC).

An FDC is an alternate way of presenting the cumulative distribution function (CDF) of streamflow. FDC presents a complement to the CDF for a series of daily streamflow calculations for a particular river basin. It portrays the percentage of time a given flow is equaled or exceeded over a historical period. A probability mass function that summarizes the magnitude and frequency of streamflow can be derived from the FDC. Vogel et al. [43] presents a brief history of the application of a flow duration curve in the utilization of water resources. They credit Clemens Herschel for the first use of an FDC in about 1880.

Weather data for a period of record can be reduced to the Typical Meteorological Year (TMY or its versions) [44]. Similarly, a given set of hydrological data can be reduced to the AFDC. The AFDC is collated based on data that spans much longer than a year sometimes known as the Period of Record Flow Duration Curve (PoRFDC) in the hydrological study. The AFDC takes long-term trends, such as one due to climate change

[45], into account. An index flow approach [10] models the relationship between an FDC and AFDC. This statistical approach is capable of reproducing some measures of central tendency (mean, median) and dispersion (variance). Basically, statistical approaches aspire to reproduce even higher order moments [46].

The hydrological cycle operates mainly due to forces of gravity and energy from the sun. Hydrologists take various approaches to model hydrological cycles and to come up with an AFDC for a river. Among them are the climatological and geomorphological approaches. The former utilizes regional climatological models (RCM) whereas the latter exploits the dynamics of active drainage networks among various other factors. These approaches are used, basically, to estimate the FDC for a river that is not gauged, which is usually the case for an MHP system.

The streamflow at an MHP site depends largely on geography and the climate in the catchment area of the river. An equilibrium water balance equation [47] can be assumed for a large catchment, over a sufficient time period. Some of these models are very explicit. They utilize Richard's multi-dimensional water balance equation [48] and aim to capture the underlying physics of the hydrological cycle at various temporal and spatial scales. There are various ideas about the model of catchment area (geography). Some utilize techniques from statistical physics [49] and electric circuits [50]. Many others have employed full-blown GIS analytics, including the physical characteristics of soil [51].

Estimating time series data based on these models requires a great deal of effort and quite a bit of data, even for the time resolution of one day. Hence, such approaches may not make a lot of sense for the performance analysis of an MHP that will require resource data set at a time resolution of an hour. There is always a trade-off between model complexity and predictive ability. Here, we will choose to follow the approach of

stochastic hydrology for disaggregation of annual or monthly flow statistics to hourly statistics.

2.4.1 Streamflow Models: Stochastic Hydrology

Historically, stochastic models of streamflow have focused on monthly and annual timescales. It is natural that there is an increasing interest in the development of stochastic models at finer timescales. Obviously, the current trend is toward hydrological models with the resolution of daily and hourly timescales [10]. Hydrologic models with daily time-scales are now commonplace in water resource engineering/planning. Data at finer resolutions may facilitate better design and the efficient operation and planning of hydro infrastructure/facilities. This is an active point of the research area in hydrology.

Disaggregation models in hydrology aspire to preserve statistical properties at more than one level of aggregation; for instance, at annual and monthly as well as daily levels. Researchers are trying to come up with a disaggregation scheme that includes a minimum number of parameters [52]. Following [53], the disaggregation approach for synthesizing streamflow data in hydrology follows some variants of a linear model of the form:

$$X_t = \mathbf{A}\, Z_t + \mathbf{B}\, V_t. \qquad \text{Equation 2.5}$$

In Equation 2.5, X_t is a vector of a disaggregated variable at a time t; Z_t is aggregate variable; and V_t is a vector of independent random innovations, usually drawn from a Gaussian distribution. A and B are parameter matrices. A is chosen or estimated to reproduce the correlation between aggregate and disaggregate flows. B is estimated to reproduce the correlation between individual disaggregate components. Many models in the extant literature make some assumptions about system dynamics that translate to the structure and sparsity of these matrices and reproduce either one or the other correlations [54] directly.

Measure–correlate–predict (MCP) like algorithms [55, 56] are also used in stochastic hydrology in order to disaggregate from monthly to daily flows at the target station based on high-resolution data at the source station. Acharya and Ryu [57] used a variation of the MCP method, named the daily streamflow index, to estimate daily streamflow at the target waterway stations located in the northwest states.

A synthesis of streamflow predicted using the stochastic disaggregation method will require a statistical model that defines the distribution of the streamflow in the river. Hydrology literature reports two classes of methods to come up with the distribution. The parametric methods approximate the nature of stream flow by some common standard distribution (Poisson, log-normal etc) whereas the non-parametric methods build distribution directly by basing their results on the historical data set. In one of the non-parametric approaches [58], the authors assume streamflow as a higher order Markov process and use the Kernel methods to estimate the joint and conditional probability function. The distribution developed in such a way is then utilized for synthesizing streamflow sequences. Almost all disaggregation schemes seem to have set their boundaries to the daily timescale. Even though there is no theoretical limit on timescale, stochastic hydrology is yet to offer an elegant method to show that synthesizing streamflow at hourly resolutions occur with acceptable accuracy. Rainfall modeling also seems not to resolve time scales sufficiently [59]. This coarse resolution may be due to the complexity associated with modeling at such temporal (and spatial) scales and the unavailability of data to validate any disaggregated sequence of streamflow.

Stochastic Analysis Modeling and Simulation (SAMS) is a tool developed at Colorado State University for the simulation of hydrologic time series such as annual and monthly streamflow. A current version, SAMS 2007 [60], allows for the generation of synthetic series at seasonal rates, such as quarterly and monthly scales. Another popular synthetic streamflow generation package SPIGOT [61] is based on linearizing the transformations

of the historical streamflow time series [54]. Neither SAMS nor SPIGOT offers an option to generate the hourly synthetic streamflow required for the performance analysis of hybrid systems within the framework of Hybrid2.

The National Weather Service (NWS) uses various models such as the lumped Sacramento Soil Moisture Accounting Model (SAC-SMA) for its river forecasts [62]. The Distributed Model Intercomparison Project (DMIP) [63] compares the output of various models with hourly data from the USGS. These models require inputs that are rarely fulfilled for an MHP site. A GIS/MATLAB based Toolkit, SMART [51] utilizes Richard's water balance equation [48] in large upland catchments to model various hydrological parameters including downstream runoff. It could be a great tool for estimating the daily flow for an MHP application, hydropower in general, where geography is the significant driver of rainfall-runoff transformations. Its inputs are digital elevation model (DEM) data, land cover, soil type and the time series of rainfall. For a site that is not gauged, which is typical for an MHP project, rainfall data may also come from the Global Precipitation Measurement (GPM) [64] or the Tropical Rainfall Measuring Mission (TRMM) [65] database. However, estimation for the hourly time series of streamflow, this toolkit requires the historical hourly meteorological dataset. Such data sets are scarce in Nepal and other developing regions of the world.

Other data-driven methods such as artificial neural networks (ANNs) have also been applied to various hydrological problems [66]. A motivation for ANN may be to capture nonstationarity, nonlinearity and inhomogeneity (i.e., statistical properties that vary by streamflow states) characteristics embedded into the physics of the hydrological cycle. Besaw et al. [67] test two ANNs to forecast streamflow in water basins that are not gauged. Their model inputs use time-lagged climate data consisting of the daily average temperature, total precipitation, and time-lagged estimates of flow. ANNs require a set of the historic dataset for the training and testing of the model consisting of multiple layers in order to capture nonlinearity and nonstationarity. MHP sites for rural

electrification usually do not have such data, to begin with. Typical data available for such sites are the average streamflow, precipitation, and temperature at different months of a climatological year as measured by the local Meteorological Office or NASA Surface Meteorology and Solar Energy database [68].

None of these models discussed above, by default, synthesize streamflow to the timescale required for the performance analysis of hybrid microhydro systems. As a result, we have to come up with our own method of calculating streamflow based on information that is available on the site in question. There are various models of FDC common among hydrologists in Nepal. We choose to use the Medium Hydropower Study Project (MHSP NEA 1997) Method recommended by Kapil Gnawali, Hydrologist Engineer, at the Department of Hydrology and Meteorology, Nepal. This method along with the stochastic modeling techniques is used in order to synthesize hourly time series of streamflow in a river. This research refrains from estimating FDC for a river that is not gauged; rather, it focuses on statistical techniques for estimating the time series. For a given AFDC, or probability distribution function, we come up with a synthetic time series of hourly flow and utilize the time series for performance analysis of HES within the framework of Hybrid2.

2.4.2 Streamflow Measurement and Estimation in Nepal

Nepal is a landlocked county in South Asia between India and China. Nepal is situated in the Hindu Kush Himalayan Region, a source of ten large Asian river systems [69]. The elevation ranges from the top of the world (Mt. Everest 8848 meter) to 70 meters within a north-south span of about 190 kilometers. There are four major river basins: Karnali, Narayani, Bagmati, Koshi. A network of about 6000 rivers and rivulets spread all over the map of Nepal. These rivers can be classified into three categories: snow-fed, rain-fed and seasonal rivers. The Department of Hydrology and Meteorology [70] maintains almost all hydrological (51) and meteorological stations (281) in Nepal.

Many remote rural villages far away from the national grid can be provided with electricity utilizing local renewable energy resource (hydro, solar and wind). A microhydro power (MHP) plant utilizes water flowing in the local rivers or rivulets to generate electricity. A small-scale project like an MHP may not be able to afford a resource assessment campaign for a year or so. In Nepal, such projects rely heavily on empirical methods such as MIP (Medium Irrigation Project) or WECS/DHM methods [71]. These methods help estimate the monthly average of streamflow based on a point/sample flow measurement taken during a day in the dry season. Such flow measurements usually are carried out using the salt dilution method [72].

Most of the feasibility study reports of MHP in Nepal use the MIP method in order to estimate the monthly means of streamflow. The Lafagad MHP (85 kW) project in Kalikot [73] is one such example. The design flow (Qdesign) is based on a firm flow that is available about 90% of the time, about 11 months of a year [13]. The MIP method, developed in 1982, divides Nepal into seven hydrological regions [71], see Figure 2.5. This method can provide an estimate of average monthly flow based on a point measurement during the dry season and the catchment area of the river.

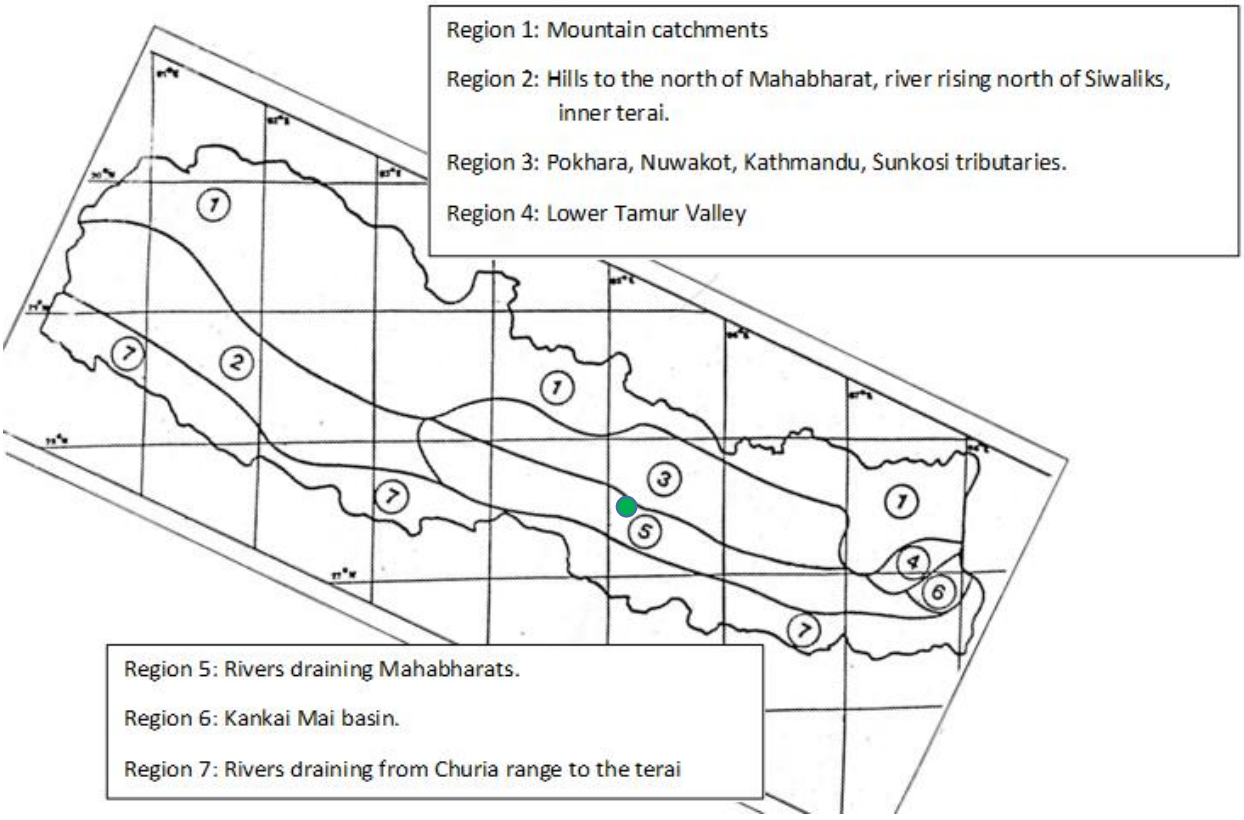

Figure 2.5: MIP Regions of Nepal [74]

A green dot in Figure 2.5 marks the Thingan Project. This project resides in MIP region 5 consisting of tributaries draining Mahabharats region.

There have been various efforts toward creating a flow estimation model for Nepal. A software package, HydraA-Nepal [8] can provide a long-term flow duration curve based on information about catchment boundary for any site in Nepal. HydraA-Nepal utilizes the results of multivariate regression analysis techniques using the low flow statistics (Q95) and key characteristics of 40 gauged catchments in order to estimate the overall streamflow.

In summary, a detailed feasibility study of MHP projects in Nepal relies on estimates of the monthly means of streamflow along with the AFDC. Such a study may benefit from the performance analysis of the system. For the performance analysis of any hybrid

MHP system to be accurate enough we will have to estimate the hourly time series of streamflow based on data that is already available for the site in question.

2.5 Subsystems of the Hybrid Energy System

The HES we study here includes three subsystems: Microhydro Power (MHP) Plant, Solar PV Array, and Wind Turbine. For completeness of this study, we present an overview of basic principles of operation of these subsystems of the HES. For a detailed and authoritative account of this extensive subject, readers are recommended to follow a standard textbook on each subsystem. A brief introduction in this section serves merely to illustrate a few aspects relevant to this research.

This section introduces those three subsystems of HES and models for the subsystem, including a model for the storage system we use for this study. We start with the MHP system, its components and operation principles, and review efficiency of Pelton and Cross-flow turbines briefly. These two turbines are used widely in MHP systems all over the world. The MHP section is followed on by sections on Solar PV and Small Windpower subsystems. We conclude this section with a short description of a model of a storage system that utilizes the lead-acid battery.

2.5.1 Microhydro Power System

A) Introduction

A microhydro power (MHP) system converts the energy of flowing water into electrical energy. The energy of water drives a water turbine coupled with a generator which converts the mechanical energy into electrical energy. We can find literature that describes current status and prospects of MHP [75] in developing and developed regions. The US Department of Energy recommends MHP systems to reduce electricity bills by homeowners and small business owners. In a country like Nepal with abundant streams and favorable geography, MHP systems have become one of the pillars for electrification of rural areas located far away from the grid.

There are various types of turbines utilized in MHP systems. An impulse turbine uses kinetic energy whereas the reaction turbine can use both pressure and kinetic energy of flowing water. Turbine selection for a site mainly depends on flow rate and head available at the site, among many other parameters. Table 2.2 presents some tentative selection criteria of water turbines suitable for low, medium and high head [72].

Table 2-2: Turbine Selection for Microhydro Power

Turbine	Head		
	High	Medium	Low
Impulse	Pelton	cross-flow	cross-flow
	Turgo	Turgo	
	Multi-jet Pelton	Multi-jet Pelton	
Reaction		Francis	Propeller
		Pump-as-Turbine	Kaplan

There can be a large variety of designs of microhydro turbine. In Nepal, two types of turbine designs are most common for rural electrification: Pelton and Cross-flow. Figure 2.6 portrays sketches of these two impulse turbines.

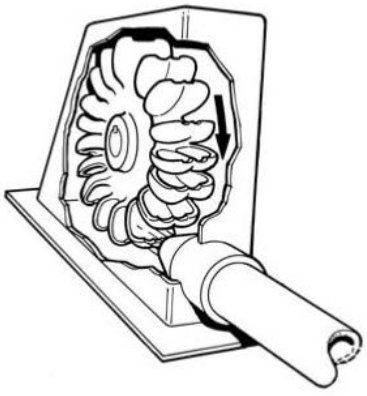

a) Pelton Turbine [76]

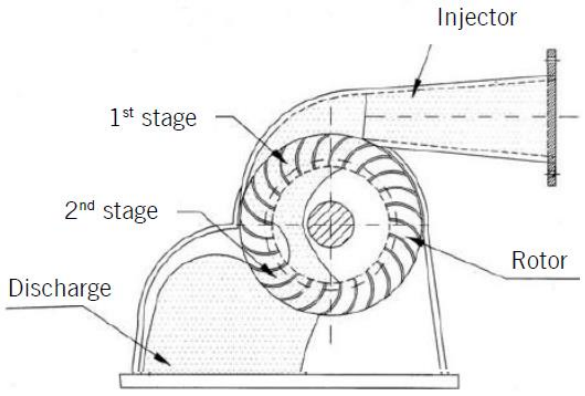

b) Cross Flow Turbine [77]

Figure 2.6: Water Turbines used in MHP systems in Nepal

The Thingan HES project utilizes a 20 kW Pelton turbine. The specification of the MHP plant [15] is presented in Table 2.3.

Table 2-3: Specification of Microhydro System at Thingan Village

Turbine Type	Pelton
Flow rate	27 liters/second
Gross head	135 m
Penstock diameter	150 mm
Pitch circle diameter	295 mm
Generator type	Synchronous
Generator capacity	50 kVA

B) Components of Microhydro System

An MHP plant utilizes various components in order to generate electric power. In general, various components of an MHP plant can be grouped into three: a) Civil, b) Mechanical, and c) Electrical components. Figure 2.7 of an MHP system is from a design manual [72]. Some of the components of the MHP system are:

a) Intake weir and Settling basin
b) Channel
c) Forebay tank
d) Penstock
e) Power House

These components are labeled in Figure 2.7. The intake weir diverts a portion of streamflow in the river along the channel for production of electricity. The forebay tank can hold some water and help maintain uniform flow in the penstock which carries water down to the turbine in the power-house that contains a generator and other balance of system components.

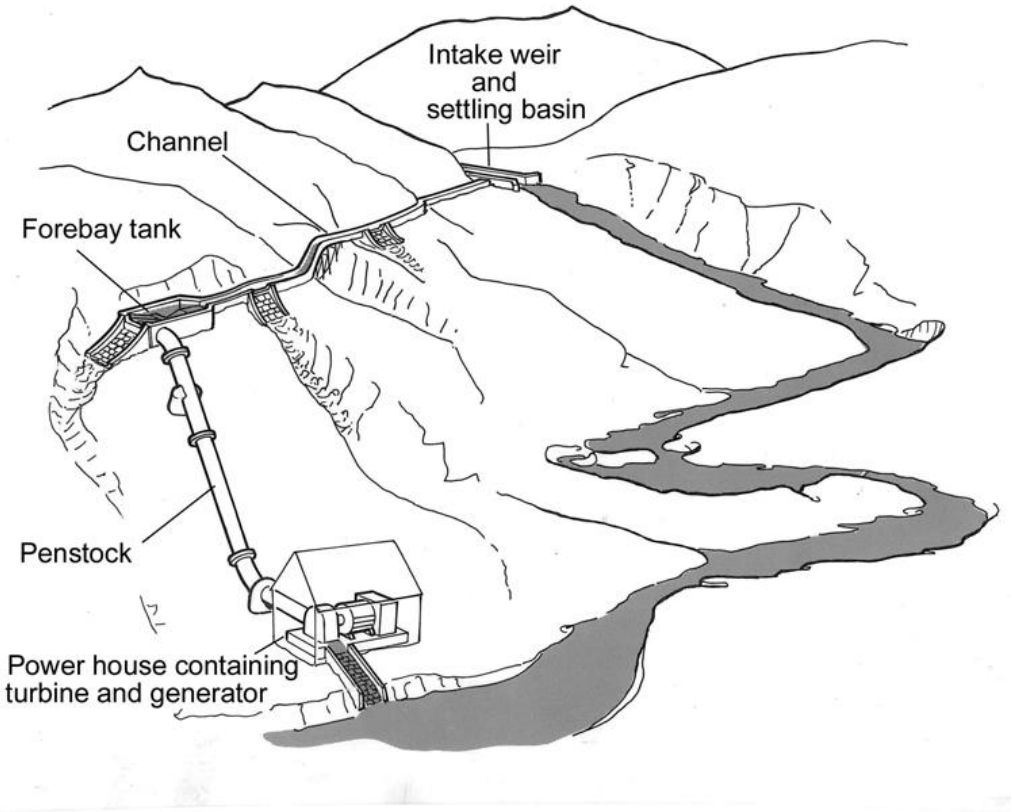

Figure 2.7: Layout of Microhydro System [72]

The water diverted at the Intake Weir goes back to the same river downstream after it passes through the turbine.

C) Basic Principle of Hydraulic Turbines

A hydraulic turbine converts the energy of the flowing water into mechanical energy. One dimensional steady flow energy equation for this energy transformation, with usual notation, is:

$$\dot{Q}_h - \dot{W} = \dot{m}[(h_2 - h_1) + \frac{1}{2}(c_2^2 - c_1^2) + g(z_2 - z_1). \qquad \text{Equation 2.6}$$

Here, we follow notation/symbol from a textbook [78]. In Equation 2.6 the 'c_i' stands for the velocity of water at section 'i'. This leads to the generic equation of power (P) = $\dot{W}$ = $\rho Q g h$; where h = $z_1 - z_2$, and $\dot{m} = \rho Q$. The enthalpy and velocity are the same at the entrance of the Forebay tank and the tailrace of the turbine, i.e $h_2 = h_1$ *and* $c_2 = c_1$.

Torque is equal to the rate of change of angular momentum. Following usual notation in Figure 2.8, the conservation of angular momentum leads to

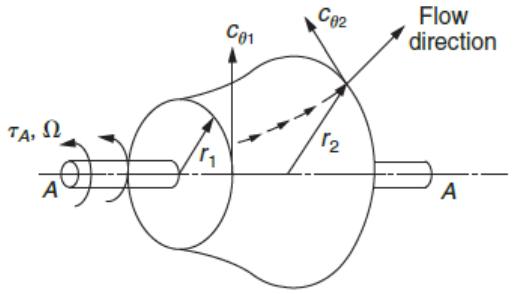

Figure 2.8: Torque and Flow for a Turbomachinery [78]

Torque = $\tau_A = \dot{m}(r_1 C_{\theta 1} - r_2 C_{\theta 2})$. The turbine blade speed (U) = r Ω.

Using symbols in Figure 2.8 the Euler Work Equation for a turbine:

$$W_t = \tau_A \Omega = \dot{m}(U_1 C_{\theta 1} - U_2 C_{\theta 2}). \qquad \text{Equation 2.7}$$

Equations 2.6 and 2.7 describe the power and the torque generated by a hydraulic turbine.

D) Efficiency of Turbine: Pelton and Cross-flow

The efficiency of a turbine can be calculated from work done by the turbine given by the Euler work equation, Equation 2.7, and energy available in the flowing water.

i. Pelton Turbine

Figure 2.9 presents a velocity diagram [78] as water passes through the bucket of a Pelton turbine. Here, U is the blade speed, c_1 is the speed of water coming out of the nozzle. Hence relative velocity w_1 at which water impinges on the bucket is $c_1 - U$. The water leaves the bucket at angle β_2 relative to the direction of the blade motion. Here, the friction factor k is defined in terms of relative velocities as $w_2 = k\, w_1$.

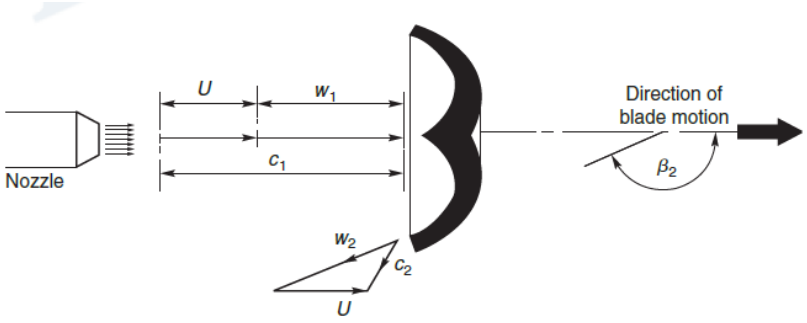

Figure 2.9: Flow geometry of a Pelton runner [78]

An expression of efficiency:

$$\text{An efficiency of Pelton Turbine Runner } \eta_R = \frac{\text{Work done}}{\text{Energy of water}}$$

$$\eta_R = 2\,U\,(c_1 - U)(1 - k\cos\beta_2)/c_1^2$$

$$= 2\,v\,(1 - v)(1 - k\,cos\beta_2).$$

Equation 2.8

Here $\nu = \frac{U}{c_1}$ is the blade speed to jet speed ratio.

The efficiency, as suggested by Equation 2.8, is mainly a function of the speed ratio (ν), friction factor (k), angle (β_2) made by deflected water with the direction of blade motion. For a detailed derivation, readers are referred to a textbook [78].

ii. Cross Flow Turbine

In a cross-flow turbine water passes across the turbine blades. A basic design consists a cylindrical runner with curved blades fixed on the outer rim. Water enters from the top, stage I in Figure 2.10, and flows through the blades twice as it passes across the runner. A cross-flow turbine is sometimes also called Bánki-Michell turbine, after those inventors who developed and patented the design as early as 1903.

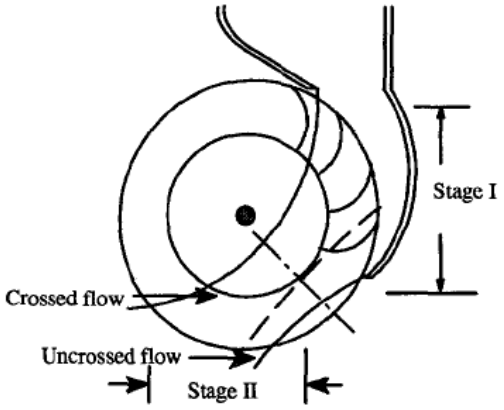

Figure 2.10: A Typical flow in a Cross-flow Turbine [79]

In Nepal, microhydro technology started getting into shape after Balaju Yantra Shala (BYS) was established in 1960 with assistance from Swiss Development Cooperation [80]. Design of cross-flow turbine started then with hand regulated design T1 for operation of agro-processing units. By now, the design has been through various iterations leading to design T16 which can generate electricity maximum at about 80% efficiency. One of the leading innovators of the Cross-flow Turbine technology, Ossberger Turbines [81], Inc. claims a peak cross-flow efficiency of 87%. Figures 2.11(a) and (b) present a picture of T12 and a cross-section of T16 by a Nepalese designer Krishna Bahadur Nakarmi. The BYS has been extremely helpful in adapting this technology to the capacity of local workshops in Nepal. Nowadays, most of the components of MHP can be produced locally.

Nepal Micro Hydropower Development Association (NMHDA) publishes various design tools for development of the microhydro sector. Cross-flow turbines are also popular in Africa. Nile Basin Capacity Building Network has produced a document on design and fabrication of cross-flow turbine [82].

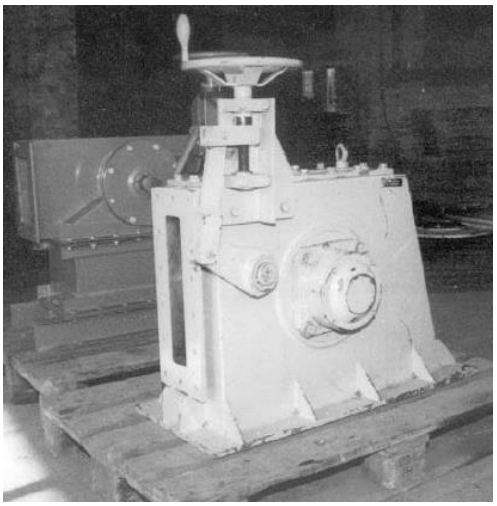

a) T12 Design BYS Nepal [2]

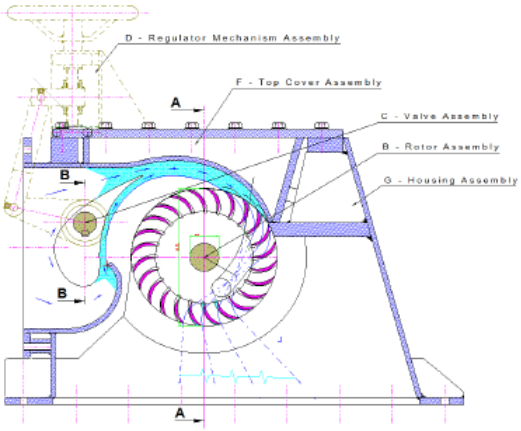

b) A cross-section of T16 Design [2]

Figure 2.11: Cross-flow turbine in Nepal

A detailed derivation of the efficiency of a cross-flow turbine may be found in [83]. Figure 2.12 shows a flow geometry of a cross-flow turbine [79]. The nozzle directs flow into the runner at an angle of attack α_1. As derived by one of its inventors Donat Bánki, the fundamental expression for maximum efficiency η_{max} of a cross-flow turbine is,

$$\eta_{max} = \cos^2\alpha_1.$$

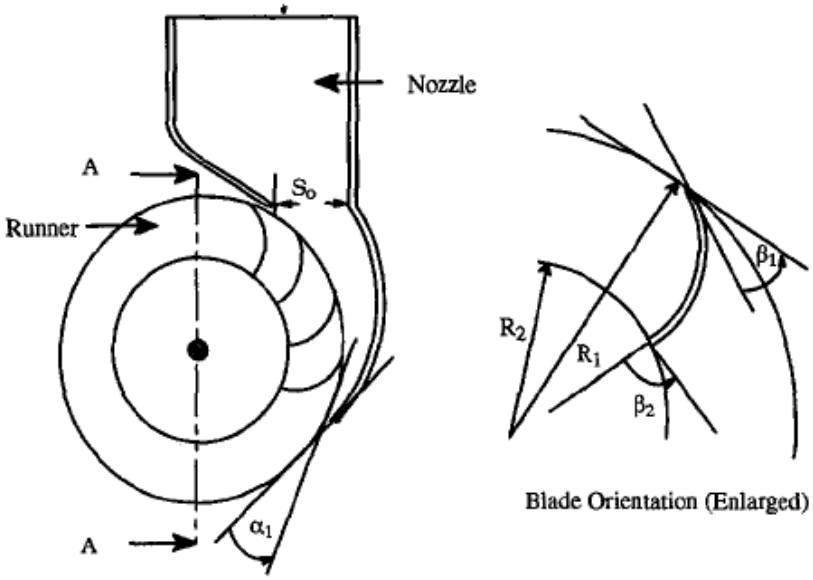

Figure 2.12: Flow geometry of a Cross-flow Turbine Runner

Desai [84] as a part of his PhD thesis at Clemson University, carried out a parametric study of the cross-flow turbine to identify optimal design parameters, and to quantify the effect of key parameters influencing the maximum efficiency. Saeed Rajab Yassen [85] utilizes a commercial CFD code (ANSYS CFX) to model internal flow through a cross-flow turbine. By analyzing the internal flow, his PhD thesis aims to optimize the performance of a selected turbine by establishing the optimal turbine's design parameters for a given site. Some scholars [86] in Pakistan have attempted to standardize the design of cross-flow turbine to the site conditions.

The cross-flow turbines work well in low/medium head and are easy to manufacture in a local workshop in developing countries like Nepal. Hence they are popular for rural electrification. As their designs are yet to be standardized, the performance of turbines used in MHP systems varies widely among the manufactures in Nepal. Figure 2.13 presents efficiency of some MHP utilizing cross-flow turbines in Nepal [5]. The rated capacities of these MHP systems range from 12 kW to 56 kW.

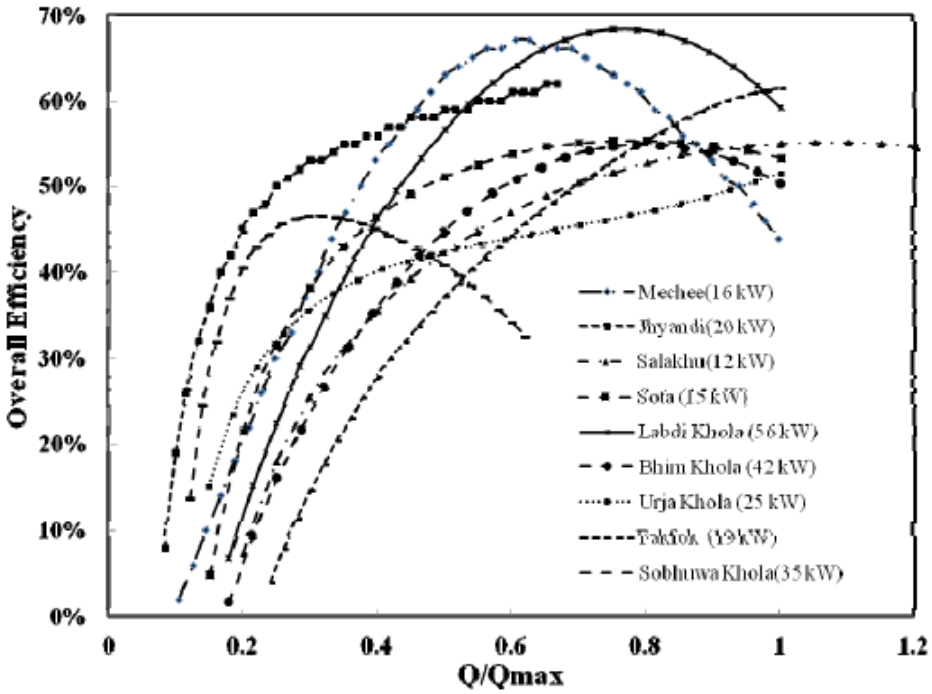

Figure 2.13: Cross Flow Turbine Efficiency of some MHP systems in Nepal [5]

The overall efficiency, based on these field observations, seems to vary widely across MHP sites and capacity range. These efficiency data, including the one in Figure 1.2 for Pelton turbines, suggest that the generic model of MHP with constant efficiency would not suffice to model a regulated water turbine we propose to study in this research. We would need a detailed model to capture this ground reality of MHP in the developing countries.

2.5.2 Solar PV System

A photovoltaic cell converts energy from the sun directly into electrical energy by a mechanism known as the photoelectric effect. A PV cell consists of semiconductor material blended with impurities such as phosphorus or boron with silicon to form n-type or p-type material. At the interface of the p-n junction, there exists an electric field. When photons from sunlight impinge on a very thin layer of N-type silicon, the free electrons ejected receive energy enough to flow in the external circuit resulting in an electric current. A number of such cells can be connected to generate a useful power enough to serve an electric load. To increase the output voltage, multiple panels are connected in series, while panels can be connected in parallel to increase the current (and power at a given voltage). A collection of such cells sealed in a laminate is known as a module, see Figure 2.14. A module is the building block of PV panel and array used in HES for rural electrification.

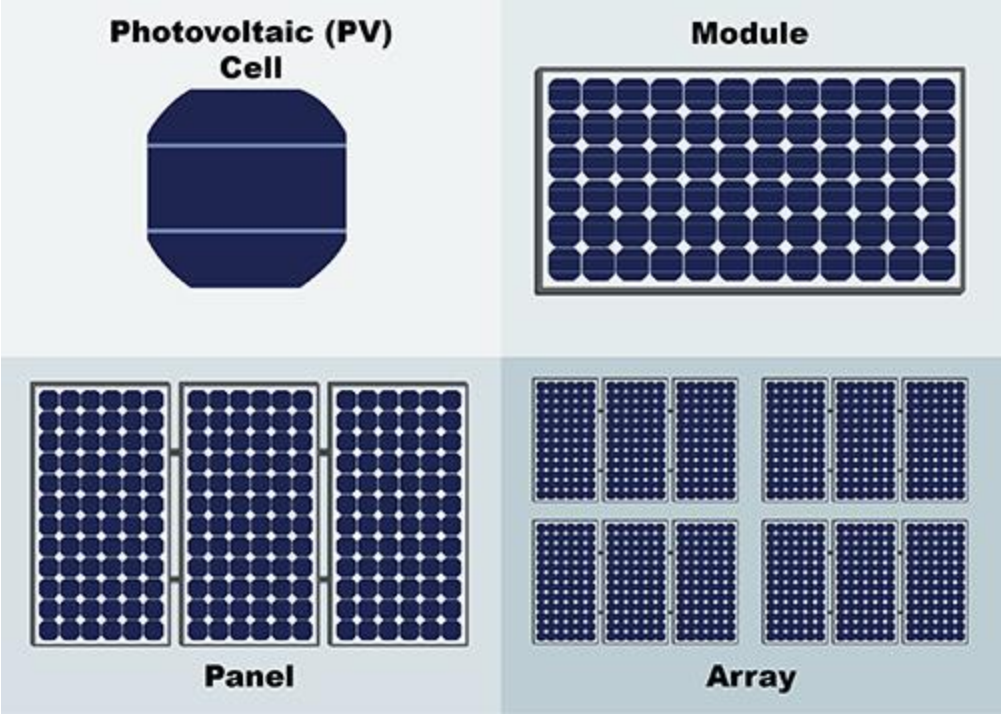

Figure 2.14: Solar PV cell, Module, Panel and Array [87]

There are various types of PV cells [88, 89]. The crystalline silicon (cSi) dominates the current market share. Thin-film solar cells are gaining popularity recently. The following photovoltaic materials can be deposited into the substrate to form thin-film solar cells:

a) Cadmium telluride (CdTe),
b) Copper indium gallium selenide(CiS),
c) Amorphous silicon (a-Si), and
d) Organic photovoltaic cells (OPC).

The Crystalline Silicon (cSi) is the basis of the mono- and polycrystalline silicon solar cells. Figure 2.15 presents the current and voltage relationship for a 120 W polycrystalline panel [90], at three level of irradiance 200 W/m^2, 800 W/m^2, and 1000 W/m^2.

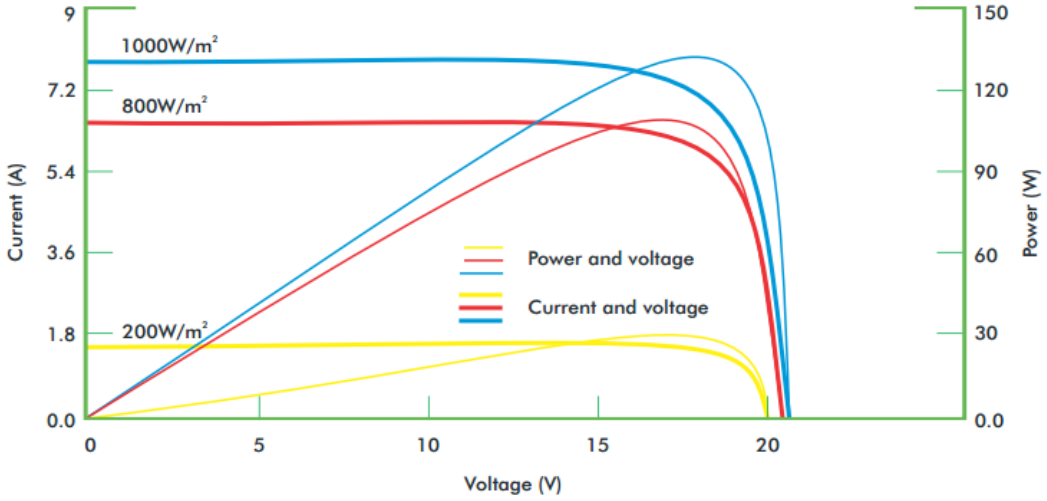

Figure 2.15: PV characteristics of a PV Module

PV panels are characterized by their current-voltage relations. The relationship may vary with solar radiation level and temperature of the cell. As portrayed in the secondary axis, the range of voltages over which a given panel performs effectively, say at maximum power, is relatively limited. A PV module specification includes short-circuit current (I_{SOC}) and open circuit voltage (V_{OC}) among other figures of merit.

The contemporary research on PV cell has a focus on enhancing the optical and electrical properties to enhance its efficiency [91]. In 1960's, Shockley has contributed to the thermodynamic limit on the efficiency of silicon-based solar cells under certain assumptions [92]. New cells are being developed to defeat some assumptions made for silicon-based solar cells about the thermodynamic limit. Such cells are sometimes referred to as the third-generation cells. The most studied third-generation cells are [93]: the Intermediate band solar cell, the multi-exciton generation solar cell, and the hot carrier solar cell.

RETScreen uses PV array model based on work by Evans [94]. The array is characterized by average efficiency which is a function of average module temperature Tc.

$$\eta_p = \eta_r \, (1 - \beta_p (T_c - T_r)) \qquad \text{Equation 2.9}$$

The T_c is a function of monthly clearness index and average monthly ambient temperature, given by Evan's formula:

$$T_c - T_a = (219 + 832\,\overline{K_t})\frac{NOCT-20}{800}. \qquad \text{Equation 2.10}$$

NOCT is the Nominal Operating Cell Temperature. The β_p in the Equation 2.10 is a coefficient that depends on the type of PV module considered.

Performance analysis of a PV array requires a model of the PV module that constitutes it. There are numerous models ranging from simple idealized model to a detailed complex model that aim to capture physical processes within a cell. A simpler model may approximate only the power output at a given radiation level whereas more detailed models also provide some methodology for calculation of current, voltage, and power at different operating conditions including ambient temperature.

In general, an analytical model of a PV cell incorporates some diode. The popular ones are the one-diode or the two-diode models with various logic in order to extract/estimate module parameters. There are models which use only one parameter to models that use five and more parameters. A review of methods to extract parameters from the manufacturers' data sheet or a set of measured I-V curves [95] can be found in review articles such as [96, 97].

A generic model of PV module is normally based on a one-diode equivalent circuit that describes the current and voltage (I-V) relationship. The cell temperature and ambient temperature affect this relationship. The temperature effects are described by equation consisting band-gap, a constant specific to the material of the cell, ambient temperature, and parameters that may influence heat transfer phenomenon. Some authors [98] have proposed two-diode equivalent circuit to predict the performance of PV array better at low irradiance level. There are many other models of PV module developed for a specific application. A 2009 report by Klise and Stein [31] have

documented PV Models developed and used by Sandia National Laboratories. This document contains more details than the one similar report [99] published earlier.

The original version of Hybrid2 contains a one-diode equivalent model for PV based on research carried at the University of Wisconsin [100]. We use the similar one-diode equivalent PV model but with new algorithms to estimate model parameters.

2.5.3 Small Windpower System

A windpower system converts energy in the wind into electrical energy. A horizontal axis wind turbine (HAWT) for rural electrification, Figure 2.16, is generally comprised of a rotor, a generator mounted on a frame on a top of a tower, a tail vane to guide rotor, and balance-of-system components. A large system may have active yaw system in place of the tail vane, and many other components. The rotor converts the kinetic energy of air into mechanical energy to drive the generator that produces electrical energy. The balance-of-system components help ensure the electricity so generated confirms to the local electric standards in terms of voltage and frequency.

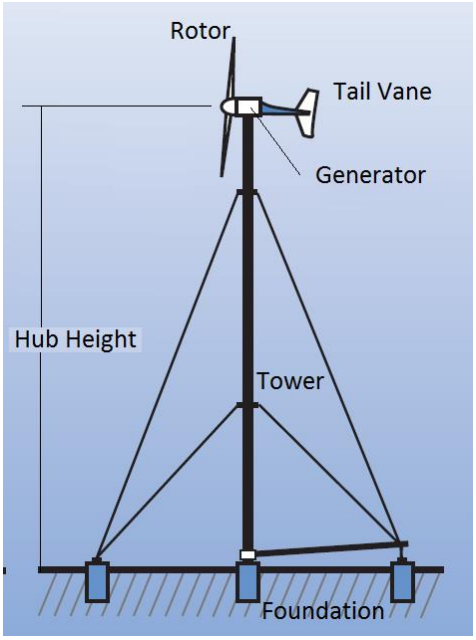

Figure 2.16: A HAWT with Tilt-up Tower, Adapted from [101]

There are various documents published in order to educate consumers interested in small windpower technologies. A Consumer's Guide [101] published by the US Department of Energy provides information about small wind electric system. It includes information for various phases of planning, installation, and maintenance of the system. The Canadian Wind Energy Association (CanWEA) has a guide for purchasing a small wind power system [102]. Likewise the case of hydropower, there is no consensus on the classification of wind turbine system. This report from CanWEA classifies wind turbine systems below 300 kW as a "small wind" category. A website [103] from the Danish Wind Industry Association provides a lucid explanation of wind energy system. Hugh Piggott maintains a website [104] that may help beginners design and manufacture small wind turbine for battery-charging applications.

Recently, Alternative Energy Promotion Center (AEPC) in Nepal is actively pursuing development of hybrid energy system for rural electrification. Figure 2.17 portrays a 5 kW wind turbine, a subsystem of HES the center has installed at Dhaubadi, Nawalparsi, Nepal with support from Asian Development Bank. The HES consists of two wind turbines, 5 kW each, and Solar PV, 2.16 kWp, and provide electricity to a rural community of 46 households.

Figure 2.17: A Hybrid Energy System for Rural Electrification in Nepal

For performance analysis, wind turbine subsystem at a site may be defined by the resource and specification of the wind turbine. The performance of wind turbine at various wind speeds is expressed in terms of a power curve. A power curve relates wind speed at the hub height to the power the wind subsystem will deliver, assuming certain standard atmospheric conditions. Figure 2.18 displays a power curve of a typical 10 kW wind turbine (Bergey EXCEL 10). This turbine starts generating power at a cut-in speed of about 3 m/s and reaches the rated power of 10 kW at about 11.5 m/s. For safety, the wind turbine will have to shut down above cut-out speed.

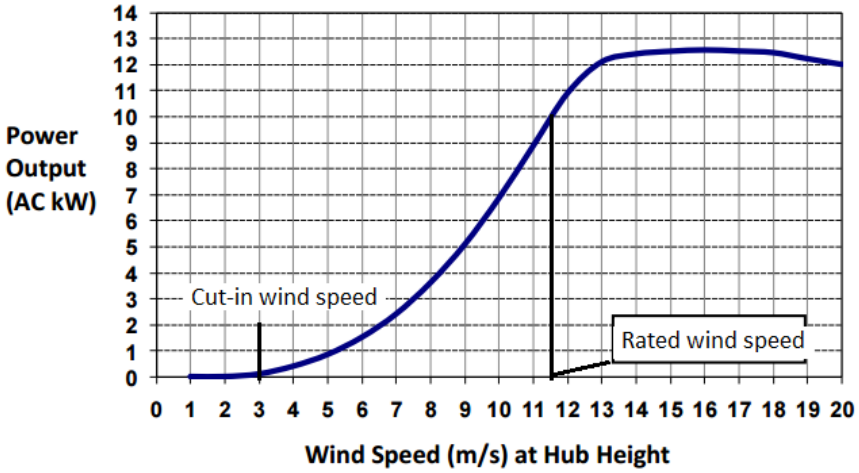

Figure 2.18: Power output curve Bergey EXCEL 10

The equation for power P of a wind power system at speed v between cut-in and cut-out speed will have a form:

$$P = \frac{1}{2}\,\eta\, C_p\, \rho\, A\, v^3. \qquad \text{Equation 2.11}$$

Here A is swept area of the rotor, η is the efficiency of the generator, and ρ is the density of air. The maximum value of power coefficient C_p derived based on the 1D momentum theory is 16/27, also known as the Betz Limit. Its derivation and various aspects of wind energy are explained in a textbook [23].

A representative time series of wind speed at the hub height, together with site-specific power curve (corrected for the density of air and other conditions) can describe the operation of the wind turbine system for a given climatological year. Estimating long-term wind speed based on data collected during resource assessment phase may involve a number of steps. It is often the case that the hub height of the wind turbine differs from height at which wind resource is measured using anemometers. Such is a case, we have to take into account variation in wind speed with height, also sometimes known as the wind profile. The common methods are the power law profile and logarithmic profile [23]. If resource measurement is carried out at a location different

than where the wind turbine will be sited, it may also require some sort of spatial modeling. For advance topic on resource assessment and power estimation of wind turbine systems readers are referred to standard texts [105, 23].

For the performance analysis of the wind turbine subsystems, we will use a power curve corrected for the site-specific conditions. The power curve method estimates the performance based on average value of wind speed at the hub-height for the time step of the simulation. The current trend for the time step of utility-scale wind turbine system simulation is 10 minutes or less. Ours is a different application. In this long-term performance analysis, we will use a time step of an hour.

2.5.4 Battery Model

Storage is an important component of HES that utilize variable renewable energy resources. A storage system enhances system reliability by managing deficit or excess power and helps ensure demand and supply of power at given point of time in sync with each other, where possible. HES for rural electrification in developing countries typically use lead-acid batteries for economic reasons, mainly due to lower upfront cost. There are various types of lead-acid batteries, such as Flooded, Sealed, VRLA (valve regulated), AGM (Absorbed Glass Matte), etc.

There are various types of models of the lead-acid battery for various applications. Some complex models are used in battery design and electrical engineering. Jongerden and Haverkort [106] have some suggestions on choosing a model for the battery. The authors suggest an analytical model for performance modeling and discuss two analytical models. The kinetic battery model (KiBaM) [107] is based on chemical kinetics, and the other one diffusion mechanism of the ions in the electrolyte [108]. This study will use the KiBaM which is elegant and extensively tested in-house. The KiBaM utilizes three capacity parameters to characterize a battery. These parameters are: Maximum Discharge Capacity (q_{max}), Capacity Ratio (c) and Rate Constant (k). Figure

2.19 illustrates the KiBaM model. The model views a battery as a two compartments syste; one contains available charge (q_1) and the other bound charge (q_2). The width of a compartment that contains available charge is 'c' and the combined volume is qmax. The two compartment has a fixed conductance k'.

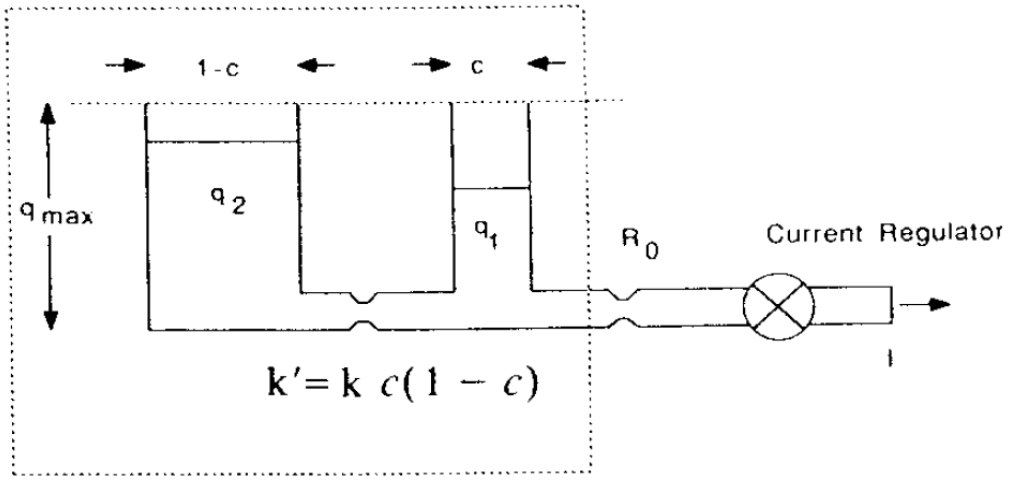

Figure 2.19: Kinetic Battery Model (KiBaM) [107]

A non-linear least square curve fitting using Marquardt technique, as described in [109] is used for estimating these parameters for the lead acid battery system used in this study. The curve-fitting in MATLAB utilizes the following equation from [107] to estimate those three parameters from the discharge data that can be obtained from the specification of the lead-acid battery.

$$I_{T=t} = \frac{q_{max}\, c\, k}{(1 - e^{-k\, t})(1 - c) \; + \; k\, c\, t}$$

Equation 2.12

The state of charge (SOC) is a parameter to keep track of energy available in the battery bank at a given time step. The system can only accept charge or discharge for a range [SOC(min), SOC(max)], as illustrated in Figure 2.20. We can limit the maximum energy transaction for a time step to a fraction of $\mathrm{E}_{\mathrm{rated}}$.

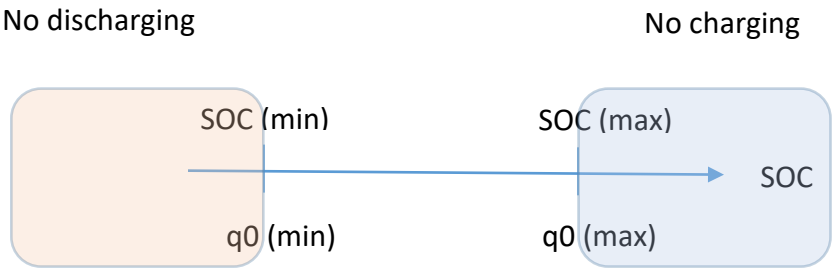

Figure 2.20: Range of SOC for the Battery Bank

The maximum discharging and charging current at a given time is a function of the current state of charges. Assuming nominal voltage, the following equations [107] are used to compute maximum currents as a function of the total charge q_0 and the available charge $q_{1,0}$ at the beginning of the time step.

$$I_{d,max} = \frac{k\, q_{1,0}\, e^{-kt} + q_0\, k\, c\, (1 - e^{-kt})}{1 - e^{-kt} + c(k\, t - 1 + e^{-kt})}.$$

Equation 2.13

$$I_{c,max} = \frac{-k\, c\, q_{max} + k\, q_{1,0}\, e^{-kt} + q_0\, k\, c\, (1 - e^{-kt})}{1 - e^{-kt} + c(k\, t - 1 + e^{-kt})}.$$

Equation 2.14

We use the KiBaM Model with a time step of an hour. For this time step, energy and power flow from the battery bank equal to each other in magnitude. The charging and discharging rates are assumed constant over a time step. A linear efficiency is assumed, which is a constant for a given transaction of energy (Eneed) irrespective of charging or discharging case. Following [110] efficiency of the battery bank is modeled using the following linear equation,

$$\eta(B) = b_1 - b_2 \frac{|E_{need}|}{E_{rated}};$$ Equation 2.15

where b_1 = 0.898, b_2 = 0.173, and $\mathrm{E_{rated}}$ is the rated energy capacity of the battery bank in kWh.

There are advanced models in order to model the variations in voltage and lifetime of lead-acid batteries [111]. We do not include voltage variations and the lifetime of the battery in this study.

2.6 Regulation of Hybrid Microhydro Systems

IEEE standard 1207-2011 [112] provides a guide for the application of turbine governing systems for hydroelectric generating units. A mismatch between generation and consumption may lead to a distorted alternating current in terms of frequency/harmonics. Such distorted electricity may not be used in all electrical appliances. A governing mechanism of a hydroelectric project aims to stabilize frequency at various load conditions.

The governor systems for a hydroelectric application may be classified into the following three categories: a) mechanical governors, b) mechanical–hydraulic governors, and c) electro-mechanical governors. Large-scale hydroelectric projects use mechanical-hydraulic governors. A version of electro-mechanical governors known as electric servomotor is sometimes used for simulation studies of microhydro plant. None of these governors has found a niche in microhydro applications. Microhydro uses a demand-side power management device known as electronic load controller (ELC). ELC is one of the most vulnerable components of the MHP systems [113].

In the section that follows, we will first review the history of governing mechanism of hydroelectric projects in general, and the latter section will focus on that of microhydro projects. In the last subsection, we present a review of some relevant previous studies.

2.6.1 Governing Mechanism: Hydroelectric Project

One of the foremost governors used in a hydroelectric project is called the flyball governor. As the speed of the water turbine goes above its limits, the fly-balls in Figure

2.21 (a) from [114] and b from [3], move outwards due to the centrifugal action and alter the position of the valve. This outward motion gradually reduces the flow through the turbine and help maintain the speed of the turbine. In summary, the governor serves mainly two purposes:

a) Maintain speed of the turbine; and
b) Conserve water.

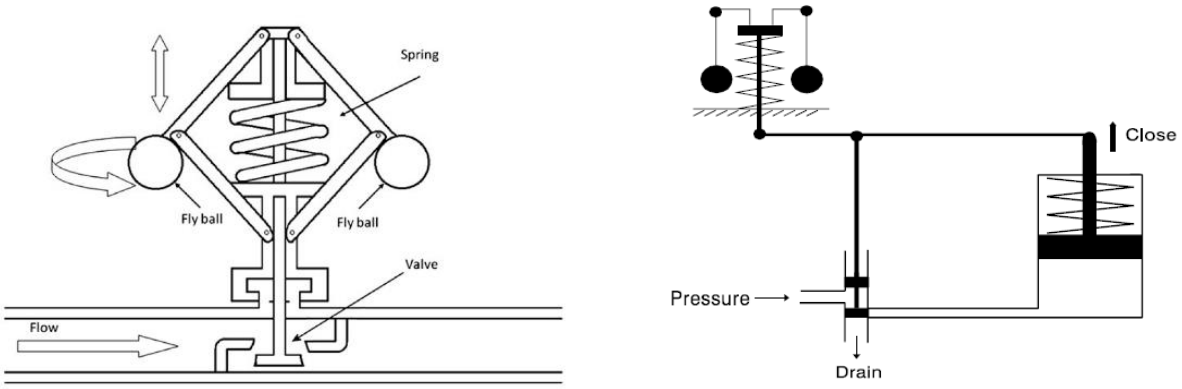

a) Flyball Governor – an illustration b) Speed droop governor

Figure 2.21: Flyball Governors

Karl Heinz Fasol [115] has documented a short history of the control mechanism for hydropower applications. Over last 100 years, the flyball was the only component to control the running speed of hydraulic turbines. Mead patented a flyball governor in 1787. The various iterations of the flyball governor were the mainstay of the control of hydroelectric turbine well into the twentieth century. This first generation of centrifugal governors has a large inertia and time constant. It takes them a long time to respond to a step load. They offer proportional control, and hence do not offer a solution to the steady state error at various turbine speeds.

Mechanical governors with actuators (pneumatic or electrical) help solve some of those steady state issues. These governors utilize a fixed control in the form of the PID control. The parameters of the PID control could be optimized for a given desired response specific to the site conditions. As a turbine has to operate intelligently across varying

conditions, even the PID control was not enough. This led to the next generation of governors known as Electronic Governors. Electronic governors utilize Programmable Logic Controllers (PLC). The computation power of PLC module provided better transient responses and offered a possibility of consolidating various advance controls to a single point/location. A detailed overview of the development of control system for hydropower applications is available in [114, 116].

2.6.2 Governing Mechanism: Microhydro Project

There are basically two methods of control for an MHP Plant. These methods may well be called: a) supply-side control, and b) demand-side control. For supply-side control, the power MHP generates can change in response to the load by adjusting the supply of water through the turbine by some governing mechanism [3]. Conversely, in the demand side control, power generation of the MHP remains constant normally at the nameplate capacity of the MHP. The excess power over the load is managed by utilizing an electronic load controller and a ballast/dump load, see Figure 2.22.

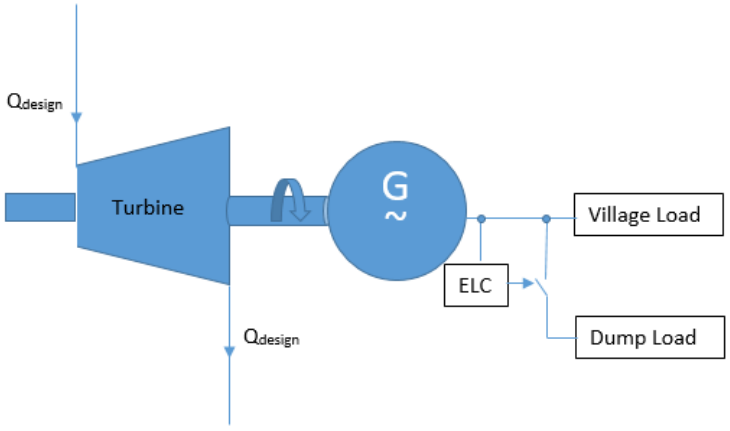

Figure 2.22: Electronic Load Controller [117]

MHP systems do not employ the supply-side controls for various reasons. They employ the demand-side controller shown in Figure 2.22. Henderson [117], as a part of his PhD thesis at The University of Edinburgh, has designed an electronic load governor for the MHP systems. There are various types of ELC [113, 118]. ELC is a standard component

of the demand side control of an MHP. This mode of control focuses only on the stability of the grid on the demand side but fall short of optimal resource utilization on the supply side.

Mathematically, the function of the ELC can be described by the following equation:

$$P(MHP) = P(ELC) + P(VLOAD), \qquad \text{Equation 2.16}$$

where,

P(MHP) = power generated by the microhydro plant, which is practically a constant ;

P(ELC) = Power the ELC diverts to the ballast/dump load; and

P(VLoad) = Power consumed by the village load.

A typical MHP system in Nepal utilizes an ELC in order to stabilize frequency to a nominal value (say 50 Hz). The ELC is a power management device that is connected to the output terminals of a generator. The generation and consumption of electricity may change with time for various reasons. This imbalance may lead to a net force which may accelerate or decelerate the system away from a specific RPM required by the synchronous generator. This deviation may result in a frequency different than the nominal value. The ELC routes generation excess of the demand to a dump load, making sure that power generated at any instant of time is approximately equal to village load plus load diverted to the dump load, and thus help maintain the frequency of the system to a nominal value.

As described above, ELC does help stabilize the frequency, but it does not alter the flow of water through the turbine. The turbine always runs at a set capacity, typically at the design capacity and utilizes design flow rate (Qdesign). To conserve water, we may want to introduce a flow control device that will receive feedback from the ELC and operate an actuator, linear or rotational, accordingly. We will not need a precise control of the supply of water through the turbine. The purpose here is to conserve water during dry

season utilizing a simple yet robust technology. A given amount of water will then be able to produce electricity for a longer duration with minimum dissipation in the ballast load.

2.6.3 Previous Studies: Flow Control and Energy Management

In the last section, we discussed two types of control strategies for the MHP systems. In this study, we are interested in the supply side control in order to conserve water as well as to minimize energy dissipation in the ballast.

For the supply side control, some authors use an electric servomotor. The servomotor consists of a motor coupled to a position sensor for feedback. It helps maintain precise control of the spear of the nozzle, Figure 1.3, in order to supply the required flow through the turbine. An IEEE working group on prime mover and energy supply has documented hydraulic turbine control model for system dynamic studies [119].

In a dynamic study of control for MHP systems, Hanmandlu and Goyal [120] have used a Type Zero servomechanism. A feedback mechanism of Type Zero is generally referred to as a regulator system. A regulator system maintains parameters such as torque of the turbine, or the frequency to a constant value even though the load may vary with time. Such mechanism may utilize terminal voltage or frequency of system excess of the base value (50 Hz or 60Hz) for the feedback. For various reasons, such servomotors have never been incorporated in the design of MHP in Nepal and elsewhere. An MHP will require a robust and cost-effective control. A purpose of the supply side control is to conserve water. It may not need the precise control an expensive servomotor can offer because this control has to work in conjunction with the ELC.

In another supply-side control study, Dolla and Bhatti [121] have proposed dividing the water flow through the penstock into a number of parallel pipes and utilizing motor operated valves to close or open the flow as demand may fluctuate. Figure 2.23

illustrates their concepts. By doing so, this study aims at reducing the size of the ballast/dump load, which otherwise need to be about the same size as the nameplate capacity of the MHP system.

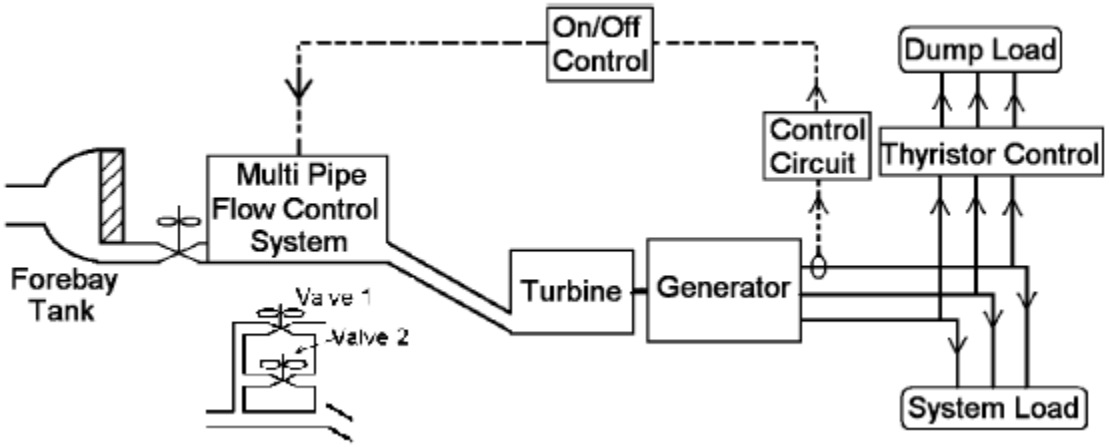

Figure 2.23: A model of Flow Control in a small Hydropower [121]

Scherer et al. [122] presents advances in the modeling and control of MHP systems with induction generators. This is one of the few papers which models MHP with flow regulation. In this paper, the authors describe the controllers for microhydro power stations for islanded operation based on a nonlinear model of the hydraulic turbine. It presents some new methods of control for speed, voltage, and frequency for an induction generator not yet common for MHP in Nepal. MHPs in Nepal mostly use synchronous generators and utilize the demand side control, the ELC.

Rajesh Saiju [123] analyzed a hybrid power system utilizing microhydro solar, wind and diesel generator. His research utilized MATLAB/Simulink model of subsystems to come up with an Energy Management Unit. This research simulates microhydro plant with a mechanical governor, similar to the small/large hydropower plant with a reservoir. For various technical and economic reasons, such governors have never made it to MHP. The water reservoir has been conceived as an energy storage unit. Many existing MHPs in Nepal can hold water enough for a few hours at design flow (Qdesign). It does not take into account nonlinear characteristics of the water turbine at partial load.

Ahmad Suliman [124] attempted to emulate dynamics of MHP and constructed a laboratory scale test system. A DC Motor is utilized to model a water turbine. In this study, the effect of regulating the turbine is modeled by controlling the DC input voltage through a delay loop to mimic time lag associated with the operation of the control valve. Raju Gupta [125] programmed a KV-300 PLC to demonstrate certain control functions applicable to small hydropower. Automatic unit starting sequence, emergency & fault shutdown, load control, speed control of turbine have been reported in the lab settings for an MHP of size less than 10 kW.

Binayak Bhandari [126] designed and evaluated the first tri-hybrid system in Nepal, as a part of his PhD work at the Seoul National University. The hybrid energy system [15] consisting of microhydro, solar PV, and wind turbine is installed at Thingan village of Makawanpur District in Nepal. His team has published a review paper [127] on mathematical modeling of a hybrid renewable energy system. In a separate paper, Bhandari et al. [128] present the optimization scheme used for the tri-hybrid system at the Thingan village.

Ajai Gupta [129] has modeled hybrid system consisting of both renewable source (hydro, biomass, biogas and solar PV) and conventional power (diesel) for provisions of electricity in remote rural villages in India. This research look at technical and economic sustainability aspect of the plan of the Government of India, to electrify remote rural villages utilizing renewable energy.

Energy management is an essential aspect of the HES that utilize variable renewable energy resources. The management strategies can affect the system design/sizing and operations as well. A review paper [130] summaries various energy management strategies utilized in the HES. Recently various dynamic programming techniques, such as Q-Learning [110] are being proposed for micro-management of storage systems. A

performance modeling technique can help find a macrolevel optimal energy management strategy for given site conditions.

Barley and Winn [131] compare nature of some of the dispatch strategies of a wind-diesel system with strategy having perfect knowledge of future load and wind conditions, idealized predictive dispatch. The load following strategy, in which the generator is regulated to follow the load excess of the wind turbine was found to be as cost-effective as the idealized predictive dispatch. Barley [132] has made an attempt to come up with a general dispatch strategy of the HES based on three non-dimensional parameters viz. wind-load ratio (WLR), diesel-load ratio (DLR) and fuel to battery cost ratio (FBCR). These non-dimensional parameters are defined as follows:

- WLR: Average wind power to the average load;
- DLR: Diesel rated power to the average village load; and
- FBCR: a dimensionless parameter in which the fuel cost, in conjunction with the genset fuel curve and the round-trip storage efficiency, is compared to the battery wear cost.

There have been consistent efforts to improve design and operation of HES utilizing various techniques such as performance modeling to the dynamic models utilizing artificial intelligence. However, the hybrid microhydro system is yet to incorporate a supply-side control to regulate flow through the turbine in response to the load variations. We will propose a simple but a robust flow control method that will work in conjunction with the electronic load controller (ELC) used in MHP system. The technical performance of hybrid microhydro system will be then estimated incorporating the flow control method.

2.7 Conclusions

A hybrid energy system (HES) for this study consists of hydroelectric (<100 kW), solar PV and wind turbine subsystems. We surveyed the underlying models of subsystems of the

leading software for the performance analysis of hybrid microhydro systems. The microhydro power (MHP) models are lacking details needed to reflect ground reality accurately. The MHP resource models are inadequate for supporting modeling effort at finer resolution; they also do not resonate/link well with the work of hydrologists who study water resource modeling. In addition to the electronic load controller (ELC) an MHP system uses to comply with the electricity standards, there is room to regulate MHP in order to prolong the supply of electricity during dry seasons by conserving water. Simple yet robust engineering and economical solution that addresses these issues may improve the HES design and add to the integration of renewable energy resources for rural electrification.

CHAPTER 3

DEMAND AND RESOURCE ASSESSMENT

3.1 Introduction

Demand and resource assessments are crucial steps for system sizing and performance evaluation of a rural electrification project. The electricity demand of a rural village may depend on the socio-economic condition of the village among various factors. Naturally, the demand may also grow over time.

Sometimes, a resource assessment campaign is too expensive for a rural electrification project, which usually is a non-bankable project. Hence, many such projects may not have data at a sufficient resolution (say hourly or sub-hourly scales). A typical rural electrification project in Nepal bases its design on statistics of renewable energy resource from various databases and some field verification and/or measurement. One database popular among system designers is the NASA Surface meteorology and Solar Energy Database. The database provides statistics mostly at monthly timescales.

System sizing and performance analysis of a hybrid system depend on accessibility and accuracy of demand and resource data. The finer the resolution of the dataset the more accurate may be the design of the hybrid energy system. A general design may be based on the monthly or daily energy balance. Some industry standard software tries to emulate energy balance at hourly or sub-hourly scales. Available dataset does not always support such effort, and hence we need to make some assumptions and synthesize the data for finer timescales.

In this study, we will use secondary data published elsewhere. The data are mostly on monthly timescales, except for a few days of wind and solar resource measurement carried out at one minute and five-minute intervals respectively. We will synthesize data

at an hourly time scale and carry out performance analysis of the existing hybrid microhydro system, and alternative system designs we may propose for the site.

In the following section, we discuss in detail about data utilized for this study and underlying assumptions regarding the data synthesis. The demand data are taken from a rural village powered by a microhydro power plant. This dataset was obtained from Nepal Electricity Authority in 2010. The solar resource data come from a nearby site measured a few years back. The wind data are synthesized following the method used in HOMER. The hydro resource data are synthesized taking into account regional hydrology and daily rainfall statistics.

3.2 Demand Assessment

The demand assessment of a remote rural village involves data collection and analysis from all stakeholders of the rural electrification project. Details of how to assess the consumer load demand for a decentralized wind-diesel system is described in [133]. The D-Lab's at MIT has developed an Energy Assessment Toolkit [134] to facilitate a part of the process. It involves interviews with key informants such as a) household, b) business, c) supply chain, d) community institutions, e) community leaders, etc. The Toolkit aspires to capture details about the level of current energy access and expenditure, and aspirational energy, etc. for a market-based initiative.

Some institutions conduct a baseline survey of various assets to facilitate the demand assessment and project design. Such a survey tries to capture individual, social and natural assets in the purview of the rural community. Sometimes, a survey may unveil latent information which may not come out in the conventional demand assessment approach. An essence of the survey is to evaluate the need and affordability of the rural community in the question. A baseline survey may provide a datum against which a

rural electrification project can be appraised and evaluated in future for changes it may bring into the rural community.

We may find templates for load/demand assessment of rural electrification projects that various organizations use. These templates try to capture best the load as a function of time of the day and day of the year. The Hybrid2 software package developed at UMass comes with an MS Excel Template for 'REMOTE COMMUNITY LOAD CALCULATION.'

Based on a pilot study conducted for six households in Thingan, Bhandari et al. [15] have estimated a peak load of about 40 kW at 6:00 and 19:00 hours. Instead, for this study, we use the consumption data obtained from the Nepal Electrical Authority (NEA) in a rural village elsewhere. This data set was measured back in 2010 and spans about 3.5 months. We normalized the consumption data by the peak load to estimate the diurnal profile of the electric demand of the Thingan Village. Figure 3.1 presents the base load, morning and evening peaks. We calculate the total load by multiplying the normalized load profile by the total 187 households in the village and the specific allocation. The Alternative Energy Promotion Center (AEPC) in Nepal recommends specific allocation of 125 Watt per household, excluding community and commercial use.

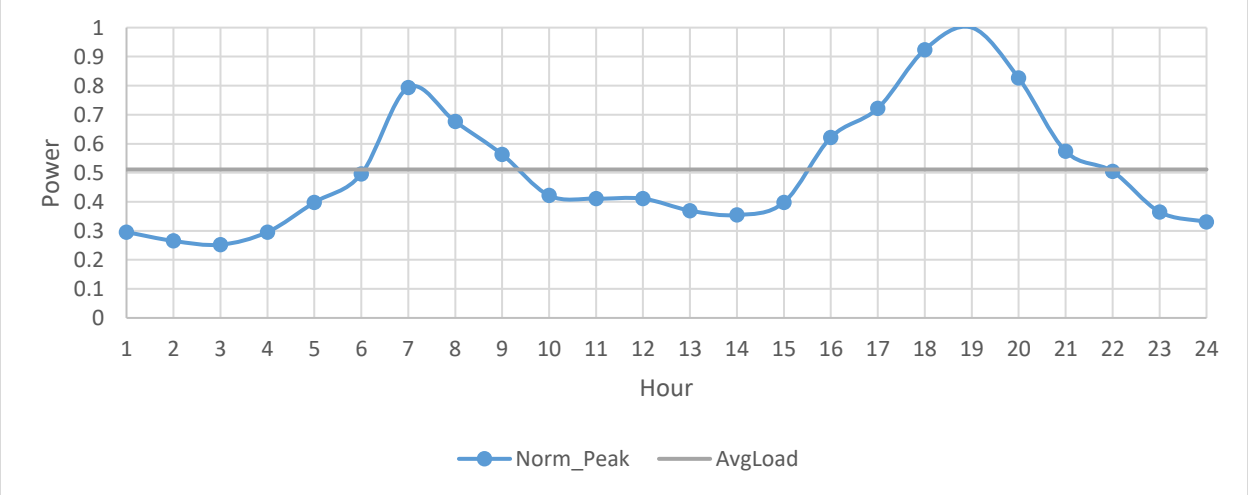

Figure 3.1: Diurnal Load Profile

3.2.1 Load Model

A purpose of a load model is to estimate the load (kW) at each of the 8760 hours in a year. Hybrid2 uses monthly measures of central tendency (average, minimum, maximum) along with autocorrelation factor and diurnal scaling parameters in order to synthesize the time series of hourly load data. As we do not have monthly statistics, we model hourly load at Thingan following the method used in HOMER. This method does not take into account load variations within weeks and seasons.

The load at Thingan is simulated using the following equations:

$$\text{Load}(t) = \text{Nominal Load } L(t) \times \text{alpha}, \qquad \text{Equation 3.1}$$

$$\text{where, alpha} = 1 + \delta(\text{daily}) + \delta(\text{hourly}).$$

The Nominal Load is based on the diurnal load profile in Figure 3.1. There are two factors this model uses – the daily and hourly perturbation (δ) factors. These factors are assumed normally distributed with mean zero and standard deviation equal to σ(daily) = 15%, and σ(hourly) = 5%. In short, $\delta \sim N(0, \sigma)$. Table 3-1 summarizes the basic statistics of the load. The standard deviation for a given hour is assumed constant throughout a year.

Table 3-1: Basic statistics of load profile in kW

Central Tendency	
Mean (μ)	11.86
Median	10.31
Minimum	3.54
Maximum	35.83

Dispersion	
Standard Deviation (σ)	5.26
First Quartile (Q1)	7.85
Third Quartile (Q3)	14.92
Inter Quartile Range (Q3-Q1)	7.07

A MATLAB code to generate the load is documented in Appendix A.2.1.

3.3 Resource Assessment

The monthly resource data estimate at the Thingan Project is taken from the various sources including the NASA Surface meteorology and Solar Energy database. The streamflow is estimated using the MIP method recommended for a detailed feasibility study of microhydro projects in Nepal. The MIP method help estimate the monthly average of the streamflow based on the size of catchment and a spot measurement during the dry season.

To carry out performance analysis in the framework of Hybrid2 we will need resource and load data at a sufficient resolution (say hourly or sub-hourly scales). We approached one of the authors of the paper in which data were published to see if they can share data at a finer resolution for academic use. Following his suggestion, we are using some data from their published papers. Some of these data including the 1-minute wind speed for couple days in September are documented in [15]. Table 3-2 presents monthly resource data Bhandari et al. used for the optimization of hybrid renewable energy power system at Thingan [128]. Even though the speed-up factor of wind speed over the hill [135] is not well accounted for in the paper, we use the same dataset for performance analysis of the tri-hybrid system to facilitate cross-comparison where applicable.

Table 3-2: Monthly statistics of Renewable Energy Resource at Thingan

Month	**Wind Speed**	**Solar Insolation**	**Flow**
	m/s	kWh/m2/day	Liter/sec
Jan	5.25	4.26	35
Feb	5.70	5.15	32
Mar	6.00	6.18	31
Apr	6.00	6.76	28
May	5.40	6.68	26
Jun	4.50	5.75	28
Jul	3.60	4.79	33
Aug	3.60	4.80	35
Sep	3.60	4.56	32

Oct	4.50	5.13	35
Nov	3.20	4.72	35
Dec	5.10	4.15	35

Feasibility study of hybrid microhydro projects in Nepal are based mainly on monthly statistics of renewable resources. It is often the case information is cross verified through site verification and spot validation of resources attested by local stakeholders. The Thingan project is just another example not an exception.

In the following subsections, we present some measured meteorological data in the neighborhood of the project site, and an hourly time series synthesis based on monthly statistics where applicable. Each subsection elaborate typical data measurement of the each of the three resources we use, and methodology for data synthesis or downscaling.

3.3.1 Hydro Resource

A) Hydro Resource Measurement

The guidelines for feasibility study recommend various methods to estimate the flow of a river/rivulet for MHP application. Alternative Energy Promotion Centre (AEPC) has prepared a guideline [13] to provide a basis for consultants to undertake detailed feasibility studies including technical design for micro-hydropower projects in Nepal.

There have been various studies for the regionalization of the hydrologic behavior of rivers in Nepal. For a not-gauged river, which is generally a case with a microhydro plant, the following are the two methods used for estimating the monthly streamflow:

a) Medium irrigation project (MIP) Method , and

b) WECS/DHM Method.

The medium irrigation project (MIP) method divides Nepal into seven hydrological regions. It supplies monthly means of specific run-off of a river per unit catchment area, e.g. in Liter/second/ km^2. The average monthly flow rates can be estimated based on

flow measurements during lean seasons, November to April as recommended by the guidelines [13] and the size of the catchment area applicable to the intake from a topographic map.

The second method is named after Water and Energy Commission Secretariat (WECS) / Department of Hydrology and Metrology (DHM), the agency which helped develop the method back in 1982. The WECS/DHM considers entire country as one hydrological regime. However, it does divide the country into regions for low flows, long-term flows and flood flows [71]. It is the former method, the Medium Irrigation Project (MIP) method, which the AEPC recommends for the flow measurement and verification.

Table 3-3 lists the equipment for streamflow measurement based on the range of flow and uncertainty. Three sets of consistent measurement (within 10%) are required for discharge measurement.

Table 3-3: Flow Measurement Equipment

Equipment	Preferable limits (lps)	Acceptable limit (lps)
Bucket	Up to 10	Up to 30
Conductivity meter	Up to 500	Up to 1500
Current meter	Above 200	As per equipment specification

There is a web-based GIS tool [136] to identify off-grid MHP sites in Nepal based on remote sensing data. This academic tool is at an early stage of development. Nonetheless, it can be helpful during the prefeasibility study of some hybrid MHP sites.

For this study, we use hydrological-meteorological data in the region with the daily acquisition, and the monthly streamflow at the site.

B) Streamflow Data Synthesis

The monthly statistics of streamflow need to be converted to data at a resolution at which the performance analysis is carried out. This analysis is usually carried out at a time step of an hour or less. Hence, the data synthesis algorithm is required to convert the monthly statistics to the daily and hourly flow rates. The algorithm can harness regional characteristics of the hydrology cycle and daily precipitation data, where available.

The Thingan Hybrid Energy System Project site is located in Ghalegau, Thingan -3 of the Makawanpur district (Latitude: 27°26'35.60"N; Longitude: 85°14'42.20"E, WGS84, 1354 m ASL). There are a few meteorological and hydrological stations in that region. Figure 3.2 presents those stations. The Rajaiya hydrological station (# 0460) in the Rapti River is at about 24 km west of the project site. This station has a historical record of daily streamflow since 1963. The three meteorological stations also have a provision for daily acquisition of data. The nearest meteorological station is Makwanpur Gandhi (# 0919). This station is at about 6.25 km 40 degree west of the south from the project site.

Figure 3.2: Hydrological and Meteorological Stations in the vicinity of the Project site

For a feasibility study of MHP project in Nepal, we may have monthly means of streamflow for the climatological year and AFDC or probability density function (PDF) derived from the AFDC. The monthly means as well as the AFDC are estimated using the Medium Hydropower Study Project (MHSP) method. There are various models of AFDC, including the multivariate regression based model the software package HydraA-Nepal [8] offers. One of our objectives here is to estimate hourly time series of streamflow for the climatological year for performance analysis within the framework of Hybrid2.

We propose two stochastic methods to estimate the time series. The first method utilizes the local hydrological data, while the second method makes use of both hydrological and meteorological data available in the region. These methods are documented in Chapter 4.

3.3.2 Solar Resource

A) Solar Resource Measurement:

The Solar Constant is the power received from the sun by a unit area perpendicular to the radiation at a mean earth-sun distance outside of the earth atmosphere. Its value is about 1353 W/m^2. The earth atmosphere scatters incoming radiation from the sun. Hence a surface of the earth may receive both scattered and undisturbed components of the solar radiation. The radiation, thus technically, can be composed of two components: direct and diffuse. The direct component is the undisturbed component of radiation from the sun reaching the surface. The diffuse component adds to the surface as a result of scattering of light by the atmosphere and some other processes. Hence, we may write: Total radiation = Direct + Diffuse radiation. The direct radiation is also known as beam radiation.

A pyranometer (such as LI-COR LI-200R by NRGSystems [137]) measure a combination of direct normal irradiance and diffuse horizontal irradiance in Watt/m^2. The CMP6 (by

Kipp & Zonen [138]) is another common pyranometer used for global solar radiation measurement research on a plane/level surface [139]. A calibrated PV may also be used for the solar resource measurement purpose – a use of a reverse engineering method. To measure beam radiation, we will need a pyrheliometer that always points toward the sun by some tracking mechanism. Besides these devices, sunshine recorder and cloud-cover recorder are also utilized to enhance solar radiation measurement process.

One can integrate the irradiance (W/m^2) on a surface over a time to get net irradiation (J/m^2) on the surface. The typical time spans are monthly, daily and hourly scale. Solar energy irradiation is referred to as insolation. In standard notation, H is the insolation for a day and I is the same for an hour. The integration may have to carry out in the solar time taking the rotation of earth into account.

Measured hourly solar radiation data is not readily available for many areas of Nepal. The solar resource data was measured at the Thingan project site for a few days at five-minute intervals [15]. The data are not available throughout the year, or at the least not accessible to us. However, a site nearby Thingan, Sundarighat has measured hourly solar data for more than a year. The Kathmandu Upatyaka Khanepani Limited (KUKL) Sundarighat is a site where one of the first grid-connected solar power plants in Nepal was built around February 2012. The 680 kWp system supplies electricity to the water treatment plant which supplies drinking water to the Kathmandu Valley.

We will use the measured data at Sundarighat, which is at about 26 km at a bearing of 10.52 degrees from the project site. The Sundarighat site that belongs to the Kathmandu Upatyaka Khanepani Limited (KUKL) has measured solar radiation data at a horizontal surface, and a surface inclined 30° with horizontal. The hourly data measured on the horizontal surface from April 1994 through March 1995 is used for this study. Figure 3.3 presents monthly statistics of daily radiation and clearness index.

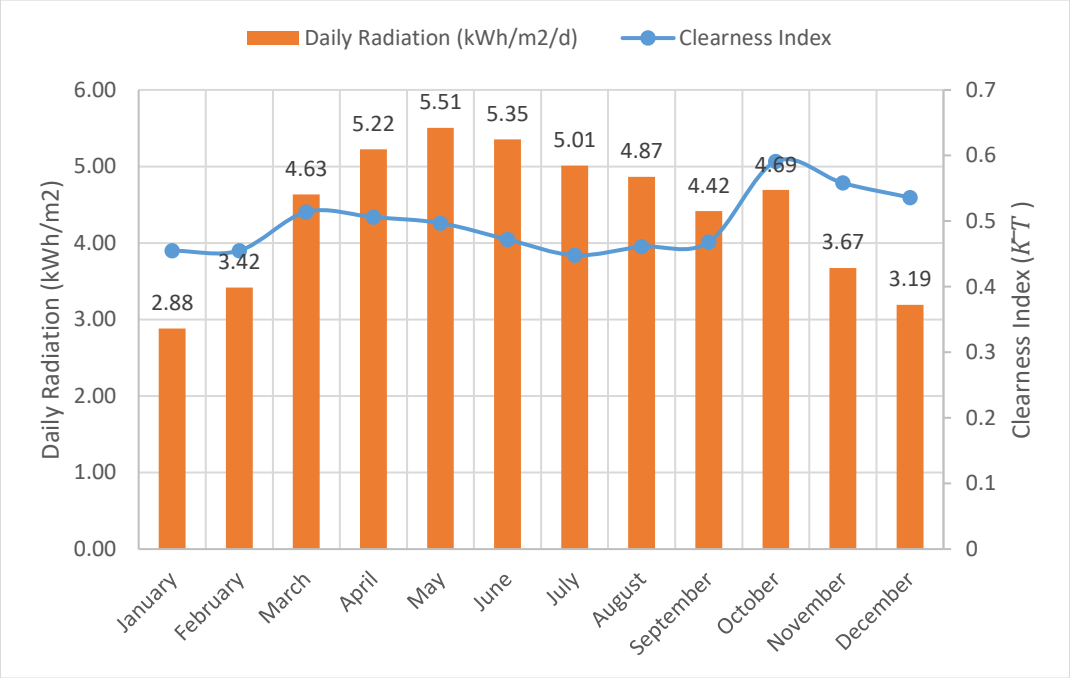

Figure 3.3: Horizontal Radiation at Sundarighat

B) Solar Data Synthesis

Graham and Hollands [140] have described a stochastic procedure to generate synthetic hourly solar radiation. Their algorithm generates the hourly data from monthly means $\bar{K}_T$ of the daily radiation and latitude of the place. HOMER uses this algorithm to synthesize the hourly data required for the simulation. Hybrid2 utilizes a pdf of the clearness index and calculated extraterrestrial radiation to synthesize the solar data.

As we have measured data for the entire year in the region, we will refrain from synthesizing the data for solar energy resource. This study uses the measured data at Sundarighat on a horizontal surface.

3.3.3 Wind Resource

A) Wind Resource Measurement

A typical wind resource assessment campaign may consist of the installation of a meteorological tower with various sensors in order to measure wind speed and direction, and how these quantities may vary with height above the ground level. An anemometer measures the horizontal wind speed, and wind vane measures the direction the wind blowing from. To estimate the density of the flowing air more accurately, we can add the temperature and pressure sensors on the list of sensors.

These sensors record data at some sampling rate, say of about ½ Hz, and compute basic statics (such as average, standard deviation, minimum, and maximum) for an interval. A typical interval used in wind resource assessment ranges from 10 mins to an hour. A detailed guide for wind resource assessment can be found in a handbook such as the one published by AWS Truewind [141].

Most of the rural electrification projects cannot afford meteorological tower of their own but rely on wind maps or secondary data based on some mesoscale models. For the Thingan project, the wind resource was measured utilizing The RainWise® WindLog at height 3.5 meters above the ground. Some data collected at 1-minute interval are published in [15]. Wind resource data at the site are not available for the whole year. We synthesize hourly time series of wind resource based on the published data and a resource assessment carried out at the nearest location, within the same climatological regime.

B) Wind Data Synthesis:

Synthesizing hourly wind data based on the monthly means is a daunting task. Data synthesis algorithms often use statistical characteristics of the wind speed data to calibrate a stochastic model and then generate a simulated wind speed time series [142]. These algorithms strive for retaining the sequential and distribution properties of the underlying data set. Hybrid2 and HOMER both provide ways to synthesize the data based on various inputs.

The current version of Hybrid2 software comes along with a "Data Synthesizer Beta". The synthesizer has a provision for synthesizing time series of wind, solar and load data. The wind data synthesizer can synthesize data based on two common distributions popular in wind resource assessment: Rayleigh and Weibull. The essential input parameters of wind data synthesizer are:

a) Average wind speed and standard deviation,

b) Autocorrelation coefficient for a given lag, and

c) Diurnal and/or long-term scaling parameters.

The scaling parameters include hour/day of the maximum value and a ratio of maximum to the average for the wind resource. These input parameters may be estimated for a site in question based on the wind data collected in the same climatological region.

HOMER synthesize hourly time series of wind speed from monthly means based on four parameters about the site in question. These parameters are:

a) Weibull shape factor (k)

b) Autocorrelation factor (R)

c) Diurnal pattern strength (δ)

d) Hour of peak wind speed (ϕ)

According to the HOMER help file [143], Weibull shape factor (k) is a measure of the long-term distribution of wind speeds. The Autocorrelation factor (A) is a measure of the hour-to-hour randomness of the wind speed. Diurnal pattern strength (δ) is an indicator of how strongly the wind speed depends on the time of day. Hour of peak wind speed (ϕ) is the time of day that tends to be windiest on average. HOMER has documented values of these parameters for TMY Typical Meteorological Year (TMY)) wind data for each of the 239 stations in the US National Solar Radiation Data Base.

HOMER uses the following equation to find out the best fit parameter based on the time series of wind resource data.

$$U_i = \overline{U}\left\{1 + \delta \cos\left[\left(\frac{2\pi}{24}\right)(i - \phi)\right]\right\} \text{ for I = 1, 2, ...24.} \qquad \text{Equation 3.2}$$

The Weibull parameters, the shape factor (k) and scale factor (c) are computed fitting the given dataset to the Weibull distribution:

$$p(U) = \left(\frac{k}{c}\right)\left(\frac{U}{c}\right)^k exp\left[-\left(\frac{U}{c}\right)^k\right] \qquad \text{Equation 3.3}$$

Both these factors are a function of average wind speed $\overline{U}$ and standard deviation σ_U . Some essential analytical and empirical equations to compute these factors are provided in [23].

Based on wind resource measured at a nearby site within the same district, we use the following values of the parameters for the wind data synthesis.

Shape Factor (k)	1.62
scale Factor (c)	5.25 m/s
Autocorrelation factor (R)	0.813
Diurnal pattern strength (δ)	0.211
Hour of peak wind speed (ϕ)	17

The hour of peak wind speed (ϕ) taken as 17 based on the 1-min wind resource data measured at the site [15]. HOMER Legacy (v2.68 beta, February 8, 2012) is utilized in order to synthesize hourly time series of the wind resource data based on the monthly statistics and parameters above.

The standard deviation of horizontal wind speed is estimated using the Normal Turbulence Model [144] described in IEC 61400-1 for wind turbine class IIIC. This turbulence model is based on the Mann and Kaimal Model. We choose to use the

following equation in order to calculate the standard deviation at the hub height speed (V_{hub}):

$$\sigma = I_{ref}\,(0.75\,V_{hub} + b);\quad b = 5.6\ m/s \qquad \text{Equation 3.4}$$

Here, I_{ref} is the expected value of turbulence intensity at 15 m/s, which is equal to 0.12 for the class IIIC, see Table 3-4. The variation of the turbulence intensity represented by the Equation 3.4 is plotted in Figure 3.4.

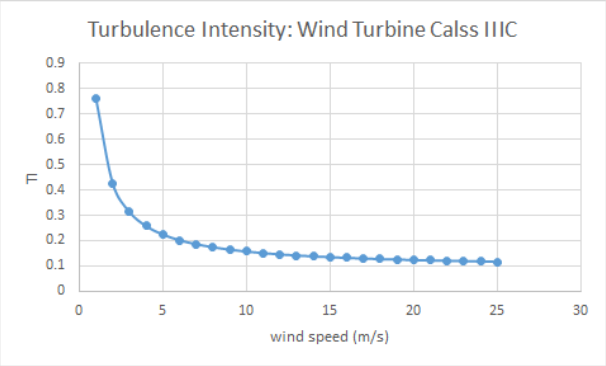

Figure 3.4: Turbulence Intensity for Wind Turbine Class IIIC

Table 3-4: Wind turbine class, IEC 61400-1

Wind Turbine Class		I	II	III	S
Vref	(m/s)	50	42.5	37.5	values specified by the designer
A	Iref(-)	0.16			
B	Iref(-)	0.14			
C	Iref(-)	0.12			

The standard deviations of wind speed and load are required in order to compute the net load variability which in turn is used estimate the range of loads to be anticipated within the time step of the modeling. The maximum value of the load determines the control strategy of dispatchable generators such as the regulated MHP and the battery system.

CHAPTER 4

HYDRO RESOURCE DATA SYNTHESIS: DOWNSCALING

4.1 Introduction

The hydrological cycle is a result of mainly two driving forces of nature, namely, the force of gravity and the energy from the Sun. Hydropower resource at a point on the surface of the earth is a result of the hydrological cycle. Hydrologists study about measurement and estimation of hydropower resources, among others. A study of water resource is carried out in terms of some measurable properties of local geography and climate. A steady-state water balance equation for a given basin/catchment area can be written in terms of the drainage (B) and the surface runoff (R). The runoff depends on precipitation (P), Infiltration (I), evapotranspiration (E). Following [47], we may write:

$$\text{Streamflow, } Q = B + R = B + P - E - I. \qquad \text{Equation 4.1}$$

In Equation 4.1 above, we have parameters of the geography and the local climate. For practical purpose, the hydrological resource can thus be studied based on some model of geography and the rainfall. A model of geography is beyond the scope of this research. Hence, we study water resource, a time series of streamflow to be more specific, as a function of rainfall and other dynamical properties of catchment such as auto-regression and correlation, etc. Another motivation for this is that metrological stations that measure the rainfall are more readily available in the developing world than the hydrological stations which measure streamflow generally at daily timescales.

For performance analysis in the framework of Hybrid2, we will require a time series of streamflow at a resolution of hourly time scales or better. Many microhydro sites in the developing world reside in a basin that is not yet gauged. However, we may have a record of meteorological data. Reporting the statistics of the daily temperature, and aggregate rainfall has been a norm of the weather news even in the developing

countries. The meteorological and hydrological stations in the neighborhood of the Thingan Project are indicated in Figure 3.2. At best, hydro resource data available for such MHP sites could be:

a) monthly means of streamflow,
b) Annual flow duration curve,
c) Daily rainfall.

We will need to synthesize an hourly time series {q(t)} of streamflow. Synthesizing such a dataset, given only the hydro resource data mentioned above, is a statistically indeterminate problem. That is, there are not enough equations to determine a unique solution pertaining to the time series. In other words, this downscaling problem is not well-posed. Accordingly, the {q(t)} may not be unique. In the following sections, we present some methods in order to synthesize an hourly time series of streamflow. The output of the methods is compared with the measured data at a hydrological station (USGS site # 07332500) in the Blue River, Oklahoma.

4.2 Theory: Downscaling of MHP resource

A typical time series model of hydro resources may have various components in order to characterize the streamflow in a particular basin. In the time series analysis, we normally break the series into the following four, namely, a) Trend (T), b) Seasonal (S), c) Cyclic (C) and d) Random (R) components. A model of time series Xt utilizes these components. The following are two models widely used in time series analysis,

Additive Model: $X_t = T_t + S_t + C_t + R_t$, and Equation 4.2

Multiplicative Model: $X_t = T_t \times S_t \times C_t \times R_t$. Equation 4.3

This study uses the Additive Model for synthesizing a time series of streamflow. In the Multiplicative Model, the components may not be necessarily independent. Here we use statistical techniques to assemble components. Random variables are easier to handle when they are independent than when they are uncorrelated.

Let us assume the following notations for streamflow Q and its components.

Notation	Components of Q
Q – streamflow	T- Trend
Q – daily mean	S – Seasonal
$\underline{Q}$ – monthly mean	C- cyclical
q – hourly mean	R – Random

In this notation, Q(T), Q(S), Q(C) and Q(R) represent the trend, seasonal, cyclical and random components of the daily streamflow respectively. The trend component Q(T) of the streamflow may take into account changes associated with the climate change (temperature, precipitation, etc.). The seasonal component Q(S) attempts to capture seasonality of the local hydrological cycle whereas the cyclic component Q(C) aims at any long-term variations in the streamflow of timescales greater than a year. We model Q(S) as a deterministic component while Q(R) as a stochastic component of the streamflow. Here, the deterministic component aims to reproduce the serial correlation of time series, whereas the stochastic component aims to capture the probability distribution derived from the AFDC.

Below we propose two parsimonious approaches for synthesizing an hourly time series of streamflow. The followings are the assumptions made into these approaches:

i. The seasonal (S) component can be estimated based on some historic/empirical data in the region.
ii. There are gauged stations available in the neighborhood of the MHP site which bear similar geographic and climatological signature/characteristics.
iii. q(R) ~ Q(R), that is the model for the random component of hourly stream flow can be estimated from the daily streamflow.
iv. The climate variables are stationary.

A time series of streamflow may be decomposed using the additive model as:

$$\{Q\} = \{Q(T)\} + \{Q(S)\} + \{ Q(C)\} + \{ Q(R)\} \quad \text{Equation 4.4}$$

For AFDC, the underlying series is a periodic function with a time period of one year. The effects of trend and cyclic components are taken in to account into the time series of AFDC. Therefore, we may write:

$$\{Q\}_{AFDC} = \{Q(S)\}_{AFDC} + \{Q(R)\}_{AFDC}. \quad \text{Equation 4.5}$$

We model $\{Q(S)\}_{AFDC}$ as a deterministic component of the stationary time series, while the random component $\{Q(R)\}_{AFDC}$ has been treated as a stochastic component.

The two methods we propose to estimate an hourly time series of the streamflow deals $\{Q(R)\}_{AFDC}$ differently. We have the distribution of $\{Q\}_{AFDC}$ and the monthly means $\{\underline{Q}\}$ for the climatological year, to begin with. In the following sections, two methods are discussed to estimate the seasonal component, the first component of the Equation 4.5.

4.2.1 Estimation of Seasonal Component

We propose to estimate the seasonal components by two methods. The first method utilizes only the monthly average values $\{\underline{Q}\}$ of the streamflow. The second method utilizes the normalized daily streamflow in the region as well as the monthly average value at the site in question. Mathematically, the two methods can be expressed in functional form as

- Method 1: $\{q(S)\} = f(\underline{Q})$,
- Method 2: $\{q(S)\} = f(Q/\bar{Q}, \underline{Q})$.

A) Method 1: Based on Monthly Averages

In this method, we assign mean streamflow $\underline{Q}$ for a given month to the mid-point hour of the month. For example, $\underline{Q}$ of month May to noon of May 16 which translates to hour 3252 of 24 x 365 hours in a year. The value for each hour of the year is interpolated then based on the twelve monthly means estimated from the MIP method. Mathematically

Q(S) = f(Q̲).This interpolated value will serve as the deterministic component Q(S) of the streamflow. The stochastic component {Q(R)} will be simulated based on the Equation 4.5.

Figure 4.1 presents an estimate of {Q(S)} at the Rajaiya station (#0460) for May. We overlay streamflow data for May 2007 for a comparison. These estimates are well within one standard deviation of the daily average for the month based on the long-term historical dataset (1963- 2010).

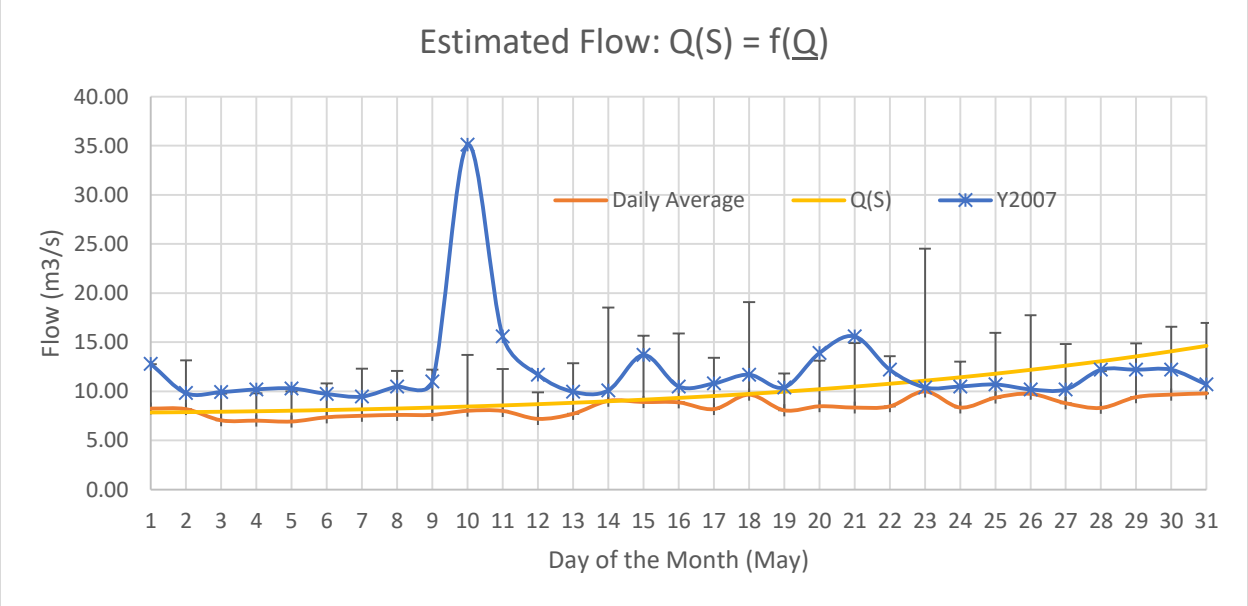

Figure 4.1: Estimation of Seasonal Component of Streamflow

B) Method 2: Based on Normalized time series and Monthly Averages

Let Q_t represents the observed daily streamflow at day t at a gauged station in the neighborhood of the MHP site. In our case, the Rajaiya hydrological station (# 0460) in the Rapti River, Figure 3.2, can serve as a gauged station. Following discussion about time series forming the AFDC, we can write:

$$Q_t = Q_t(S) + Q_t(R). \qquad \text{Equation 4.6}$$

In this method we estimate $Q_t(S)$ = f(Q(gauged)/Q̲(gauged) , Q̲(site)).

This equation can be normalized with the mean value of the streamflow $\bar{Q}$ over the period of the record, which is at the least greater than a year. Hence, we get

$$Q_t/\bar{Q} = Q_t(S)/\bar{Q} + Q_t(R)/\bar{Q}. \quad \text{Equation 4.7}$$

The normalized daily flow, the left-hand side of Equation 4.7 at the gauged station is used as an estimate of Q(S) at the project site. We calculate Q(S) by multiplying the normalized time series of flow at the gauged station by the annual average streamflow at the project site. The average value may be inferred from the AFDC. The area under the AFDC represents the volume of the water flowing in the time frame described by the abscissa. Obviously, the time frame for the AFDC is a year. The average value is then calculated by dividing the total volume of the water by the whole time, 365 days. This average value may also be calculated based on the monthly means if such data are available for the project site.

This estimation of Q(S) may reflect seasonal characteristics of streamflow at the site to some extent if the gauge's station and the site both have similar regional characteristics. The $q_t(S)$ will be interpolated then based on $Q_t(S)$. Figure 4.2 presents an estimate of hourly streamflow during dry seasons at Thingan based on data at the Rajaiya station (#0460).

The month of May is the critical month for the design of the hybrid microhydro system at Thingan Village. The HES would be designed around this month, sometimes also known as the design month. The estimates of Q(S) around the design-month of May is presented in Figure 4.2. The Thingan MHP system has the design flow rate (Qdesign) equal to 27 Liters/second. Based on the estimate of the seasonal component for the year 2010, the month of July seems to be the most critical for the MHP system at Thingan. The hydrograph for the month of July is at the lowest among the dry months most of the time, although it peaks up toward the final week of the month.

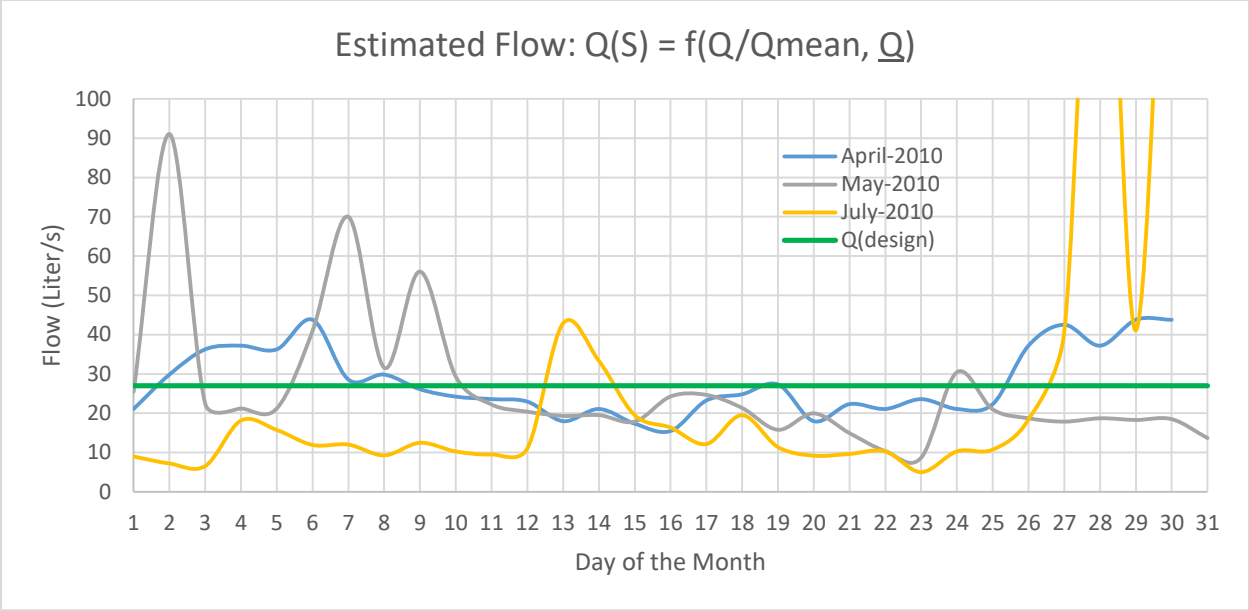

Figure 4.2: Regional Estimation of Seasonal Component of streamflow

The random component $\{Q_t(R)\}$ has to be superposed with the $\{Q_t(S)\}$ to obtain $\{Q_t\}$. The hourly time series $\{q_t\}$ may also be estimated from the daily time series $\{Q_t\}$ utilizing some interpolation techniques because the water flow in streams and rivers changes relatively slow, except after a storm.

4.2.2 Estimation of Random Component

We need to estimate the mean, variance and distribution functions of Q(R). Based on Equation 4.5, we can express Q(R) as,

$$Q = Q(S) + Q(R),$$

$$\Rightarrow Q(R) = Q - Q(S). \qquad \text{Equation 4.8}$$

Let's represent Q and Q(S) by two random variables X and Y respectively. Hence, Q(R) is a random variable which is a linear combination of two random variables: X = Q and Y = Q(S). Let Z = Q(R) = a X + b Y. Here a = 1, and b = – 1.

The mean and variance of the linear combination of the random variables can be expressed as:

$$\text{E(aX + bY)} \quad = a\,E(X) + b\,E(Y) = a\mu_X + b\mu_Y, \qquad \text{Equation 4.9}$$

$$\text{Var(aX + bY)} \quad = a^2\sigma_X^2 + b^2\sigma_Y^2 + 2ab\,Cov(X,Y),$$

$$= a^2\sigma_X^2 + b^2\sigma_Y^2 + 2ab\,\sigma_X\,\sigma_Y\,\rho(X,Y) \text{ ; where } (X,Y) = \frac{Cov(X,Y)}{\sigma_X\,\sigma_Y}.$$

Equation 4.10

If the correlation coefficient $\rho(X,Y)$ is positive, by subtracting the random variables we can even lower the variance of Q(R) than the case when they are uncorrelated or/and independent.

Let Q = k Q(S) where k is a random variable with k > 0. Hence, Q(R) = (k –1) Q(S). I propose to select Q(S) such that $\overline{\mathrm{Q}}(\mathrm{S}) = \overline{\mathrm{Q}}$, which imply $\overline{\mathrm{Q}}(\mathrm{R}) = 0$. Next, we will need to estimate the variance of Q(R) given the Q(S). The variance can be estimated by the following equation:

$$\sigma_R^2 = (k-1)^2\sigma_S^2 \qquad \text{Equation 4.11}$$

Distribution Functions of Q(R)

The random component Q(R) is one function of two random variables [145] as described by Equation 4.8. To estimate distribution functions of Q(R), we can start with joint probability density function. Let f_{XY} be the joint probability density function of X = Q and Y = Q(S). By definition, it is a non-negative function with the total area under the curve is equal to 1. Mathematically,

$$\int_{-\infty}^{\infty}\int_{-\infty}^{\infty} f_{XY}(x,y)dx\,dy = 1. \qquad \text{Equation 4.12}$$

The joint cumulative density function$\mathrm{F}_{XY}(\mathrm{x},\mathrm{y}) = \mathrm{P}[(\mathrm{X} \le \mathrm{x}) \cap (\mathrm{Y} \le \mathrm{y})]$. The cumulative density function is:

$$F_{XY}(x_o,y_o) = \int_{-\infty}^{y_o}\int_{-\infty}^{x_o} f_{XY}(x,y)dx\,dy. \qquad \text{Equation 4.13}$$

$\mathrm{F}_{XY}(x, y)$ is a monotonically increasing function [0, 1]. $F_{XY}(\infty, \infty) = 1$.

These two distribution functions have the following usual relationship,

$$f_{XY}(x, y) = \frac{\partial^2 F_{XY}(x,y)}{\partial x\, \partial y}. \qquad \text{Equation 4.14}$$

Let Z = X – Y such that X ≥ 0 and Y ≥ 0. This corresponds to region Q ≥ 0 and Q(S) ≥ 0.

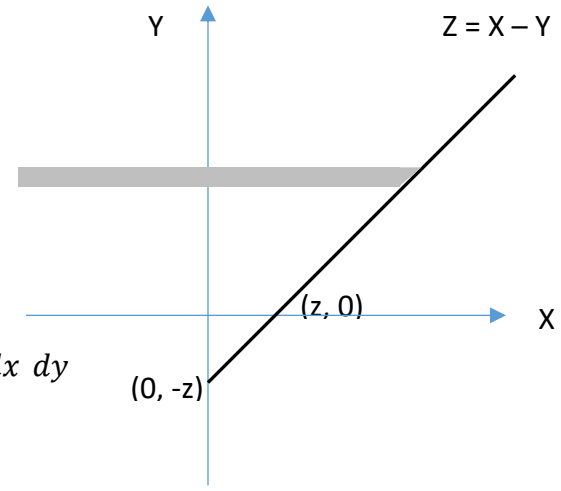

$$\mathrm{F}_Z(z) = P[Z \leq z] = P[X - Y \leq z]$$

$$= \int_{-\infty}^{\infty} \left(\int_{-\infty}^{z+y} f_{XY}(x, y) dx \right) dy$$

The probability density function is

$$f_Z(z) = \frac{d\mathrm{F}_Z(z)}{dz} = \int_{-\infty}^{\infty} \frac{\partial}{\partial z} \int_{-\infty}^{z+y} f_{XY}(x, y) dx\ dy$$

$$= \int_{-\infty}^{\infty} f_{XY}(z + y, y)\ dy$$

This is the case for our study. But our study is limited only to the first Quadrant x ≥ 0 and y ≥ 0. Hence, the above equation can be written as:

$$f_Z(z) = \int_0^{\infty} f_{XY}(z + y, y)\ dy.$$

Here the lower limit is changed from $-\infty$ to zero.

In this case we will have two cases

$$\mathrm{Z} = X - Y = \begin{cases} z > 0 & if\ x > y \\ z < 0 & if\ x < y \end{cases}$$

$$F_Z(z) = \begin{cases} \int_0^{\infty} \int_0^{z+y} f_{XY}(x,y)dx\,dy & z > 0 \\ \int_{-z}^{\infty} \int_0^{z+y} f_{XY}(x,y)dx\,dy & z < 0 \end{cases}$$

Equation 4.15

Applying the Leibnitz theorem, we get

$$f_Z(z) = \begin{cases} \int_0^{\infty} f_{XY}(z+y,y)dy & z > 0 \\ \int_{-z}^{\infty} f_{XY}(z+y,y)dy & z < 0 \end{cases}$$

Equation 4.16

Leibnitz Integral Rule:

$$H(x) = \int_{a(x)}^{b(x)} g(x,y)dy$$

$$\frac{dH(x)}{dx} = \frac{db(x)}{dx} g(x,b(x)) - \frac{da(x)}{dx} g\big(x,a(x)\big) + \int_{a(x)}^{b(x)} \frac{\partial g(x,y)}{\partial x} dy$$

Equations 4.15 and 4.16 can be used to compute the distribution functions of Q(R) given the joint distribution function of Q and Q(S). Further details may be found in Chapter *Two Random Variables* of a book [145].

4.3 Downscaling Models

We propose two models for the downscaling of time series of streamflow. The Monte Carlo Markov Chain (MCMC) Method [146, 147]utilizes the distribution of Q(S) as a proposal distribution, and distribution resulting from the AFDC as the target distribution. The MCMC does not utilize the rainfall data as an input to the model. However the Autoregressive–moving-average model with exogenous inputs (ARMAX) Model does utilize the rainfall data as one of its inputs. The ARMAX model is one

example of linear input-output polynomial models. Here we use two inputs and one output model. The seasonal component Q(S) and the rainfall data serve as two inputs to the ARMAX model which outputs the streamflow time series. The ARMAX is a special case of more general Box and Jenkins [148] model.

4.3.1 Monte Carlo Markov Chain (MCMC) Theory

This theory for a sampling of data from a symmetrical proposal distribution was developed in 1953 by a team consisting of Metropolis et al. [149]. Hasting [150] expanded the theory for more general cases during the 1970s.

Assume that streamflow q has a unique stationary distribution $\pi(q)$ and transition probability P. Let transition between flow-states is ergodic, i.e $q \rightarrow q'$ is reversible, a condition for the detailed balance will require,

$$\pi(q)\, P(q'|q) = \pi(q')\, P(q|q'). \qquad \text{Equation 4.17}$$

The transition process is conceived as a process consisting of two independent steps of

a) Proposal distribution, $g(q'|q)$; and
b) Accept-Reject $A(q'|q)$ criteria.

As transition steps are independent of each other, we can write:

$$P(q'|q) = g(q'|q)\, A(q'|q). \qquad \text{Equation 4.18}$$

Substituting $P(q'|q)$ using Equation 4.17, we get

$$\pi(q')\, P(q|q')/\pi(q) = g(q'|q)\, A(q'|q)$$

or $$\pi(q')\, g(q|q')\, A(q|q')\, /\pi(q) = g(q'|q)\, A(q'|q)$$

or $$\frac{A(q'|q)}{A(q|q')} = \frac{\pi(q')}{\pi(q)}\,\frac{g(q|q')}{g(q'|q)}.$$

According to the Metropolis choice

$$A(q'|q) = min\left[1,\ \frac{\pi(q')}{\pi(q)}\,\frac{g(q|q')}{g(q'|q)}\right]. \qquad \text{Equation 4.19}$$

In this study $p_1 = \frac{g(q|q')}{g(q'|q)}$ is approximated based on a transitional probability matrix (TPM) of q(S). Two ways to estimate q(S) are discussed in Section 3.2.3. The probability

ratio $p_2 = \frac{\pi(q')}{\pi(q)}$ of the target distribution is computed from the AFDC. Figure 4.3 below presents a flowchart of by which this method is implemented in a MATLAB code.

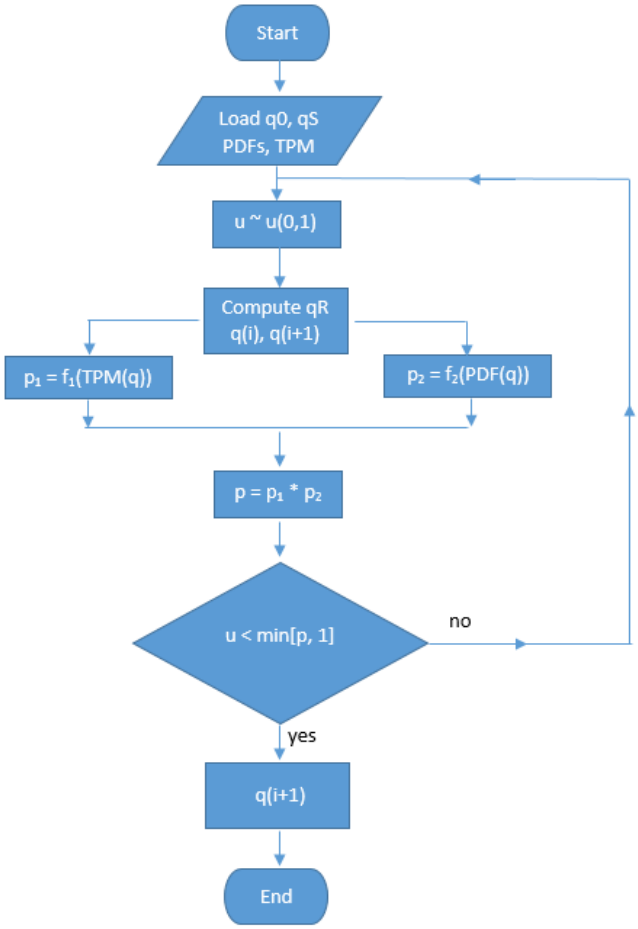

Figure 4.3: Flowchart of MCMC Method

The process begins with the initial condition q0, and a proposed time series qS of q(S). A MATLAB® script computes the PDF and CDF for q(R) = q – q(S) based on the model estimation data set, and the transition probability matrix (TPM) of q(S). Here u is a uniformly distributed random number in the interval (0, 1). The q(R) is estimated as the inverse of the CDF function F_R, i.e., $q(R) \sim F_R^{-1}(u)$. This inverse method preserves the PDF of the random variable $q(R)$ corresponding to the CDF [151]. The process is illustrated below in Figure 4.4. The q(R) is normalized value by the average value of q for the period of the record.

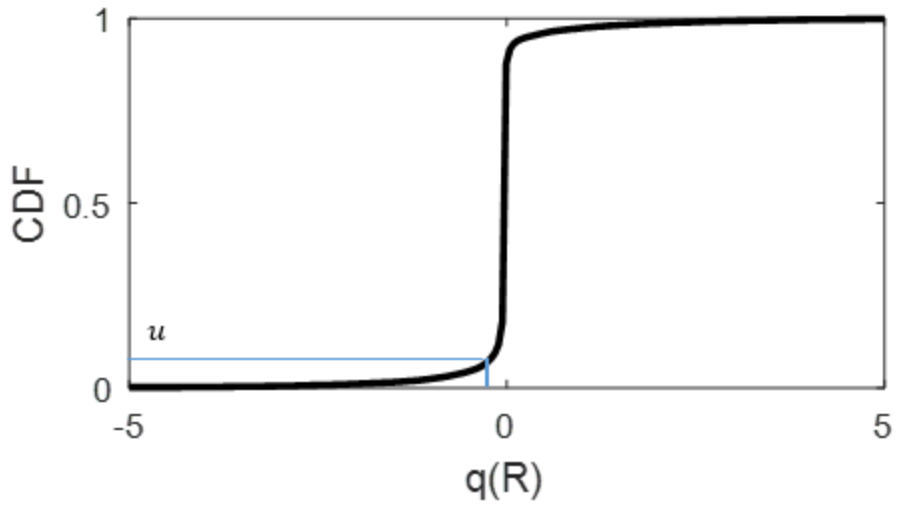

Figure 4.4: Estimation of q(R) in MCMC

In addition to synthesizing an hourly time series of the streamflow, the MATLAB® code also keeps track of acceptance rate and the percentage fit against observed data, if available. The code is documented in Appendix A.2.1.

In fact, the performance of this MCMC algorithm depends largely on the choice of q(S), the deterministic component of the streamflow. A better understanding/characterization of regional hydrology will have a positive impact on estimation of q(S). In the limit $q(S) \rightarrow q$, the synthesized data should match perfectly with the measured data set. This MCMC algorithm stands up to this expectation. This algorithm aims not merely try to match the target distribution but also to reproduce some degree of autocorrelation of time series at various lags through a better choice of q(S).

4.3.2 ARMAX Model

In Autoregressive–moving-average model with exogenous inputs (ARMAX) model we use a technique used in the identification of a system which may consist of inputs and outputs. A system may be defined as an object in which variables of various types and nature that interact to produce some observable signals. Three types of variables (u, v and w) are acting on a system below, Figure 4.5, to produce an output y.

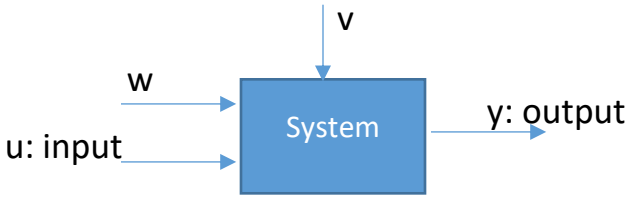

Figure 4.5: A system with various types of variables

In Figure 4.5, variables v and w represents disturbances in general. The disturbances that can be directly measured are denoted by w, and those that are only observed through their influence in the output denoted by v following notation of Lung [152]. Together these variables (u, v and w) are sometimes called external stimuli of the system. A system responds to the external stimuli to produce observable output. Table 4-1 presents some macro-variables related to streamflow modeling.

Table 4-1: Input and output of Hydro resource model

Input	Output	Disturbance
Rainfall	Streamflow	Evapotranspiration
Geography		Infiltration

We can classify systems in various ways. A dynamic system depends not only on the current external stimuli but also on their values in previous timestamps. We model streamflow as dynamics system with two inputs, namely seasonal component Q(S) and the rainfall. In some dynamical system, external stimuli are not resolved. The output of such system is known as Time Series [152]. A time series ARMA model of streamflow may not take rainfall into account, but the ARMAX model does. The rainfall can have significant contribution to the streamflow. This is one of the various reasons we have chosen the ARMAX model for this study.

An ARMAX model structure has a following form:

$$y(t) + a_1 y(t-1) + \ldots a_{na} y(t-na) = b_1 u(t-nk) + \ldots b_{nb} u(t-nk-nb+1) + c_1 e(t-1) + \ldots + c_{nc} e(t-nc) + e(t) .$$ Equation 4.20

Here e(t) is the error term. This model is a special case of more general Box-Jenkin [148] model. In short form, ARMAX model can be expressed in terms of the lag operator (z) as,

$$A(z)\, y(t) = B(z)\, u(t-nk) + C(z)\, e(t).$$ Equation 4.21

In our case we have two inputs, u_1 = Q(S) and u_2 = rainfall. Hence the model takes a form,

$$A(z)\, y(t) = \sum_i^{nu} B_i(z)\, u_i(t - nk) + C(z)\, e(t),$$

where,

$$A(z) = 1 + a_1 z^{-1} + \ldots + a_{na} z^{-na};$$

$$B(z) = b_1 + b_2 z^{-1} + \ldots\ldots + b_{nb} z^{nb+1};$$

$$C(z) = 1 + c_1 z^{-1} + \ldots\ldots + c_{nc} z^{-nc};$$

Equation 4.22

The parameters na, nb and nc are the orders of ARMAX model. The value of nk is set to unity for the rainfall and q(S). Here, we will estimate ARMAX model that adequately describes the data based on iteration of these parameters for a range of their values and the corresponding goodness of fit of synthesized data against the validation dataset. Figure 4.6 illustrates the iteration process to come up with the values of these parameters. If data has no input channels u, ARMAX reduces to the ARMA model. The ARMAX model reduces to an ARX model when C(z) = 1.

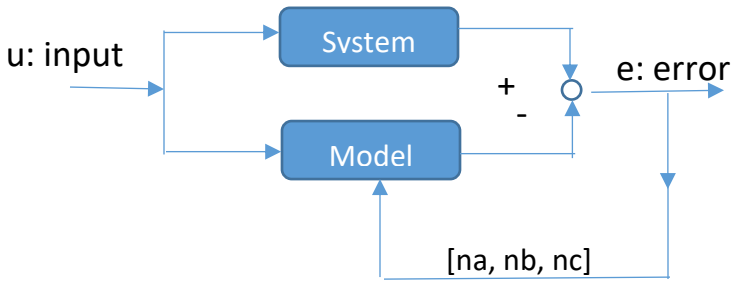

Figure 4.6: Estimation of Model Parameters

For a given set of model parameter, the coefficients a_{na}, b_{nb} and c_{nc} of Equation 4.22 are estimated by minimizing the error terms using the least-square methods. The System Identification Toolbox™ of MATLAB® has been utilized to estimate these coefficients.

Once the ARMAX model is estimated from the data set, the random component of the stream flow Q(R) can be estimated from a technique known as subreferencing of the model [153]. Subreferencing allows us to create models with subsets of inputs and outputs from existing multivariable ARMAX models. A special case of ARMAX model is ARX model. We simulate Q(R) for the ARX model utilizing steps as follows.

The ARX model, following Equation 4.21 has a form: A(z)y(t) = B(z)u(t) + e(t). This can be rearranged as:

$$y(t) = \frac{B(z)}{A(z)}\, u(t) + \frac{1}{A(z)} e(t) = G(z)u(t) + H(z)\, e(t); \qquad \text{Equation 4.23}$$

y(t) = y(system dynamics) + y(noise) Equation 4.24

In the ARX model represented by Equation 4.23, dynamic and noise models are subreferenced separately. The Q(R) corresponds to the noise model in Equation 4.24.

In one of the example we use ARX model with na = 6, nb = 4 and nk = 1. Let the model be represented as “sys = arx641”. The transfer functions for the dynamic and noise models are G and H respectively. In MATLAB® it is implemented as: G = tf(sys, 'measured'); and H = tf(sys, 'noise').

The noise variance of the model is computed from the covariance matrix of e(t). The covariance matrix of e = E[e(t) e(t)’] = λ^2 I, where $\hat{\lambda}^2 = \frac{1}{N-p}\sum_{k=1}^{N}[\hat{e}(k)]^2$. In the adjoining equation, p is the number of parameters on the ARX model. The hourly standard deviation is approximated as $\lambda(\text{hourly}) = \frac{\lambda(\text{daily})}{\sqrt{24}}$. The noise is modeled then by changing the origin and scale of the random variable as e = λX + b such that X ~ N(0, 1)

and b is the mean value which is zero for white Gaussian noise. Once these parameters are known, the random component can be simulated as q(R) = f(H, e, t). In MATLAB®, q(R) = lsim(H,e,t). This simulation results in the distribution functions PDF and CDF of the q(R) required for the downscaling of the MHP resources utilizing the MCMC method discussed in the previous section.

4.4 Validation of Model

To validate the downscaling model, we use data from the Distributed Model Intercomparison Project (DMIP) [154] of the National Weather Service (NWS). The DMIP provides hourly test datasets for comparison and validation of various distributed models in Hydrology. The DMIP has provided the hourly streamflow data from the USGS at five different locations. We use the dataset for the Blue River at Blue, OK. Table 4-2 below presents metadata of the data set used for this study.

Table 4-2: Metadata dataset at Blue River at Blue, OK

Blue River at Blue, OK	
USGS site #	07332500
Data Start Date	October 1, 1992
Data End Date	May 31, 1999
Time resolution	Hourly
Total Span	6.6 years
Data Availability	97.74 %

The rainfall data are taken from the USGS site # USC00342678 (Durant, OK). We split the combined data set into two datasets, one for the model estimation and the other for the model validation. We use the hourly time series of streamflow for the year 1995 as validation data set because of its 100% availability. The blue rectangle is the segment where we do not have the rainfall data.

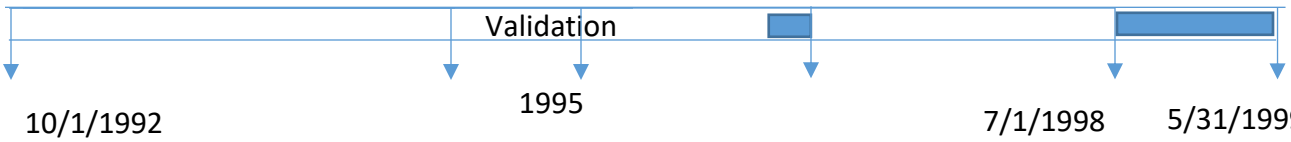

The goodness of the fit of the synthesized time series $\hat{y}$ is measured as:

$$\text{FIT} = \left[1 - \frac{NORM(y - \hat{y})}{NORM(y - \bar{y})}\right] \times 100\%. \qquad \text{Equation 4.25}$$

The RHS of Equation 4.25 is a percentage of the output variations that is reproduced by the model. A higher number may indicate a better model of the streamflow downscaling.

In the following section, we document detailed steps involved in downscaling hydro resource utilizing the two models described in Section 4.3.

A) Markov Chain Monte Carlo (MCMC) Method

The hourly streamflow data from the Blue River is normalized by the average flow. The normalized streamflow is divided into bins. Each bin represents a state of streamflow. We choose identical bin of size 0.05 for up to 1.5 times the normalized streamflow, and any other states above 1.5 are lumped together in a single bin. Hence, there are altogether 31 states of streamflow. The reason for keeping all data points above 1.5 in a single bin is because they will produce the same power, the rated power, irrespective of their magnitudes. The following two figures present the transition probability from one state to the other. It is sometimes known also as Transition Probability Matrix (TPM). The one in Figure 4.7 (a) presents TPM of q(S) while the other on the bottom, Figure 4.7 (b), is the same of the measured data q at USGS site # 07332500, Blue River, Oklahoma. Here q(S) is computed from the daily average of the measured flow by linear interpolation.

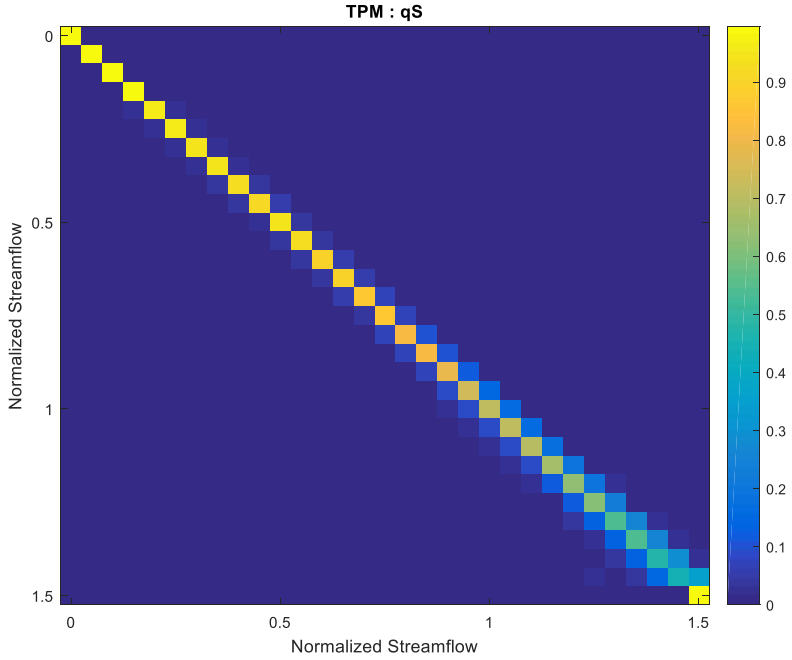

a) TPM of q(S)

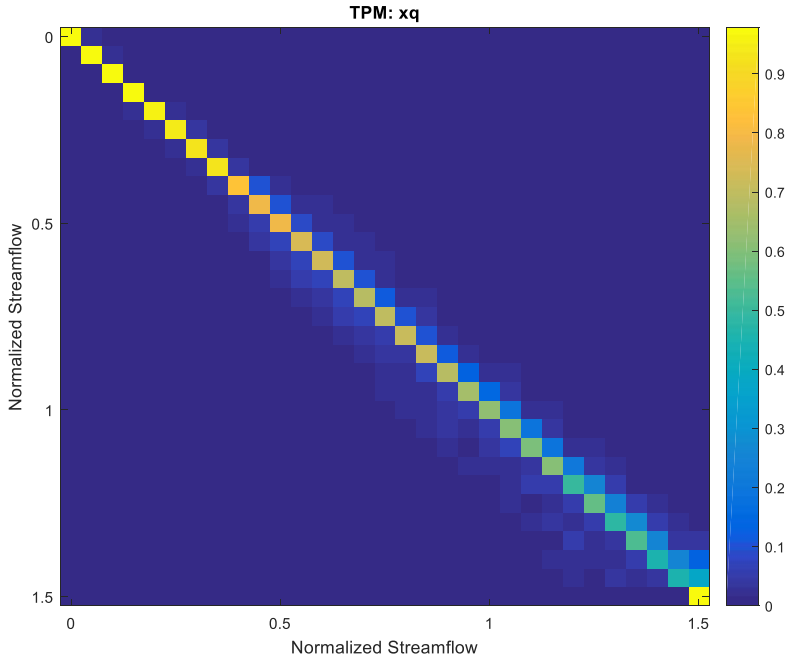

b) TPM of q

Figure 4.7: Transition probability matrices of q(S) and q.

The TPM of q(S) is a 3-band matrix almost up to the average flow, and 5-band after that. However, the TPM of q has much higher bandwidth. This difference in the bandwidth of TPMs outlines the information lost in the time series aggregation. An ideal downscaling algorithm strives for retrieving this lost information as much as possible.

An hourly time series of streamflow synthesized for the months April through June 1995 is presented in Figure 4.8. There is not a very significant difference in the trend with the measured data except it seems not to capture all peaks. This algorithm misses transient peaks at scales less than the day on which q(S) is based.

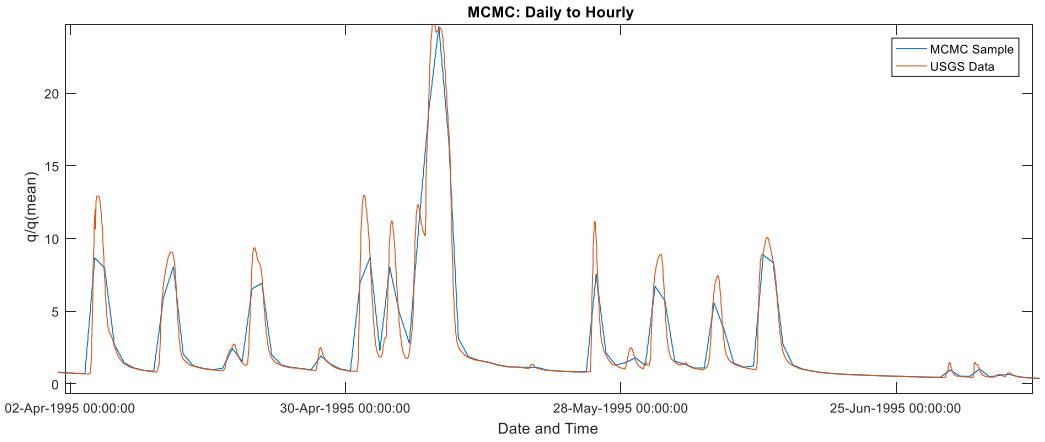

Figure 4.8: Comparison of MCMC synthesized data

As evaluated by the metric given by Equation 4.25, the synthesized data fit the USGS measured data about over 99%. The percentage acceptance of sampled data by the MCMC algorithm was about 87%. This level of performance of the MCMC algorithm may be acceptable for performance analysis of hybrid microhydro systems, where the focus is more to capture low-flow states than the transient peaks. Moreover, streamflow may not alter quite a bit within a few hours except after a storm.

B) Autoregressive-moving-average model with exogenous inputs (ARMAX) Model

The four parameters which are to be estimated in ARMAX Model represented by Equation 4.20 are [na, nb , nc, nk]. To estimate the lag nk for rainfall input, we overlay the hourly time series of precipitation and streamflow in Figure 4.9. By observation, we choose to set nk = 1 for rainfall. Here we use Multiple Input Single Output (MISO) ARMAX model. The other input is q(S), the deterministic component of the model. The value of lag nk for q(S) is also set to unity. A precise estimate of nk for rainfall may demand a detailed study of unit hydrograph [49] for a range of precipitation. This is beyond the scope of this study; we are interested only in the statistical methods of downscaling.

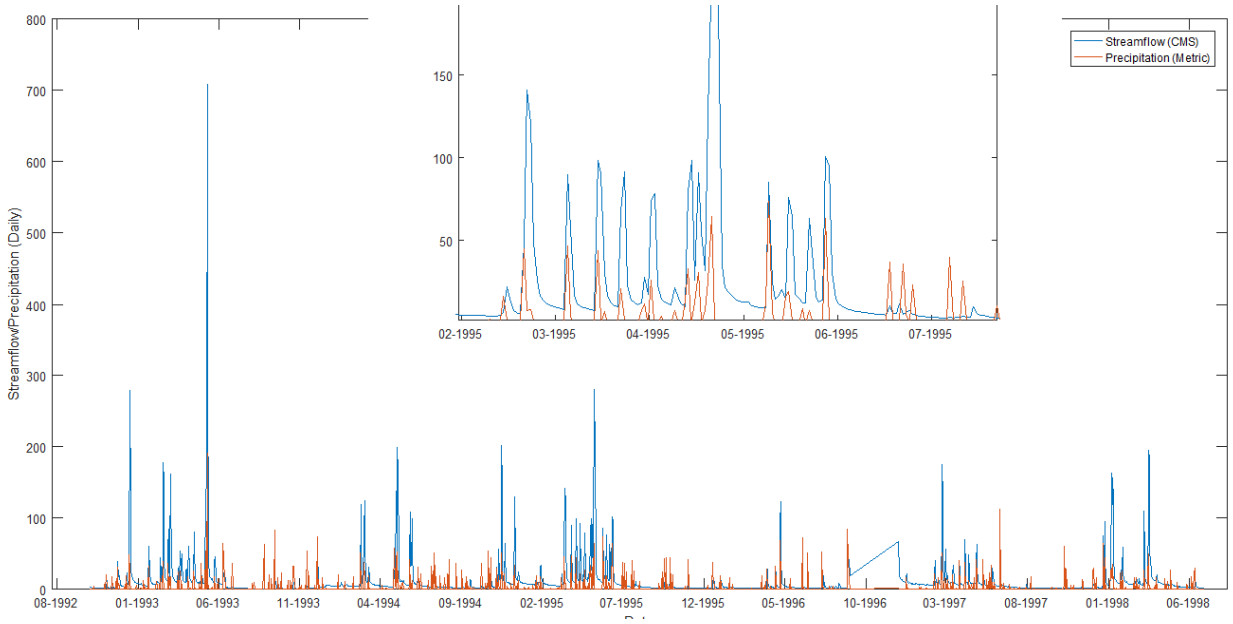

Figure 4.9: Rainfall and streamflow at Blue River, OK

The other model parameters [na, nb , nc] are determined such that the error term {e(t)} is a white noise sequence. This is how the time series models estimate disturbances v and w of the system, Figure 4.5. The effect of unmeasured disturbances is modeled as a transfer function driven by a white noise sequence. The case simplifies to an analytical solution of parameters in the case of ARX model, an ARMAX model without the moving

average terms. In ARX model, we can increase the model order until e(k) become white noise.

We overlay output of ARX (6,4,1) and ARMAX (4,4,3,1) models in Figure 4.10. It seems the ARX model can capture the time-averaged macro-dynamics as reflected in the percentage fit of over 99% as gauged by the Equation 4.25. The ARMAX term still captures the trend in measure data, but it induces some oscillations about the measured values. The ARX model captures the variations in the data set very well. However, the auto-correlation and cross-correlation functions are on the boundaries of the confidence intervals.

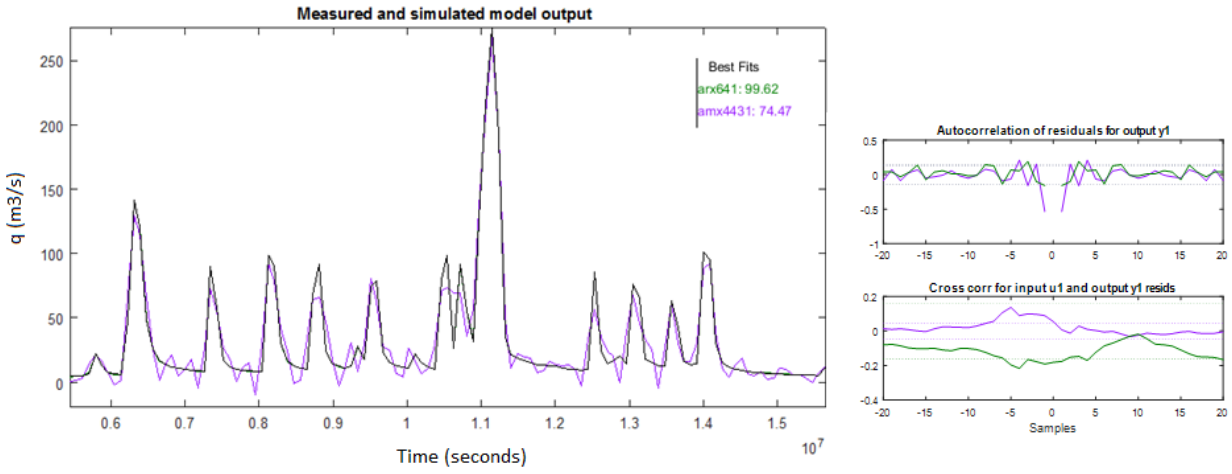

Figure 4.10: Comparison of ARMAX models with measured USGS data at Blue River.

The details of ARX (6,4,1) and ARMAX (4,4,3,1) models are documented in Appendix A.2.2. The ARX model seems to fit measured data better in this case compared to the ARMAX model. The streamflow is known to be a function of rainfall and geography. For MHP application, these model should be used with caution because the dynamic response may differ between catchment areas owing to their geography among many other factors.

4.5 Data Synthesis: Thingan Project

We use hydrological and rainfall dataset with the daily acquisition to develop an ARMAX model. The model supplies the variance required for estimating the distribution functions of the q(R). The normalized daily flow Q(S)/Q(mean) at the Rajaiya Station (#0460), Figure 3.2, is multiplied by the annual average streamflow (i.e. 232.8 Liter per second at the site) to estimate Q(S) at the project site. The hourly seasonal component q(S) is estimated by interpolation by assigning the daily Q(S) value at the noon of the day. Once we have q(S) and q(R), the hourly time series of the streamflow is synthesized utilizing the Monte-Carlo Markov chain method explained in Section 4.3. The target distribution has been derived from the AFDC at the site.

The average monthly streamflow at the project site is estimated using two local methods,

a) Medium Hydropower Study Project (NEA 1997) Method, and
b) MIP Method.

Figure 4.11 depicts the average monthly streamflow in Liter per second. The NEA's MHSP method seems to predict higher flow during the monsoon season, from June till September. During the dry season, this method predicts flow at the site lower than the flow by the MIP method.

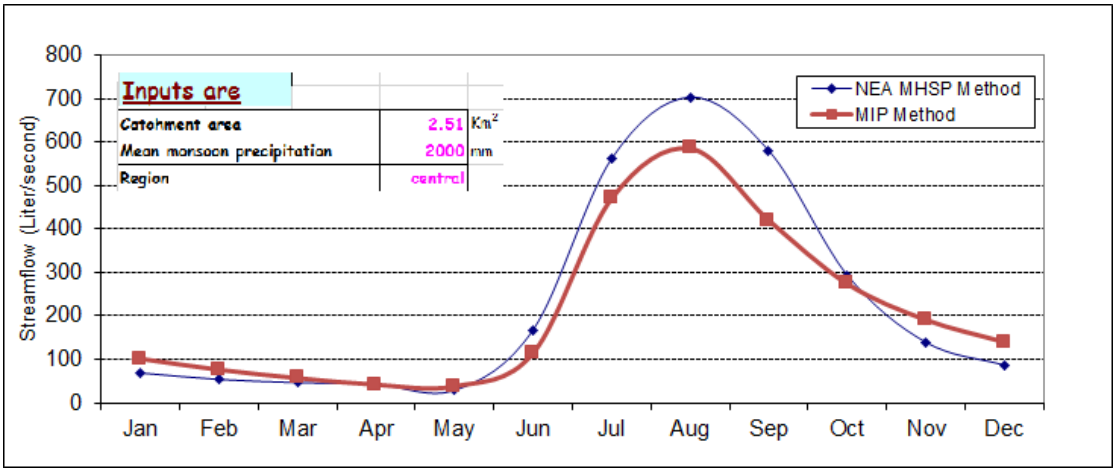

Figure 4.11: Monthly average of streamflow at the Thingan Site

Table 4.3 presents the average annual streamflow based on the two methods mentioned above. The MHSP method gives an average of 232.8 Liter per second, whereas the average value from the MIP method is 210.55 Liter per second. In this study, we use the average by the MHSP method, because the flow duration curve, Figure 4.12, used in this study is based on this method.

Table 4-3: Average annual streamflow at Thingan

Method	MHSP	MIP	Unit
Average Flow	232.80	210.55	Liter/Second

We use the hydrological data at the Rajaiya Station (#0460) from the year 2007 through 2009 and rainfall data from the Makawanpur Gandhi (# 0919). The rainfall data had two instances of "T" stands for "trace". This symbol is used when precipitation has been detected, but it isn't sufficient to measure meaningfully. We replaced these two instances with zero rainfall for practical reasons. This data acquired at the daily time step is utilized to estimate the hourly time series of streamflow at the project site.

We develop ARX model of the streamflow at the Rajaiya station considering two inputs, Q(S) and the rainfall at Makawanpur Gandhi (# 0919). The order of the model, the number of parameters of the model, is chosen such that the autocorrelation and partial correlation functions are within the confidence intervals. Among the feasible ARX models, the model with the highest best fit (%) with validation data (the year 2009) is used for this study.

Figure 4.12 presents an AFDC estimated at the project site by the NEA's MHSP method. This AFDC has only 7 data points for the entire range of streamflow. The CDF is computed as the complement of AFDC corresponding to the streamflow, as discussed in Section 2.4. The inset in the figure shows the CDF corresponding to those 7 points from the AFDC. We fitted these points based on a shape-preserving piecewise cubic

interpolation of the values at neighboring grid points. This fit allowed us to estimate CDF for a discrete set of points in the range of streamflow. Based on these CDFs values, we compute the PDF by numerical differentiation utilizing the central difference method. We choose to use the central difference method because it is second order accurate (truncation error ~ $O(h^2)$) and known to provide better results compared to the forward or the backward differentiation methods.

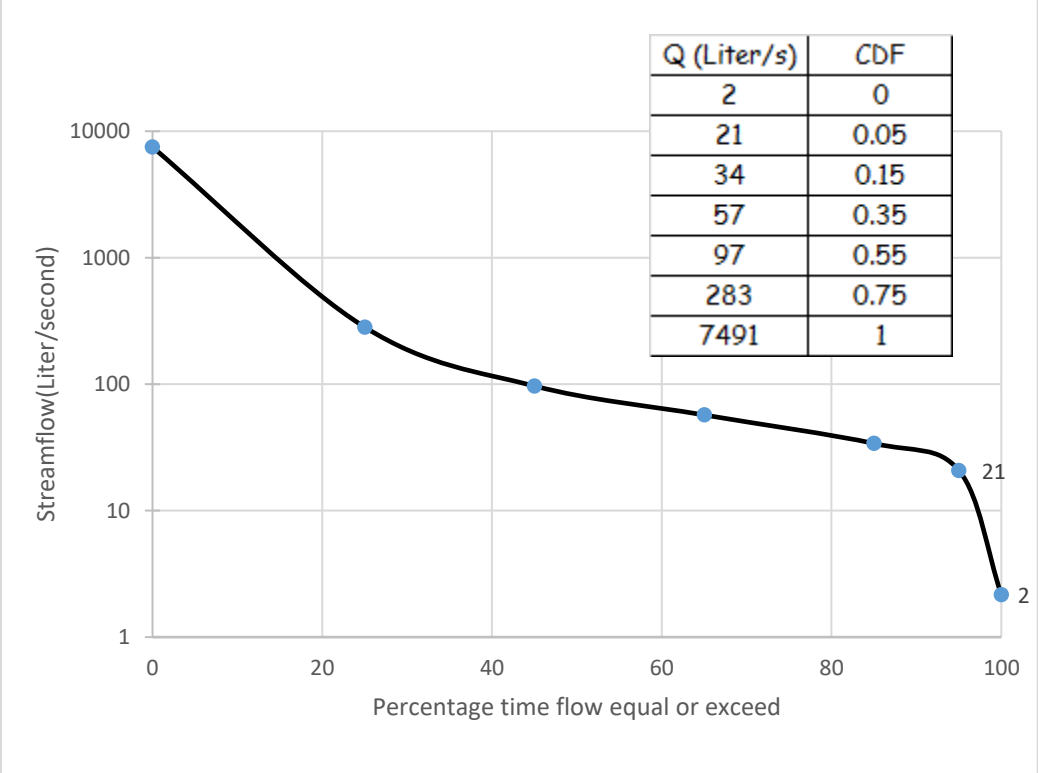

Figure 4.12: Annual Flow Duration Curve at Thingan

We found the Gamma distribution the best fit to the AFDC at the site. Figure 4.12 compares the PDF of the streamflow at the site with a PDF based on the gamma distribution. The Gamma distribution with the shape parameter 'a' and the scale parameter 'b' is given as:

$$y = f(x\,|a,b) = \frac{1}{b^a\,\Gamma(a)}\,x^{a-1}\,e^{\frac{-x}{b}} \qquad \text{Equation 4.26}$$

The two parameters in Equation 4.26 are estimated using the non-linear least square methods. We estimated a = 1.7138; and b = 0.2276. The MCMC method can use either PDF to synthesize an hourly time series of the streamflow. In this study, we choose to use PDF derived directly from the AFDC, not the best fitted Gamma distribution.

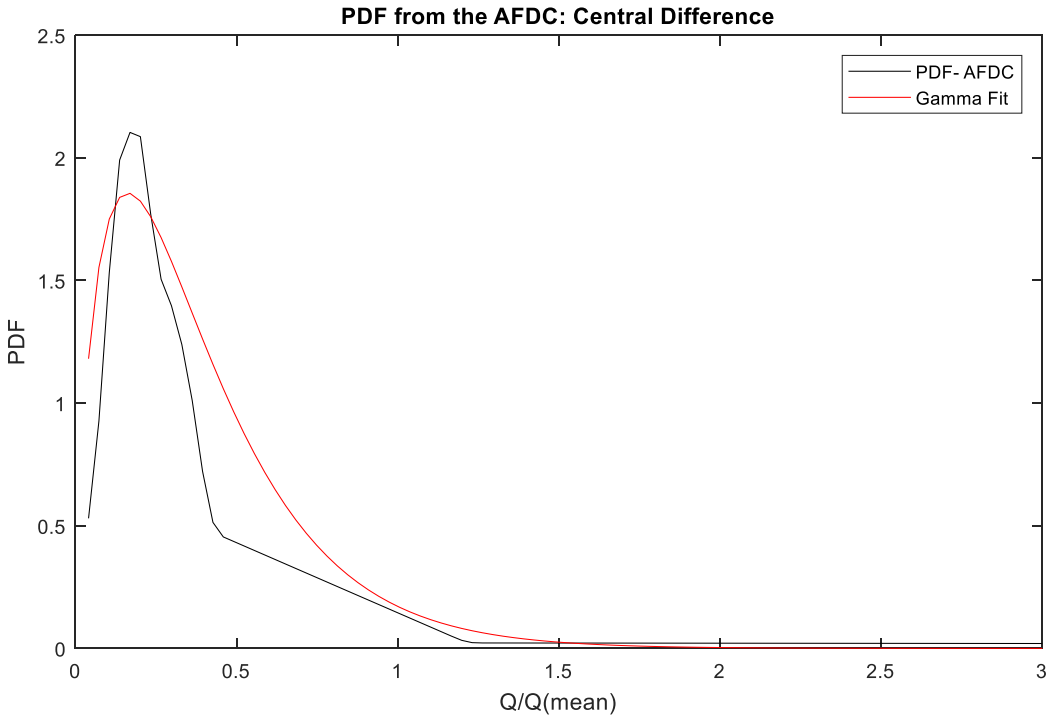

Figure 4.13: PDF of streamflow at the site

The simulated q(R) sequence is obtained from the ARX model (arx512) fitted for the data set at the Rajaiya station. The noise variance from the model came out to be λ^2 = arx512.NoiseVariance = 215.25 CMS. The noise model $H(z)$, discussed in Section 4.4.2, is found to be

$$H(z) = \frac{14.67}{1 + 0.3455\,z^{-1} + 0.449\,z^{-2} + 0.4655\,z^{-3} + 0.4422\,z^{-4} + 0.4616\,z^{-5}}$$

The inputs for the simulation of q(R) are H, eh and t. The eh is calculated as eh = $\frac{\lambda}{\sqrt{24}}\,e(t)$, where $e(t)$ is a normally distributed white noise sequence. The q(R)

normalized by the average flow rate, Q(mean) = 26.683 CMS at the Rajaiya Station (#0460) is used for synthesizing hourly time series at the project site.

Figure 4.13 presents CDF of the simulated {q(R)} on the secondary y-axis. On the x-axis, we have a histogram of normalized streamflow. The histogram is calculated from the CDF. The bar heights are normalized so that the area of the histogram is equal to 1. This CDF is one of the inputs for the Monte-Carlo Markov chain synthesis based on the Metropolis-Hastings algorithm. We use this algorithm because the proposed q(S), in general, can have a non-symmetric transitional probability matrix.

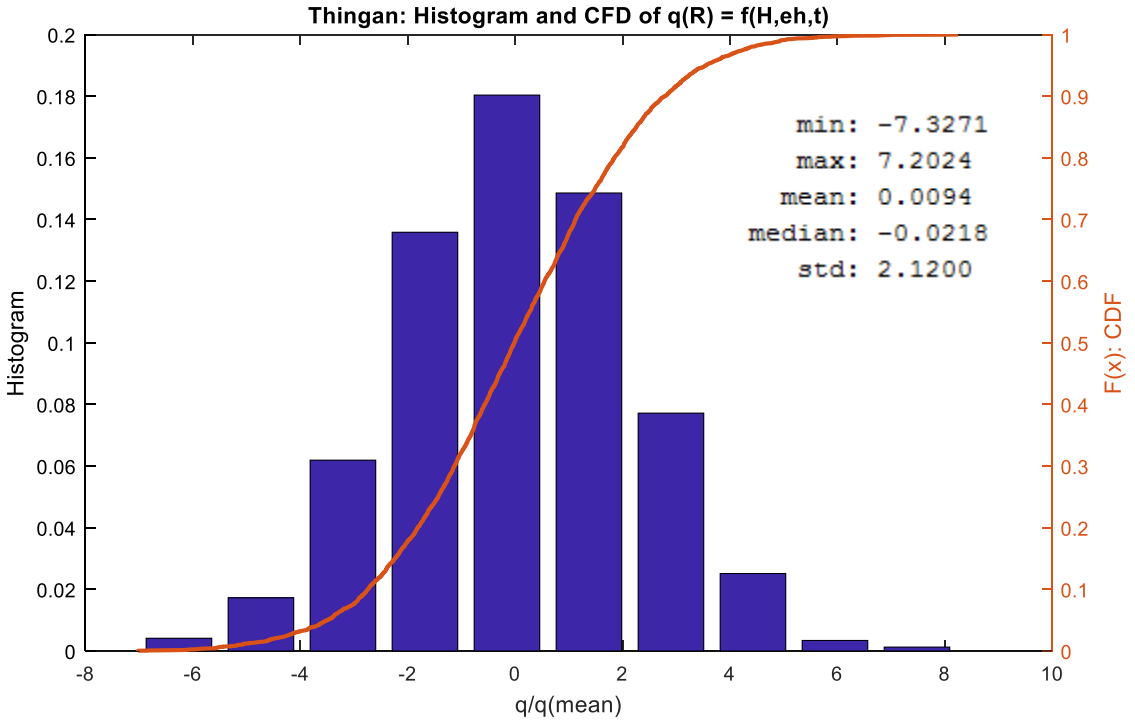

Figure 4.14: Distributions of q(R) at Thingan site

Figure 4.15 presents the deterministic q(S) and random q(R) components of the streamflow at Thingan. The contribution of q(R) is not very significant; it contributes only about three orders of magnitude less of q(S). This may be because our algorithms focus more on low-flow states, those up to 1.5 times the average values. Flow states higher than this threshold value are lumped into a single state.

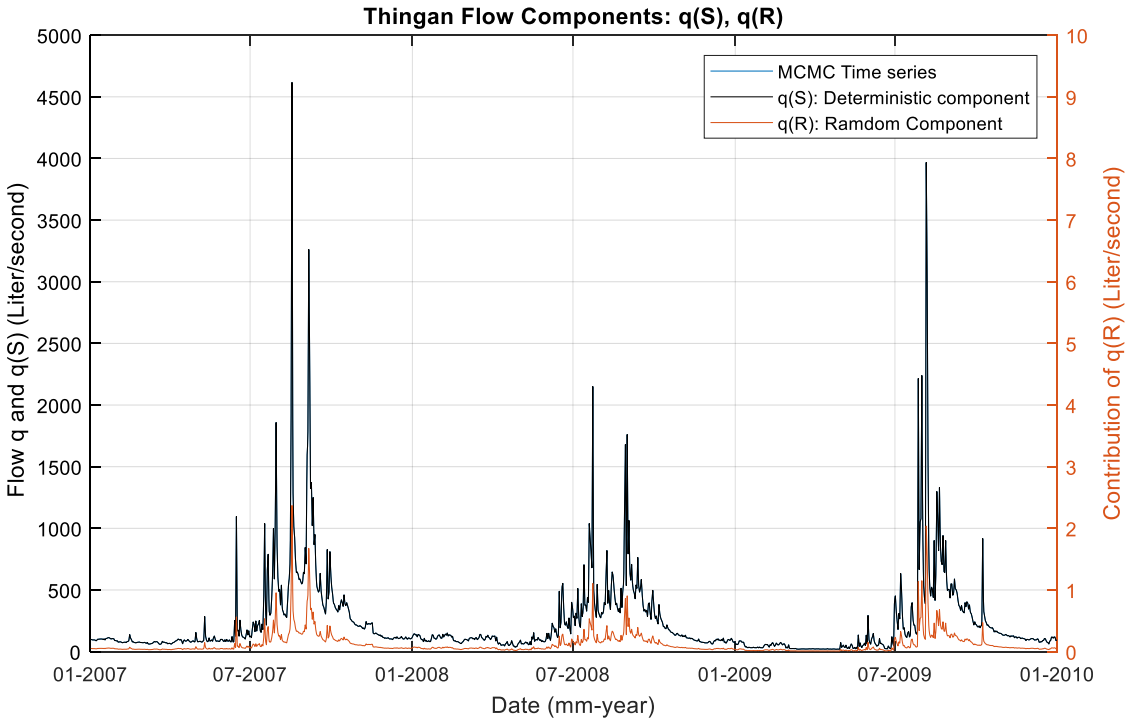

Figure 4.15: Hourly time series and components of stream flow at Thingan

A MATLAB® script and Monte-Carlo Markov chain function used for producing various figures above are documented in Appendix A.2.1. The script (mcmcThingan.m) utilizes a function (mcmc.m) in order to synthesize an hourly time series of streamflow at the Thingan site. We chose to use synthesized data for the year 2009 for performance analysis of the hybrid MHP systems.

4.6 Conclusions

In this chapter, we developed and validated a new statistical method for synthesizing an hourly time series of streamflow for a basin with limited hydrological information typical of site for a microhydro plant. The method utilizes a constrained Monte Carlo Markov Chain method for downscaling of the streamflow given an annual flow duration curve. Multiple Input Single Output (MISO) model utilizes a daily precipitation dataset as well as seasonal hydrological characteristics in the neighbourhood of project site in question in order to synthesize an hourly time series of streamflow.

CHAPTER 5

PERFORMANCE MODELS: HYDRO, SOLAR, AND WIND

5.1 Introdution

A hybrid energy system consists of subsystems consisting two or more generators and balance of the system. A performance model of a generator relates inputs (resource information) to the output (electric power). In Hybrid2 the performance of each system is characterized by power flows. Accordingly, the output of performance model, in general, is the average power (kW) generated within the given time step. We will use the following a generic model of a system shown in Figure 5.1 to describe the performance models of the subsystems comprising the hybrid microhydro system.

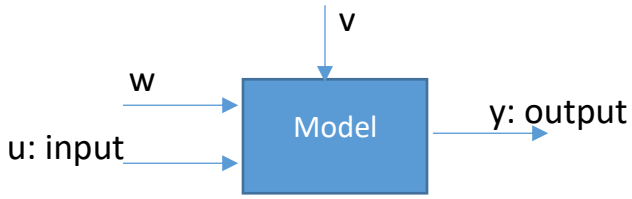

Figure 5.1: A generic model of a system

Here the input consists of the parameters that may characterize the renewable resource. Not all environmental variables pertaining to the system can be measured. Such variables are sometimes known as disturbances. Here w represent the disturbances that can be measured and v that may not be measured directly. Table 5-1 provide an example input and outputs as it may apply to a solar PV performance model.

Table 5-1: Input and output of a solar PV model

Input	Output	Disturbance
Solar Irradiance (W/m^2)	PV Power	Wind speed/ Humidity
Ambient Temperature (Tamb)	Current/ Voltage	Air mass

5.2 Microhydro Model

In general, microhydro systems utilize unregulated turbines. In this study, we evaluate a method to regulate microhydro systems employing Pelton turbine. A regulated MHP system responds to the variations in the load by self-adjusting the flow through the turbine (Qturbine). Figure 5.2 illustrates a model of the regulated MHP we propose for this study. Here SOW = state of water, a variable to quantify the size of the pond.

One of the objectives here is to conserve water, especially during the dry seasons when the streamflow may go below the design flow (Qdesign). The water conservation will be accompanied by less dissipation of excess energy in the dump load, and extended life of the electronic load controller (ELC). As indicated in the Literature Review, ELC is one of the most vulnerable components of the MHP systems.

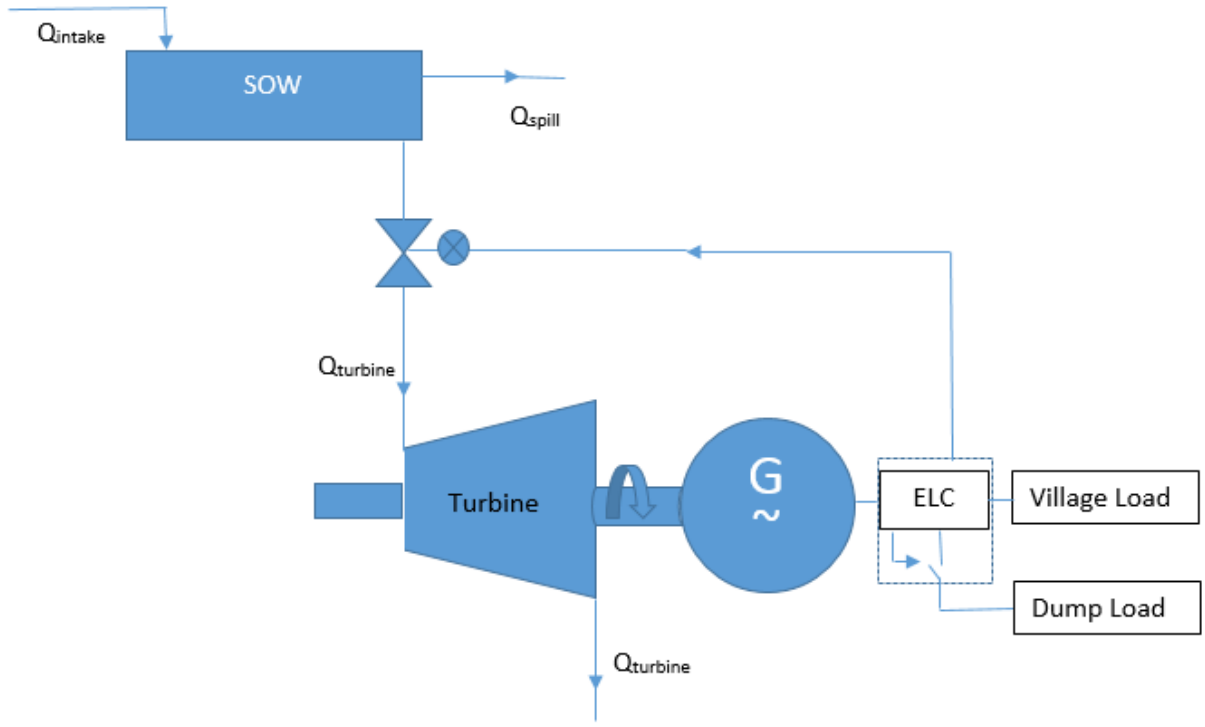

Figure 5.2: A model of Regulated MHP system

The generic equation for an MHP system, with the usual notion, is

$$P = \eta \rho Q g h. \qquad \text{Equation 5.1}$$

We will normalize the Equation 5.1 by the rated power (Pdesign) to get

$$\frac{P}{P_{design}} = \frac{\eta}{\eta_{design}} \frac{Q}{Q_{design}}. \qquad \text{Equation 5.2}$$

On the RHS, we have two normalized quantities. The first term $\frac{\eta}{\eta_{design}}$ describes the performance of the MHP system at partial load, which we will need to characterize a regulated turbine. For a given penstock pipe, this term is a function of the Reynold number. Figure 5.3 presents various terms of Equations 5.1 and 5.2 for an MHP system in Nepal that utilizes a 20 kW Pelton turbine. The normalized power is plotted on the left y-axis and the efficiency on the right y-axis at various fractions of the design flow rate.

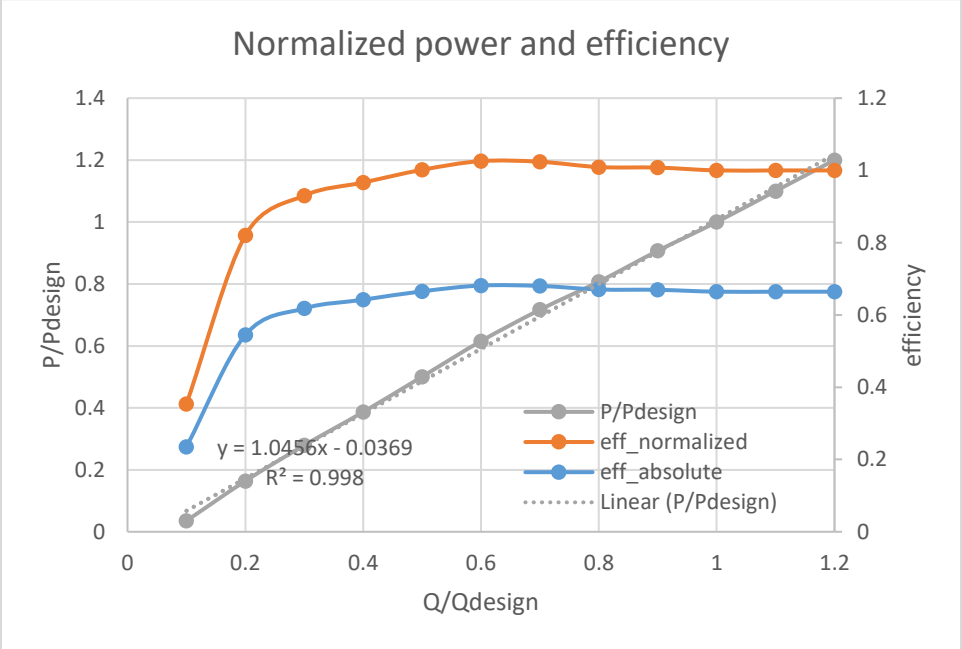

Figure 5.3: Part load efficiency of a generic 20 kW Pelton Turbine

The least-square estimates of the parameters for the normalized power are shown in Figure 5.3. The linear trend line model has a slope 1.0456 and an intercept 0.037. The standard errors of the slope, intercept and the normalized power estimates are 0.015, 0.011 and 0.018 respectively. To keep it more general, we evoke a model of normalized power based on a truncated power series as

$$\frac{P}{P_{design}} = a_0 + a_1\left(\frac{Q}{Q_{design}}\right) + a_2\left(\frac{Q}{Q_{design}}\right)^2. \qquad \text{Equation 5.3}$$

Table 5-2 presents the parameters of the model for the 20 kW MHP systems along with corresponding coefficients of determination (R^2). The first order model has two parameters and the second order model has three parameters.

Table 5-2: Model parameter for the MHP system

Model for efficiency	Coefficients	R^2
First Order	a_0 = - 0.0369; a_1 = 1.0456; a_2= 0	0.9980
Second Order	a_0 = - 0.0804; a_1 = 1.2318; a_2= -0.1432	0.9998

Equation 5.3, with Q/Qdesign $\geq$ 0.2, is a model of the regulated MHP system we propose for the performance analysis of MHP systems. The R^2 value for the first order model is 0.998. Even this first order linear model seems to capture efficiency variation adequately at the partial load.

This study considers the MHP system as a dispatchable system. The control system will dispatch the power generated from other resources (solar PV and wind turbine) and the unmet load will be served by the MHP system and battery system. The Thingan HES has a grid-tied inverter (3kW) to feed power from the solar PV and wind turbine into the grid. Such an inverter cannot function independently of the grid. Hence the MHP system should be in operation when there is a need for power. The minimum value of Q/Qdesign for the MHP system has been set to 0.2 to keep it operating.

For a given time step, we will know the required power (Pneed) of MHP system based on the energy balance principle Hybrid2 utilizes [4]. The flow corresponding to the required power (Pneed) can be calculated using Equation 5.3. To be precise, Q/Qdesgin = min {0.2, 1.2}.

The Bernoulli Equation can be utilized to calculate valve opening/positioning corresponding to the flow. The control system will receive this feedback from the ELC, and command the actuator to position the valve accordingly. A water balance equation for the pond will provide the State of Water (SOW) at the beginning of the next time step. Here we reproduce a figure from Section 1.7: Definition of Terms.

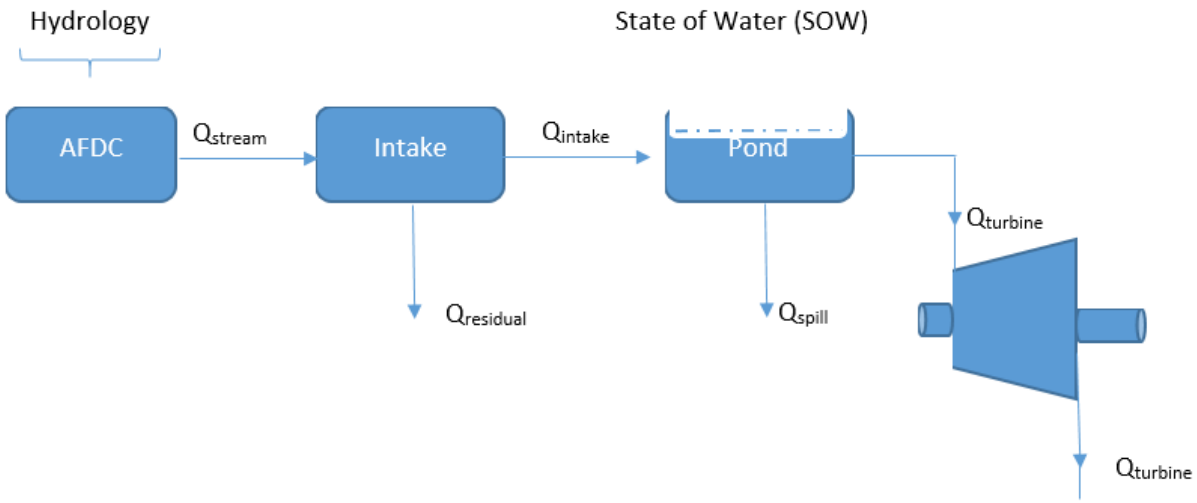

The model of intake will have a form of a low pass filter, which will depend on the height of the intake weir/dam, h_{intake}. Let $Q_{intake|max} = k * \sqrt{h_{intake}}$. Equation 5.4 describes the model of the intake in mathematical form.

$$Q_{intake} = \begin{cases} \min(Qstream - Qresidual;\ Q_{intake|max}) & \text{if } Qstream > Qresidual \\ 0 & \text{if } Qstream \leq Qresidual \end{cases}$$

Equation 5.4

In this study, we choose to use $Qresidual = 0$, and $Q_{intake|max} = 1.2\ Q_{design}$.

5.3 Solar PV Model

A solar PV model takes solar irradiance and other environmental variables such as an ambient temperature as inputs to yield the electric power, the output of a PV module. In general, solar PV performance models may be classified into two broad categories, namely a) linear model, and b) nonlinear model.

The linear model assumes a linear relationship between irradiance and the dc output power (kW) of the module. The power output is assumed directly proportional to the irradiance. These models sometimes also utilize temperature coefficient of maximum power to compute the power output. The main purpose of the nonlinear PV model is to capture accurately the steady-state current-voltage relationship of the PV panel at various irradiance and ambient temperature. Back in 1967, J. D. Sandstrom [155] has published one of the earliest analytical methods for predicting solar cell current-voltage curve as a function of incident solar intensity and cell temperature.

There are varieties of non-linear models of a solar PV module. Some models use only the Manufacturer's Data Sheet (or Specification) while others utilize entire I-V curve (I-V pair for zero through Voc) or the data matrix from the standard test such as IEC 61853-1. The following are the list of models available in the System Advisor Model [156] (version 2017.1.17) being developed at the National Renewable Research Laboratory.

- Simple Efficiency Module Model
- CEC Performance Model with Module Database
- CEC Performance Model with user Specification
- SANDIA PV Array Performance Model with Module Database
- IEC 61853 Single Diode Model

Most of these models are based on empirical data. Some technical details of these empirically based models are documented in [157, 158]. The SANDIA model, which many users consider the best in the empirical class, is documented in [159]. Continuous improvement in the technology and manufacturing process may render some Module Database obsolete, because these modules may have been upgraded or are no longer manufactured.

It may not always be practical to base a project design on the empirical PV models. At the different stages of project development, information available to the project

designer may be limited. Here we use a solar PV model which depends mainly on a manufacturer's datasheet. Another motivation is to make use of the science of solar cell, where applicable, and utilize a minimum number of model parameters without compromising much on the performance of the model. Naturally, a parsimonious model inherits some tradeoff between complexity and accuracy.

The most current version of Hybrid2 (version 1.3f, April 2011) utilizes the PV model that was developed by researchers at the University of Wisconsin documented in [100, 160]. It is a one-diode equivalent model as presented in Figure 5.4. Here we use a version of the PV Model adapted from the class notes by Prof. Manwell, as taught in a Spring 2016 course at University of Massachusetts [161]. This model is a one-diode equivalent model as well. Nonetheless, it utilizes extended auxiliary equations and improved algorithms in order to extract model parameters.

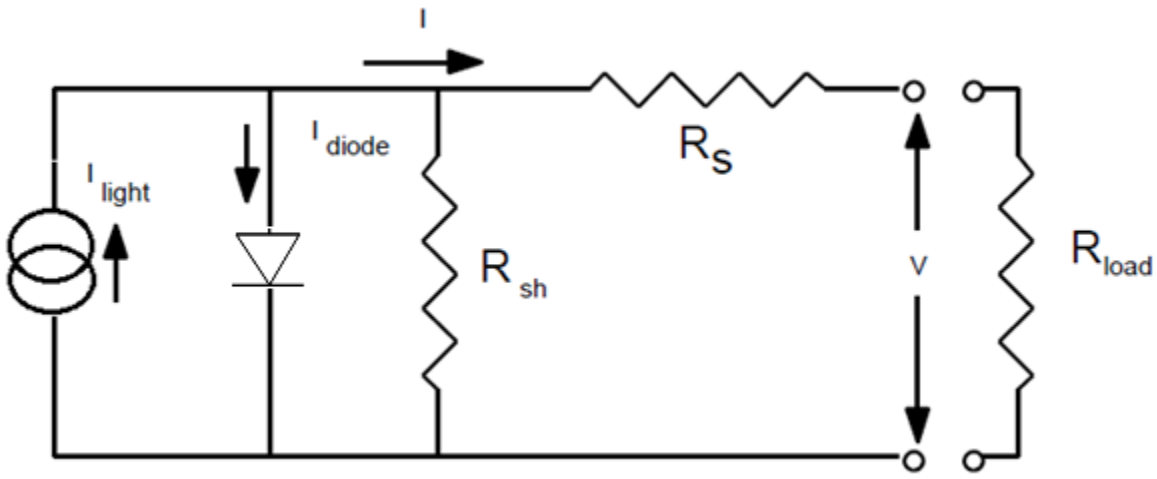

Figure 5.4: An equivalent circuit of a PV panel

This improved model also uses the Shockley ideal diode equation, an equation named after co-inventor William Bradford Shockley of the bipolar junction transistor. However, the method used to compute parameters and underlying assumptions are slightly different.

The Shockley equation gives diode current as,

$$I_{diode} = I_0 \left(exp^{\frac{V_D}{m V_T}} - 1\right) \quad \text{Equation 5.5}$$

where,

I_0 = reverse saturation current

V_D = voltage across the diode

V_T = thermal voltage.

The thermal voltage is calculated as $\frac{\kappa T}{e}$, where *e* is the charge on an electron (1.6022 x 10^{-19} C), κ is Boltzmann's Constant (1.38066 x 10^{-23} J/K), and *T* is the absolute temperature of the cell (K). This voltage is is about 25.7 mV at 25 °C.

The ideality factor m take into account for imperfection at junctions as observed in a real diode, especially carrier recombination as the charge carriers cross the depletion region. It has a value between 1 and 2 based on the degree of recombination in the different region of a diode. If recombination in depletion region is dominant, m tends to 2. In solar cells where the recombination in each region is comparable, m is somewhere in between [162].

Given the equivalent circuit of a PV Panel in Figure 5.4, the voltage across diode $V_D = V + I\,R_s$. If there are N cells in the module, we use $V_D = V/Ncells + I\,R_s$. The current flowing through the load can be expressed as:

$$I = I_L - I_D - I_{Sh} = I_L - I_0\left\{\exp\left(\frac{V/N_{cells} + I\,R_s}{mV_T}\right) - 1\right\} - \frac{V + I\,R_s}{R_{sh}} \quad \text{Equation 5.6}$$

This equation tries to approximate I –V Characteristic of a solar cell. Similar equations can also be derived by taking into consideration the dynamics of holes and electrons in the solar cell [162]. Equation 5.6 contains five parameters, namely the light current I_L, the diode reverse saturation current, the shunt resistance R_{sh}, the series resistance R_s,

and ideality factor m. The values of these parameters may depend well on the level of irradiance and the operating temperature of the cell (Tc). The estimates for these parameters may come from

a) Manufacturer's data sheet, known also as a specification of the PV Module; and/or
b) A set of measured I-V curves, such as one stipulated by the IEC 61853-1.

Effect of R_s and R_{sh}: Parasitic Resistances

These resistances are the electrical representation of energy losses that occur in a real cell. The metal contacts, the curvature of the path and transverse current between the emitter and front grid to collect the current give rise to the series resistance [162]. The series resistance arises mainly due to practical reasons associated with connection and collection of electric currents. The shunt resistance represents any high-conductivity parallel paths which may exist due to imperfect crystals and impurities in and near the junction [163]. The shunt resistant aggregates the imperfection in the cells or modules. These resistances are sometimes known as parasitic resistances owing to their net effect which reduces the energy flow in the external load.

a) Effect of the Series Resistance R_s

To study the effect of the series resistance (R_s), let's assume R_{sh} is very large, or infinite in Equation 5.6. Because of its position in the circuit, the series resistance will not have any effect on the open circuit voltage. A higher value of R_s will result in a higher voltage across the diode, and hence decreasing the current I through the load. This relationship is illustrated in Figure 5.5 (a) for a single silicon cell [162].

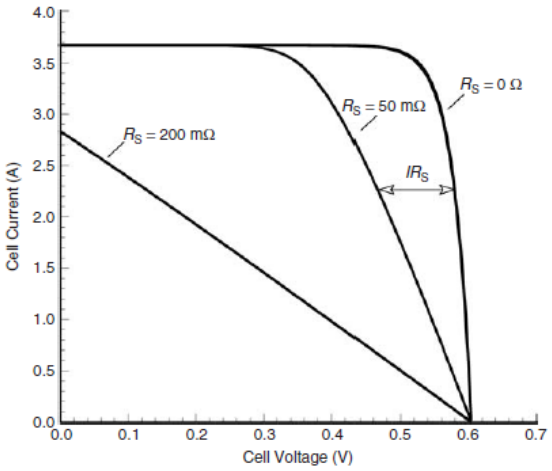

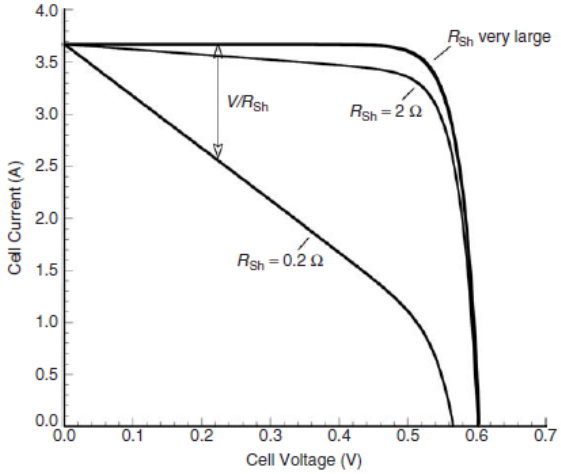

a) Series resistance at R_{sh} -> ∞ b) Shunt Resistance at $R_s = 0$

Figure 5.5: Effect of Parasitic Resistance on cell current and voltage [162]

b) Effect of the Shunt Resistance R_{sh}

To study the effect of the shunt resistance, let's assume $R_s = 0$. This translates into that the voltage across the diode, shunt, and load are the same. At constant voltage current is inversely proportional to resistance. If we lower Rsh further, a higher current will go through the shunt and less current will be available to flow through the load. This will decrease in open circuit voltage but will have no effect on the short-circuit current as depicted in Figure 5.5 (b).

A manufacturer's datasheet normally supplies: 1) short circuit current, $I_{SC,\,ref}$, 2) open circuit voltage, $V_{OC,ref}$, 3) maximum power point circuit, $I_{mp,ref}$, and voltage, $V_{mp,ref}$, (all of the previous at rated conditions of 1000 W/m^2 and 25° C) 4) short circuit current temperature coefficient, $\mu_{I,SC}$, 5) open circuit voltage temperature coefficient, $\mu_{V,OC}$, and 6) the number of cells in the panel, N_{cells}. These figures of merit for an AstroPower 120 W PV Module is presented in Table 5-3 for reference. The datasheet is documented in the Appendix B.2.

Table 5-3: Parameters of AstroPower 120 W PV module

Parameters	Symbol	Unit	Value
Peak Power	Wp	Watts	120
Number of Cells	N_{cells}		36
Open Circuit Voltage	$V_{OC,ref}$	Volts	21
Short Circuit Current	$I_{SC,\ ref}$	Amps	7.7
Maximum Power Voltage	$V_{mp,ref}$	Volts	16.9
Maximum Power Current	$I_{mp,ref}$	Amps	7.1
Short circuit Temp. Coefficient	$\mu_{I,SC}$	mA/C	3.5
Open Circuit Voltage Coefficient	$\mu_{V,OC}$	V/C	-0.08

Temperature coefficients may be given in different units such as A/°C, or %/°C, or /°C. Nowadays, some PV datasheet also provides the coefficient of maximum power, fill factor, etc. The fill factor is some measure of the radius of curvature of the I-V curve about the maximum power point.

In some cases, we may have a set of measured I-V curves at some irradiance and temperature combination. IEC 61853-1:2011 [164] describes requirements for evaluating PV module performance in terms of power (watts) rating over a range of irradiances and temperatures. This standard aim to provide a full set of characterization parameters for the module under various values of irradiance and temperature. The IEC-61853 - 1 defines a matrix of 23 temperature and irradiance pairs. A single diode model based on IEC-61853 test data set is documented by Dobos & MacAlpine [157]. A report from the Sandia National Laboratories [95] provides a more detailed method to estimate parameters of a single diode model of PV module that makes use of a full range of available I-V curves.

Here we take a practical approach that uses the manufacturer's datasheet. We make some simplifying assumptions/approximations to develop auxiliary equations to estimate the I-V characteristics of a solar PV module as a function of irradiance and cell temperature. Figure 5.6 presents current and voltage characteristics of an Astropower

120W module at five levels of irradiance 200 W/m2 through 1000 W/m2 at equal increment. This four-parameter model has the following assumptions:

1) Identical cells in the module;
2) m and R_s stay constant for a range of operating conditions;
3) Rsh $\rightarrow \infty$;
4) Spectral properties of solar radiation same at various air masses;
5) Light current is proportional to the Irradiation.

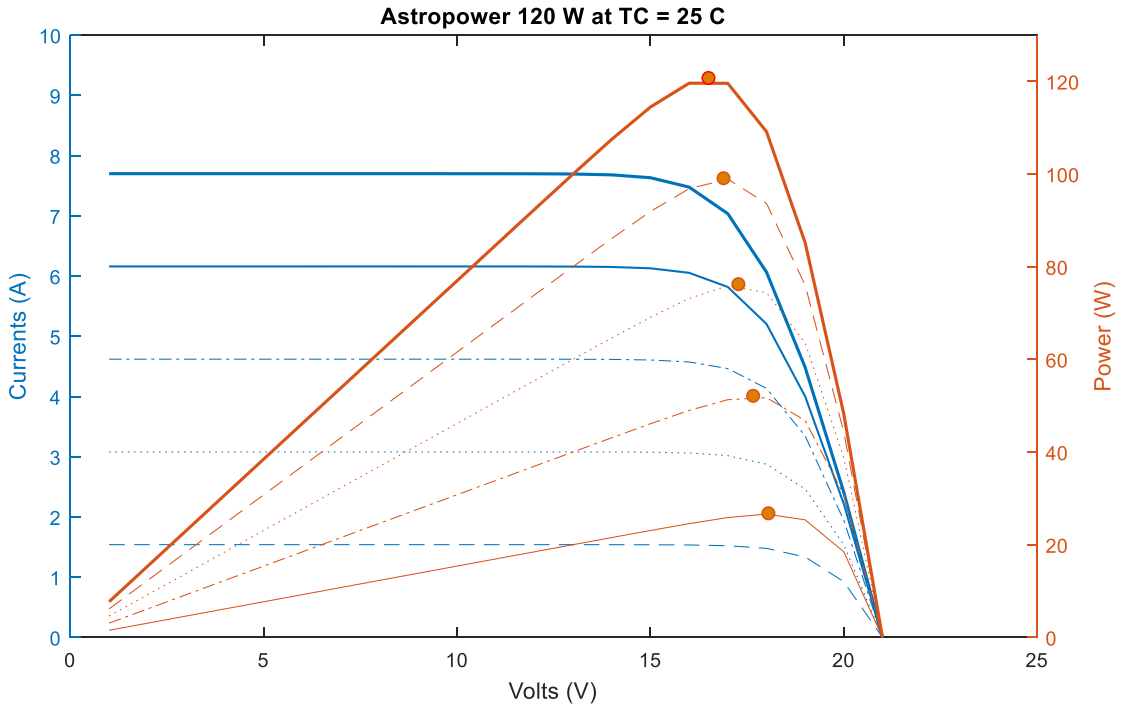

Figure 5.6: I-V cure of Astropower 120W module at the various level of Irradiance.

In a modern PV cell, the shunt resistance R_{sh} is very high. Hence we can neglect current I_{Sh} through it [4]. The Equation 5.6 can then be written as,

$$I = I_L - I_D = I_L - I_0 \left\{ \exp\left(\frac{V / N_{cells} + I R_s}{m V_T} \right) - 1 \right\}$$

Equation 5.7

The Equation 5.7 above is implicit in I. To solve this equation we may have to follow the iterative process: you need to guess I, predict it, then adjust the guess.

Under short circuit, the diode current is very small so the short circuit current and light current are the same. This case may also be approximately valid for a condition other than the ref conditions [165] :

$$I_L = I_{SC}$$ Equation 5.8

At open circuit there is no current, the exponential term >> 1 so the reverse saturation current for reference conditions, $I_{0,ref}$, is given by

$$I_{0,ref} = I_{L,ref} \exp\left(-\frac{V_{OC,ref} / N_{cells}}{mV_{T,ref}} \right) = I_{SC,ref} \exp\left(-\frac{V_{OC,ref} / N_{cells}}{mV_{T,ref}} \right).$$ Equation 5.9

The series resistance R_s can be calculated based on the data using Equation 5.7. At maximum power condition corresponding to the reference conditions, i.e. 1000 W/m^2 and 25 C, to the Equation of R_s in terms of values is:

$$R_s = \frac{mV_{T,ref} \ln\left(\frac{I_{L,ref} - I_{mp,ref} + I_{0,ref}}{I_{0,ref}} \right) - V_{mp,ref} / N_{cells}}{I_{mp,ref}}.$$ Equation 5.10

For conditions other than the reference conditions, we assume *m* and R_s stay constant. The relation between current, *I* and voltage, *V*, is given by Equation 5.7:

Auxiliary equations

These are equations that help to solve I and V as f(GT, TC). These auxiliary equations are derived from the Temperature Coefficients (μ), dimensionless Irradiance correction factor (λ) and assuming the light current is proportional to the irradiance.

The temperature coefficients of PV cells are usually supplied in the specification of PV Module either in per unit percentage or as their derivative about the reference conditions. Here we use the later definition.

The short circuit temperature coefficient of current,

$$\mu_{I,SC} = \left.\frac{d(I_{SC})}{dT}\right|_{GT} = \left.\frac{I_{SC} - I_{SC,ref}}{T_C - T_{C,ref}}\right|_{GT} \quad \text{Equation 5.11}$$

The open circuit temperature coefficient of voltage

$$\mu_{V,OC} = \left.\frac{d(V_{OC})}{dT}\right|_{GT} = \left.\frac{V_{OC} - V_{OC,ref}}{T_C - T_{C,ref}}\right|_{GT} \quad \text{Equation 5.12}$$

Some manufacture nowadays also report the temperature coefficient of maximum power, $\mu_{P,mp}$. In this study, we do not use it directly because it may not be available for all PV modules.

Following the definition of the coefficients above, at a given GT, current and voltage at a temperature other than reference condition can be approximated as

$$I_{SC} = I_{SC,ref} + \mu_{I,SC}(T_C - T_{C,ref}) = I_{SC,ref} + \Delta T_C \mu_{I,SC}, \quad \text{Equation 5.13}$$

$$V_{OC} = V_{OC,ref} + \mu_{V,OC}(T_C - T_{C,ref}) = V_{OC,ref} + \Delta T_C \mu_{V,OC}. \quad \text{Equation 5.14}$$

Here, we use $\Delta T_C = T_C - T_{C,ref}$.

The Translation Equations help translate PV performance values from one set of temperature and irradiance conditions to any other set of conditions. There are various equations in order to translate performance of PV cell at one pair of (GT, TC) to the other. Such equations are documented in IEC 891 or its current version IEC 60891:2009. An NREL subcontracted report suggests a new equation for translating the open circuit voltage [166]. Adapted from [167, 168], we model $V_{OC} = f(G_T,\ T_C)$, as follows:

$$V_{OC} = = V_{OC,ref}\left(1 + \Delta T_C \frac{\mu_{V,OC}}{V_{OC,ref}} + \lambda \ln\left(\frac{G_T}{G_{T,ref}}\right)\right). \quad \text{Equation 5.15}$$

Here λ is a dimensionless Irradiance correction factor.

For other temperatures, we model the thermal voltage (V_T) , light current (I_L) and reverse saturation current(I_0) as follows.

$$V_T = V_{T,ref}\,\frac{T}{T_{ref}} \qquad \text{Equation 5.16}$$

At different radiation, G_T, or temperature, T_C, (in Kelvin) than reference conditions, light current is:

$$I_L = \frac{G_T}{G_{T,ref}}\left[I_{L,ref} + \mu_{I,SC}\left(T_C - T_{C,ref}\right)\right] \qquad \text{Equation 5.17}$$

For reverse saturation current, use:

$$I_0 = \frac{G_T}{G_{T,ref}}\left(I_{SC,ref} + \Delta T_C \mu_{I,SC}\right)\exp\left(-\frac{\left(V_{OC,ref} + \Delta T_C \mu_{V,OC}\right)/N_{cells}}{mV_{T,ref}\left(T_C / T_{C,ref}\right)}\right) \qquad \text{Equation 5.18}$$

For convenience, one can use: $I_{SC} = \frac{G_T}{G_{T,ref}}\left(I_{SC,ref} + \Delta T_C \mu_{I,SC}\right)$. This Isc is f(GT, TC) which is more general than the one given by Equation 5.13 . Accordingly, we may write Equation 5.18 in short form as,

$$I_0 = I_{SC}\exp\left(-\frac{V_{OC}/N_{cells}}{mV_{T,ref}\left(T_C / T_{C,ref}\right)}\right). \qquad \text{Equation 5.19}$$

Estimation of m and R_s: Improving the Fit

The ideality factor m can be assumed 1.5 and compute various parameters using equations above. However, we can utilize the following equations to estimate the factor m and the series resistance R_s utilizing the current and voltage values at the maximum power point (MPP) from the manufacturer's data sheet.

At the MPP, the following first derivative should vanish, i.e.,

$$\left.\frac{dP}{dV}\right|_{MPP} = 0\ ; \qquad \text{Equation 5.20}$$

As P = I V, we get the following using the Chain rule,

$$\frac{dP}{dV} = \frac{d(IV)}{dV} = I + V\frac{dI}{dV}\ ; \qquad \text{Equation 5.21}$$

Using Equation 5.20,

$$\left.\frac{dI}{dV}\right|_{MPP} + \frac{I_{mp}}{V_{mp}} = 0. \qquad \text{Equation 5.22}$$

The first term of the above equation can be obtained by differentiating Equation 5.7 with respect to V,

$$\frac{dI}{dV} = -I_0\ exp\left(\frac{\frac{V}{N_{cells}} + I\ R_s}{m\ V_T}\right)\left[\frac{1}{N_{cells}\ m\ V_T} + \frac{R_s}{m\ V_T}\frac{dI}{dV}\right]. \qquad \text{Equation 5.23}$$

Bringing dI/dV together, we get

$$\frac{dI}{dV} = -\left[\frac{N_{cells}\ m\ V_T}{I_0} exp\left(-\frac{\frac{V}{N_{cells}} + I\ R_s}{m\ V_T}\right) + N_{cells}\ R_s\right]^{-1} \qquad \text{Equation 5.24}$$

Using Equation 4.18,

$$\frac{V_{mp}}{I_{mp}} - \left[\frac{N_{cells}\ m\ V_T}{I_0}\ exp\left(-\frac{\frac{V_{mp}}{N_{cells}} + I_{mp}\ R_s}{m\ V_T}\right) + N_{cells}\ R_s\right] = 0 \qquad \text{Equation 5.25}$$

The value of m can be estimated from above Equation 5.25. Here R_s, I_0 are a function of m. Hence this equation needs to be solved iteratively as shown in Figure 5.7 until the value of RHS converges to a specified tolerance.

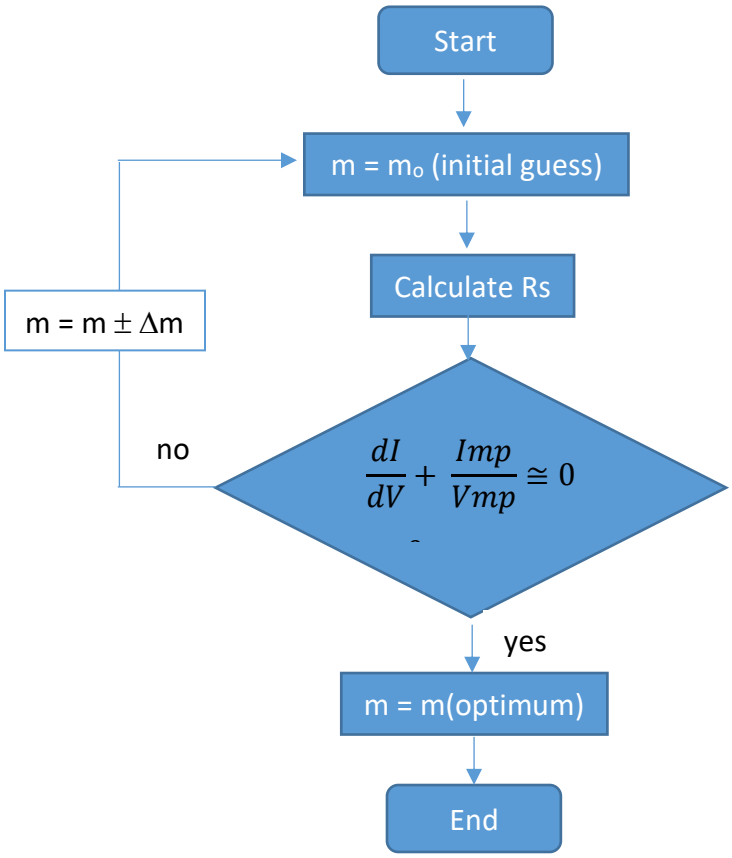

Figure 5.7: Flow chart for estimation of m and Rs

Cell Temperature

The performance of a PV module depends on irradiance and the cell temperature. Each parameter of the Equation 5.7 may well be a function of the cell temperature which in turn may depend on irradiance level and ambient temperature.

To calculate the cell temperature, we may use a standard method such one used for calculating the efficiency of flat plate solar collectors [169]. A heat transfer based method will require an estimate of the overall heat transfer coefficient (U) in W/m^2 °C in each time steps. This coefficient is one of the most complex parameters to estimate accurately because it depends on the environmental conditions as well as on the

mounting of the panels [170]. There are practical engineering approaches to go around this complexity. An MS thesis by Neises [171] at the University of Wisconsin-Madison has come up with Nominal Operating Cell Temperature (NOCT) model which is included in System Advisor Model developed at NREL [156].

For this study, we will use a simple steady-state energy balance around the PV cell. The fraction of the solar energy not converted into electrical energy is responsible for the change in temperature of PV cells. Hence we may write,

$$G_T(1-\eta) = U(T_C - T_{amb}). \qquad \text{Equation 5.26}$$

The cell temperature is estimated by rearranging equation above,

$$T_C = T_{amb} + G_T(1-\eta)/U\ . \qquad \text{Equation 5.27}$$

We estimate U using the typical operational specification that is included in PV Module specification. For AstroPower 120W Module (AP-120), the NOCT is 45°C which is calculated at the irradiance of 800 W/m^2, Tamb = 20°C, and wind speed of 1 m/s. Following Equation 5.26, this results in U = 28.16 W/m^2.

In the case the ambient temperature is not available, we will assume the cell temperature is equal to the NOCT. In this study, we will use the following simplified model of the cell temperature:

$$T_C = T_{amb} + 0.0312\ G_T. \qquad \text{Equation 5.28}$$

Load Matching: Renewable Only system

For one of the three design options, the renewable only system, there will be no battery storage in the system. The Grid-Tied Inverter (GTI) is connected directly to the grid. The GTI mirrors the amplitude and frequency set by the grid and operates as a current source inverter [172]. In such a directly-coupled configuration, it is crucial to match outputs of PV array with that of the grid. The load variation will have an impact on the output of the PV array.

For a directly coupled solar system it is important we design the system such that the overall system is optimized for long-term operation. We need to match the load characteristics to the characteristics of the PV array. Kou et al. [160] extracted the third order polynomial relation among current, voltage, flow and head from the specification of pump-motor. The polynomial relationship is then utilized in order to design an optimal direct-coupled water pumping system and estimated the long-term performance. In general, the load could be represented by a polynomial of form I = *f* (V). A general n degree polynomial will have a form:

$$I = a_n V^n + a_{n-1} V^{n-1} + \cdots \ldots + a_2 V^2 + a_1 V + a_0 . \qquad \text{Equation 5.29}$$

In MATLAB, this polynomial can be represented by vector p of length n + 1, where

$$p = [a_n, \ a_{n-1}, \ldots \ldots a_2, \ a_1, a_0].$$

Linear load is a resistive load. The linear and quadratic load may be special cases of interest:

a) Linear Load I(L) = $a_1 V + a_0$

$$p = [0, \ a_1, a_0]$$

b) Quadratic Load I(Q) = $a_2 V^2 + a_1 V + a_0$

$$p = [a_2, \ a_1, a_0]$$

We test the load matching algorithm considering linear and quadratic loads. Table 5.4 presents two quadratic and linear loads tested against Astropower 120 W (AP-120) Module with n = 36 cells. The results shall be compared with the graphical solution obtained from the analytical equations and the digitized I-V curves utilizing data reverse engineering software DataThief [173]. In Figure 5.8, we illustrate graphical solution for two linear loads.

Table 5-4: Test Load Cases for directly coupled PV System

Quadratic Load		Linear Load	
Load	Equation	Load	Equation
L(Q1)	I(Q1) $= 0.06V^2 - 0.6V + 1.5$	L(L1)	I(L1) = -75 + 5 V
L(Q3)	I(Q3) $= \frac{V^2}{2.8} + 2 = 0.357\ V^2 + 2$	L(L2)	I(L2) = -10 + 1.25

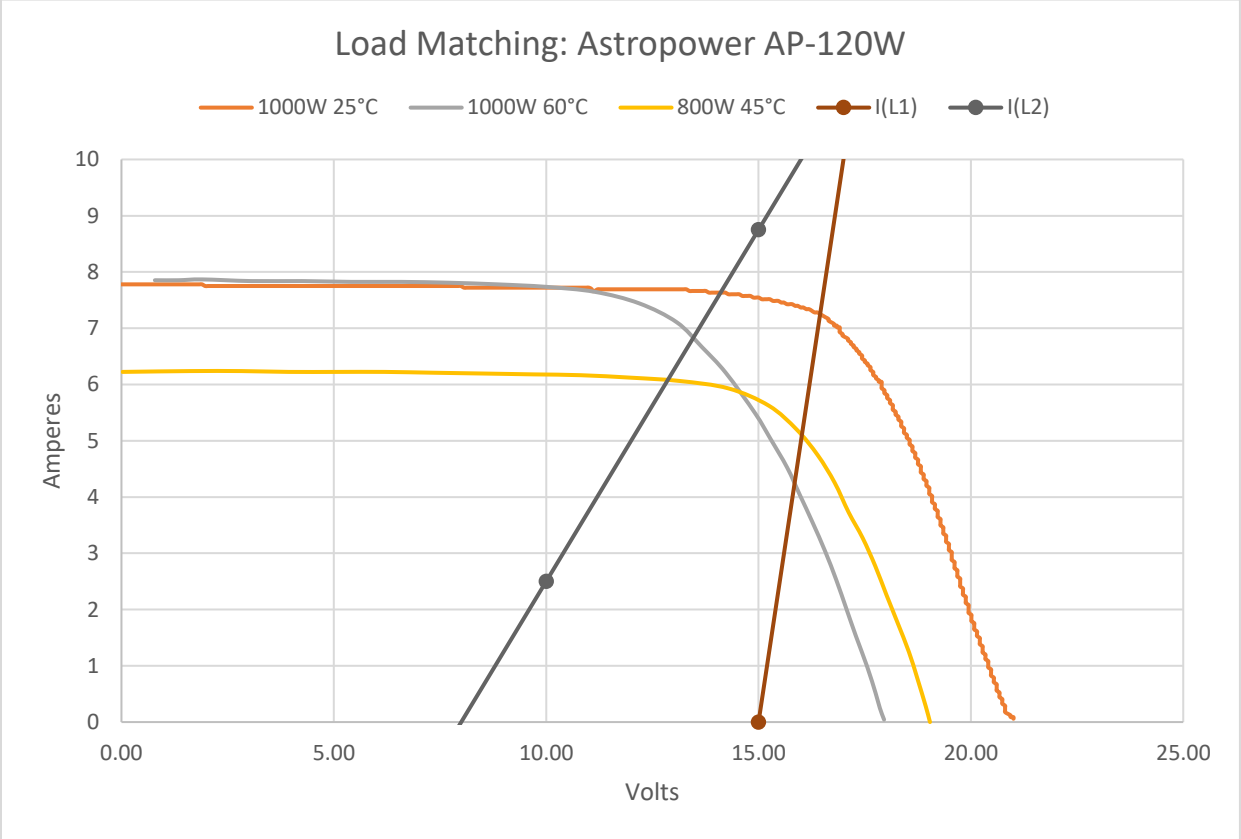

Figure 5.8: Load matching for a directly coupled PV system

A grid-tied solar inverter can also be linked internally with the maximum power point tracking (MPPT) systems [174]. 'Grid-tied Solar Micro Inverter with MPPT' is one of such devices by Texas Instruments [175]. In this study, we did not consider such advanced grid integration options.

5.4 Wind Turbine Model

We will use a simplified version of the wind turbine performance model documented in the Hybrid2 Theory Manual [4]. Our performance model deals with only one turbine at a time. It does not attempt complex interactions among turbines within a wind farm. This is rarely a case for rural electrification involving hybrid microhydro system.

5.5 Integrated Model

We propose to simulate hybrid microhydro systems within the framework of Hybrid2 developed at the Renewable Energy Research Laboratory (RERL), University of Massachusetts. The principles of Hybrid2 code are documented well in its Theory Manual [4]. The probabilistic/time-series performance analysis approach of Hybrid2 bases on the energy balance in each time step. The energy balance is an essential feature of time series (or quasi-steady state) approach for the simulation to be internally consistent. In other words, the demand and supply of electricity are matched in each time step of simulation in order to make sure the electricity confirms to the voltage and frequency set by the electricity standards. The energy balance we will use for this study is sketched in Figure 5.9. This study will use the standard time step of an hour. Any fluctuation in the loads at lower time scale shall be assumed normally distributed about the mean value and will be handled using the probabilistic approach used in Hybrid2.

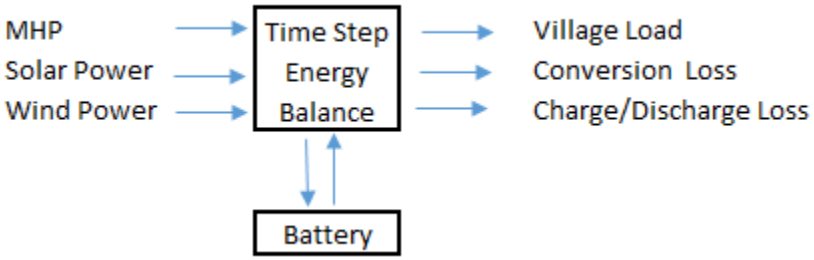

Figure 5.9: Schematic of Energy Balance

This research focuses on the development of an MHP module and its integration with other renewable resources. An MHP module primarily consists of models for the resources and the generator. In the section it follows, we propose resource models to generate an hourly time series of streamflow and a model of regulated MHP systems. Such a model can be utilized to evaluate alternate designs that may include a regulated microhydro system along with a small pond to store water.

A flowchart portrayed in Figure 5.10 outlines the integrated performance model we propose for this study. It includes the probabilistic approach within the time step of modeling and dispatch strategy based on the net load. Taking inter-temporal variations into account in tandem with quasi-static simulation is one of defining features of Hybrid2. This feature is included in this model in a simplified way. This model shall be used to study the following three cases:

a) Existing system: Unregulated MHP and battery,
b) Renewable + battery system: regulated MHP,
c) Renewable Only system: regulated MHP.

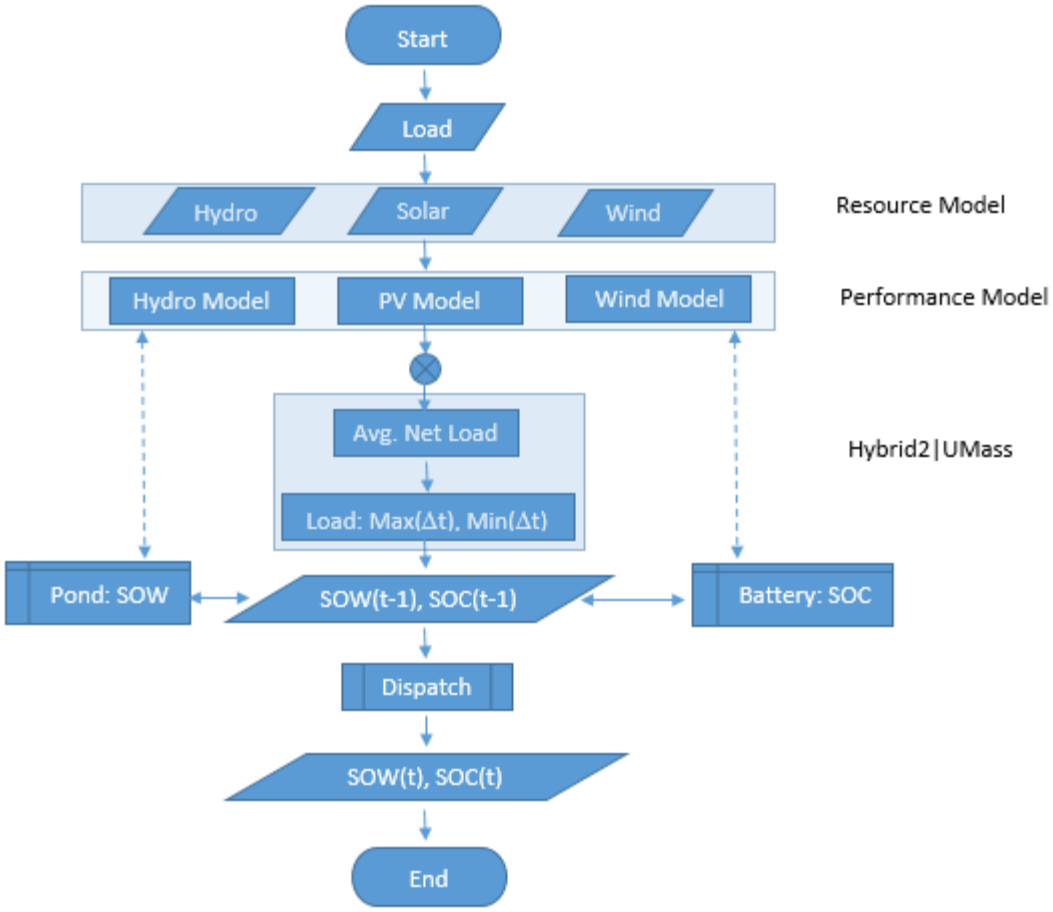

Figure 5.10: Integrated model of hybrid MHP system in the framework of Hybrid2.

A detailed method in order to characterize the Net Load is documented in the Hybrid2 Manual [4] in Section: Principles of Hybrid2 Code. The Net Load is assumed to be distributed normally with a standard deviation which is a function of standard deviations of wind speed and loads. A concept of disregarded net load probability has been used to compute the maximum and minimum load for each time step. The Error Function has been utilized to calculate the load extremums: "Load: Max(Δt), Min(Δt)". The next section elaborates some of these calculations.

5.6 Performance Metrics: Unmet Load

Of various performance metrics of HES, an unmet load is one of the defining variables for its analysis. In this section, we briefly describe how the integrated model presented in the previous section is used to calculate the unmet load. This method of calculation is an extension of the Hybrid2 method [4], and uses the similar notations:

$\bar{L}$ = Mean net load,

$\bar{W}$ = Mean wind power,

$\bar{S}$ = Mean solar PV power,

H = Dispatchable microhydro up to H(max),

B = Dispatchable battery power up to B(max),

C(xi) = Constraints of subsystem xi, includes generators plus battery,

V = Wind speed.

Note that we have prioritized the dispatch of generators/storage in order: i) solar + wind, ii) microhydro and iii) battery. The unmet load can be calculated based either on the average load or on the maximum load. The probabilistic approach of the Hybrid2 leads to minimum and maximum values of the load for a given time step of the simulation.

A. Unmet Load (Average)

The unmet load based on the average load is

Unmet load (Average) = $\delta(\bar{L} - \bar{W} - \bar{S}$ – H (max) – B(max)), Equation 5.30

$\forall$ C(subsystem) = True,

where $\delta(x) = x$ if $x > 0$; and

$= 0$ if $x \leq 0$.

B. Unmet Load (Maximum)

The unmet load (maximum) within the time step of simulation is calculated based on the Net Load and standard deviations of the load as well as the wind power.

Net Load $\bar{N} = \bar{L} - \bar{W} - \bar{S}$ Equation 5.31

The variability of the Net Load $\sigma_N^2 = \sigma_L^2 + \sigma_W^2$. The standard deviation of wind power is calculated using $\sigma_W = \bar{W}\, F_{WPT}\, \frac{\sigma_V}{\bar{V}}$, where the wind power turbulence factor $F_{WPT} = 1.5$, a value for a single turbine. The load is assumed distributed normally with standard deviation σ_N. Load L in a time step can take any value in the range $[(\bar{N} - n\,\sigma_N) < L < (\bar{N} + n\,\sigma_N)]$. The user can choose a value of n; by default n = 2 which correspond to a probability p of about 0.945. If n = 3, p = 0.997. More discussion on the relationship among fluctuations in wind speed, wind power and load can be found in the Hybrid2 manual [4].

Unmet load (Maximum) = $\delta((\bar{N} + n\,\sigma_N)$ – H (max) – B(max)). Equation 5.32

For each time step, we calculate maximum dispatchable power 'GPMax' which is a sum of H (max) and B(max). The GPMax is then compared against NLMax = $\bar{N} + n\,\sigma_N$ to evaluate if the hybrid MHP system has enough reserve to deliver the unmet load.
The MATLAB® code used for computing unmet load is documented in Appendix A.1. This code utilizes a function `probHy2` documented in Appendix A.2.2.

5.7 Conclusions

In this section we described various performance models used in this study. A non-dimensional model of MHP performance is proposed for regulated MHP plant. The two-parameter model is based on a truncated power series. The coefficients are estimated based on an empirical data using the least-square methods. A minor revision has been proposed to the UMass Model for PV panel performance. The revision may help capture I-V curves better for thin-film based PV panel. An integrated model of Hybrid2 has been expanded to include MHP module.

CHAPTER 6

ANALYSIS OF THE HYBRID SYSTEM

6.1 Introduction

The hybrid energy system at Thingan consists of tripartite generators and a storage system. Figure 6-1 depicts a sketch of the tri-hybrid system. The base configuration includes subsystems as tabulated in an inset at the bottom right corner. The Grid-Tied Inverter (GTI) manages typically two-way energy transaction between the storage (battery bank) and the electric grid. At Thingan, the GTI is used to route excess power into the mini-grid connecting the two villages [15]. We are interested in the optimal size of the regulated MHP for various configuration of storage systems enclosed in the grey boxes. The regulated MHP system, as discussed in previous sections, is comprised of a Flow Control Devise (FCD) and State of Water (SOW_{max}) that characterizes maximum volume of water in cubic meters the pond can hold.

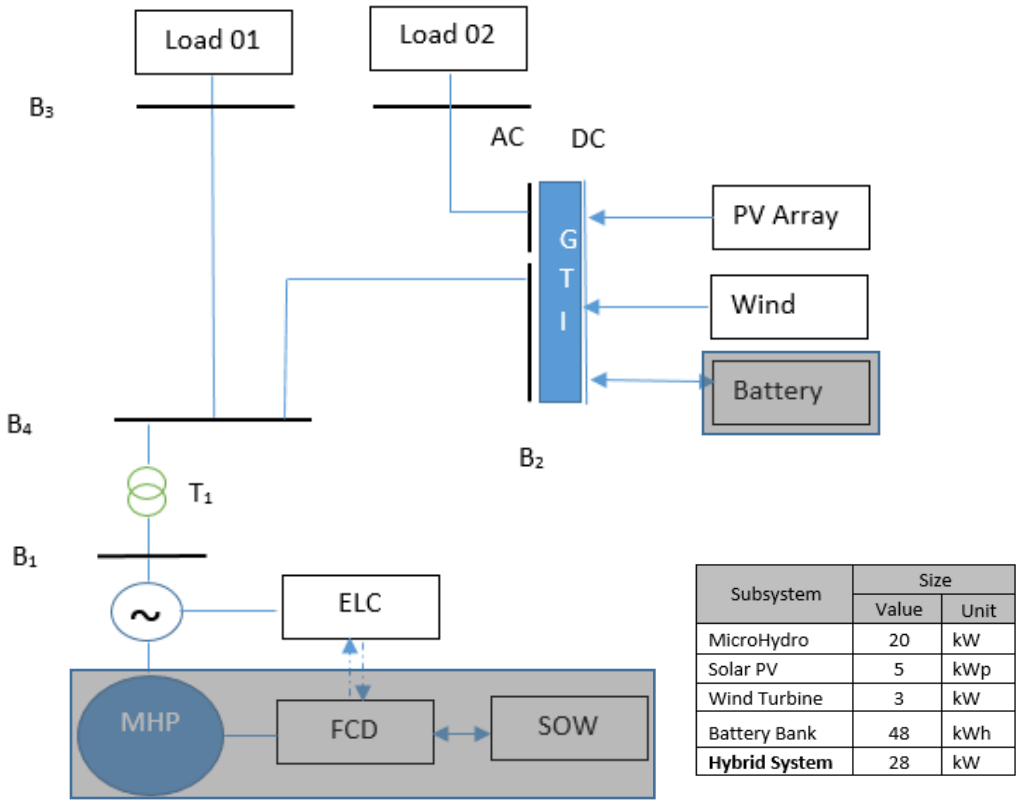

Subsystem	Size	
	Value	Unit
MicroHydro	20	kW
Solar PV	5	kWp
Wind Turbine	3	kW
Battery Bank	48	kWh
Hybrid System	28	kW

Figure 6.1: Trihybrid system at Thingan

In this Chapter, we summarize results of integrating various resource and performance models we discussed in the previous section. These models are implemented in MATLAB® environment. We simulate various configurations in order to identify configuration that delivers the best technical performance within the class. For a given load, we are interested in exploring a relationship between the design flow rate, Qdesign, of the MHP system and corresponding size of the pond (SOW_{max}). Obviously, we want to come up with a minimum size system (MHP + storage) that can deliver on the design load requirements stipulated by the Multi-Tier framework [176]. An hourly time series consisting of load and electricity supply shall be analyzed in order to infer the technical performance of various configurations of hybrid MHP systems.

6.2 Analysis Matrix and Statistics

We analyze HES for a range of MHP size and the maximum size of the pond (SOW_{max}) for three configurations of the battery bank. Table 6-1 presents ordered pair of MHP size in kW and pond size in SOW. Those three configurations of battery bank consist two, one and zero number of the string respectively. Each string is comprised of 20 lead-acid batteries (Exide 12 V/100 Ah). For regulated MHP system, we compare various statistics for each of 77 ordered pairs indicated in Table 6-1 below.

Table 6-1: Performance Analysis Matrix

$SOW_{max}\downarrow$ P(MHP)$\rightarrow$		MHP size (kW)										
		20	21	22	23	24	25	26	27	28	29	30
Pond size (SOW)	0	X	X	X	X	X	X	X	X	X	X	X
	0.25	X	X	X	X	X	X	X	X	X	X	X
	0.5	X	X	X	X	X	X	X	X	X	X	X
	0.75	X	X	X	X	X	X	X	X	X	X	X
	1	X	X	X	X	X	X	X	X	X	X	X
	1.25	X	X	X	X	X	X	X	X	X	X	X
	1.5	X	X	X	X	X	X	X	X	X	X	X

For each ordered pair (also called configuration) we run hourly performance simulation over a year. Based on the resulting time series of performance data, we compute statistics described in Table 6-2. These statistics can inform the configuration that can deliver best technical performance with reference to the load profile.

Table 6-2: Performance Statistics

SN	Description	Unit	Symbol
1	Unmet Load Hours: Average Load	Hours	umLh
2	Unmet Load kWh	kWh	umLkW
3	Unmet Load Spinning Reserve Ratio	-	umLsr
4	Unmet Load Hours: Net Max Load	Hours	sRh
5	Spinning Reserve Ratio: Net Max Load	-	sR
6	Excess Energy Hours	Hours	exEnh
7	Excess Energy kWh	kWh	exEnkW
8	Energy In Battery Bank (Hours)	Hours	Ein_h
9	Energy In Battery Bank (kWh)	kWh	Ein
10	Energy Out Battery Bank (Hours)	Hours	Eout_h
11	Energy Out Battery Bank (kWh)	kWh	Eout
12	Energy Needed from MHP	kWh	Hydro_Phneed
13	Energy Served by MHP	kWh	Hydro_Phserved
14	Extra Running Hours of reg-MHP	Hours	exEn_regHydro_h
15	Extra Energy from reg-MHP	kWh	exEn_regHydro
16	Extra Hours compared to unReg-MHP	Hours	exEn_Load_h

Sometimes identification of an optimum configuration could easily be a subjective question demanding a tradeoff between various competing statistics. We handle such situation case by case basis. A marginal economic analysis technique which we will touch upon in a subsequent section can be of a help. A detailed uncertainty estimation is beyond the scope of this thesis. We incorporate uncertainty tangentially by taking a factor of safety in size of the design.

6.3 Unregulated MHP System

The existing HES at Thingan employs an unregulated MHP system. This system does not have a pond. Hence, we simulated the performance of HES only in one dimension - the MHP size ranging from 20 to 30 kW. Figure 6-2 presents hours of the unmet load based on the average load and the maximum net load within an hour, which is the default time step of the simulation.

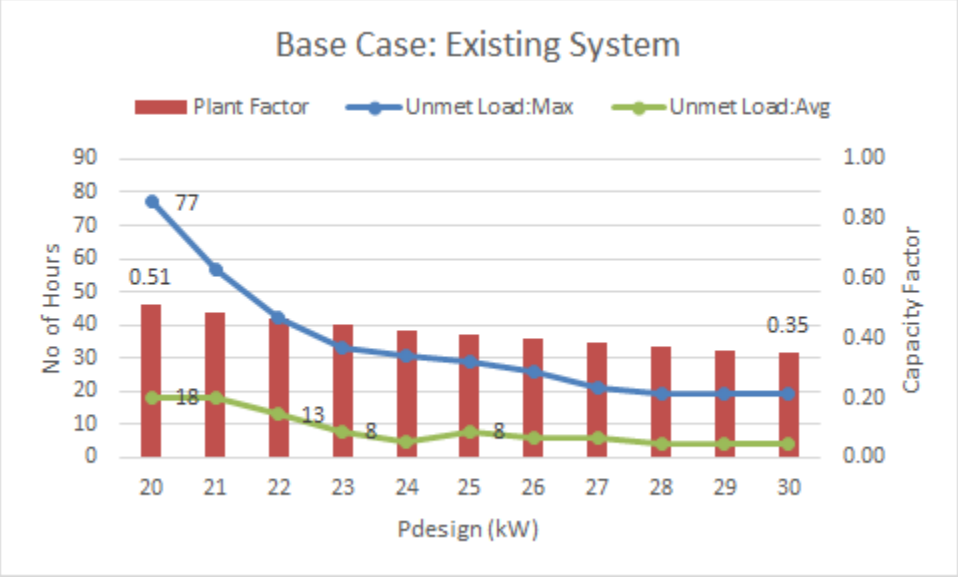

Figure 6.2: Unmet load in hours – Case C01

In a typical year, this long-term performance analysis shows that the existing unregulated system (i.e., 20 kW MHP) may miss delivering the load 18 hours on average. However, if we consider the inter-hourly normally distributed variation, this system might miss load 77 hours in a typical year. If the MHP size is increased to 23 kW, these two unmet loads decrease to 8 hours and 33 hours respectively. Beyond this size, the unmet hours (based on the Net Maximum Load) decrease asymptotically. The capacity factor of existing MHP plant is about 0.51, which decreases almost linearly to 0.35 if the size is increased to 30 kW.

It is essential to look at the performance of the storage system to have a better hold on the sizing of a HES. Figure 6.3 presents statistics of battery bank utilization for the given range of MHP size. The number of hours energy is taken out of the battery bank decreases from 855 to 212 hours in a typical year as MHP size increased to 30 kW. The existing system utilizes the battery bank about 9.7% of the time, mainly during the evening peak-hours. On average 4.78 kWh is exported during those peak-hours. This value reaches a minimum value of 3.73 kWh for an MHP size of 25 kW.

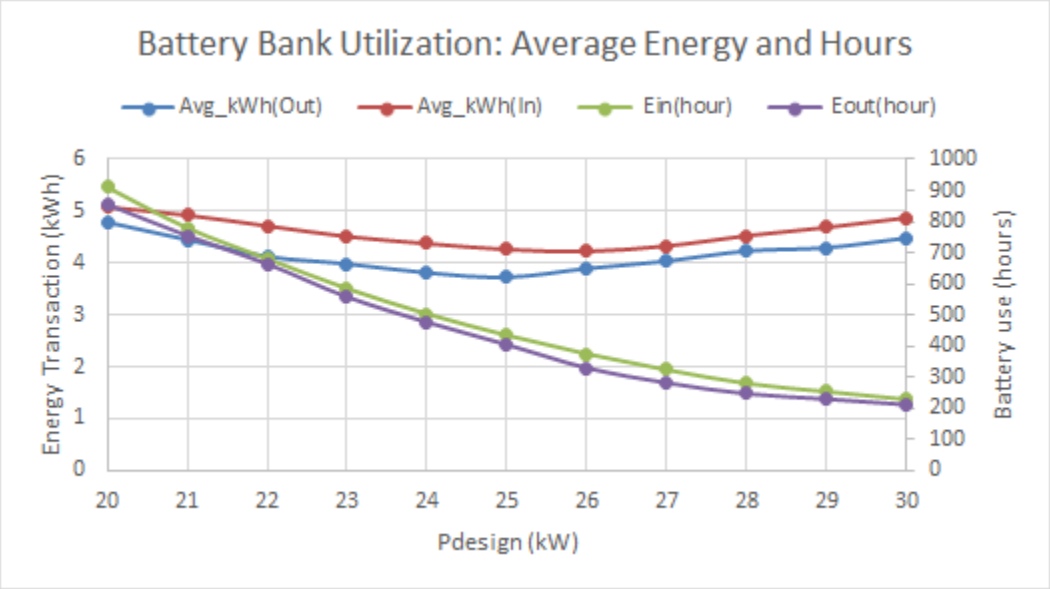

Figure 6.3: Battery bank utilization

6.4 Regulated MHP System

A regulated MHP system utilizes a flow control device (FCD) together with a small pond that can store water enough for an hour or two. Unlike the unregulated system, it is assumed in this study that a regulated MHP system can deliver maximum power 1.2 times its rated capacity.

6.4.1 Renewable and Battery system

In this case, we study MHP systems along with a battery bank half the size of the existing system. This results to one string of battery bank consisting 24 kWh storage. Likewise in the previous case study, we simulate MHP systems ranging from 20 to 30 kW. However, unlike the previous one, this configuration includes a pond. We choose to increment size of pond (SOW) by 15 minutes with upper limit set to 1.5 hours.

Figure 6.4 presents a contour plot of the unmet load in hours for a range of analysis matrix, see Section 6.2. The optimal design for best technical performance came out to be 24 kW MHP system with SOW = 1.0 Hours. This design will deliver the average load all year around except less than three hours in a typical year. The same value based on the Net Maximum load is found to be 29 hours. This unmet load translates to almost 100% reliability of the hybrid MHP system.

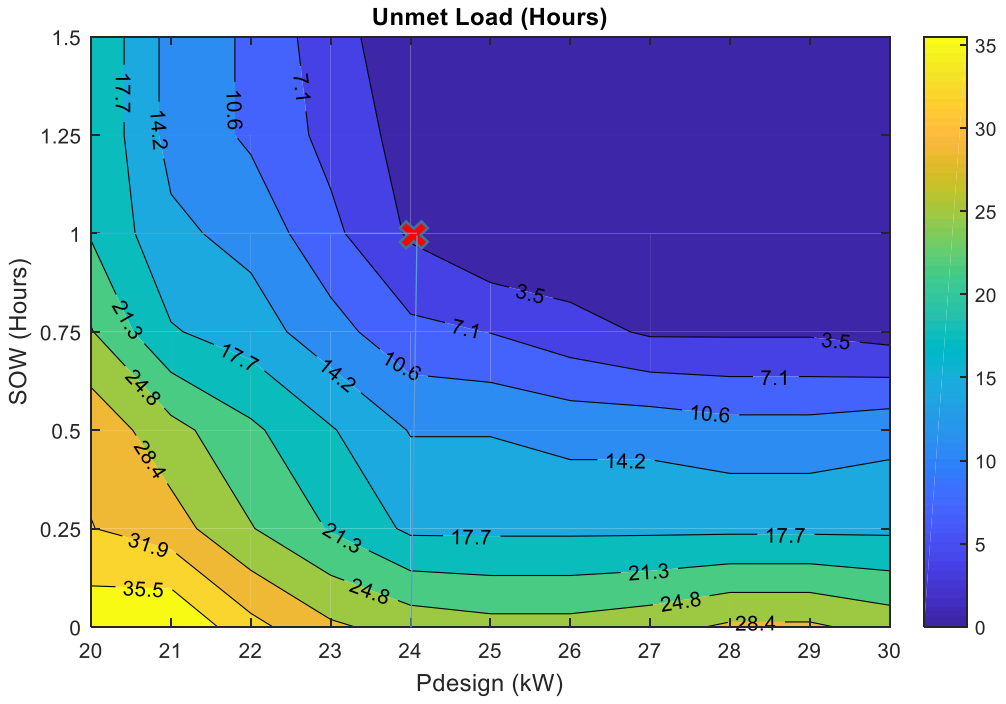

Figure 6.4: Unmet Load in hours – Case C02

The optimal technical design is marked by a red cross in Figure 6.4. We will carry out a detailed economic analysis for this design in the next section.

The Unmet Load can be expressed either in hours or in kWh. We summarize in Figure 6.5 the total unmet load in kWh for the analysis matrix in Table 6-1. For configurations P(MHP) ≥ 24 and SOW ≥ 1.0, the unmet load based on average is almost nil. This region is depicted in Figure 6.5 by a flat surface painted in a dark blue color.

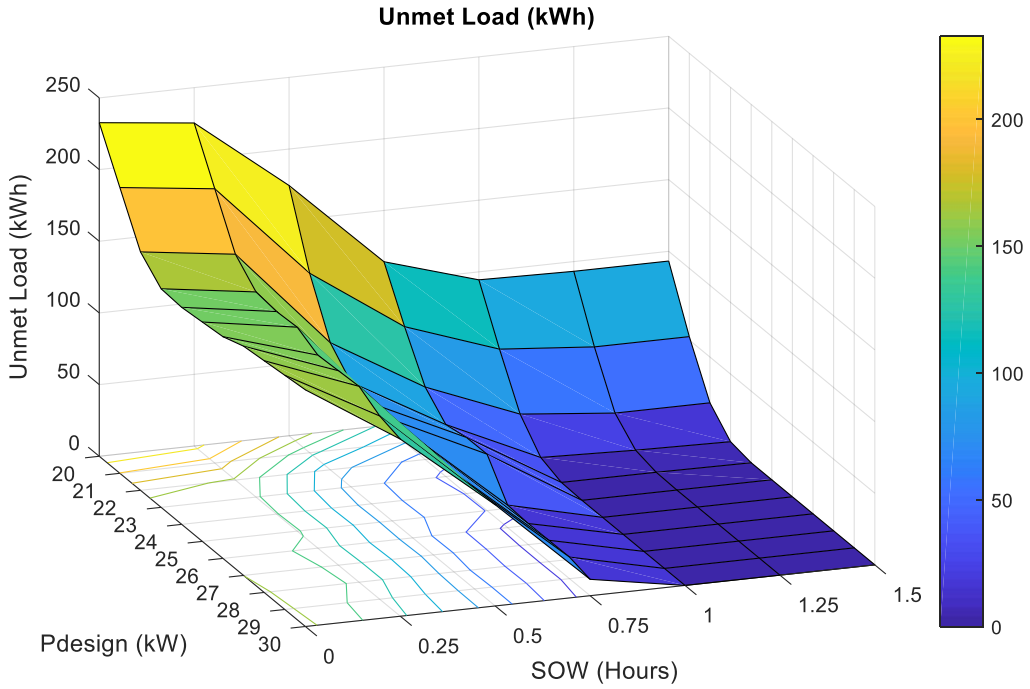

Figure 6.5: Unmet Load in kWh – Case C02

The unmet load for unregulated MHP was about 50 kWh. For this regulated MHP case with half the battery size, the unmet load for the base 20 kW MHP system increases to 232 kWh in a typical year.

A battery bank utilization plot can provide important information about this class of HES. A filled contour plot of Energy-out of the battery bank is displayed in Figure 6.6. The design (P(MHP) = 24 | SOW = 1.0) we have selected for this class is marked by a red

cross. Average energy out from the battery bank for this design is about 227 kWh in a year.

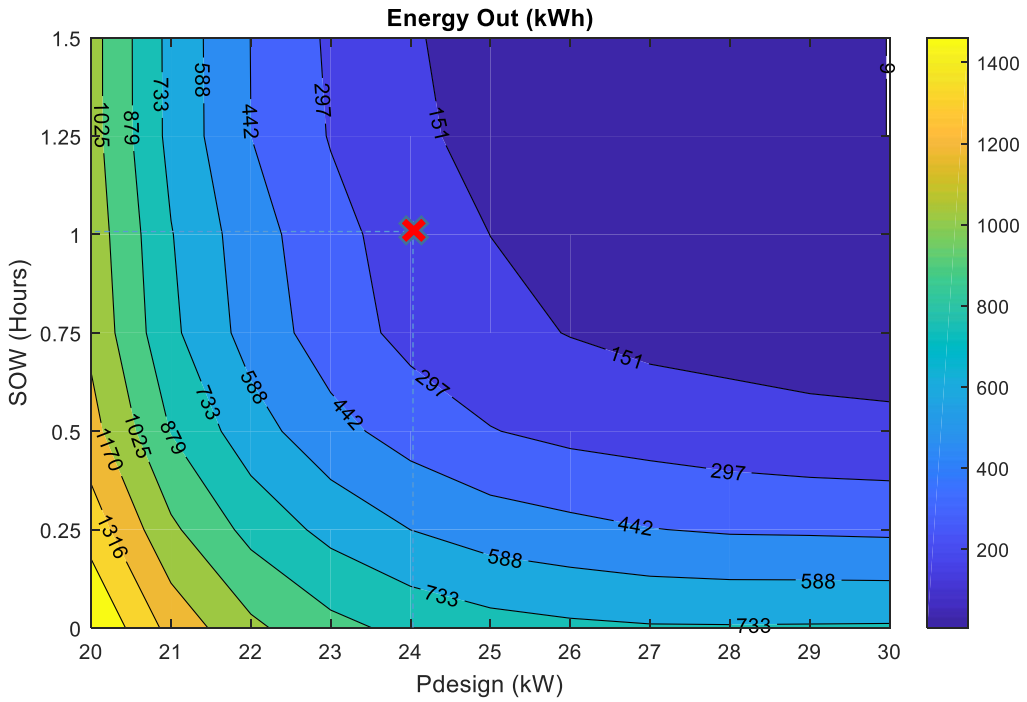

Figure 6.6: Battery bank utilization – Case C02

The isoquants representing energy-out from the battery seems to follow a Cobb-Douglas function of the form: $A\, x_1^{\alpha_1} x_2^{\alpha_2}$, where x_1 may represent Pdesign (kW) and x_2 the SOW.

6.4.2 Renewable Only system

This class of system utilizes a regulated MHP, but there is no battery bank as such. To simulate this system, we set up the number of string parameter to zero in the MATLAB code. Figure 6.7 portrays a filled contour plot of the unmet load in hours for a range of the analysis matrix discussed in Section 6.2. The RE only design C03 we have chosen for an economic analysis is marked by a red cross, as usual. The C03 design with P(MHP) = 26 kW | SOW = 0.75 misses the average load less than 35 hours in a year.

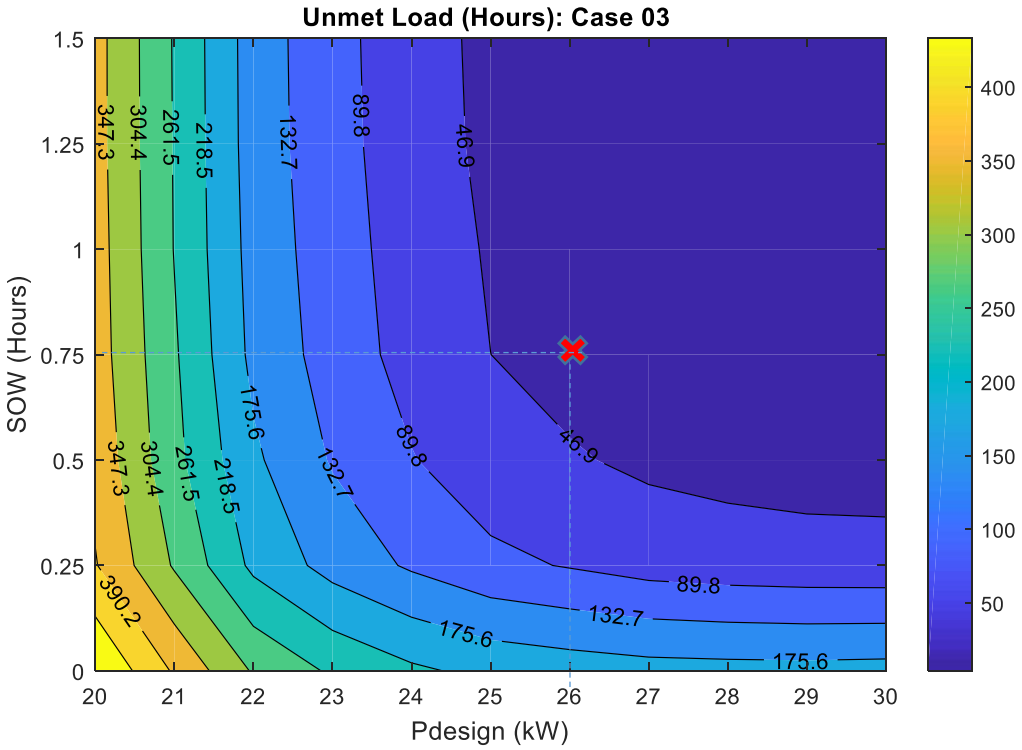

Figure 6.7: Unmet load in hours – Case C03

6.5 Case Studies: Optimal Configurations

The three classes of Hybrid MHP system we discussed in previous sections are:

1) Base case - Existing system (unregulated microhydro plant),
2) Renewable + battery system (with regulated microhydro plant), and
3) Renewable only system (with regulated microhydro plant).

The optimal configuration within each class was selected considering technical performance only, with focus on minimizing the MHP size and/or size of the pond. Table 6-3 presents three configurations, one on each class we aim to study further. It includes the MHP size and the storage system for those three cases.

Table 6-3: Configuration of three case study.

Cofiguration	MHP	Pond		Battery
	kW	SOW_{max}	m^3	kWh
Base Case: C01	20	–	–	48
RE + Battery: C02	24	1.00	117	24
RE-Only: C03	26	0.75	100	–

The configurations C02 and C03 utilize regulated MHP systems. These configurations deliver best technical performance in terms of serving the load among the various options within each class. These configurations represent optimum sizes in order to serve the load profile [176]. In the following section, we present some performance statistics for those three configurations, C01 through C03, presented in Table 6-3. The economics of HES is documented in the next chapter.

6.6 Technical Performance: Statistics

In this section, we look at how various configurations perform with respect to the load profile. The load is assumed normally distributed within an hour considering inter time step variations in the wind and load [4]. We make a comparison based on two statistics, the average load and the maximum load within each hour.

1) Unmet Load

The reliability of HES may be accounted for in terms of the number of hours the total generation misses the total demand in a typical year. If we base our calculation on the average load in an hour, the existing system at Thingan misses delivering load about 18 hours in a year. This number rises to 77 hours based on the maximum load within an hour. The latter is a more realistic statistics for the unmet load. Figure 6.8 presents this unmet load for the three configurations C01 through C03. The renewable only system (C03) fails to deliver the load about 5.20 percent of the time in a typical year.

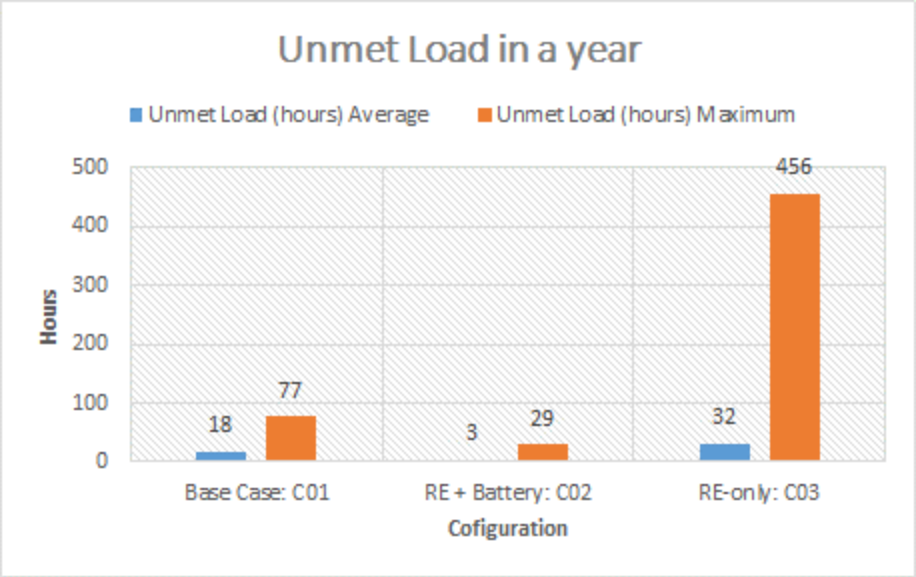

Figure 6.8: Unmet load in a typical year

For the case C03, there is a significant difference between the unmet loads. This is mainly because the system size in this case is less than the evening peak loads and there is no battery to absorb excess demand. Out of the 456 hours, it misses 243 hours at 7:00 PM and 101 hours at 8:00 PM. Here, we have considered 15% load variability within a day in addition to 5% variability within the time step.

We calculated the time the maximum load is not met within each hour of the unmet load in a year. These configurations C01 – C03 miss the maximum load on average about 20.28 minutes, 19.56 minutes, and 13.53 minutes respectively in those hours (marked by the orange columns in Figure 6.8). We will drill down into those unmet load hours to get a little more sense of load shedding within an hour in the following paragraph.

2) Distribution of Unmet Load: Maximum Load

A HES may miss the maximum load just for a few minutes in an hour. Accordingly, a load-shedding may only occur only a few minutes in an hour, not the whole hour. Figure 6.9 presents a distribution of a six-minute-segments of an hour the load is not delivered for configurations C01 through C03. Indicated by a data label, the Renewable-only

configuration C03 misses load just by less than 6 minutes for 50 % of total hours (N = 456 hours) of the unmet load in a typical year. In other words, out of 456 hours, the C03 configuration misses 228 hours of the load just by a few minutes (less than 6 minutes).

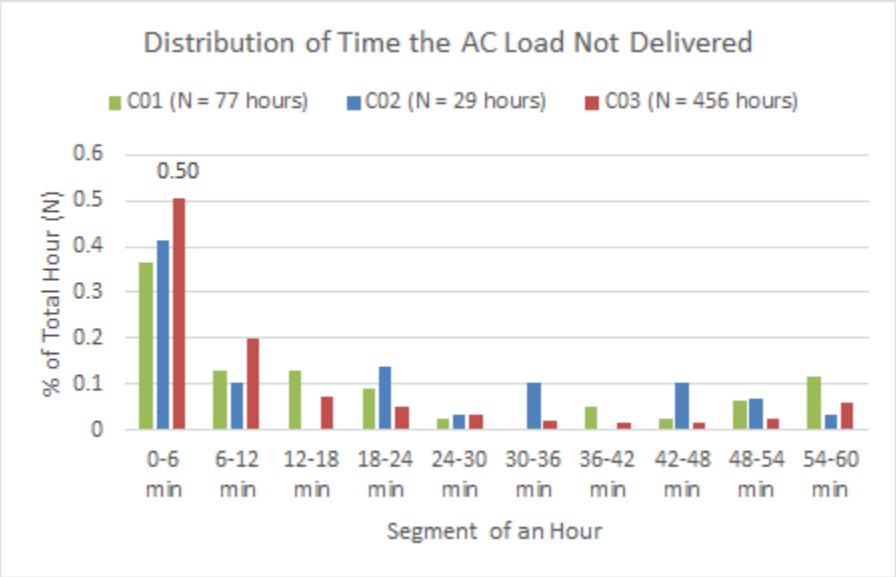

Figure 6.9: Time the AC load not delivered

In the future, a load-shedding for smaller segment of an hour may be handled by some superconducting magnetic or capacitor storage [177].

3) Unmet Load: Morning and Evening

The Multi-Tier Framework for Measuring Energy Access for HH supply [20] differentiate availability in the evening and the whole day. For this analysis, morning hours are considered 4:00 through 8:00 AM and evening hours are taken as 6:00 PM through 10:00 PM. First two of three configurations meet the morning peak the whole year but the third configuration C03 misses the same three days in a year. Figure 6.10 presents the number of days the electricity may not be available for a segment of evening hours in a typical year. The existing system C01 misses load 42 days at 7:00 PM, 29 days at 8:00 PM, and only six days at 9:00 PM in a typical year.

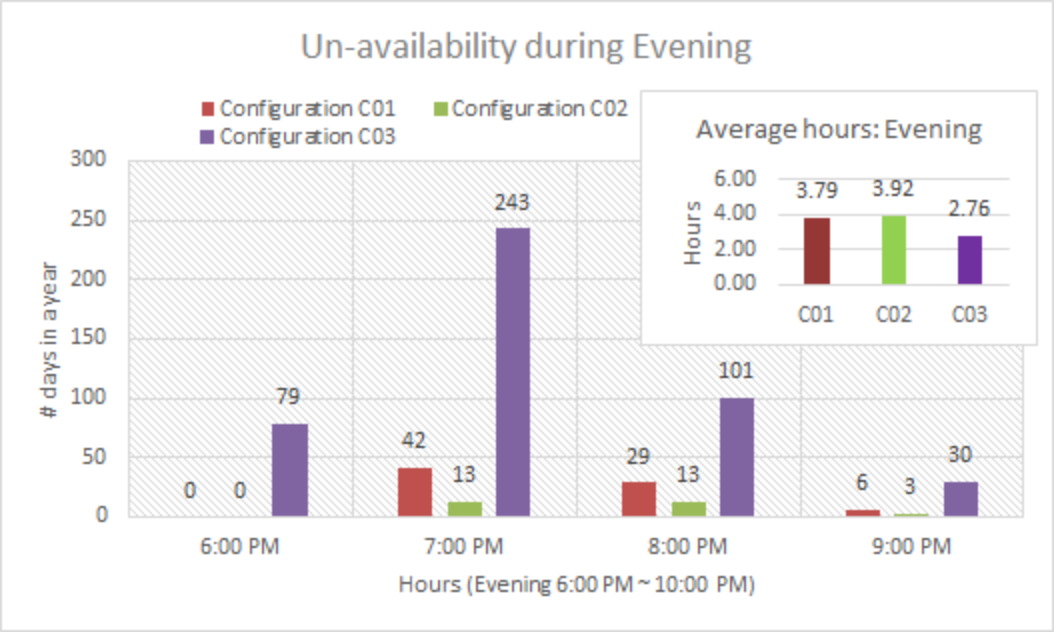

Figure 6.10: Availability hours/evening

A HES may not miss load throughout an hour but only a fraction of the hour. In the inset of Figure 6.10, we present average hours those three configurations deliver load. The configuration C01 through C03 deliver load on average about 3.79, 3.92 and 2.76 hours per evening. In order to qualify for the Tier 3 access, a HES must supply load greater than 3 hours in the evening. Accordingly, configurations C01 and C02 meet the requirements of the Tier 3 energy access while the configuration C03 does not. For completeness, we present here a segment of the Multi-Tier Framework [19] from Table 2-4.

Attribute		Metric	Tier 0	Tier 1	Tier 2	**Tier 3**	**Tier 4**	**Tier 5**
	Availability	Hours/day		> 4 hrs	> 4 hrs	> 8 hrs	> 16 hrs	> 23 hrs
		Hours/evening		> 1 hrs	> 2 hrs	> 3 hrs	> 4 hrs	> 4 hrs

All those configurations meet hours/day availability for the Tier 3 which should be greater than 8 hours a day. For the analysis above, we did not take into account the deferred load which may accumulate as a result of load-shedding.

6.7 Conclusions

We simulated the long-term technical performance of hybrid MHP systems in a framework of the Hybrid2 tool. For an hourly synthesized load profile, we explored the relationship among the size of MHP plant and storage (water in a pond and electricity in a battery bank) in order to identify optimum size of hybrid MHP system that can deliver a load profile.

For three classes of hybrid MHP system, one unregulated and the other two regulated MHP systems, we identified optimal configurations that can deliver the best technical performance within each class. We looked at the MHP size ranging from 20 – 30 kW at an increment of 1 kW, battery size ranging from two, one and zero strings, and pond size ranging from 0 to 1.5 SOW_{max} for the regulated MHP system. These optimal configurations, C01 through C03, for the three class of hybrid MHP system are reproduced in a table below (see Table 6.3). The Base Case (C01) consists of a 20 kW unregulated MHP system and 48 kWh battery bank comprised of two strings of batteries, 24 kWh each. The other two configurations, C02 and C3, utilize regulated MHP systems 24 kW and 26 kW in size along with 117 m^3 and 100 m^3 water storage ponds respectively.

Cofiguration	MHP	Pond		Battery
	kW	SOW_{max}	m^3	kWh
Base Case: C01	20	–	–	48
RE + Battery: C02	24	1.00	117	24
RE-Only: C03	26	0.75	100	–

The configurations C01 and C02 meet the availability requirement of HES under the Multi-Tier framework [176] for measuring energy access, but configuration C03 fails to do so. The latter configuration can deliver load only 2.76 hours/evening while the framework demands 3 hours per evening. A detailed analysis may help improve the

feasibility study guidelines for microhydro plants, and operation and maintenance of hybrid microhydro systems, especially during the dry seasons.

CHAPTER 7

THE ECONOMICS OF HYBRID SYSTEM

7.1 Introduction

Initial capital cost is the majority of the overall cost of hybrid energy systems that utilize renewable energy resources. The total cost consists of the capital cost of each subsystem and a fixed cost which is independent of the system configurations. The fixed cost includes the site development, any auxiliary buildings that may be necessary to house subsystems comprising the hybrid system, and O&M cost that may consist of wages of system operators and/or annual maintenance contract cost with some Rural and Renewable Energy Service Companies (RuRESCo) [29].

The economic analysis of the hybrid microhydro system is based on a dataset of projects installed earlier in Nepal [178]. We compute standard economic metrics such as a) Net Present Cost (NPC), and b) Levelized Cost of Energy (LCOE). We also carry out sensitivity analysis to evaluate sustainability of the HES based on current practices at the site in Nepal.

For each subsystem, we look at the capital cost, subsidy, O&M cost, and replacement cost. We do not include the environmental cost or any externalities because such costs are minuscule compared with the overall capital cost, and also the decommissioning and restoration at the end of the active life of the component. In Nepal, there is no production incentive ($/kWh) for renewable energy. The interest rate is taken from the Clean Energy Development Bank, acquired recently by the NMB Bank [179]. We base the discount rate on the real interest rate that includes the monetary (general) and energy inflation rate together.

7.2 Background

The economics of hybrid MHP system depends mainly on socio-economic conditions of the community in which the system resides [180]. The overall impact of access to energy on the economic development of a community could easily be a subjective analysis. A kWh generated from a hybrid system can have different functions and hence different economic impact/value depending on what we utilize the energy for. The same energy can dissipate on a dump load, or light a LED bulb to facilitate teaching and learning activities for hours, or even, in the extreme, save a life in a health post.

In addition to the regular household application of energy, a decentralized energy system may include community service and productive-use of energy [181]. A workshop organized by GEF and FAO in June 2002 has come up with the following working definition of the productive use of energy.

> "In the context of providing modern energy services in rural areas, a productive use of energy is one that involves the application of energy derived mainly from renewable resources to create goods and/or services either directly or indirectly for the production of income or value."

It is a complex task to evaluate the value of a unit of energy. It may depend on specific context and also on idiosyncratic view of the assessor. Various studies have concluded that access to electricity is a necessary condition for economic development. Aligning electrification programs with other development programs may incur a better value of a unit of energy, compared with sectoral productivity. Nonetheless, production of income is also influenced by the productive use of the energy and saved-time from chores.

The conventional economic metrics, however, may not suffice to evaluate/appraise all decentralized applications. Financially unprofitable MHP systems can exhibit strong positive impacts on the lives of the poor people, and can also achieve wide range of

quite different objectives [182]. A broader development framework that includes social-cost benefit analysis may be a more appropriate framework for an appraisal of a rural electrification project far away from the national grid. Whatsoever it is, we limit our study to conventional economics metrics.

The hybrid MHP systems are known to be marginal in economic sense. Economics of small-scale systems is very site specific. They can hardly recoup the initial capital investment for various reasons. In this study, we will look at the conventional economic indicators like c/kWh, or $/kW to make sense of these systems with reference to the utility-scale systems and general trend at the regional and national level. At planning level, cost per household may still be a useful matrix, and we always strive for minimizing the cost for a given level of energy services among alternatives.

7.3 Method and Scope of Economic Analysis

An Economic analysis involves a set of standard steps that consider a notion of time value and the opportunity cost of an investment. We use a method adapted from a guide [183] published by Asian Development Bank. A typical economic analysis of an HES project may consist of steps [184] as follows.

- Identification of project benefits and costs
- Economic valuation of benefits and costs
- Benefit valuation in different sectors
- Investment decisions and criteria
- Sensitivity and risk analysis
- Project sustainability.

In this analysis, we do not include indirect costs and benefits. Sometimes, analysts practice of internalizing the externalities in order to encompass the broader positive impacts an HES might induce. Such tangential benefits are out of the scope of this study. This study refrains from benefit evaluation in different sectors. Benefits are the revenue collected as tariffs from beneficiary households, productive-end uses, and grid

interaction, if any. We exclude decommissioning and restoration costs at the end of the active life of the component. The salvage value may offset those costs.

7.4 Cost and Benefit: Hybrid System

There has been some recent efforts toward classification and standardization of nomenclature of costs [185] associated with the minigrid system. We will classify cost into the four categories: a) capital cost per kW, b) subsidy per kW, c) O&M cost per year and d) replacement cost at the end of useful life of subcomponents. The fixed capital and O&M costs of the hybrid energy system are also included at a system level. We choose not to include environmental cost and benefit in this study. These four categories of cost are explained below.

a) Capital cost

   The capital cost includes overall investment made in the year at which the hybrid system begins its operation, sometimes known also as year 'zero' in the economic analysis. Any prior cost associated with site development are projected to year zero taking time value of money into the account.

b) Subsidy: a negative capital cost

   A subsidy is a financial aid that helps to lower the capital cost of RE project. A subsidy may be given to an RE system for various reasons. Some pronounced reasons are: to overcome market barriers, to enhance public welfare, or to enact some economic/environmental policy. In Nepal, a subsidy may depend on the size of the project or on the number of beneficiary households. Alternative Energy Promotion Center (AEPC) manages the subsidy in RE sector on behalf of the Government of Nepal. The subsidy allotment for each subsystem has been taken from these two policy documents: a) Renewable Energy Subsidy Policy 2016, and b) MHP Subsidy Delivery Mechanism 2013. In some cases, an MHP system may qualify for an additional transport subsidy based on the remoteness of the project.

c) O&M cost

The O&M costs may include service (e.g., annual maintenance contract) and any consumable items associated with the subsystem. A wind turbine may require a service every two years. Such O&M costs can be aggregated to the fixed O&M cost of the overall system, including the wage of the operators

d) Replacement cost

Some components (e.g., battery bank) of the system may have an effective life less than the life of the project, which is typically considered 20 years for HES. A battery bank of a useful life of 7 year needs to be replaced twice during the project life cycle of 20 years. A replacement cost incurs at discrete interval equal to effective life of the component. A component may have a positive salvage value at the end of the project life.

7.4.1 System Configuration and Parameters

The hybrid system has base configuration presented in Table 1-1. A new configuration, which is a focus of this study, consists of a regulated MHP system with a pond to manage water effectively during dry seasons. We study this regulated system together with a battery bank half the size of the base configuration. This configuration we have named as Configuration 02 or Case Study 02. The third configuration is a renewable only system – a system without battery bank. Under the renewable only system, named here Configuration 03 or Case Study 03, we study if a HES can still meet the Tier 3 design requirement of the Multi-Tier Framework for Measuring Energy Access [176]. A lead-acid battery bank is the weakest link of a HES system, known infamously for environmental reasons. We want to look at the performance of the system without the battery bank. The regulated system allows us to vary flow of water through turbine without dissipating much excess energy.

Two design variables of our interest are the minimum size of MHP plant and the corresponding optimum size of the pond to meet a load with an acceptable reliability.

Table 7-1 presents the size of various subsystem we consider for an economic analysis. These configurations follow on from the previous chapter.

Table 7-1: Various configuration and storage capacity

Cofiguration	MHP	Pond		Battery
	kW	SOW_{max}	m^3	kWh
Base Case: C01	20	–	–	48
RE + Battery: C02	24	1.00	117	24
RE-Only: C03	26	0.75	100	–

For configuration C02 and C03, we also carry out marginal cost-benefit analysis. This marginal analysis brings out if incremental benefits are enough to cover incremental cost with reference to the base case scenario (C01).

7.4.2 Cost of System/Subsystems

In this analysis, we explore MHP plants ranging from 20 kW to 30 kW. Accordingly, we will need an analytical equation (or a look-up table) of the cost of the system for each discrete size of MHP system we may explore.

The cost of a Pelton Turbine is sometimes expressed in terms of Cobb-Douglas function [186] of Power (P) and head (H). In a review article [187], authors from Indonesia have proposed the following relation:

$$Cost\ \left(\frac{€}{kW}\right) = 17{,}693\ P^{-0.3644725}\ H^{-0.281735}. \qquad \text{Equation 7.1}$$

This relationship resembles the generalized Cobb-Douglas function $f(x) = A\prod_{i=1}^{N} x_i^{\alpha_i}$, where $\alpha_i$is the elasticity parameter for input x_i. Following Equation 7.1, $\alpha_1 + \alpha_2 < 1$, the cost of Pelton turbine decreases with scale. The larger the size, the lower is the cost per kW of the MHP plant.

Some fixed costs of MHP system do not scale up in proportion to the size of the plant. This reflects the economy of scale of MHP system. However, for a higher side of the range, say for above 80 kW, sometime we may need a high voltage transmission, (transformers, etc.) which may add substantial cost to the initial capital cost. This cost of electric/transmission work normally increases with the size of the MHP plant [18]. In general, the higher the size and head the lower the cost per kW of the MHP system in Nepal.

Through a nodal program known as the National Rural and Renewable Energy Program (NRREP) [188] the Government of Nepal expects to install about 25 MW of mini and microhydro in order to benefit additional 150,000 remote households utilizing community electrification. Our cost estimate is based on the NRREP Baseline Document [178] published by the AEPC. Considering microhydro installations (Mid July 2011 - mid July 2012) in the range 20 – 30 kW, we have come up with Equation 7.2 for the cost of an MHP system in Nepal.

$$Cost\ \left(\frac{\$}{kW}\right) = 12{,}317\ P^{-0.445}. \qquad \text{Equation 7.2}$$

For the base configuration C01 with P(MHP) = 20 kW, we use 3247$/kW. As the size increases, P(MHP) = 30 kW, the cost decreases to 2711 $ /kW. The initial capital cost decreases by about 16% for the range of MHP plant in the analysis matrix Table 6-1.

The cost of MHP systems in Nepal are studied extensively [189, 18] . In 2008 US$, the cost per installed kW capacity varied from US$ 1850 to US$ 3455. Adjusting this cost to 2018 US$, the cost per kW will be in the range US$ 3042 to US$ 5681. Figure 7.1 presents a breakdown of total costs of five microhydro power plants [18]. The largest portion of the initial capital cost belongs to the electrical equipment, followed on by civil infrastructure and mechanical equipment. The turbine is included in the mechanical and the generator in an electrical category. Nonetheless, initial capital costs ($/kW) of MHP plants are found to be very site specific in general.

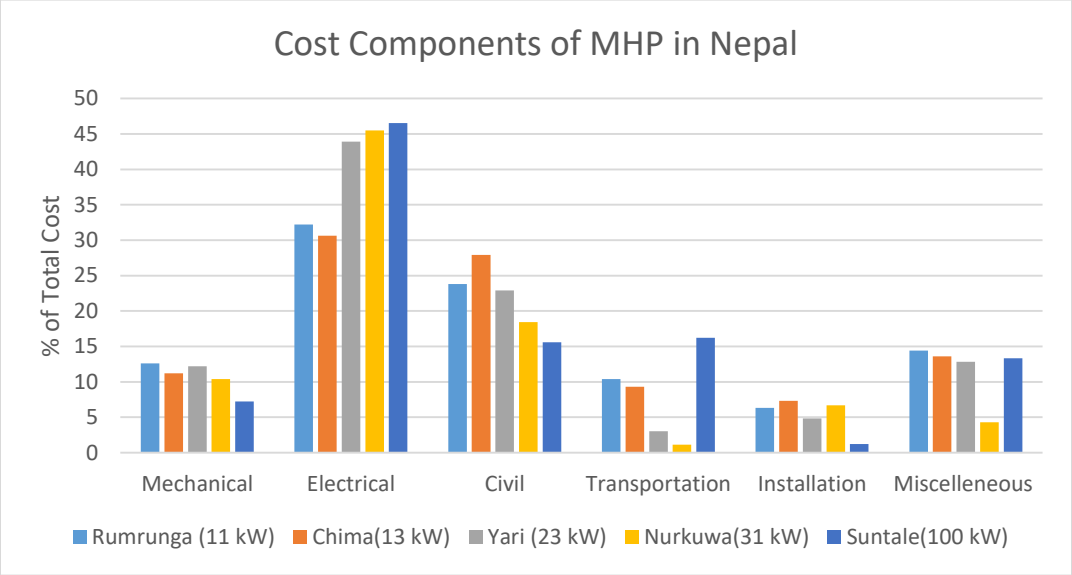

Figure 7.1: Cost components of MHP in Nepal [18]

Not all the cost details are published for the HES at Thingan [16, 128]; hence it was not possible to aggregate cost in the categories we break them down at the beginning of Section 7.4. Some costs are taken from similar HES in Nepal [29, 190]. For economic analysis, we use cost structure presented in Table 7-2.

Table 7-2: Capital and O&M Costs for economic analysis.

Subsystem	Size		Life Time	Capital cost		O&M cost
	Value	Unit	Years	US$	Unit	US$
MicroHydro	20	kW	20	3247	$/kW	100
Solar PV	5	kWp	20	5215	$/kW	10
Wind Turbine	3	kW	20	2937	$/kW	500
Battery Bank	48	kWh	7	376	$/kWh	50
Pond	117	m3	20	10	$/m3	50
Hybrid System	28	kW	20	4952	$/kW	1710

We expect innovation in storage system [191] will bring down the cost of battery bank in Nepalese market by 40% every seven years. Hence, we use only 60% of the initial

capital cost of the battery bank as a replacement cost. The O&M costs inflate at a fixed monetary inflation rate for the lifespan of the hybrid MHP systems.

7.4.3 Benefits of Hybrid Energy System

There are numerous developmental benefits that a HES can bring about in a community without access to electricity. Benjamin Sovacool [192] has reviewed the connection between modern energy services and development covering education, health, environment, etc. Many of these benefits are very site-specific and hard to quantify with a common yardstick. A typical rural household may use electricity for lighting, cooking, recreational and productive end uses such as agro-processing or other small enterprises. The affordability or willingness-to-pay may sometimes hinder many households to use electricity from the HES for cooking or space-heating. The traditional energy resources a HES may replace, or complement does not generally pass through a cash economy. In such informal sector of an economy, it is difficult to access the overall benefits in monetary terms with accuracy. Access to modern energy services may also save time from doing household chores. This time can be utilized to benefit oneself and family.

Here we will focus only the monetary benefits recovered by selling electricity to the households or enterprises. Such benefits come in the form of tariffs collected from the consumers. Sometimes tariffs are engineered to promote sustainability of operation and maximize public welfare. An electricity tariff for a HES, just like a utility scale tariff, may comprise of a fixed base cost per month plus variable cost that may change during the time of the day or season [193]. A tariff system for a small HES system should be easy to implement, at the same time be able to ensure accountability of energy use and to recuperate operational cost, at the least.

In summary, the benefits we include in this economic analysis is tariff collected monthly from the households and enterprises. The costs include initial capital cost, O&M cost and replacement cost, etc.

7.5 Economic Parameters and Metrics

7.5.1 Economic Parameters

Economic parameters for analysis of the HES at Thingan has been compiled from the various source. The interest rate is taken from the Clean Energy Development Bank, acquired recently by the NMB Bank [179]. We base the discount rate on the real interest rate that includes the monetary (general) inflation and energy inflation rate together. The general inflation data comes from the national accounts dataset published by the World Bank [194, 195]. Table 7-3 presents some economic parameters used in this study. Further details are available in Appendix B.2.

Table 7-3: Economic Parameters

Symbol	Value	Unit	Definition
i	16.00%	%	Nominal/Bank Interest rate
π	5.10%	%	General inflation rate: Monetary
πe	2.50%	%	Inflation rate of energy
r	10.37%	%	Real interest rate
T	20	years	HES economic lifespan
coe	7.30	NRs/kWh	The Economic value of energy

The bank interest rate is higher than the real interest rate because of the general inflation rate. The Fisher Equation relates the nominal interest rate (i) to the real interest rate (r). This equation can be expressed as,

$$r = \frac{1+i}{1+\pi} - 1 = \frac{i-\pi}{1+\pi}. \qquad \text{Equation 7.3}$$

Generally the energy inflation rate is greater than the general inflation rate. On the contrary, it is the other way around in this study. In Nepal, the energy market is regulated partly by the government. The economic value of energy is obtained from the "Grid Connected Alternative Energy Development Guideline 2074" published by the Ministry of Energy in Nepal [196]. It is based on tariff for the energy consumption block in the range 21-50 units (Single Phase) by the national utility [197]. The foreign

exchange rate is taken from the Central Bank of Nepal [198]. We use average selling rate for the year 2017 as an exchange rate, which turns out to be 1US$ = NRs 104.50.

7.5.2 Net Present Cost

The total Net Present Cost (NPC) represents the full cost of a system. The NPC condenses all the costs and revenues that occur within the project lifetime into a single lump sum in present dollars, with future cash flows discounted back to present using a discount rate. Costs may include capital costs, replacement costs, O&M costs, insurance costs, etc. Revenues may include income from selling electric power to the customers, plus any salvage value at the end of the project lifetime. When calculating the NPC, costs are positive, and revenues are negative, which is opposite to the process for calculating the net present value.

The net present cost of establishing and operating a stand-alone renewable energy system, NPC^{RE}, can be represented as:

$$NPC^{RE}(E) = \sum_{n=1}^{N} (k_n^{RE} - s_n^{RE})\, W_n(E) + \sum_{t=1}^{T} \frac{o_t^{RE} - R_t^{RE}}{(1+i)^t} + MG(E)$$

Equation 7.4

where:

E is the designed total annual electricity supply target in kWh, based on the assessment of electricity demand in the village,

N is the total number of renewable energy technologies adopted,

T is project lifespan in year,

i is the discount rate in % (normally taken as the interest rate),

$W_n(E)$ is the installed capacity for nth type of RET, in kW, optimized in a portfolio way to meet the load demand in the village, in kW

k_n^{RE} is the unit capital cost for the nth type of RET, in US$ per kW,

s_n^{RE} is the subsidies from all sources for the nth type of RET, in US$ per kW,

o_t^{RE} is the O&M costs in year t, in US$, which includes and the cost of replacing energy storage systems (e.g., the battery bank),

R_t^{RE} is the revenue in year t, in US$, from tariff,

$MG(E)$ is the NPC associated with the marginal cost of energy to meet demand forecast.

7.5.3 Levelized Cost of Energy

The levelized cost of energy (LCOE) is defined as the price at which electricity services generated from a specific source must be paid to break even over the lifetime of the project. It is very beneficial to calculate such costs for different approaches to meet the same electricity demand and find out which approach is the most efficient. The LCOE for a hybrid energy system for rural electrification can be calculated as:

$$LCOE^{RE} = \frac{\sum_{n=1}^{N}(k_n^{RE} - s_n^{RE})\, W_n(E) + \sum_{t=1}^{T} \frac{o_t^{RE}}{(1+i)^t}}{\sum_{t=1}^{T} \frac{E_t}{(1+i)^t}}$$

Equation 7.5

Equations 7.4 and 7.5 are adapted from a paper published earlier [29].

7.5.4 Payback Period

The HES at Thingan can never pay back the initial investment at the present cost of energy which is about 6.98 cents/kWh. The NPC was found to be positive for all those three optimal configurations, see economic metrics in Figure 7.2. The economics might look different if there was an option of grid interaction as the MHP can run at the rated power and be able to sell excess amount to the grid. A study by AEPC has shown MHP systems with more than 25 kW capacity, at a distance of less than 3 km from the existing 11kV line, are financially viable for grid connection [199].

7.6 Case Studies and Scenarios

In this section, we present a summary of economic analysis carried out using MS Excel (documented in Appendix B.2) with the existing tri-hybrid system at Thingan as the base case. Basically, we are interested in those three configurations, see Table 7-1. These configurations deliver a best technical performance meeting the hourly time series of the load among the various options we study within each configuration.

We look at Levelized Cost of Energy (LCOE) and Net Present Cost (NPC). These economic metrics are computed for various configurations. Figure 7.2 presents the LCOE on the primary axis and NPC in Thousands on the secondary axis. For the Base Case (C01) we present those values for cases with the subsidy and without the subsidy. The LCOE = 0.20 $/kWh (with subsidy) and LCOE = 0.35 $/kWh (without subsidy). The NPC for these two cases is $90,018 and $217,753 respectively.

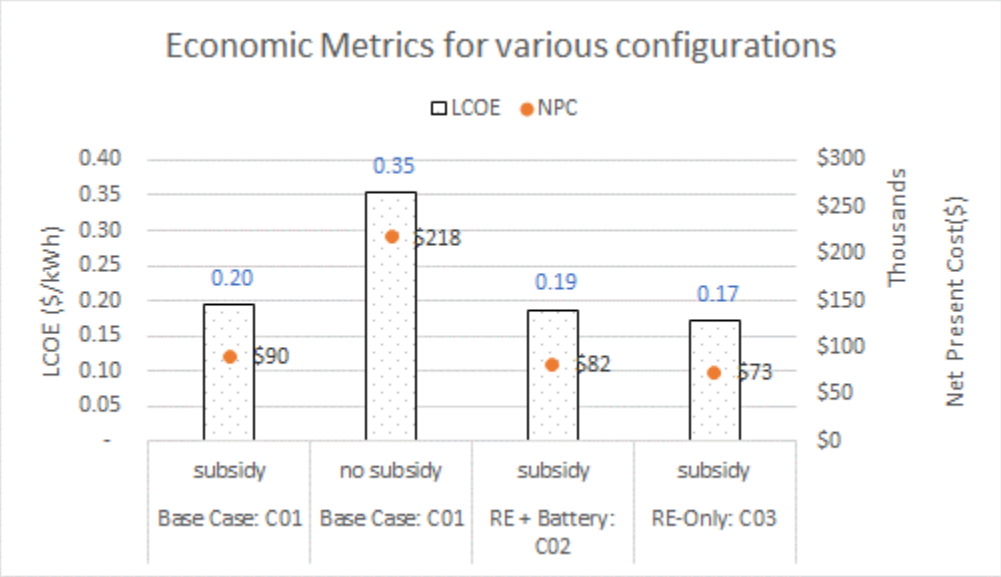

Figure 7.2: Economic Metrics for various configuration, with/without subsidy

For the regulated systems, the LCOE is found not very significantly different than the base configuration (C01). The LCOE for RE + Battery (C02) and RE-Only (C03) configurations are found to be a cent and three cents cheaper respectively in comparison to the base configuration. The NPC is preceded by the $ sign and expressed

in Thousands. For configuration C02 and CO3, the NPC turned out to be 82,336 and 72,919 respectively.

A study published in 2013 claims the LCOE of MHP plants in Nepal varies between 0.28 and 0.35 USD/kWh for the 25 kW plant, and between 0.25 and 0.30 USD/kWh for the 50 kW plant [200]. Unlike a stand-alone MHP system, our case is different. Here we are dealing with a tri-hybrid system that includes solar PV and wind turbine systems. In the following subsection, we present a breakdown of the cost as well as the assumptions we have made in this economic analysis.

7.6.1 Scenario C01: Base case: Existing tri-hybrid system

A summary of the estimated cost of the HES at Thingan is presented in Table 7-4. All costs are presented in US Dollars at the average exchange rate for the year 2017, the base year for this study.

Table 7-4: Cost breakdown of typical HES in Nepal

Description	Capital Cost	O&M Cost per year	Replacement Cost	Subsidy amount	Total Cost
Hybrid Energy System	**138,668**	**1,710**		**33,493**	**105,176**
Microhydro	64,950	150		23,923	41,176
Wind Turbines	8,811	500		3,589	5,722
Solar Panels	26,075	10		5,981	20,104
Battery	18,048	50	60.00%		18,098
Balance of Plant | Accessories	15,507				15,507
Installation	5,278				5,278
Mini-grid	**117,803**			**94,242**	**23,561**

The cost of 11 kV distribution system is $ 11,797 per km, and the same for 400/230 V distribution system is $ 3817 per km. The former is about 4 km, and the latter is estimated to be 18.5 km based on a map in [15]. In Nepal, a utility-compatible grid may qualify to receive a subsidy up to 80% of the designated rate for the region.

The NPC and LOCE calculate utilizing Equations 7.4 and 7.5 are presented in Table 7-5. The LCOE with subsidy and without subsidy turned out to be $ 0.20/kWh and $ 0.35/kWh respectively.

Table 7-5: LCOE and NPC for C01(base case)

Description	Subsidy	w/o Subsidy
Levelized cost of energy(LCOE)	0.20	0.35
Net Present Cost (NPC)	90,007	217,742

An MS Excel® sheet with a detailed cash-flow that includes values of all economic parameters for the Base Case C01 is documented in Appendix B.2.1.

7.6.2 Scenario C02: Regulated MHP with storage (pond + battery)

This case incorporates dispatchable generator, a regulated MHP in addition to the battery bank. By regulating the flow of water through the turbine, along with a small pond, it was possible to consider battery bank half the size of the base case. Along with it brings some extra civil work and associated costs. Table 7-6 lists an estimate of marginal benefits and cost of this configuration with reference to the base case C01 presented in the previous section.

Table 7-6: Benefit and cost of configuration C02.

Marginal cost	**$9,147**		**Marginal Benefits**	**$10,193**
Pond (117 m3) | SOW_{max} = 1.0	$1,166		Less battery size	$9,024
Flow control device (FCD) | Accessories	$3,023		ELC Life	$1,130
Incremental cost/subsidy: 4 kW MHP	$4,958		Energy value (50 extra hours)	$38
Life of FCD (years)	5		Life of battery bank	7

The effective life of a flow control device is assumed to be about five years. We will evaluate the economics of downsizing the battery bank against the cost of the regulating the MHP system and associated support structure, the pond in this case. In some cases, this pond may be incorporated with some geological feature along the power canal.

7.6.3 Scenario C03: Renewable only system:

This case is similar to the previous configuration except that it does not utilize the lead-acid battery bank at all. The best technical performance was with MHP plant of size 26 kW. Following the template in the previous case, Table 7-7 lists estimate of marginal benefits and the marginal cost of this configuration with reference to the base case.

Table 7-7: Benefit and cost of configuration C03.

Marginal cost	**$11,467**		**Marginal Benefits**	**$18,922**
Pond (100 m^3) | SOW_{max} = 0.75	$1,007		Less battery size (48 kWh)	$18,048
Flow control device (FCD) | Accessories	$3,023		ELC Life	$1,130
Incremental cost/subsidy 6 kW MHP	$7,437		Energy value (33 fewer hours)	-$256
Life of FCD (years)	5		Life of battery bank	7

We can compare cash flows for those three configurations. The annual and cumulative cash flows over lifespan are depicted in Figure 7.3 for all three configurations. For configuration C01 through C03, the cumulative cash flows hit a deficit of $31,304, $16,446 and $5,310 respectively.

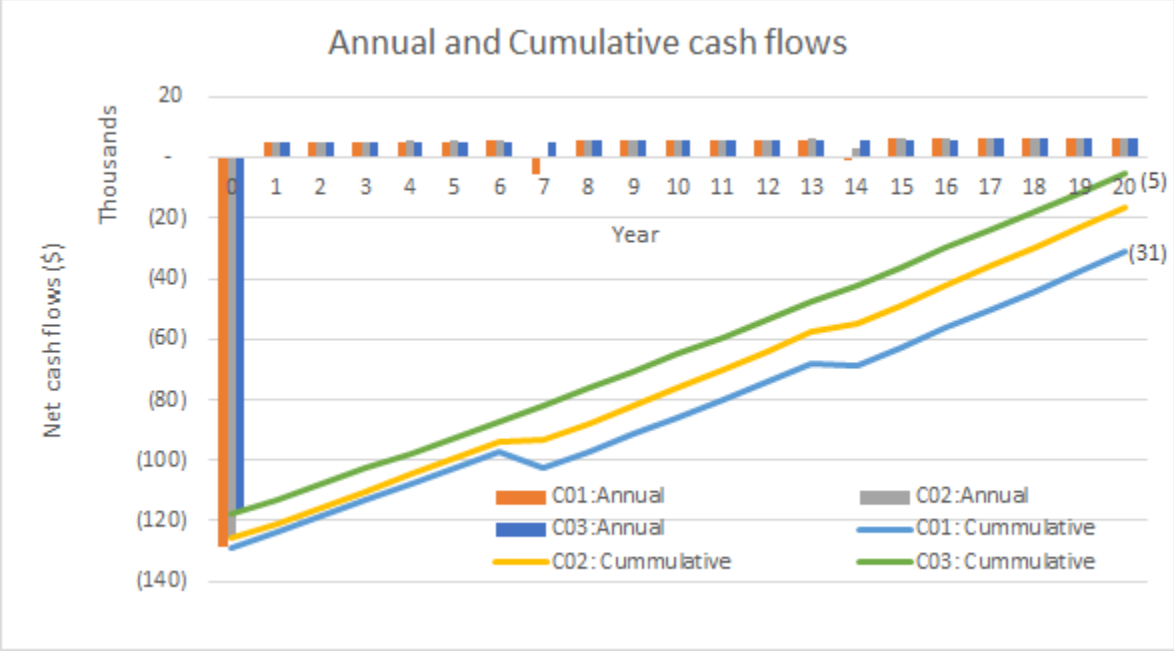

Figure 7.3: Annual and Cumulative cash flows

In Table 7-8 we organize the Levelized Cost of Energy (LCOE) and the Net Present Cost (NPC) for various configurations including the one without the subsidy. The LCOE is the least for the Renewable-Only configuration C03. The NPC of those three configurations, C01 through C03, calculated based on annual cash flows presented in Figure 7.3, are $90,018, $82,336 and $72,919 respectively.

Table 7-8: LCOE and NPC of various configurations

Economic Metric	Base Case: C01 subsidy	Base Case: C01 no subsidy	RE + Battery: C02 subsidy	RE-Only: C03 subsidy
LCOE	0.20	0.35	0.19	0.17
NPC	$90,018	$217,753	$82,336	$72,919

Even though the NPC of configuration C03 may look better, in fact, we are not comparing here an apple to apple. Configuration C03 does not deliver the same technical performance to that of C02 configuration. The C02 configuration misses inter hourly maximum load only 0.26 % of the time whereas the C03 configuration misses the load at about 5% of the time in a typical year.

7.7 Sensitivity and Risk Analysis

A sensitivity analysis evaluates how a variable of interest in the economic model may respond to a range of dependent variables. The economic model may have a set of assumptions about value and range of the underlying variables. These assumptions may have some degree of uncertainty and error. A sensitivity analysis evaluates how robust is the variable of interest under alternative assumptions.

A HES that utilizes the local renewable resource for rural electrification is a capital-intensive project. The upfront capital is a real chunk out of the total cost of the system. Hence operational sustainability of the HES may be sensitive to the cost of capital, subsidies, and cost of energy it may collect from the consumers. Most of the HES deployed in Nepal for rural electrification are not bankable, hardly can they recoup the

initial capital investment. A motivation here is to evaluate the operational sustainability of hybrid microhydro system under alternative assumptions.

We looked at how sensitive the NPC and LCOE are with the capital cost and the discount rate which usually is taken as the interest rate charged by the bank for clean energy projects. Table 7-9 presents the result of interest rage ranging from 3.0% to 18.0%. The real interest rate, an interest rate adjusted for both the monetary and energy inflation, is 10.5%. This is the interest rate for the base case. As anticipated, both the NPC and LCOE increase with an increase in the discount rate.

Table 7-9: Sensitivity analysis with the discount rate

Sensitivity to the Discount Rate								
	Unit	-7.5%	-5.0%	-2.5%	Base Case	2.5%	5.0%	7.5%
Discount Rate	%	**3.0%**	**5.5%**	**8.0%**	**10.5%**	**13.0%**	**15.5%**	**18.0%**
Net Present Costs (NPC)								
Base Case: C01	US$	57,516	72,187	82,682	90,360	96,102	100,487	103,903
RE + Battery: C02		46,562	62,638	74,207	82,717	89,111	94,014	97,845
RE-Only: C03		36,043	52,558	64,496	73,314	79,963	85,075	89,078
Levelized Cost of Electricity (LCOE)								
(Subsidy)Base Case: C01	US$	0.127	0.148	0.171	0.196	0.223	0.251	0.281
(No Subsidy)Base Case: C01		0.216	0.259	0.306	0.357	0.412	0.469	0.528
RE + Battery: C02		0.121	0.141	0.164	0.189	0.215	0.243	0.271
RE-Only: C03		0.110	0.129	0.151	0.174	0.198	0.224	0.251

For every percentage point increase in the discount rate the LCOE increase by about 0.0094 cents/kWh. The cost of energy has an opposite effect on the NPC of the hybrid MHP system. For three cases, the NPC decrease by about $9047, $9081 and $8756 for every NRs (equivalent to about 1 cent) increase in cost of energy. The equations used in order to calculate these numbers are depicted in Figure 7.4 by the trend equations.

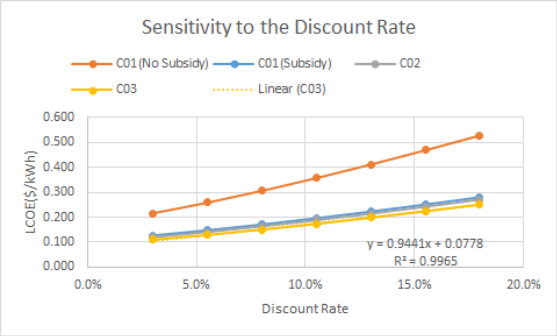

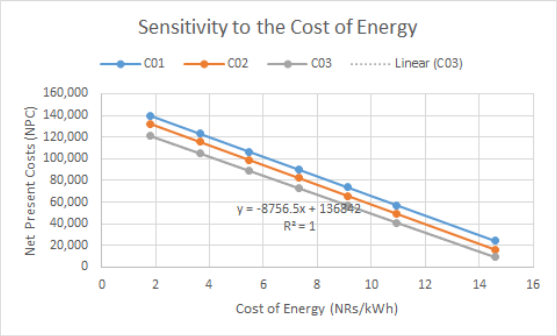

a) Discount Rate b) Cost of Energy

Figure 7.4: Sensitivity analysis

We used MS Excel function "What-If Analysis" tool to carry out the sensitivity analysis presented above. More details are documented in Appendix B.2.5.

There are several risks associated with hybrid MHP system. Nepal is one of the most vulnerable countries in the world due to the climate change. There are reports that Nepal is losing its glaciers at an alarming rate, at the same time the snow-line in the mountains are gradually moving up. Those changes are echoed in more frequent extreme events such as droughts, storms, floods, etc. These events are not favorable for hydropower production. In some MHP plants, the original turbine is replaced by a turbine of lesser capacity due to the decreased water flow [196]. In addition to climate change, Nepal is prone to earthquake due to its location – it is situated at the boundary of tectonic plates. A recent earthquake in April 2015 has created a havoc in the country. The quake threatened many hydropower plants. Even though the civil works do not amount much as the large-scale hydropower plants, apparently, an earthquake can induce a damage a MHP plant. A part of civil work (head works, power cannel etc.) may subside during an earthquake. We have added a pond in the configuration. Although the size of the pond is less than 125 m3, it can possess a risk to infrastructure and life.

7.8 Sustainability of Hybrid Energy Systems

Sustainability of HES in Nepal may be approached through two routes: strong and weak sustainability. A strongly sustainable project generates revenue to recover the initial capital cost and projected O&M cost over the lifespan of the project. On the other hand, a weakly sustainable project does not generate enough revenue to replace major components as they wear out and thus not allow the project to continue indefinitely. Some pilot projects are supported by grant from development agencies, which may not have a burden of recovering the capital cost, can go for a tariff designed for a weakly sustainable operation.

Sustainability is a crucial issue for off-grid electrification in Nepal and elsewhere [201, 202]. A recent study weighs various dimensions, namely economic, social, environmental, and technical dimensions, on sustainability assessment of a micro hydropower plant in Nepal [180]. The social dimension ranks highest followed by environmental, economic, and technical dimensions.

An economical sustainably of HES depends mainly on two factors: a) interest rate and b) tariff collected from customers. Figure 7.5 presents the NPC for a matrix consisting 49 different interest rate and tariff for the base case C01. The ordered pairs with negative NPC, which translates to a positive NPV, are marked with red labels in the figure.

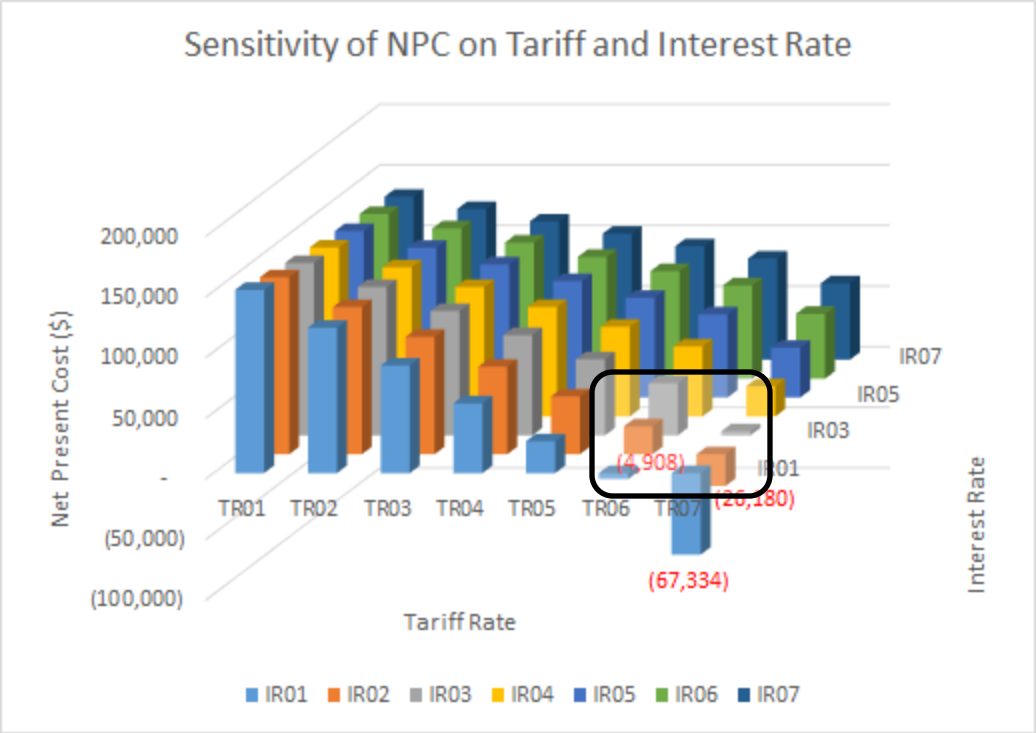

Figure 7.5: Sensitivity of NPC on tariff and interest rate

Table 7-10 presents NPC data in the neighborhood where NPV is positive, marked in the figure above by a black rectangle. At a tariff rate of 10.5 cents/kWh, the internal rate of return (IRR) turned out to be 3.38%. A number in parentheses represents a negative value.

Table 7-10: Net Present Cost

Net Present Cost	Tariff Rate (TR06) = 10.5 cents/kWh	Tariff Rate (TR07) = 14.0 cents/kWh
Interest Rate (IR01) = 3.0%	(4,908)	(67,334)
Interest Rate (IR02) = 5.5%	23,004	(26,180)
Interest Rate (IR03) = 8.0%	43,002	3,321

The initial capital cost and affordability are two major issues for sustainable operation of HES in Nepal. Even though a subsidy policy somehow addresses this issue, it is still an issue as reflected in the IRR to breakeven the HES. Electricity in rural areas of Nepal is mainly used for recreational use (e.g. Lighting). Lower productive use of energy makes

the economic situation even worse. A low tariff rate is an open issue for sustainability, but a high tariff rate is an issue for affordability, in turn, to the project's sustainability [203].

7.9 Conclusions

Hybrid MHP systems are known to be marginal in the economic sense. The Thingan project is just another example, not an exception. Even at a tariff rate 50% higher than that of the utility-rate and discount rate of 10.37%, the project seems not to recover initial investment as reflected by the NPC values in the Table 7-10. All three configurations we choose to study do not differ significantly in economic metrics, especially in terms of LCOE. The Renewable Only system has the least LCOE and NPC among the three cases we study here, Table 7-11. The LCOE for this case is about 17 cents/kWh and NPC is about $ 72,919. This analysis supports a case for a subsidized loan in addition to the present rate of subsidy designated for microhydro-solar-wind power generation.

Table 7-11: Summary of Economic Analysis

Description	Base Case: C01		RE + Battery: C02	RE-Only: C03
	Subsidy	w/o Subsidy	Subsidy	Subsidy
Levellized cost of energy (LCOE)	0.20	0.35	0.19	0.17
Net Present Cost (NPC)	90,018	217,753	82,336	72,919
Total Cost	128,736	256,471	126,033	117,722
Capital cost	256,471	256,471	258,552	252,633
Subsidy	127,735	-	132,520	134,912
NPC for O&M/Replacement	27,329	27,329	23,799	20,250

Affordability of customers and productive end-use may affect economic analysis. These areas are not explored in this analysis. An economics analysis presented above assumes a normal course of operation, does not include unexpected O&M costs which often are known to derail an HES. We don't take into account the effect of climate change on precipitation and in turn to the streamflow. The streamflow is assumed stationary with a periodicity of a year.

Economic analysis suggests a regulated MHP together with ELC, as reflected by the lower LCOE and NPC, delivered the technical performance above stipulated by the Global Tracking Framework. Such a system enhances reliability as well as helps reduce the size of lead-acid battery bank. However, one should not accept this recommendation at a face-value; a detailed site-specific analysis is warranted before implementing any regulated MHP systems.

CHAPTER 8

SUMMARY AND FUTURE WORK

This thesis presents a detailed approach toward performance analysis of hybrid microhydro system based on data available for a typical site. A new concept of incorporating a small pond with a regulated MHP system has been tested in the framework of Hybrid2 tool developed at the University of Massachusetts. A small pond can complement a battery bank for a hybrid MHP system.

A long-term performance analysis of microhydro plant requires an hourly or sub-hourly time series of streamflow. Such data series are scarce for a not-gauged river basin. Some hydrological modeling tools, however, can provide an estimate of annual flow duration curve (AFDC) even for a not-gauged river basin. We adopt the additive model of time series decomposition and develop a Multiple Input Single Output (MISO) model in order to synthesize an hourly time series of stream flow. The MISO model is based on the AFDC and take into account of daily precipitation dataset as well as of regional hydrological characteristics. A non-dimensional performance model of an MHP is developed based on empirical data. We integrate these models and simulate the long-term performance of a tri-hybrid system consisting of hydropower, solar PV and wind turbine.

8.1 Summary of findings

The following bullet points summarize findings of this study. These points are organized in the order of the chapters presented in this thesis.

- We developed a new Multiple Input Single Output (MISO) model for downscaling of flow in a river. Our model makes use of ARMAX time series model and the Monte-Carlo Markov Chain (MCMC) algorithm and generate streamflow data to an hour or sub-hourly time scales.

- The MISO hydro resource model we have developed in this thesis has been validated utilizing hourly data from the Blue River at Blue (USGS site # 07332500) in Oklahoma.
- We propose a two-parameter performance model of MHP system based on empirical data. This non-dimensional model may reflect the performance of MHP system better at part-load compare to the conventional one-parameter model.
- A minor revision of the UMass PV Model developed by Prof. Manwell has been proposed. The revised Open Circuit Voltage (Voc) model captures the performance of thin-film based solar PV panel better. A new analytical equation has been added to the set of equations in order to improve estimation of the diode-ideality factor (m), one of the four parameters of the solar PV Model.
- For three classes of hybrid MHP systems, one unregulated and two regulated, we identified three configurations, one on each class, that deliver best technical performance. Out of these configurations, C01 through C03, the renewable-only system (C03) does not meet the availability requirements of the Multi-Tier Framework [19] for measuring energy access for household supply.
- Even with the existing subsidy of about $ 1200/kW, the hybrid MHP system at Thingan does not attend the grid parity regarding the Levelized Cost of Energy (LOCE). The table below presents LCOE and the Net Present Cost (NPC) for four scenarios we have studied in this study.

Economic Metric	Base Case: C01 subsidy	Base Case: C01 no subsidy	RE + Battery: C02 subsidy	RE-Only: C03 subsidy
LCOE	0.20	0.35	0.19	0.17
NPC	$90,018	$217,753	$82,336	$72,919

- The hybrid MHP system at Thingan is marginal in an economic sense. This project can never recover the initial capital cost at current rate of tariff which is about 7 cents/kWh.
- At twice the existing rate of tariff and half the interest rate, the configuration C02 may barely recover the initial capital cost, excluding the subsidy.

8.2 Suggestions for Future Research

The work presented in this thesis may open up some new research questions, at the same time this study could be improved in various ways. The following are some suggestions for a vision of regulated MHP system laid down in this thesis.

We introduced a concept of automated flow control device (FCD) for a regulated MHP system. This device may not require complex specifications of the mechanical governor because it will work in parallel with the electronic load Controller. Whatsoever it is, we did not design FDC in details. A detailed design of such a device and full-scale testing is recommended.

The hydro resource model we have developed in this thesis has been tested only for one site. The model can be tested for basins with varying hydrological signature. The model may allow us downscaling of streamflow to the time scale of minutes or less. Such is a case, this work may facilitate dynamic modeling of the hybrid MHP system at an ungauged basin. A synthesized data set at high resolution should be satisfactory except for a case of a storm. We don't know it for sure.

The hydro resource model and the performance model of MHP system we developed in this research could be integrated with Hybrid2 to come up with an updated version for general public use.

APPENDICES

The MATLAB simulation codes necessary in order to reproduce analysis presented in this thesis is documented in appendix A. The section B presents all other appendices indicated in this dissertation. We start with the main file used for the system level control, and order all other codes (includes Function, Scripts etc.) in the order discussed in the thesis. The version of the MATLAB is '9.2.0.556344 (R2017a)'. In order to run the program, it is recommend that all codes are placed in the current working directory.

A.1 The Main File: System Level Control

Filename	Type	Description
Hy2MHPmodule2Clean.m	Main File	System level control and simulation
SumStatsAnalysis.m	Data Analysis	Data Analysis Script/Plots

```
% System level control of Dispatchable Generators
clearvars; clearvars -global
% Global Variable: Design and Control Variables
global Pdesign Qdesign sowm
global qmax c_kibam k_kibam sys_volt n_string bErated

%% Microhydro: Specification
% P = [20 21 22 23 24 25 26 27 28 29 30];         % Design size
P = [26];                                        % Configuration Study

% ps = [0 0.25 0.5 0.75 1 1.25 1.5];              % pond size
ps = [0.75];                                     % Configuration Study
nP = length(P);
nps = length(ps);
sumSize = nP * nps;
sumFile = zeros(sumSize, 18);
%% Configuration of the MHP Systems
% Here are three cases we are studying: Use GUI UI_Thingan.fig Later
% Case01: Existing system - Base case ( unregulated microhydro plant),
% Case02: Renewable + battery system (with regulated microhydro plant),
% Case03: Renewable only system (with regulated microhydro plant).

Case01 = false; Case02 = false; Case03 = true;

% A radioButton tells which one is true - at least one is true always.
% In all cases the output stored in the same table column

%% Case01:Existing system - Base case ( unregulated microhydro plant),
if Case01 == true
    hflag = 0;      % unregulated hydro
    bflag = 1;      % battery in the system
    cName = 'Case01';
```

```
end

%% Case02:Renewable + battery system (with regulated microhydro plant),
and
if Case02 == true
    hflag = 1;       % regulated hydro
    bflag = 1;       % battery in the system
    cName = 'Case02';
end
%% Case03:Renewable only system (with regulated microhydro plant. No
battery
if Case03 == true
    hflag = 1;       % regulated hydro
    bflag = 0;       % no battery
    cName = 'Case03';
end


%% Loading the resource file : Time series collection
tic
load('tscThingan.mat');             % Resource File: Time Series

nhours = length(ThinganMain.ThinganLoad.Data);

netLoad = zeros(nhours, 4);

for i = 1: nhours

  % load function argument from the time series collection dataset.

    Load = ThinganMain.ThinganLoad.Data(i, 1);       % Average Load in
hour i
    sigma_L = ThinganMain.ThinganLoad.Data(i, 2);    % stDeviation of
Load
    gen_wind = ThinganMain.Windgeneration.Data(i, 1); % Power from wind
turbine
    gen_solar = ThinganMain.Solargeneration.Data(i, 1);
    % gen_solar is not used to calculate Mean Net Load in probHy2.
    V = ThinganMain.Windresource.Data(i, 1);          % Wind speed
    sigma_V = ThinganMain.Windresource.Data(i, 2);    % stDeviation of
Wind speed

    % Details of the Theoretical Basis Time Series/Probabilistic Method
    % see HYBRID2 THEORY MANUAL (Nov 1998)
    % compute min/max load using the function probHy2

    [ NLmin, NLmax ] = probHy2( Load, gen_wind, gen_solar, sigma_L,
sigma_V, V );

    netLoad(i, :) = [i, NLmin, NLmax, (NLmin+ NLmax)/2 ];
    % Include sigma_N for load description and analysis

end
```

```
%% Battery in the system: Battery specification and capacity constants
sys_volt = 0.24;        % 12 V/each * 20 count on one string
n_string = 0;           % # of parallel strings
% % m_cells = 20;
% % v_cell = 12;       % emf of each cell
% bErated = n_string * m_cells * v_cell;
bErated = 24 * n_string;           % 24 kWh/string
% Maximum dispatch capacity
qmax = 109.146;
% capacity ratio (c)
c_kibam = 0.174;
% rate constant(k)
k_kibam = 6.103;

%% Computational Matrix Loop
for ii =1:nP

Pdesign = P(ii);  % This is a design variable.
% Pdesign = 22;  % This is a design variable.
Qdesign = 27*Pdesign/20;           % 27 liters/second
% Pdesign = 20;  % 20 kW, the rated power of MHP Plant
% Qdesign = 27;           % 27 liters/second

%% Update Qin in ThinganMain.Hydroresource.Data - Qstream is 3rd column
% Load a timeseries for template and tscollection: ThinganMain

% load('dbThingan.mat');
% load('tscThingan.mat');

% Load Hydroresource data Qintake based on Qstream and Qresidual
% This can be included in the loop below for code performance
% http://www.mathworks.com/help/matlab/math/matrix-indexing.html
% This array opeartion saves 25 seconds compare to for loop below
% Qresidual = 0;              % A regulatory parameter 2/1/2018
Qin_max = 1.2 * Qdesign;    % A design parameter
Qstream = ThinganMain.Hydroresource.Data(:,3);
filter = Qstream > Qin_max;         % Qstream - Qresidual
ThinganMain.Hydroresource.Data(:,1) = Qstream;      % Qstream -
Qresidual
ThinganMain.Hydroresource.Data(filter,1) = Qin_max;

%This for loop can come out - as it is independent of Pdesign and sowm

    for jj = 1: nps

sowm = ps(jj);               % maximum size of the pond (hours @
Pdesign)
% sowt = 1.5;      % threshold for reg hydro control - design
% Pdesign = 20;
% sowm = 6;        % maximum storage: 6 hour full load.
sowi = sowm;       % initial condition of pond storage - start full
hydroStats = zeros(nhours, 6);
battStats = zeros(nhours, 8);
```

```
% Variable Initialization for dispachable generators
% State of initial charge: Initial conditions
% Initial cap of Battery Bank (%SOC) = 75%
% we use q10 = 0.75*62 = 46.5    q0 =  0.75 * qmax
q10 = 46.5;
q0 = 52.5;         % qmax = 70 assumed of testing - handle with global
SOC = q0/100;       % Temporary fix
SP = 0.85;          % 85% of SOC setPoint of Battery
SPflag = 1;         % SetPoint flag for Dispatch Control
Qspill = 1;
% Icmax = 0;           % For initialization

[ Idmax, Icmax ] = KiBaMmax(q10, q0, 1 );

%% Loop through the hours so that we have hydro and battery stats
for j = 1: nhours

% Generate the function arguments for regulated MHP

ANLoad = netLoad(j,4);

% Dispatch Strategy in General

% Phneed = netLoad(j,3) + (1 - SOC)* Pdesign * bflag * Qspill * SPflag;

% We may also need battery setpoint flag - not to charge above it.

bPower = - Icmax * sys_volt;      % Icmax is -ve by convention
bbe = bbefficiency(bPower , bErated, bflag);
bPower = bPower/bbe;

% Phneed = netLoad(j,3) - Icmax * sys_volt * bflag * Qspill * SPflag;
Phneed = netLoad(j,4) + bPower * bflag * Qspill * SPflag;

Qin = ThinganMain.Hydroresource.Data(j,1);

% Phneed    PhServed    SOWf    Qspill  Qspill_flag

[Phserved, sowf, Qspill] = regMHP(Phneed, Qin, sowi, sowm, hflag);
Phmax = regMHP(1.5*Pdesign, Qin, sowi, sowm, hflag);
% urPhmax = regMHP(1.5*Pdesign, Qin, sowi, sowm, 0);
urPhmax = unregMHP(Qin);
% This version doesn't account for Qspill - just raise a flag

hydroStats(j, :) = [Phneed, Phserved, sowf, Phmax , urPhmax, Qspill];

% This may need to set to zero when bflag = 0 for clean up

pneed = round(ANLoad - Phserved, 2);      % this could be +ve or -ve
 % handle battery bank eficiency case when dicharging
 if sign(pneed) == 1            % + ve is discharging
    bbe = bbefficiency(pneed , bErated, bflag);
    pneed = pneed/bbe;
 end
```

```
[ q10n, q0n, pserved, Idmax, Icmax, cflag ] = KiBaM( q10, q0, 1, pneed,
bflag);

% Check if system have enough reserve to meet the NLmax
% Max from the battery: Idmax * SysVoltage
% Max from the Hydro: 1.2Pdesign given SOW, Qin,
GPMax = Phmax + Idmax * sys_volt * n_string;   % Max power that can be
generated

battStats(j, :) = [pneed, pserved, q10n, q0n, Idmax, Icmax, cflag,
GPMax];
%% initial condition of SOC and SOW for next timestep.
sowi = sowf;    % for hydro
q0 = q0n;       % for battery
q10 = q10n;     % for battery
SOC = battStats(j,4)/100;        % We may not need this - always carry
of previous steps
% SPflag = sign(SP - SOC);
    if SOC < SP
        SPflag = 1;
    else
        SPflag = 0;
    end
Qspill = hydroStats(j, 6);  % for Dispatch decision

end

% From a single table we need to compute useful results, stats and
plots
% create a temporary DataTable or store on one of timeseries data
lhbStat = [netLoad hydroStats battStats];

% RC02 = array2table(A ,'VariableNames',{'NLmin','NLmax', 'AvgNLoad'});

% clearvars -except lhbStat ThinganMain

% Colunm names given to the variables for easy reading/statistics

% RName = strcat('R', cName);      % date 2/5/2018 - Case and Result

RC02 = array2table(lhbStat ,'VariableNames', {'nhour','NLmin',
'NLmax',...
    'AvgNLoad', 'Phneed', 'Phserved', 'sowf', 'Phmax' ,'urPhmax',
'Qspill',...
    'pneed', 'pserved', 'q10n', 'q0n', 'Idmax', 'Icmax', 'cflag',...
    'GPMax'});

return

% break

% clearvars -except RC02 ThinganMain Pdesign sowm  ii jj
% writetable(RC02,'test2.xlsx','Sheet',1);
```

```
% Now calculate statistics for comparisions
% capacity shortage
% renewable fraction

% Unmet load - has two element greater due to float error with Excel
idx01 = find(RC02.Phneed > RC02.Phserved & RC02.pneed > 0 ...
& RC02.pserved < RC02.pneed);
umLkW = sum(RC02.pneed(idx01) - RC02.pserved(idx01));
umLh = length(idx01);
umLsr = mean(RC02.GPMax(idx01)./RC02.NLmax(idx01));

% Spinning reserve : Enough
idx02 = find(RC02.GPMax <= RC02.NLmax);
sRh = length(idx02);
sR = mean(RC02.GPMax(idx02)./RC02.NLmax(idx02));        % fraction

% Excess Energy
idx03 = find(RC02.Phneed < RC02.Phserved & RC02.pneed < 0 ...
&  RC02.pneed< RC02.pserved);
exEnh = length(idx03);
exEnkW = sum(abs(RC02.pneed(idx03) - RC02.pserved(idx03)));

% Battery Energy IN/OUT
idx04 = find(RC02.pserved < 0);
idx05 = find(RC02.pserved > 0);
Ein_h = length(idx04);
Eout_h = length(idx05);
Ein = sum(RC02.pserved(idx04));
Eout = sum(RC02.pserved(idx05));
Ein_avg = Ein/Ein_h;
Eout_avg = Eout/Eout_h;

% MicroHydro Statistics
Hydro_Phneed = sum(RC02.Phneed);
Hydro_Phserved = sum(RC02.Phserved);

% Advantage of regulation and Pond in terms of kWh
idx06 = find(RC02.urPhmax < Pdesign & RC02.Phmax > RC02.urPhmax);
extEn_regHydro = sum(RC02.Phmax(idx06)) - sum(RC02.urPhmax(idx06));
extEn_regHydro_h = length(idx06);        % Hour(SOW) in MS Excel
idx07 = find(RC02.Phserved > Pdesign);  % Hour(Phserved>Pdesign)
% Load served above Pdesgin because of Pond
extEn_Load_h = length(idx07);

% renamed to Extra Energy due to regulated Hydro

toc

simID = (ii-1)*nps + jj;
% Store result for various case Pdesign and Sown on 1/31/2018
sumFile(simID,:) = [Pdesign, sowm, umLh, umLkW, umLsr, sRh, sR, ...
    exEnh, exEnkW, Ein_h, Ein, Eout_h, Eout, Hydro_Phneed, ...
    Hydro_Phserved, extEn_regHydro_h, extEn_regHydro, extEn_Load_h];
```

```
    end
end

% sName = strcat('sum', cName);            % summary name
sumFile = array2table(sumFile ,'VariableNames', {'Pdesign', 'sowm', ...
    'umLh', 'umLkW', 'umLsr', 'sRh', 'sR', 'exEnh', 'exEnkW',
'Ein_h',...
    'Ein', 'Eout_h', 'Eout', 'Hydro_Phneed', 'Hydro_Phserved',...
    'extEnregHydro_h', 'extEnregHydro', 'extEn_Load_h'});
```

A.2 Load Model

Morning and evening peaks are approximated by the normal distributions, and added to the base load to create an hourly time series of load for a year.

Filename	Type	Description
Thinganload_generator.m	Resource Model	Hourly load generation
probHy2.m	Resource Model	Inter-hourly load distribution

A.2.1 Hourly load synthesizer

Filename: Thinganload_generator.m

```
% Load Estimate based on Diurnal Profile
hr = load('ThinganLoad.txt');      % Load diurnal Nominal Load (hourly)
% plot(hr)

% Variations in load: Daily and with in the time steps
dnoise = 0.15;
tnoise = 0.05;
m = 365;        % number of days on a typical year
n = 24;
d_alpha = normrnd(0, dnoise, [m, 1]);
t_alpha = normrnd(0, tnoise, [m, n]);

% Load variation alpha = 1 + alpha(daily) + alpha(timestep)
alpha_ = zeros(m, n);
for i = 1: n
temp = 1 + d_alpha(:,1) + t_alpha(:,i);
alpha_(:,i) =temp;
temp = [];
end;

% Duplicating matrix for array operation -
year_load = repmat(hr', m, 1);
year_load_final = year_load.*alpha_;

%[m n] = size(load_time_series)
% Transpose column to daily - to calculate mean/st dev - column wise
col_year_load = year_load_final';
```

```
load_time_series = reshape(year_load_final',m*n,1);

% plot daily mean and standard deviation of the load...
mu = mean(col_year_load);
sigma = std(col_year_load);
plot( mu, 'o-')
hold on
plot(sigma)
xlabel('Days in a year')
ylabel('Daily Average Load in kW')
xlim([0 365])
hold off
%reshape(load_time_series',m*n,1);
```

A.2.2 Inter-temporal load estimation

Filename: probHy2.m

- `function [ NLmin, NLmax ] = probHy2( Load, gen_wind, gen_solar, sigma_L, sigma_V, V )`

```
% This function handles probabilistic method within time step
% Example [ NLmin, NLmax ] = probHy2( 24.5, 2.45, 3.42,  2.43,
1.26.5.2)
% Input : It search from the tscollection object based on heading name.
% confidence interval of probability | Disregarded net load probability
% Let user choose confidence interval in terms of P
% xn    Probility(P)
%     sigma_1 = 0.6826895;
      sigma_2 = 0.9544997;
%     sigma_3 = 0.9973002;
%     sigma_4 = 0.9999366;
%     sigma_5 = 0.9999994;
% Reference: http://mathworld.wolfram.com/ConfidenceInterval.html

% Disregarded net load probability PDNL - based on 2sigma

n = sqrt(2)* erfinv(sigma_2);

PDNL = 0.5* erfc(n/sqrt(2));


    % calculate Mean net Load(MNL)
    % MNL = Load - gen_wind;
    MNL = Load - gen_wind - gen_solar;

    %Consider net load based charging of battery if available
    %Load following during high net load and
    %cycle charging during period of low net load

    % calculate variability of wind power from wind speed variability
    n_WT = 1;                   % Number of wind turbine
    F_WPT = 1.5;                % Wind power turbulence factor
```

```
    sigma_W = sqrt(n_WT)* F_WPT * gen_wind * sigma_V/V;

    % Variability of the net load
    sigma_N = sqrt( sigma_L^2 + sigma_W^2);

    % Wind Farm - Here we do for Single Wind Turbine

    % Assume or calculate
    % This steps can also be calculated as MNL +/- n * sigma_N
    [Load] = norminv([PDNL, 1-PDNL],MNL, sigma_N);
    % we can pass Load as outpur_args and separate min and max later
    NLmin = Load(1);
    NLmax = Load(2);

end
```

A.3 Hydro Model

Filename	Type	Description
mcmc.m	Resource Model	General MCMC method for Blue River
mcmcThingan.m	Resource Model	MCMC method adapted to Thingan site
Armax_Rajaiya.sid	Resource Model	System Identification based model MATLAB
regMHP.m	Performance Model	MHP performance model

A.3.1 MCMC Model

FileName: mcmc.m

```
function [ ts_sample, paccept, pfit ] = mcmc( ts_dh, tpm_qS, ...
                                pdf_cdf_qR, pdf_xq)
% This is functional form of MCMC Algorithm for downscaling of
streamflow
%   INPUT
%     ts_dh:  Time series of q(S)
%     tpm_qS: TPM of q(S) =
%     pdf_cdf_qR: Distribution Functions of Q(R)
%     pdf_xq): Target distribution derived from the AFDC
%   OUTPUT
%       ts_sample is normalized flow by default
%        pfit is calculated based on ts_dh and ts_sample
%      For Blue River pfit was calculated based on hourly time series
data.
% This script synthesize timeseries of streamflow based on data
% prepared based on hourly timeseries of Blue River in Oklahoma

% load mcmc_br.mat
% load ts_br.mat
```

```
% This funciton will require the following input
% a) initial value q0
% b) nsamples - a year 8760 hours
% c) target pdf
% d) proposal pdf: TPM(initial state x, final state y). q(y|x)

% normalize the timeseries ts_dh - because our TPM is on normalized
scale
ts_dhn = ts_dh/mean(ts_dh);

%ts_mhn = ts_mh/mean(ts_mh);
% ts_dhn = qS_mh;     % For monthly to hourly data

% Duplicate the timeseries to store mcmc samples and set data value
zero
ts_sample = ts_dhn;
ts_sample.Data = 0;

% Load initial value and length of dataset
nsamples = length(ts_dhn.Data);

% Bin size of TPM
nsize_tpm = 0.05;

% Unique CDF for interpolation: Ramdom Distribution
[C, ia, ic] = unique(pdf_cdf_qR(3,:));
xqR = pdf_cdf_qR(1,ia);
vqR = pdf_cdf_qR(3,ia);

% Unique PDF for interpolation: Target Distribution Normalized
[CT, iaT, icT] = unique(pdf_xq(2,:));
xq = pdf_xq(1,iaT);
vq = pdf_xq(2,iaT);

% Metropolis-Hasting
% if initial value q0 is given
 % qS1 = q0
qS1 = ts_dhn.Data(1); qR1 = 0;
% qS1 = qS_mh.Data(1); qR1 = 0;     % For monthly data
 q0 = qS1 + qR1;
ts_sample.Data(1) = q0;
counter = 1;          % while loop count
 taccept = 0;         % total accepted samples
% redundant variable which serve same purpose as nsamples - for debug

for i = 1: (nsamples - 1)

    % next qS value from - q
    qS2 = ts_dhn.Data(i + 1);

    accept = false;

    while ~accept
    % Find qR from
```

```
    x = rand();
    vq_p = interp1(vqR, xqR, x);
    % This need to be double check - temporary fix
    if isnan(vq_p) vq_p = 0; end


    % Find TPM for both ways transitions
    idx1 = ceil((qS1 + qR1)/nsize_tpm);
    idx2 = ceil((qS2 + vq_p)/nsize_tpm);

    % Handle when idx is greater than 30
    % our bin size are upto 1.5Q - all rest
    if idx1 > 30 idx1 = 31; end
    if idx2 > 30 idx2 = 31; end

    % Correction if idx came out to be negative
   if idx1 <= 0  idx1 = 1; end
   if idx2 <= 0  idx2 = 1; end
    % Compute probability ratios
    p1 = tpm_qS(idx2, idx1)/tpm_qS(idx1, idx2);
    %if isnan(p1) p1 = 0; end        % For Monthly

    p2 = interp1(vq, xq, qS2)/interp1(vq, xq, qS1);
    % if isnan(p2) p2 = 0; end        % For Monthly
    %p = p1 * p2;

    % Count acceptance percentage
    counter = counter + 1;

    % Acceptance Criteria - gives logical variable for accept/reject

    accept = x < min(1, p1*p2);

    % fprintf('Just finished iteration #%d\n', counter);

    end

    % Write sample as a timseries object

    % if accept ts_sample.Data(nsamples + 1) = qS2; end
    ts_sample.Data(i + 1) = qS2;

    qS1 = qS2;

    % total accepted data count
    taccept = taccept + 1;

end

% Percentage of accepted samples
paccept = (taccept+1)/counter;

% Calculate the percentage fit
```

```
% FIT = [1 - NORM(y -y_hat)/NORM(y - y_mean]*100
norm_n = norm(ts_dhn.Data - ts_sample.Data);     % numerator
norm_d = norm(ts_dhn.Data - mean(ts_dhn));       % denominator

pfit = (1 - norm_n/norm_d)*100;

end
```

FileName: **mcmcThingan.m**

```
% This script synthesizes an hourly time series at the Thingan site.
close all
clear all
clc

% Load data from Rajaiya station Rajaiya.txt
Rajaiya = importfile('Rajaiya.txt', 2, 1097);
% %
*********************************************************************
% % Date    Month   Day Flow (cms)  Q/Q(mean)   Precp(0919) SiteQ(S)
% % 1/1/2007    1   1   12.2    0.457   0   106.44
% %
*********************************************************************

tsR_d = timeseries(Rajaiya.Flowcms, 1:1096, 'Name', 'Flow-CMS');
tsR_d.TimeInfo.StartDate = '31-DEC-2006 12:00:00';
tsR_d.TimeInfo.Units = 'days';
tsR_d.TimeInfo.Format = 'mm-yyyy';
tsR_d.DataInfo.Units = 'CMS';

% Loading the precipitation
tsR_d_precp = tsR_d;
tsR_d_precp.Name = 'Precipitation';
tsR_d_precp.Data = Rajaiya.Precp0919;
tsR_d_precp.DataInfo.Units = 'mm-Rain';

% Prepartion of QS for ARMAX
tsR_d_QS = tsR_d;
tsR_d_QS.Data = movmean(tsR_d.Data, 7);

tstep = 86400;              % Daily data
hyear = 8760;
dyear = 365;
nyear = 10;                  % # of years for simulation of Q(R)

% Data for ARMAX model
est_iddR = iddata(tsR_d.Data, [tsR_d_QS.Data tsR_d_precp.Data], tstep);
% The validation data set was developed as the subset of this one

% Load the existing model file from the saved mat file
load thi_amx.mat;
sys = arx512;
lambda = sqrt(sys.NoiseVariance);           % Standard Deviation
lambda_h = lambda/sqrt(24);                 % Hourly Standard Deviation
G = tf(sys, 'measured');                    % Dynamic Mo
```

```
H = tf(sys, 'noise');
e_h = randn(nyear*dyear,1)*lambda_h;
qR = lsim(H, e_h, 1:tstep: nyear* dyear * tstep);

% Interpolation based on daily and QS data
avgflow = 232.80;                       % Thingan site in Liter/se
avgflow_Rajaiya = 26.683;               % Rajaiys in CMS
ndays = length(tsR_d.Data);
tsT_d = tsR_d*avgflow/mean(tsR_d);
tsT_d.DataInfo.Units ='Liter/second';
tsT_d.Name = 'Flow Thingan';

tsT_dh = resample(tsT_d, 1:1/24:ndays);
% tsR_dh = resample(tsR_d, 1:1/24:ndays);
% tsR_dh.TimeInfo.Units = 'hours';


% creating the CDF of qR
% [f,x] = ecdf(qR);
% plot(x,f)

% Create TPM Matrix for the qS
qS = tsT_dh;
qS.Data = qS.Data/mean(qS);
qSD = qS.Data;
qSD1lag = [qSD(end); qSD(1:end - 1)];
qS_min = min(qSD); qS_max = max(qSD);
Xedges = [0:0.05:1.5 qS_max];

h2qS = histogram2(qSD, qSD1lag, Xedges, Xedges,'Normalization', 'pdf');
h2qS.Normalization = 'count';
nXnY = h2qS.NumBins;
nbins = nXnY(1);

tpm_qS = h2qS.Values;
tpm_qS_sum = sum(tpm_qS, 2);

% Each row the probability sum equal to 1
for i = 1:nbins
tpm_qS(i,:) = tpm_qS(i,:)/tpm_qS_sum(i);        % Input for MCMC
end

% x = [0 1.5];
% y = [0 1.5];
% imagesc(x, y, tpm_qS)
% colorbar

% Now we will need CDF of qR, first we will need to normalize it

qR = qR/avgflow_Rajaiya;                        % Normalization

Xedges = [min(qR):0.05:max(qR)];

h1qR = histogram(qR, Xedges, 'Normalization', 'pdf');
```

```
pdf_qR = h1qR.Values;
h1qR.Normalization = 'cdf';
cdf_qR = h1qR.Values;
qR_mid = movmean(Xedges,2,'Endpoints','discard');
pdf_cdf_qR = [qR_mid; pdf_qR; cdf_qR];      % Input for MCMC

% Target pdf from the AFDC:
cdf_afdc = [2 21 34 57 97 283 7491;0 0.05 0.15 0.35 0.55 0.75 1];
% Limit the maximum vlue to 500 Liter per second
% cdf_afdc = [2 21 34 57 97 283 400;0 0.05 0.15 0.35 0.55 0.75 1];

xcdf = cdf_afdc(1,:)/avgflow;           % Normalization
vcdf = cdf_afdc(2,:);
xq_cdf = linspace(min(xcdf),max(xcdf), 501);
vq_cdf = interp1(xcdf, vcdf, xq_cdf,'pchip');

h = xq_cdf(2) - xq_cdf(1);

% Derivative by Central Difference Method
xq_pdf= xq_cdf(2:end-1);
vq_pdf = (vq_cdf(3:end) - vq_cdf(1:end -2))/(2*h);

pdf_xq = [xq_pdf; vq_pdf];                  % Input for MCMC
% plot(xcdf, vcdf, 'r')
% hold on
% yyaxis left
% plot(xq_pdf, vq_pdf, 'k')
% legend('CDF-AFDC', 'PDF-Central')

% Does not have data to test pfit%
% start with tsR_dh_qS and create sample from this

ts_dh = tsT_dh;      % renaming of the timeseris

% clearvars -except ts_dh tpm_qS pdf_cdf_qR pdf_xq avgflow

% MCMC Function
[ ts_sample, paccept, pfit ] = mcmc( ts_dh, tpm_qS, ...
                              pdf_cdf_qR, pdf_xq);
% Here pfit gives how much q(S) is close to xq (in %)
ts_sample_unit = ts_sample * avgflow;

% Contribution of qR on the streamflow
qRc = ts_dh - ts_sample_unit;
qRc.Name ='Contribution of q(R)';
qRmax = max(qRc); qRmin = min(qRc);
plot(qRc); ylim([qRmin 1.5*qRmax]);
```

A.3.2 ARMAX Model

Filename: Armax_Rajaiya.sid

A.3.2.1 Model parameters of ARX(6,4,1)

arx641 =

Discrete-time ARX model: A(z)y(t) = B(z)u(t) + e(t)

A(z) = 1 + 0.9978 z^-1 + 0.999 z^-2 + 0.9985 z^-3 + 0.9986 z^-4 + 0.9987 z^-5 + 0.9976 z^-6

B1(z) = -0.0003516 z^-1 + 0.005088 z^-2 + 6.987 z^-3 - 0.001928 z^-4

B2(z) = -0.0001511 z^-1 + 0.0008519 z^-2 + 0.0006632 z^-3 + 4.432e-05 z^-4

Name: arx641

Sample time: 86400 seconds

Parameterization:

Polynomial orders: na=6 nb=[4 4] nk=[1 1]

Number of free coefficients: 14

Use "polydata", "getpvec", "getcov" for parameters and their uncertainties.

Status:

Estimated using ARX on time domain data "est_idd".

Fit to estimation data: 98.15% (prediction focus)

FPE: 0.3138, MSE: 0.3062

A.3.2.2 Model parameters of ARMAX(4,4,3,1)

amx4431 =

Discrete-time ARMAX model: A(z)y(t) = B(z)u(t) + C(z)e(t)

A(z) = 1 - 0.625 z^-1 + 0.9974 z^-2 - 0.3417 z^-3 + 0.7627 z^-4

B1(z) = -0.7438 z^-1 + 3.72 z^-2 - 1.444 z^-3 + 0.2608 z^-4

B2(z) = -0.004753 z^-1 + 0.01314 z^-2 - 0.01313 z^-3 + 0.005578 z^-4

C(z) = 1 - 2.353 z^-1 + 2.178 z^-2 - 0.7923 z^-3

Name: amx4431

Sample time: 86400 seconds

Parameterization:

Polynomial orders: na=4 nb=[4 4] nc=3 nk=[1 1]

Number of free coefficients: 15

Use "polydata", "getpvec", "getcov" for parameters and their uncertainties.

Status:

Estimated using PEM on time domain data "est_idd".

Fit to estimation data: 87.18% (prediction focus)

FPE: 15.01, MSE: 14.73

A.3.3 Model of Hydro Turbine: Pelton

```
function [Phserved, sowf, Qspill] = regMHP(Phneed, Qin, sowi, sowm,
flag)
%This function calculates the output of the MHP
% Qin in Liter/s -> do not normalize in argument
% sowi: initial state of water
% sowm: maxium state of water - a design parameter - relates to Qdesign
% flag: 1 (true) is regulated hydro; flag: 0 (false) unregulated hydro
% Example
% [Phserved, sowf, Qspill] = regMHP(5, 30, 4, 6, 1) regulated
% [Phserved, sowf, Qspill] = regMHP(5, 20, 4, 6, 0) unregulated

global Pdesign Qdesign

% MHP Powerplant parameters
% Pdesign = 20;   % kW
% coefficient for minimum and maximum power - a design parameter.
pratio_min = 0.2;
pratio_max = 1.2;
%Pmax = 1.2 * Pdesign;       % Maximum Power
% Qdesign = 27;   % liter/second
% sowt = 1.5;     % Minimum state of water threshold for control
```

```
sowt = min(0.2 * sowm, 0.5);
% It may be a good idea to relate it to sowm as percentage of sowm
% this is equivalent to 1.5 hour of operation at Pdesign.
% sowm = 6 - we are interested in sowmax (design parameter)
% initial sowi, sow(t-1)
% final sowf, sow(t) - at the end of current timestep

% Check if input arguments are within range.

% Performance Model: Normalized power curve
% First Order equation
% y = 1.0456x - 0.0369 ; Here y = P/Pdesign and x = Q/Qdesign = Qnorm
m_hydro = 1.0456; c_hydro = - 0.0369;
% 2nd Order equation
% a_0 =  - 0.0804; a_1 = 1.2318; a_2= -0.1432
% it will require to solve a quadratic equation and positive root only

% Flow regulation paramters and ranges - intake
% Qnorm_min = 0.2; Qnorm_max = 1.2;
Qintake_max = 1.1829;      % Intake for P = 1.2 Pdesign
% Qmin =0.226 =  6.117 liter/s              % Intake for P = 0.2
Pdesign

% Resource available on that time step
Qin_norm = Qin/Qdesign;
% This value should be less than or equal to Qintake_max

 Qin_norm = min(Qin_norm,  Qintake_max);

% Flow regulation paramters and ranges - from SOW - from storage.

% Phneed should be positive with max value as design parameter
Phneed_norm = Phneed/Pdesign;

% Phdispatch_norm is used for power supplied by the Dispatch Strategies

% if power neeed is greater than pmax - limit to the Pmax
% if power need is zero or negative - hydro should be operating at 0.2
if Phneed_norm >= pratio_max
    Phneed_norm = pratio_max;
elseif Phneed_norm < pratio_min
    Phneed_norm = pratio_min; % this would handle negative value
else
    Phneed_norm = Phneed/Pdesign ;
end

% Flow rate calculation from storage to deliver power
% used water Q/Qdesign to serve power
Qturb_norm = (Phneed_norm - c_hydro)/m_hydro;
% Qturb_norm = min(Qintake_max, Qturb_norm);
% Qturb_norm = min((Phneed_norm - c_hydro)/m_hydro, Qin_norm);

%% Here we need to handle flag - regulated or unregulated
% Irrespective of Phneed it generates Pdesing if Qin > Qdesign
if flag == 0
```

```
P_hydro = m_hydro * (Qin/Qdesign) + c_hydro;    % Normalized power

Phserved = min(Pdesign,  P_hydro * Pdesign);
sowf = 0;
        if Qin > Qdesign
            Qspill = 1;
        else
            Qspill = 0;
        end
return
end
%%

% Handle if sowi is comming negative
%  Phdispatch_norm = 0;
% If SOW is <sowt and Qin_norm - we do not operate MHP
if ((sowi <= sowt) && (Qin_norm <= 0.2))  %
    Qturb_norm = 0;          % because MHP is shutdown for safety
    Phdispatch_norm = 0;
    sowf = sowi + (Qin_norm - Qturb_norm);

    % return
% end

% Control based on Intake and SOW - state of Water;
elseif ((sowi + Qin_norm) >= Qturb_norm)
%if ((sowi <= sowt) &&  (0.2 < Qin_norm) && (Qin_norm <= Qintake_max))
    % operate if Qin_norm >= Qnorm
%     switch (Qin_norm >= Qturb_norm)
%         switch (Qin_norm <= Qturb_norm)
%     switch((sowi + Qin_norm) <= Qturb_norm)
%         case 1
            Phdispatch_norm = Phneed_norm;
            sowf = sowi + (Qin_norm - Qturb_norm) ;
             % should limit to the sowm - from input argument...
else
%         case 0
            % Do not operate MHP --->
            Qturb_norm = Qin_norm;
            Phdispatch_norm = m_hydro * Qin_norm + c_hydro;
            sowf = sowi + (Qin_norm - Qturb_norm) ;

%     end

end

% Power served in kW scale - denormalized
    Phserved = Phdispatch_norm * Pdesign;
% A flag for if the demand has been served
% If Phserved == Phneed fhydro =1; elese fhydro = 0; end
% e = 0.01*Pdesign;
% idx = find(abs(Phserved - Phneed)<=e)

% If want to store Qspill - we will need to do here.
% This is to pass a flag if there is overflow from the storage.
```

```
% Spill should be checked based on Qin not SOW, what if Qin = 500
  if sowf >  sowm
      Qspill = 1;
  else
      Qspill = 0;
  end

% should limit to the sowm - - the maximum value of the storage
    sowf = min( sowf, sowm);
    % sowf = max(0, sowf); % No negative value.

end
```

A.4 Solar PV Model

Filename	Type	Description
testsolar2Voc.m	Performance Model	Solar PV Performance model

```
% Model for PV Panel Performance J.F. Manwell, Spring 2016
% Code rewritten in MATLAB by Ram Poudel
% Updated on 6/16/2018
clear variables  clc
% Functions in scripts are supported in R2016b or later.
global TC_ref TC GT_ref IL_ref I0_ref V_thermal T_Cen2Kel lambda
global N_cells Isc V_OC_ref I_mp V_mp m_ideal Isc_coeff Voc_coeff Rs

%% Given conditions to calculate
GT = 800;           % W/m2 GT_test
T_amb = 25;         % Centigrade
TC = 25;            % Cell temperature
U_panel = 25;       % 25 W/m2.C

%% Some constants/Inputs
k_boltz = 1.3807e-23; % Boltzman constatnt J/K
e_charge = 1.6022e-19; % Charge of an electron
GT_ref = 1000; % W/m2
TC_ref = 25; % C
T_Cen2Kel = 273.15; % Centigrade to Kelvin scale
V_thermal = k_boltz * (TC_ref + T_Cen2Kel)/e_charge;

%% Panel Inputs
% load 'AP1206PVSpec.m' for Astropower 120W PV Module
% AP1206PVSpec

%% Panel Inputs AP1206PVSpec
N_cells = 36;
Isc = 7.7; % Short circuit current in A
V_OC_ref = 21.0; % Open circuit voltage in V
I_mp = 7.1;   % Maximum power current at Ref.
V_mp = 16.9;   % Maximu power voltage at Ref.
% m_ideal = 1.5;   % ideality factor
m_ideal = 0.8624;   % iterated to d(P)/dV = 0
```

```
lambda = 0;

Isc_coeff = 0.0006; % Ampere/Centigrade
Voc_coeff = -0.08; % Voltage/Centigrade

% Dimensions
Length = 1.476; % meter
Width = 0.66; % meter
Area = Length * Width;

% %% This PV Pannel Input for 200 W Panel Example by Prof. Manwell
% N_cells = 54;
% Isc = 8.21; % Short circuit current in A
% V_OC = 32.9; % Open circuit voltage in V
% I_mp = 7.61;    % Maximum power current at Ref.
% V_mp = 26.3;    % Maximu power voltage at Ref.
% m_ideal = 1.5;    % ideality factor
% lambda = 0;
%
% Isc_coeff = 0.00318; % Ampere/Centigrade
% Voc_coeff = -0.123;  % Voltage/Centigrade
%
% % Dimensions
% Length = 1.425; % meter
% Width = 0.99; % meter
% Area = Length * Width;

% %% Fist Solar FS-267 Module PMax = 67.5 Watt: From Data Sheet
%
% N_cells = 116;
% Isc = 1.18; % Short circuit current in A
% V_OC_ref = 87; % Open circuit voltage in V At GT = 1000 W/m2
% % V_OC = 79.63;    % At GT = 200 W/m2
%
%
% I_mp = 1.05;    % Maximum power current at Ref.
% V_mp = 64.6;    % Maximu power voltage at Ref.
% m_ideal = 1.25;    % ideality factor
% % lambda = 0.0514; % Irradiance correction factor for V_OC - Fitting
% lambda = 0;
% % lambda = 0.09617; % calculated from the data sheet
%
%
% Isc_coeff = 0.04* Isc/100 ; % % given in %/C
% Voc_coeff = -0.25* V_OC_ref/100;  % given in %/C
%
% % Dimensions
% Length = 1.2; % meter
% Width = 0.6; % meter
% Area = Length * Width;
%
del_TC = TC - TC_ref;           % T_amb is different temperature
V_OC = V_OC_ref *(1 + del_TC * Voc_coeff/V_OC_ref + lambda *
log(GT/GT_ref));

%% Panel calculated vlaues
```

```
% step 1: choose a value of m
% step 2
IL_ref = Isc;
I0_ref = Isc * exp(-V_OC_ref/(N_cells * m_ideal * V_thermal));

% steps 3
lnbrack01 = log((IL_ref - I_mp + I0_ref)/I0_ref);   % temporary dum
Rs = ((m_ideal * V_thermal * lnbrack01) - V_mp/N_cells)/I_mp;

V_count = round(V_OC);

VITable = zeros(V_count,20);
PMaxTable = zeros(5, 3);

for i = 1: 5
    GT = i * 200;

% V_OC = 4.6357ln(GT) + 55.177; % For FS-267
% Voc/Vocref = 0.0532ln(GT/GT_ref) + 1.0013         % Normalized scale
% Irradiance correction factor at constant temperature

    for V = 1: V_count
        I = 0;
        LS = 0;         % LeftStart
        RS = Isc;       % RightStart
        tol = 1e-4;
        I = TSearchPVIV(I, V, TC, GT, LS, RS, tol );
        % write in a table
        %  [ I ] = TSearchPVIV(I, V, TC, GT, LS, RS, tol )



        VITable(V, 1) = V;
        VITable(V, i + 1) = I;


    end
    % This is for MPPT power are various GT
        Pmax = 0;
        [P_mppt, V_mppt ] = MPPTPower(Pmax, TC, GT, 0, V_OC, tol );
        PMaxTable(i,:) = [GT, P_mppt, V_mppt];

end
clear I % In order that function may not assume it by default

%% Generation of IEC-61853 Data for Validation/Comparison
% IEC61853 Single Diode Model: System Advisor Model 2017
% Procedure for Applying IEC-61853 Test Data to a Single Diode Model
% Aron P. Dobos, Sara M. MacAlpine (2014)

% GTset = [100, 200, 400, 600, 800, 1000, 1100];
% TCset = [15, 25, 50, 75];
%
% n1 = length(GTset);
```

```
% m1 = length(TCset);
%
% iecData = zeros(n1*m1, 6);
% % These are the columns od data GT, TC,  P_mppt, V_mppt, V_OC, IL
%
% for i = 1: n1    % variation of GT
% for j = 1: m1     % variation of TC
%
% GT = GTset(i);
% TC = TCset(j);
%
% del_TC = TC - TC_ref;           % T_amb is different temperature
% V_OC = V_OC_ref *(1 + del_TC * Voc_coeff/V_OC_ref + lambda *
log(GT/GT_ref));
%
% Pmax = 0.75 * (GT/GT_ref) * I_mp * V_mp;         % Derating 0.75
% % Pmax = 0;
% [P_mppt, V_mppt ] = MPPTPower(Pmax, TC, GT, 0, V_OC, tol );
%
%
% IL = (GT/GT_ref) * (IL_ref + Isc_coeff * del_TC);
%
% % Voc = V_OC + del_TC * Voc_coeff;    % V_OC is Global but Voc is
local
%
% iecData(4*(i-1)+ j, :) = [GT, TC,  P_mppt, V_mppt, V_OC, IL];
%
% end
%
% end


% %% For Load Matching Linear and Qudratic Load
% % Two Algorithms: Bisection and substitution.
%
% PowerMat = zeros(20, 9);
%
% for i = 1: 20
%     GT = i * 50;
% % Just a Initial guess for Pmax to start MPPT Search
% Pmax = 0.75 * (GT/GT_ref) * I_mp * V_mp;         % Derating 0.75
% % Pmax = 0;
% del_TC = TC - TC_ref;
% V_OC = V_OC_ref *(1 + del_TC * Voc_coeff + lambda * log(GT/GT_ref));
%
% [P_mppt, V_mppt ] = MPPTPower(Pmax, TC, GT, 0, V_OC, tol );
%
% % Load matching
% % p = [0.015, 10, -200];
% %  p = [0.06, -0.6, 1.5];
%    p = [0.01, 0.01, 0];    % Value from Prof. Manwell PVModel 2017
%
% % p = [0.357, 0, 2];   % positive offset of 2
% % Linear Load
% % p = [0, 0.2, -4];        % we do not have this option handled
offset + ve
```

```
%
% %[P_Load, V_Load, I_Load ] = loadMatch(0, p, TC, GT, LS, RS, tol);
% [P_Load, V_Load, I_Load ] = loadMatch(0, p, TC, GT, tol);
% % This algorith has some problem at lower GT <= 200
%
% [P_Load2, V_Load2, I_Load2 ] = loadMatch2(0, p, TC, GT, tol);
%
% PowerMat(i,:) = [GT, P_mppt, V_mppt, P_Load, V_Load, I_Load, P_Load2,
V_Load2, I_Load2];
%
% % % step 7: Recalculate TC based on assumed U
%
% end

%% Efficiency of panel is Power/GT * Area
% % eff_panel = I_* V_ / (GT * Area);
% % TC = T_amb + GT *(1 - eff_panel)/U_panel;
%
% % step 8 : Iterate on cell temperature untill convergence

%% Includes all the functions required for Solar Module

function [ dI_abs ] = PVIVZero( I, V, TC, GT )
%This calculate difference in current between user supplied and the
Equation
%   Detailed explanation goes here
global TC_ref GT_ref IL_ref V_thermal T_Cen2Kel
global N_cells Isc V_OC_ref m_ideal Isc_coeff Voc_coeff Rs lambda

% Later may include as Global variable
I_ = I;
V_ = V;


% step 4
del_TC = TC - TC_ref;           % T_amb is different temperature
IL = (GT/GT_ref) * (IL_ref + Isc_coeff * del_TC);

% step 5: reverse saturation current I0

V_OC = V_OC_ref *(1 + del_TC * Voc_coeff/V_OC_ref + lambda *
log(GT/GT_ref));

num_exp05 = -(V_OC)/N_cells;     % temporary dum
den_exp05 = m_ideal * V_thermal * (TC + T_Cen2Kel)/(TC_ref +
T_Cen2Kel);
I0 = (GT/GT_ref) * (Isc + del_TC * Isc_coeff)*
exp(num_exp05/den_exp05);


temp = exp((V_/N_cells + I_ * Rs)/(m_ideal* V_thermal)); % bracket
missed

I_temp = IL - I0* (temp - 1);
```

```
dI_abs = abs(I - I_temp);

end

% For Tstart we may not need TC, GT etc when we on same script.

function [ I ] = TSearchPVIV(I, V, TC, GT, LS, RS, tol )
% This uses a Ternary Search, adapted from the one given in
% https://en.wikipedia.org/wiki/Ternary_search
% LS: Left Start
% RS: Right Start
% tol: tolearance

% check if LS < RS or equal etc functional check.

% Initialization
Left = LS;
Right = RS;
LThird = Left;
RThird = Right;
% if LS and RS is not given use LS = 0 and RS = Isc

% Later may include as Global variable
% I_ = I;
V_ = V;

tol_cal = RS - LS;
n =0;           % While loop counter and control
while tol_cal > tol
    n = n +1;
%     dI_abs_LThird = PVIVZero(LThird, V_, TC, GT);
%     dI_abs_RThird = PVIVZero(RThird, V_, TC, GT):
%     if  dI_abs_LThird > dI_abs_RThird
%
    if (PVIVZero(LThird, V_, TC, GT) > PVIVZero(RThird, V_, TC, GT))
        Left =  Left + (Right - Left)/3;
        %LThird = Left + (Right - Left)/3; - This is mistake
    else
        Right = Right - (Right - Left)/3;
        % RThird = Right - (Right - Left)/3; - This is mistake
    end

    LThird = Left + (Right - Left)/3;
    RThird = Right - (Right - Left)/3;

    tol_cal = abs(Right - Left);
    I = (Left + Right)/2;

    % While loop count and control
        if n > 100
            I = NaN;
        break
        end
```

```
end


end

%% Includes all the functions required for a Solar Module


function [ dPdV_abs ] = midealZero( Imp, Vmp, TC, GT )
%This calculates dP/dV at maximum power point, and pass error
global TC_ref GT_ref IL_ref V_thermal T_Cen2Kel
global N_cells Isc V_OC_ref m_ideal Isc_coeff Voc_coeff lambda


IL_ref = Isc;
I0_ref = Isc * exp(-V_OC_ref/(N_cells * m_ideal * V_thermal));


% steps 3 - this is valid for other hence I_mp changed to Imp
lnbrack01 = log((IL_ref - I_mp + I0_ref)/I0_ref);   % temporary dum
Rs = ((m_ideal * V_thermal * lnbrack01) - V_mp/N_cells)/I_mp;


% step 4
del_TC = TC - TC_ref;           % T_amb is different temperature
IL = (GT/GT_ref) * (IL_ref + Isc_coeff * del_TC);

% step 5: reverse saturation current I0

V_OC = V_OC_ref *(1 + del_TC * Voc_coeff/V_OC_ref + lambda *
log(GT/GT_ref));

num_exp05 = -(V_OC)/N_cells;     % temporary dum
den_exp05 = m_ideal * V_thermal * (TC + T_Cen2Kel)/(TC_ref +
T_Cen2Kel);
I0 = (GT/GT_ref) * (Isc + del_TC * Isc_coeff)*
exp(num_exp05/den_exp05);


temp = exp((V_/N_cells + I_ * Rs)/(m_ideal* V_thermal));
I_temp = IL - I0* (temp - 1);

dI_abs = abs(I - I_temp);

end


function [P_mppt, V_mppt ] = MPPTPower(Pmax, TC, GT, LS, RS, tol )
% Maximum Power Point Calculation
% In this case we don't know voltage
% we search range of voltage from zero to VOC
% This uses TSearchPVIV to get current, and uses P = IV
```

```
global V_OC_ref
% Pmax = 0;
% what is I here??/


% Initialization
I = Pmax/(0 + V_OC_ref);
Left = LS;
Right = RS;
LThird = Left;
RThird = Right;
% if LS and RS is not given use LS = 0 and RS = VOC

tol_cal = RS - LS;
n =0;           % While loop counter and control
while tol_cal > tol
    n = n +1;
% This gives current for voltage LThird and RThird
    ILThird = TSearchPVIV(I, LThird, TC, GT, LS, RS, tol);
    IRThird = TSearchPVIV(I, RThird, TC, GT, LS, RS, tol );

    P1 = ILThird * LThird;
    P2 = IRThird * RThird;

        if  P1 < P2
        Left =  Left + (Right - Left)/3;

        else
        Right = Right - (Right - Left)/3;

        end
    LThird = Left + (Right - Left)/3;
    RThird = Right - (Right - Left)/3;

    tol_cal = max(abs(Right - Left), abs(ILThird - IRThird));

    V_mppt = (Left + Right)/2;
    P_mppt = V_mppt * (ILThird + IRThird)/2;

    % While loop count and control
        if n > 100
            V_mppt = NaN; P_mppt = NaN;
        break
        end
end
end


function [P_Load, V_Load, I_Load ] = loadMatch(Pmax, p, TC, GT, tol )
% Load match for Linear/Quadratic load I(Q) = I(Q) = a0 + a1* V + a2 V2
% % Here p = [a2 a1 a0] for linear put a2 = 0
% we search range of voltage from V(I=zero) to VOC
% This uses TSearchPVIV to get current, and uses P = IV
```

```
global V_OC_ref Isc
% Pmax tell which module to use for load matching AP-120 or AP-200 W

% Here p = [a2 a1 a0] for linear put a2 = 0
% p = [0.015, 10, -200];
% I(Q) = -200 + 10 * V + 0.015 * V^2;

% Isc = 7.1;
% Here a0 should be less that Isc
if p(3) > Isc
I_Load = NaN; V_Load = NaN; P_Load = NaN;
return
end

a = roots(p);

% roots has to be real and positive
% a = (a(a>= 0) && a(a == real(a));
% Filter imaginary value if any
a = a(a == real(a));
% Filter for negative value if any bacause V is positive only
a = a(a >= 0);

%  Count the lenght of a and This value should be less than  Voc
if length(a) == 1 && a < V_OC
    LS = a;
elseif a > V_OC
    LS = NaN;
    return
else
    LS = 0;
end

% Right start should be V_OC
RS = V_OC;

% Initialization
I = Pmax/(0 + V_OC_ref);
Left = LS;
Right = RS;

% if LS and RS is not given use LS = 0 and RS = V_OC

tol_cal = RS - LS;
n =0;           % While loop counter and control
while tol_cal > tol
    n = n +1;
    c_mid = (Left + Right)/2;

    % This gives current for voltage LThird and RThird
    ILThird = TSearchPVIV(I, Left, TC, GT, 0, Isc, tol);
    IRThird = TSearchPVIV(I, c_mid, TC, GT, 0, Isc, tol );
```

```
    % Calculate current from the load
    ILoad_left = polyval(p, Left);
    ILoad_right = polyval(p, c_mid);

    dI_left = ILThird - ILoad_left;
    dI_right = IRThird - ILoad_right;


    % check for tolerance here
    %     tol_cal = abs(Right - Left);
    tol_cal = abs(c_mid - Left);        % Voltage based tolerance

        if  sign(dI_left) == sign(dI_right)
            Left = c_mid;          % Mid voltage

        else
            Right = c_mid;

        end
%     LThird = Left + (Right - Left)/3;
%     RThird = Right - (Right - Left)/3;

    I_Load = (ILThird + IRThird)/2;
    V_Load = (Left + Right)/2;
    P_Load = V_Load * I_Load;

    % While loop count and control
        if n > 100
            V_Load = NaN; I_Load = NaN; P_Load = NaN;
        break
        end
end
end


function [P_Load2, V_Load2, I_Load2 ] = loadMatch2(Pmax, p, TC, GT, tol
)
% Load match for Linear/Quadratic load I(Q) = I(Q) = a0 + a1* V + a2 V2
% % Here p = [a2 a1 a0] for linear put a2 = 0
% we search range of voltage from V(I=zero) to VOC
% This uses TSearchPVIV to get current, and uses P = IV

global V_OC Isc
% Pmax tell which module to use for load matching AP-120 or AP-200 W

% Here p = [a2 a1 a0] for linear put a2 = 0
% p = [0.015, 10, -200];
% I(Q) = -200 + 10 * V + 0.015 * V^2;

% Isc = 7.1;
% Here a0 should be less that Isc
if p(3) > Isc
I_Load2 = NaN; V_Load2 = NaN; P_Load2 = NaN;
return
```

```
end

a = roots(p);

% roots has to be real and positive
% a = (a(a>= 0) && a(a == real(a));
% Filter imaginary value if any
a = a(a == real(a));
% Filter for negative value if any bacause V is positive only
a = a(a >= 0);

%  Count the lenght of a and This value should be less than  Voc
if length(a) == 1 && a < V_OC
    LS = a;
elseif a > V_OC
    LS = NaN;
    return
else
    LS = 0;
end

% Right start should be V_OC
RS = V_OC;

% Initialization
I = Pmax/(0 + V_OC);
Vguess = (LS + RS)/2;


% if LS and RS is not given use LS = 0 and RS = V_OC

tol_cal = Isc - I;          % Initialisation anything will work here.

% store function how it works
n =0;           % While loop counter and control
while tol_cal > tol
    n = n +1;
    % This gives current for voltage LThird and RThird
    IVguess1 = TSearchPVIV(I, Vguess, TC, GT, 0, Isc, tol);

    IL2 = polyval(p, Vguess);

    Imid = (IVguess1 + IL2)/2;

    pnew = p;
    pnew(length(p)) =  pnew(length(p)) - Imid;  % new offset = a0 -
IVguess

    % From Prof. Manwell PV Model 2017
    % V_guess_3 = (-a1_ + Sqr(a1_ * a2_ - 4 * (a0_ - I_) * a2_)) / (2 *
a2_)

    Vnew = roots(pnew);
    Vnew = Vnew(Vnew >= 0 &  Vnew == real(Vnew));
```

```
    % Sometimes there may be two roots that may satisfy condition
above.
    if length(Vnew) > 1
%         Vnew = Vnew(1); % or Vnew(2)
        Vnew = min(max(Vnew), V_OC);   % bring back to knee region
    end

    if isempty(Vnew) == 1
%         Vnew = NaN;
        V_Load2 = NaN; I_Load2 = NaN; P_Load2 = NaN;
        break
    end

    IVguess2 = TSearchPVIV(I, Vnew, TC, GT, 0, Isc, tol);
    IR2 = polyval(p, Vnew);

%       tol_cal = abs(Vguess - Vnew);
      tol_cal = max( abs(Vguess - Vnew), abs(IVguess1 - IVguess2));

%      In a linear region Voltage should be tolarence calculation
variable
%      In the curve/knee region current should be tolarence calculation
variable

     dI_left = IVguess1 - IL2;
     dI_right = IVguess2 - IR2;


    I_Load2 = (IVguess1 + IVguess2)/2;
    V_Load2 = (Vguess+ Vnew)/2;
    P_Load2 = V_Load2 * I_Load2;


     if  sign(dI_left) ~= sign(dI_right)

          Vguess = (Vnew + Vguess)/2;

        else
          Vguess = Vnew;

     end


    % While loop count and control
        if n > 100
            V_Load2 = NaN; I_Load2 = NaN; P_Load2 = NaN;
        break
        end
end
end
```

A.5 Wind Model

Filename: This model was implemented in MS Excel and data imported in MATLAB®.

A.6 Battery Model: KiBaM

Battery parameters, and simulation model for the storage.

Filename	Type	Description
KiBaM.m	Performance Model	Kinetic Battery Model
KiBaMmax.m	Maximum Power	Maximum current of KiBaM Model
bbefficiency.m	Efficiency In/Out	Battery bank efficiencey
KiBaMpar.m	Script	Battery parameters estimator

A.6.1 KiBaM Model

```
function [ q10n, q0n, pserved, Idmax, Icmax, cflag ] = KiBaM( q10, q0,
tstep, pneed, flag)
% Returns state of charge (SOC) using KiBaM Model given the intial SOC
& power
% Ref: Manwell & McGowan (1993); Solar energ Vol. 50 No 5. pp 399-405
% Detailed explanation goes here
% q10: the amount of available charge
% q20: the amount of bound charge
% q0 = q10 + q20 - total charge.
% q10 and q0 are in Ah; tstep in hours, and pneed in kW
% Syntax: [q10n, q0n, pserved, Idmax, Icmax, cflag] = KiBaM( 56, 85, 1,
2.5, 1)
% Sign convention: If pneed is +ve we discharge battery.

% Declare some global variables when we integrate codes
global sys_volt n_string
global qmax c_kibam k_kibam bErated

% bbe = bbefficiency(pneed, bErated);     % Battery bank efficiency
% pneed = bbe * pneed;                    % Update pneed to take
efficiency

%% There is no battery in the system
Idmax = 0; Icmax = 0; cflag = 0;      % initialization of new added
variable 1/11/2018
if flag == 0
    q10n = 0;
    q0n = 0;
    pserved = 0;
%     Idmax = 0; Icmax = 0;
return
end
%% There is battery in the system
% % Maximum dispatch capacity
% qmax = 109.146;
```

```
% % capacity ratio (c)
% c_kibam = 0.174;
% % rate constant(k)
% k_kibam = 6.103;

emkt = exp(-k_kibam*tstep);

% Battery bank parameters : m cells in a string and n strings
% n_string = 1;
% m_cells = 20;
% v_cell = 12;       % emf of each cell
% sys_volt = (m_cells * v_cell)/1000;       % in kV b/c pneed will be
in kW

% Efficiency function

pneed = pneed/n_string;              % This variable needs to be updated
nom_cap = 100;  % Nominal Ah - 1
min_soc = 0.2;
q0_min = min_soc * nom_cap;
q0_max = nom_cap;

q10_min = c_kibam * q0_min;     % minimum free charge allowed

% Calculate the maximum discharging and charging current based on SOC
% calculate Idmax
[ Idmax, Icmax ] = KiBaMmax(q10, q0, tstep );


% Limit the maximum battery power to serve to - 75% of pmax
% pmax = sys_volt * nom_cap;                   % This should base on
SOC/q0- not nom_cap
 pmax = sys_volt * q0;                        % Idmax or q0??
% if (abs(pneed) > (0.95* pmax))   abs removed b/c hindering charging
too

 if (pneed > (0.95* pmax))               % If more than 18 kW - hindered
charging also
   % May be we want to set pneed to
    q10n = q10; q0n = q0; pserved = 0;
    return
end
% Limit charging and dischargin at given SOC
% check if arguments are within the limit of SOC - min and max
% No discharging below q0_min - to maintain battery life


if (q10 < q10_min && q0 < q0_min && pneed > 0)  % limit on free charge
on 1/21/2018
    q10n = q10; q0n = q0; pserved = 0;
    return
end

% No charging after maximum q0 - full charge
```

```
if (q0 >= q0_max && pneed < 0)          % >= updated on 1/23/2018
    q10n = q10; q0n = q0; pserved = 0;
    return
end

% Here pneed could be positive or negative - unmetpower after hydro
% pneed > + is discharing case
Ineed = pneed/sys_volt;

% Hybrid2 has Charge Rate Limit (A/Ah remaining) ~ 5

switch (Ineed > 0)       % has to be a logical operator
    case 1 % Discharging case
%           % calculate Idmax
% Check if Id is equal to Ineed or Idmax
        if Ineed > Idmax
            Icur = Idmax;
        else
            Icur = Ineed;
        end


    case 0  % Charging case
        % calculate Icmax

% Limiting to the maximum charing current Icmax.
        if  Ineed > Icmax
            Icur = Ineed;
        else
            Icur = Icmax;
        end

    otherwise
        q10n = q10;
        q0n = q0;
%        soc
        Icur = 0;
end

% Calculation of new states of charges q1 and q2

q1_first = q10 * emkt;
q1_second = (q0 * k_kibam * c_kibam - Icur)* (1-emkt)/k_kibam;
q1_third = - Icur * c_kibam * (k_kibam * tstep - 1 + emkt)/k_kibam;

% Here rounding is to avoid value like q10n =  2.6645e-15
q10n = round(q1_first + q1_second + q1_third, 2);


q2_first = (q0 - q10) * emkt;
q2_second = q0 * (1 - c_kibam) * (1 - emkt);
q2_third = - Icur * (1-c_kibam) * (k_kibam * tstep - 1 + emkt)/k_kibam;

q20n = q2_first + q2_second + q2_third;
```

```
q0n = q10n + q20n;

q0n = min(q0n, nom_cap);        % to handle numerical overflow eg
100.23

% Upadate maximum charging and discharging currents
[ Idmax, Icmax ] = KiBaMmax(q10n, q0n, tstep );

% Here we need to pass Icmax and Idmax based on new q0n and q10n
% Check if battery charging or discharging here - this is dumb
e = 1e-3;               % general tolearance

if q0n > q0
    cflag = 1;           % charging flag
elseif (abs(q0n - q0) <= e)
    cflag = 0;
else
    cflag = -1;         % discharing flag
end

% Power serverd by the battery bank
pserved = Icur * sys_volt *n_string;

% Efficiency function

end
```

A.6.2 KiBaMmax Model

```
function [ Idmax, Icmax ] = KiBaMmax(q10, q0, tstep )
%   This function calculates the maximum charging and discharging
current

global qmax c_kibam k_kibam

% qmax = 109.146;
% % capacity ratio (c)
% c_kibam = 0.174;
% % rate constant(k)
% k_kibam = 6.103;


emkt = exp(-k_kibam*tstep);

% Calculate the maximum discharging and charging current based on SOC
% calculate Idmax
num_Idmax = k_kibam * q10 * emkt + q0 * k_kibam * c_kibam * (1 - emkt);
den_Idmax = 1 - emkt + c_kibam * (k_kibam * tstep - 1 + emkt);
```

```
Idmax = (num_Idmax/den_Idmax);

% Calculation of maximum discharging current

num_Icmax = -k_kibam * c_kibam * qmax + k_kibam * q10 * emkt + ...
     + q0 * k_kibam * c_kibam * (1 - emkt);

den_Icmax = 1 - emkt + c_kibam * (k_kibam * tstep - 1 + emkt);

Icmax = (num_Icmax/den_Icmax);


end
```

A.6.3 Battery Efficiency

```
function [ bbe ] = bbefficiency( E_need, E_rated, bflag)
% Efficiency of Battery Bank: Linear
%   This function gives the efficiency of the battery bank

if bflag == 0
    bbe = 1;
    return
end

b_1 = 0.898;
b_2 = 0.173;
bbe = b_1  - b_2 * abs(E_need)/E_rated;

% E_need = E_need/bbefficiency;
% E_need = E_need * bbefficiency;

end
```

A.6.4 KiBaM Battery parameters estimation

```
Filename: KiBaMpar.m

bdata = load('exide100ah.txt')
t = bdata(:,1)';  % Time in hours
y = bdata(:,2)';  % Discharge current
% see Equation 2.12
fun = @(x)x(1)*x(2)*x(3)./((1-exp(-x(3)*t))*(1-x(2)) + x(3)*x(2)*t) -
y;
x0 =[125, 0.2, 2]

%Solve nonlinear least-squares (nonlinear data-fitting) problems
x = lsqnonlin(fun,x0)
x =   109.1463    0.1735    6.1031
plot(t,y,'ko',t,fun(x)+y,'b-')
xlabel('time'); ylabel('Discharge current')
```

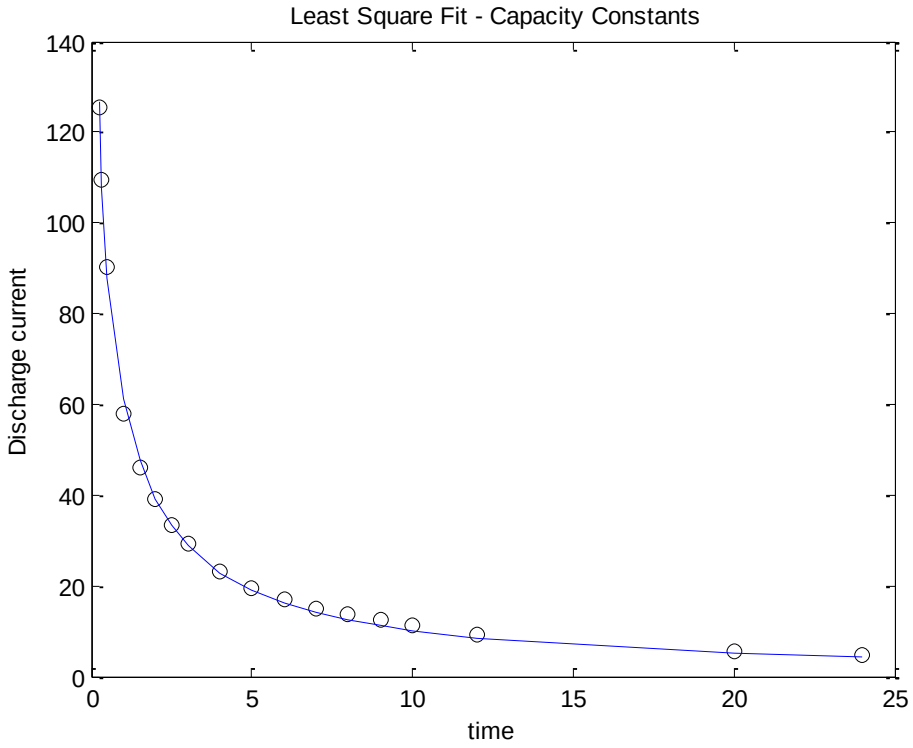


```
Data File Exide: 100 Ah (6-TCX-05G); Filename: exide100ah.txt
24     4.8    115.20
20     5.7    114.00
12     9.4    112.80
10     11.2   112.00
9      12.4   111.60
8      13.6   108.80
7      15.1   105.70
6      17     102.00
5      19.6   98.00
4      23.3   93.20
3      29.2   87.60
2.5    33.2   83.00
2      38.9   77.80
1.5    45.9   68.85
1      57.9   57.90
0.5    90.2   45.10
0.33333      109.4 36.47
0.25   125.4 31.35
```

B.1 Economic Analysis: Three Case Study

Assumption and Economic Parameters

Symbol	Value	Unit	Defintion
ib	16.00%	%	Nominal/Bank Interest rate
π	5.10%	%	General inflation rate
πe	2.50%	%	Inflation rate of energy
r	10.37%	%	Real interest rate
T	20	years	HES economic life / project lifespan
coe	7.30	NRs/kWh	Economic value of energy
E (t)	96,360	kWh	Total annual electricity supply, based on electricity demand assessment
ge	3.78%	%	Growth rate of annual electricity demand
i	10.37%	%	discount rate (normally taken as the interest rate)
N	3		the total number of renewable energy technologies adopted
Wn(E)	28	kW	installed capacity for nth RET, optimized in a portfolio way to meet the demand
k_n^{RE}		US$/kW	the unit capital cost for the nth type of RET
o_t^{RE}		US$	O&M costs in year t, which includes costs for replacing energy storage systems
s_n^{RE}	125,000	NRs./kw	Subsidies for microhydro-solar-wind power generation
	15,000	NRs./hh	Subsidy per household
R_t^{RE}			Revenue in year t from electricity tariff plus other source
sgRE	80%		Subsidies for grid compatible mini-grid/grid-extension
forex	104.5	NRs/US$	Exchange rate in the base year - average value

B.1.1 Base Case C01: Existing System

Year	Discount Factor	Capital Cost | Revenue	O&M Cost	Replacement Cost	Subsidy amount	Total Cost
0	1.000	256,471	-	-	127,735	128,736
1	0.906	(6,731)	1,710	-	-	(5,021)
2	0.821	(6,900)	1,753	-	-	(5,147)
3	0.744	(7,072)	1,797	-	-	(5,276)
4	0.674	(7,249)	1,841	-	-	(5,407)
5	0.611	(7,430)	1,888	-	-	(5,543)
6	0.553	(7,616)	1,935	-	-	(5,681)
7	0.501	(7,806)	1,983	10,842	-	5,019
8	0.454	(8,001)	2,033	-	-	(5,969)
9	0.411	(8,202)	2,083	-	-	(6,118)
10	0.373	(8,407)	2,136	-	-	(6,271)
11	0.338	(8,617)	2,189	-	-	(6,428)
12	0.306	(8,832)	2,244	-	-	(6,588)
13	0.277	(9,053)	2,300	-	-	(6,753)
14	0.251	(9,279)	2,357	6,505	-	(417)
15	0.228	(9,511)	2,416	-	-	(7,095)
16	0.206	(9,749)	2,477	-	-	(7,272)
17	0.187	(9,993)	2,539	-	-	(7,454)
18	0.169	(10,243)	2,602	-	-	(7,641)
19	0.153	(10,499)	2,667	-	-	(7,832)
20	0.139	(10,761)	2,734	-	-	(8,027)
NPC		190,423.90	16,778	7,068	127,735	86,535.45

Description	Subsidy	w/o Subsidy
Levellized cost of energy	0.19	0.35
Net Present Cost	86,535	214,270
Capital Cost	128,736	256,471
NPC for O&M/Replacement	23,846	23,846
Cumulative Discount Factor	8.30	8.30

B.1.2 Case C02: Renewable + battery system

Description		Capital Cost	O&M Cost per	Replacement	Subsidy amount	Total Cost
Hybrid Energy System		**140,750**	**1,710**		**38,278**	**102,472**
Microhydro		71,866	150		28,708	43,308
Wind Turbines		8,811	500		3,589	5,722
Solar Panels		26,075	10		5,981	20,104
Battery		9,024	50	60.00%		9,074
Pond (117 m3)		1,166	50			1,216
Balance of Plant | Accessor		18,530				18,530
Installation		5,278				5,278
Mini-grid		**117,803**			**94,242**	**23,561**
Year	Discount Factor	Capital Cost |	O&M Cost	Replacement	Subsidy amount	Total Cost
0	1.000	258,552	-	-	132,520	126,033
1	0.906	(6,906)	1,710	-	-	(5,196)
2	0.821	(7,074)	1,797	-	-	(5,277)
3	0.744	(7,247)	1,889	-	-	(5,358)
4	0.674	(7,423)	1,985	-	-	(5,438)
5	0.611	(7,605)	2,086	-	-	(5,518)
6	0.553	(7,790)	2,193	-	-	(5,598)
7	0.501	(7,981)	2,305	5,444	-	(232)
8	0.454	(8,176)	2,422	-	-	(5,754)
9	0.411	(8,376)	2,546	-	-	(5,830)
10	0.373	(8,581)	2,676	-	-	(5,906)
11	0.338	(8,791)	2,812	-	-	(5,979)
12	0.306	(9,007)	2,955	-	-	(6,051)
13	0.277	(9,227)	3,106	-	-	(6,121)
14	0.251	(9,454)	3,265	3,267	-	(2,923)
15	0.228	(9,686)	3,431	-	-	(6,255)
16	0.206	(9,924)	3,606	-	-	(6,317)
17	0.187	(10,167)	3,790	-	-	(6,377)
18	0.169	(10,417)	3,983	-	-	(6,434)
19	0.153	(10,673)	4,186	-	-	(6,487)
20	0.139	(10,936)	4,400	-	-	(6,536)
NPC		191,056	20,250	3,549	132,520	82,335.98

B.1.3 Case C03: Renewable Only System

Description		Capital Cost	O&M Cost per	Replacement	Subsidy amount	Total Cost
Hybrid Energy System		**134,831**	**1,710**		**40,670**	**94,161**
Microhydro		75,130	150		31,100	44,180
Wind Turbines		8,811	500		3,589	5,722
Solar Panels		26,075	10		5,981	20,104
Battery		-	-	60.00%		-
Pond (100 m3) | SOWmax =		1,007	50			1,057
Balance of Plant | Accessor		18,530				18,530
Installation		5,278				5,278
Mini-grid		**117,803**			**94,242**	**23,561**
Year	Discount Factor	Capital Cost |	O&M Cost	Replacement	Subsidy amount	Total Cost
0	1.000	252,633	-	-	134,912	117,722
1	0.906	(6,612)	1,710	-	-	(4,902)
2	0.821	(6,780)	1,797	-	-	(4,983)
3	0.744	(6,952)	1,889	-	-	(5,064)
4	0.674	(7,129)	1,985	-	-	(5,144)
5	0.611	(7,310)	2,086	-	-	(5,224)
6	0.553	(7,496)	2,193	-	-	(5,303)
7	0.501	(7,687)	2,305	-	-	(5,382)
8	0.454	(7,882)	2,422	-	-	(5,459)
9	0.411	(8,082)	2,546	-	-	(5,536)
10	0.373	(8,287)	2,676	-	-	(5,611)
11	0.338	(8,497)	2,812	-	-	(5,685)
12	0.306	(8,712)	2,955	-	-	(5,757)
13	0.277	(8,933)	3,106	-	-	(5,827)
14	0.251	(9,160)	3,265	-	-	(5,895)
15	0.228	(9,391)	3,431	-	-	(5,960)
16	0.206	(9,629)	3,606	-	-	(6,023)
17	0.187	(9,873)	3,790	-	-	(6,083)
18	0.169	(10,123)	3,983	-	-	(6,140)
19	0.153	(10,379)	4,186	-	-	(6,192)
20	0.139	(10,641)	4,400	-	-	(6,241)
NPC		187,581	20,250	-	134,912	72,919.00

B.1.4 Sensitivity Analysis

Sensitivity to the unit capital cost of the HES								
	Unit	-15%	-10%	-5%	Base Case	5%	10%	15%
Unit Capital Cost of HES	US$	4,210	4,457	4,705	4,952	5,200	5,448	5,695
Total Capital Cost		117,868	124,802	131,735	138,668	145,602	152,535	159,469
Net Present Costs (NPC)								
Base Case: C01	US$	69,215	76,149	83,082	90,015	96,949	103,882	110,816
RE + Battery: C02		59,454	66,388	73,321	80,255	87,188	94,121	101,055
RE-Only: C03		55,956	62,890	69,823	76,756	83,690	90,623	97,557
Levelized Cost of Electricity (LCOE)								
(Subsidy)Base Case: C01	US$	0.169	0.178	0.186	0.195	0.204	0.212	0.221
(No Subsidy)Base Case: C01		0.329	0.337	0.346	0.355	0.363	0.372	0.381
RE + Battery: C02		0.159	0.167	0.176	0.185	0.193	0.202	0.211
RE-Only: C03		0.151	0.160	0.169	0.177	0.186	0.195	0.203

Sensitivity to the Discount Rate								
	Unit	-7.5%	-5.0%	-2.5%	Base Case	2.5%	5.0%	7.5%
Discount Rate	%	**3.0%**	**5.5%**	**8.0%**	**10.5%**	**13.0%**	**15.5%**	**18.0%**
Net Present Costs (NPC)								
Base Case: C01	US$	57,516	72,187	82,682	90,360	96,102	100,487	103,903
RE + Battery: C02		46,562	62,638	74,207	82,717	89,111	94,014	97,845
RE-Only: C03		36,043	52,558	64,496	73,314	79,963	85,075	89,078
Levelized Cost of Electricity (LCOE)								
(Subsidy)Base Case: C01	US$	0.127	0.148	0.171	0.196	0.223	0.251	0.281
(No Subsidy)Base Case: C01		0.216	0.259	0.306	0.357	0.412	0.469	0.528
RE + Battery: C02		0.121	0.141	0.164	0.189	0.215	0.243	0.271
RE-Only: C03		0.110	0.129	0.151	0.174	0.198	0.224	0.251

Sensitivity to the Cost of Energy								
	Unit	-75.0%	-50.0%	-25.0%	Base Case	25.0%	50.0%	100.0%
Cost of Energy	NRs/kW	**1.825**	**3.65**	**5.475**	**7.3**	**9.125**	**10.95**	**14.6**
Net Present Costs (NPC)								
Base Case: C01	US$	139,553	123,042	106,530	90,018	73,506	56,995	23,971
RE + Battery: C02		132,111	115,519	98,928	82,336	65,745	49,153	15,970
RE-Only: C03		120,861	104,880	88,900	72,919	56,938	40,958	8,997

B.2 AstroPower 120 W PV Module

AP-120 ELECTRICAL/MECHANICAL CHARACTERISTICS

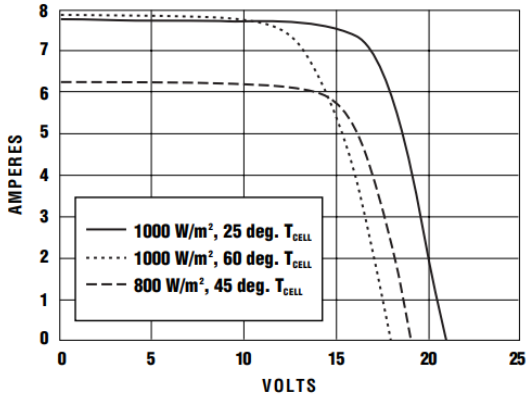

TYPICAL ELECTRICAL PARAMETERS

Peak Power *(W_p)	Watts	120
Open Circuit Voltage (V_{oc})	Volts	21.0
Max. Power Voltage (V_{mp})	Volts	16.9
Short Circuit Current (I_{sc})	Amps	7.7
Max. Power Current (I_{mp})	Amps	7.1
Short Circuit Temp. Coefficient	mA/°C	+3.5
Open Circuit Voltage Coefficient	V/°C	-0.08
Max. Series Fuse	Amps	15

@ Standard Test Conditions (defined as: Irradiance = 1000 W/m²; cell temperature = 25°C; AM 1.5G solar spectrum.)
*rated power tolerance ±10%

TYPICAL OPERATIONAL SPECIFICATIONS

Nominal Operating Cell Temp. (NOCT)	45°C (Determined under: Irradiance = 800 W/m²; ambient temperature = 20°C; wind speed = 1m/s)
Weight (Wind) Bearing Potential	50 lbs/ft² (125 mph equiv.)
Hailstone Impact Resistance	1" @ 50 mph (25.4 mm @ 80.5 kph)
Weight	26.1 lbs. (11.9 kg)
Dimensions	26.0 x 58.1 x 1.4 in. (661 x 1477 x 35 mm)

JOINT RESEARCH CENTRE
ESTI – Ispra
TÜV Rheinland

Source: http://www.cosolar.com/pdf/ap-120-new.pdf

BIBLIOGRAPHY

[1] UN, "Sustainable Development Goals," The United Nations, [Online]. Available: http://www.un.org/sustainabledevelopment/energy/. [Accessed 24 May 2017].

[2] K. B. Nakarmi, "Turbine and Drive System," in *Regional Workshop on Micro Hydro Projects*, Kathmandu, Nepal, 2010.

[3] W. Duncan and R. Cline, "Mechanical Governors for Hydroelectric Units," United States Department of Interior, Denver, 2002.

[4] J. F. Manwell, A. Rogers, G. Hayman, C. T. Avelar and J. G. McGowan, "HYBRID2 - A Hybrid System Simulation, Theory Manual," Renewable Energy Research Laboratory, Amherst, 1998.

[5] S. S. Khadka and R. K. Maskey, "Performance Study of Micro-hydropower System in Nepal," Alternative Energy Promotion Center (AEPC), Nepal, 2010.

[6] "WaterWatch," USGA, [Online]. Available: https://waterwatch.usgs.gov/. [Accessed 24 May 2017].

[7] I. D. Jones, "Assessment and Design of Small-Scale Hydro-Electric Power Plants," PhD Thesis, The University of Salford, Department of Civil Engineering, Salford, England, 1988.

[8] G. Rees, A. Gustard and S. R. Kansakar, "Development and testing of a flow estimation model for Nepal," *Journal of Hydrology and Meteorology,* vol. 1, no. 1, pp. 16- 23, 2004.

[9] M. Mimikou and S. Kaemaki, "Regionalization of flow duration characteristics," *Journal of Hydrology,* vol. 82, no. 1–2, pp. 77-91, 1985.

[10] A. Castellarin, R. M. Vogel and A. Brath, "A stochastic index flow model of flow duration curves," *Water Resources Research,* vol. 40, no. 3, 2004.

[11] B. K. Sovacool, "Energy studies need social science.," *Nature,* vol. 511, no. 7511 , p. 529, 2014.

[12] H. S. Sachdev, A. K. Akella and N. Kumar, "Analysis and evaluation of small hydropower plants: A bibliographical survey," *Renewable and Sustainable Energy Reviews,* vol. 51, pp. 1013-1022, 2015.

[13] AEPC, "A Detail Feaseability Study Guidelines for Microhydro Power Projects," Alternative Energy Promotion Center(AEPC), Nepal, Lalitpur, 2013.

[14] ESHA, "Guide on How to Develop a Small Hydropower Plant," European Small Hydropower Association, 2004.

[15] B. Bhandari, K.-T. Lee, C. S. Lee, C.-K. Song and R. K. Maskey, "A novel off-grid hybrid power system comprised of solar photovoltaic, wind, and hydro energy sources," *Applied Energy,* vol. 133, p. 236–242, 2014.

[16] Wind Energy Nepal Pvt. Ltd., "Preparing site assessment report cum intervention cost of Thingan Tri-Hybrid up gradation project Under “Support to Thingan Tri-Hybrid project in Makwanpur”," Alternative Energy Promotion Center (AEPC), Khumaltar, Lalitpur, 2015.

[17] "The Turbine Testing Lab, Kathmandu University," [Online]. Available: http://www.ku.edu.np/ttl/index.php. [Accessed 17 January 2017].

[18] K. Acharya and T. Bajracharya, "Current Status of Micro Hydro Technology in Nepal," in *Proceedings of IOE Graduate Conference*, Lalitpur, 2013.

[19] ESMAP, "Sustainable Energy for All: Global Tracking Framework," Energy Sector Management Assistance Program, 2013.

[20] International Energy Agency (IEA) and the World Bank., "Sustainable Energy for All 2017: Progress toward Sustainable Energy," World Bank, Washington, DC., 2017.

[21] I. Baring-Gould, K. Burman, M. Singh, S. Esterly, R. Mutiso and C. McGregor, "Quality Assurance Framework for Mini-Grids," National Renewable Energy Laboratory, Golden, CO 80401, 2016.

[22] National Renewable Energy Laboratory, "National Solar Radiation Data Base," Renewable Resource Data Center, [Online]. Available: http://rredc.nrel.gov/solar/old_data/nsrdb/1991-2005/tmy3/. [Accessed 24 May 2017].

[23] J. F. Manwell, J. G. McGowan and A. L. Rogers, Wind Energy Explained: Theory, Design and Application, John Wiley & Sons Ltd., 2009.

[24] S. Basso and G. Botter, "Streamflow variability and optimal capacity of run-of-river hydropower plants," *Water Resources Research,* vol. 48, pp. 1-13, 2012.

[25] "National Renewable Energy Laboratory, USA," [Online]. Available: http://www.nrel.gov/analysis/models_tools.html. [Accessed 12 January 2017].

[26] AEPC, "MINI/MICRO HYDRO," Alternative Energy Promotion Centre, [Online]. Available: http://www.aepc.gov.np/statistic/minimicro-hydro. [Accessed 29 July 2018].

[27] B. Mainali and S. Silveira, "Financing off-grid rural electrification: country case Nepal," *Energy,* vol. 36, no. 4, pp. 2194-2201, 2011.

[28] D. F. Barnes, The Challanges of Rural Electrification: Strategies for Developing Countries, Washington, DC: Resources for the uture, 2007.

[29] R. C. Poudel, "Quantitative decision parameters of rural electrification planning: A review based on a pilot project in rural Nepal.," *Renewable and Sustainable Energy Reviews,* vol. 25, pp. 291-300, 2013.

[30] S. Sinha and S. Chandel, "Review of software tools for hybrid renewable energy systems," *Renewable and Sustainable Energy Reviews,* vol. 32, p. 192–205, 2014.

[31] G. T. Klise and J. S. Stein, "Models Used to Assess the Performance of Photovoltaic Systems," Sandia National Laboratories, Albuquerque, NM, 2009.

[32] International Energy Agency, "World-wide overview of design and simulation tools for hybrid PV systems," International Energy Agency, 2011.

[33] G. Léna, "Rural Electrification with PV Hybrid Systems: Overview and Recommendations for Further Deployment," International Energy Agency, 2013.

[34] F. Milano, "The Power System Analysis Toolbox (PSAT)," [Online]. Available: http://faraday1.ucd.ie/psat.html. [Accessed 15 January 2017].

[35] "RETScreen," Natural Resources Canada, [Online]. Available: http://www.nrcan.gc.ca/energy/software-tools/7465. [Accessed 12 January 2017].

[36] Natural Resources Canada, Clean Energy Project Analysis: RETScreen® Engineering & Cases Textbook, Minister of Natural Resources Canada, 2005.

[37] T. Lambert, P. Gilman and P. Lilienthal, "Micropower system modeling with HOMER," in *Integration of Alternative Sources of Energy*, John Wiley & Sons, Inc, 2006, pp. 379 - 417.

[38] "Getting Started Guide for HOMER Legacy (Version 2.68)," HOMER Energy and National Renewable Energy Laboratory, 2011.

[39] J. F. Manwell and J. G. McGowan, "A combined probabilistic/time series model for wind diesel systems simulation.," *Solar Energy,* vol. 53, no. 6, pp. 481-490, 1994.

[40] H. J. Green and J. F. Manwell, "HYBRID2: a versatile model of the performance of hybrid power systems.," National Renewable Energy Laboratory, 1995.

[41] Wind Energy Center, University of Massachusetts, "Hybrid2," Wind Energy Center, University of Massachusetts, [Online]. Available: http://www.umass.edu/windenergy/research/topics/tools/software/hybrid2. [Accessed 12 September 2016].

[42] E. l. Baring-Gould, "Hybrid2: The hybrid system simulation model, Version 1.0, user manual. No. NREL/TP--440-21272.," National Renewable Energy Laboratory, Golden, Co, 1996.

[43] R. M. Vogel and N. M. Fennessey, "Flow-duration curves. I: New interpretation and confidence intervals," *Journal of Water Resources Planning and Management,* vol. 120, no. 4, pp. 485-504, 1994.

[44] "National Solar Radiation Data Base," [Online]. Available: http://rredc.nrel.gov/solar/old_data/nsrdb/1991-2005/tmy3/. [Accessed 24 May 2017].

[45] M. Gautam and K. Acharya, "Streamflow trends in Nepal," *Hydrological Sciences Journal,* vol. 57, no. 2, p. 344–357, 2011.

[46] I. Krasovskaia, L. Gottschalk, E. Leblois and A. Pacheco, "Regionalization of flow duration curves.," in *Climate Variability and Change—Hydrological Impacts*, Havana, Cuba, 2006.

[47] L. Monition, M. L. Nir, J. Roux and J. M. (Translator), Micro Hydroelectric Power Stations, John Wiley & Sons, 1984.

[48] L. A. Richards, "Capillary conduction of liquids through porous mediums.," *Physics,* vol. 1, no. 5, pp. 318-333, 1931.

[49] J. H. Lienhard, "A Statistical Mechanical Prediction of the Dimensionless Unit Hydrograph," *Journal of Geophysical Research,* vol. 69, no. 24, pp. 5231 - 5238, 1965.

[50] C. G. Collier, "Modelling a river catchment using an electrical circuit analogue.," *Hydrology and Earth System Sciences Discussions,* vol. 2, no. 1, pp. 9-18, 1998.

[51] H. Ajami, U. Khan, N. K. Tuteja and A. Sharma, "Development of a computationally efficient semi-distributed hydrologic modeling application for soil moisture, lateral flow and runoff simulation," *Environmental Modelling & Software,* vol. 85, pp. 319-331, 2016.

[52] E. G. Santos and J. D. Salas, "Stepwise disaggregation scheme for synthetic hydrology.," *Journal of Hydraulic Engineering,* vol. 118, no. 5, pp. 765-784, 1992.

[53] D. Valencia and J. C. Schakke, "Disaggregation processes in stochastic hydrology," *Water Resources Research,* vol. 9, no. 3, pp. 580-585, 1973.

[54] D. G. Tarboton, A. Sharma and U. Lall, "Disaggregation procedures for stochastic hydrology based on nonparametric density estimation.," *Water resources research,* vol. 34, no. 1, pp. 107-119, 1998.

[55] A. L. Rogers, J. W. Rogers and J. F. Manwell, "Comparison of the performance of four measure–correlate–predict algorithms," *Journal of Wind Engineering and Industrial Aerodynamics,* vol. 93, no. 3, p. 243–264, 2005.

[56] D. A. Hughes and V. Smakhtin, "Daily flow time series patching or extension: a spatial interpolation approach based on flow duration curves," *Hydrological Sciences Journal,* vol. 41, no. 6, pp. 851-871, 1996.

[57] A. Acharya and J. H. Ryu, "Simple Method for Streamflow Disaggregation," *Journal of Hydrologic Engineering,* pp. 509 - 519, 2014.

[58] A. Sharma, D. G. Tarboton and U. Lall, "Streamflow simulation: A nonparametric approach," *Water Resources Research,* vol. 33, no. 2, p. 291–308, 1997.

[59] D. Koutsoyiannis, "Rainfall disaggregation methods: Theory and applications," in *Workshop on Statistical and Mathematical Methods for Hydrological Analysis*, Rome, 2003.

[60] O. G. B. Sveinsson, J. D. Salas, W. L. Lane and D. K. Frevert, "Stochastic Analysis, Modeling, and Simulation (SAMS) Version 2007 User's Manual," Computing Hydrology Laboratory , Colorado State University, Fort Collins, Colorado, 2007.

[61] J. C. Grygier and J. R. Stedinger, "Spigot, a synthetic streamflow generation package, technical description, version 2.5," School of Civil and Environmental Engineering, Cornell University, Ithaca, New York, 1995.

[62] "Distributed Model Intercomparison Project," NOAA's National Weather Service, [Online]. Available: http://www.nws.noaa.gov/oh/hrl/dmip/intro.html. [Accessed 5 May 2017].

[63] M. B. Smith, K. P. Georgakakos and X. Liang, "The distributed model intercomparison project (DMIP)," *Journal of Hydrology,* vol. 298, no. 1–4, pp. 1-3, 2004.

[64] "Global Precipitation Measurement," NASA, [Online]. Available: https://www.nasa.gov/mission_pages/GPM/main/index.html. [Accessed 9 May 2017].

[65] "The Tropical Rainfall Measuring Mission (TRMM)," Goddard Space Flight Center, NASA , [Online]. Available: https://trmm.gsfc.nasa.gov/. [Accessed 9 May 2017].

[66] R. S. Govindaraju and A. R. Rao, Artificial neural networks in hydrology, Springer Science & Business Media, 2013.

[67] L. E. Besaw, D. M. Rizzo, P. R. Bierman and W. R. Hackett., "Advances in ungauged streamflow prediction using artificial neural networks," *Journal of Hydrology,* vol. 386, no. 1, pp. 27-37, 2010.

[68] "Surface meteorology and Solar Energy," Atmospheric Science Data Center, [Online]. Available: https://eosweb.larc.nasa.gov/cgi-bin/sse/sse.cgi?. [Accessed 10 September 2016].

[69] ICIMOD, "Hindu Kush Himalayan Region," ICIMOD, [Online]. Available: http://www.icimod.org/?q=1137. [Accessed 20 April 2017].

[70] "Department Of Hydrology and Meteorology," [Online]. Available: http://dhm.gov.np. [Accessed 20 April 2017].

[71] M. K. Shrestha, S. Chaudhary, R. Maskey and G. Rajkarnikar, "Comparison of the Anomaly of Hydrological Analysis Tools used in Nepal," *Journal of Hydrology and Meteorology,* vol. 7, no. 1, pp. 30-39, 2010.

[72] A. Harvey and A. Brown, Micro-Hydro Design Manual: A Guide to Small-Scale Water Power Schemes, Practical Action, 1993.

[73] Inclusive Consultants and Strength Engineering Company Pvt. Ltd, "Detailed Feasibility Study Report of Lafagad MHP (85 kW) Ramnakot VDC-06, Kalikot," Alternative Energy Promotion Center(AEPC), Nepal, Lalitpur, 2015.

[74] P. Chitrakar, "Micro-hydropower Design Aids Manual," Small Hydropower Promotion Project (SHPP/GTZ) and Mini-Grid Support Programme (MGSP/AEPC-ESAP), Kathmandu, Nepal, 2005.

[75] O. Paish, "Micro-hydropower: status and prospects," *Proceedings of the Institution of Mechanical Engineers: Part A: J Power and Energy,* vol. 216, pp. 31-40, 2002.

[76] Practical Action, "Micro-hydro Power: Technical Brief," Practical Action, 2010.

[77] Practical Action, "Michell-Banki Turbine: Technical Brief," Practical Action, Warwickshire, UK, 2012.

[78] S. L. Dixon and C. Hall, Fluid Mechanics and Thermodynamics of Turbomachinery, Butterworth-Heinemann, 2010.

[79] V. R. Desai and N. M. Aziz, "Parametric Evaluation of Crossflow Turbine Performance," *Journal of Energy Engineering,* vol. 120, no. 1, pp. 17-34, 1994.

[80] S. Shrestha and V. B. Amatya, " A Case Study of Micro-hydropower in Nepal," in *Renewable Energy Technologies: A Brighter Future*, Kathmandu, International Center for Integrated Mountain Development (ICIMOD), 1998, pp. 141-156.

[81] OSSBERGER, "Hydro," OSSBERGER, [Online]. Available: http://www.ossberger.de/cms/en/hydro/. [Accessed 3 May 2017].

[82] F. Mtalo, R. Wakati, A. Towo, S. K. Makhanu, O. Munyaneza and B. Abate, "Design and Fabrication of Cross flow Turbine.," Nile Basin Capacity Building Network, Cairo, Egypt, 2010.

[83] C. A.Mockmore and E. Merryfield, "The Banki Water Turbine," Oregon State University, Corvallis, Oregon, 1949.

[84] V. R. Desai, "A parametric study of the cross-flow turbine performance," PhD Thesis, Clemson University, Clemson, SC, 1993.

[85] S. R. Yassen, "Optimization of the Performance of Micro Hydro-Turbines for Electricity Generation," PhD Thesis, University of Hertfordshire, Hatfield, UK, 2014.

[86] J. A.Chattha, M. S. K. H. Iftekhar and S. Shahid, "Standardization of Cross Flow Turbine Design for Typical Micro-Hydro Site Conditions in Pakistan.," in *ASME 2014 Power Conference*, 2014.

[87] T. F. S. E. Center, "The Florida Solar Energy Center (FSEC)," [Online]. Available: http://www.fsec.ucf.edu/en/about/index.htm. [Accessed 20 January 2017].

[88] L. L. Kazmerski, "Photovoltaics: A review of cell and module technologies," *Renewable and Sustainable Energy Reviews,* vol. 1, no. 1–2, pp. 71-170, 1997.

[89] L. L. Kazmerski, "Solar photovoltaics R&D at the tipping point: A 2005 technology overview," *Journal of Electron Spectroscopy and Related Phenomena,* vol. 150, no. 2–3, p. 105–135, 2006.

[90] "Solar Panel Systems: 120W Solar panel specifications," CENTURION SYSTEMS PACIFIC, [Online]. Available: http://www.centsys.co.za/australia/product-documentation. [Accessed 20 May 2017].

[91] J. Wilson, "Solar Panels: an online lesson on PV Cell Efficiency and the Solar Spectrum," European Energy Centre (EEC), [Online]. Available: https://theect.org/webinar-series/pv-cell-efficiency-and-solar-spectrum.html. [Accessed 4 December 2017].

[92] W. Shockley and H. J. Queisser, "Detailed Balance Limit of Efficiency of p-n Junction Solar Cells," *Journal of Applied Physics,* vol. 32, no. 3, pp. 510-519, 1961.

[93] A. Luque and S. Hegedus, Handbook of Photovoltaic Science and Engineering, Second Edition, John Wiley & Sons, Ltd, 2011.

[94] D. Evans, "Simplified method for predicting photovoltaic array output," *Solar Energy,* vol. 27, no. 6, pp. 555-560, 1981.

[95] C. W. Hansen, "Parameter Estimation for Single Diode Models of Photovoltaic Modules," Sandia National Laboratories, Albuquerque, NM, 2015.

[96] A. M.Humada, M. Hojabri, S. Mekhilef and H. M.Hamada, "Solar cell parameters extraction based on single and double-diode models: A review," *Renewable and Sustainable Energy Reviews,* vol. 56, pp. 494-509, 2016.

[97] A. R. Jordehi, "Parameter estimation of solar photovoltaic (PV) cells: A review," *Renewable and Sustainable Energy Reviews,* vol. 61, pp. 354-371, 2016.

[98] Z. Salam, K. Ishaque and H. Taheri, "An improved two-diode photovoltaic (PV) model for PV system.," in *Power Electronics, Drives and Energy Systems (PEDES) & Power India*, 2010.

[99] D. L. King, J. A. Kratochvil and W. E. Boyson, "Photovoltaic array performance model," Sandia National Laboratories, 2003.

[100] J. A. Duffie and W. M. Beckman, Solar Engineering Of Thermal Processes, 4 Edition, New York: Wiley, 2013.

[101] National Renewable Energy Laboratory, "Small Wind Electric Systems: A U.S. Consumer's Guide," Energy Efficiency and Renewable Energy, U.S. Department of Energy, 2007.

[102] "Small Wind Turbine Purchasing Guide: Off-grid, Residential, Farm & Small Business Applications," Canadian Wind Energy Association (CanWEA), 2008.

[103] "Windpower Wiki," Danish Wind Industry Association, [Online]. Available: http://www.windpower.org/en/knowledge/windpower_wiki.html. [Accessed 26 May 2017].

[104] H. Piggott, "Old Homepage," Scoraig Wind Electric, [Online]. Available: http://www.scoraigwind.com/. [Accessed 26 May 2017].

[105] B. H. Bailey, S. L. McDonald, D. W. Bernadett, M. J. Markus and K. V. Elsholz., "Wind resource assessment handbook: Fundamentals for conducting a successful monitoring program," National Renewable Energy Lab., Golden, CO (US); AWS Scientific, Inc., Albany, NY (US), 1997.

[106] M. Jongerden and B. Haverkort, "Which battery model to use?," *IET Software,* vol. 3, no. 6, p. 445–457, 2009.

[107] J. F. Manwell and J. G. McGowan, "Lead Acid Battery Storage Model for Hybrid Energy Systems," *Solar Energy,* vol. 50, no. 5, pp. 399-405, 1993.

[108] D. Rakhmatov and S. Vrudhula, "An analytical high-level battery model for use in energy management of portable electronic systems," in *Proc. Int. Conf. Computer Aided Design (ICCAD'01)*, 2001.

[109] J. F. Manwell and J. G. McGowan, "Extension of the kinetic battery model for wind/hybrid power systems," in *Fifth European Wind Energy Association Conference (EWEC '94)*, 1994.

[110] Q. Wei, D. Liu and G. Shi, "A Novel Dual Iterative Q-Learning Method for Optimal Battery Management in Smart Residential Environments," *IEEE Transactions on Industrial Electronics,* vol. 62, no. 4, pp. 2509-2518, 2015.

[111] H. Bindner, T. Cronin, P. Lundsager, J. F. Manwell, U. Abdulwahid and I. Baring-Gould, "Lifetime Modelling of Lead Acid Batteries," Risø National Laboratory, Roskilde, Denmark, 2005.

[112] "IEEE Guide for the Application of Turbine Governing Systems for Hydroelectric Generating Units," Institute of Electrical and Electronics Engineers, 2011.

[113] J.Chan and W. Lubitz, "Electronic load controller (ELC) design and simulation for remote rural communities: A powerhouse ELC compatible with household distributed-ELCs in Nepal.," in *Global Humanitarian Technology Conference (GHTC),2016*, 2016.

[114] G. A. Munoz-Hernandez, S. P. Mansoor and D. I. Jones, Modelling and controlling hydropower plants, Springer Science & Business Media, 2012.

[115] K. H. Fasol, "A short history of hydropower control," *IEEE Control Systems,* pp. 68 - 76, 2002.

[116] N. Kishor, R. Saini and S. Singh, "A review on hydropower plant models and control," *Renewable and Sustainable Energy Reviews,* vol. 11, p. 776–796, 2007.

[117] D. Henderson, "A three phase electronic load governor for micro hydro generation," PhD Thesis, The University of Edinburgh, 1992.

[118] N. P. Gyawali, "Universal electronic load controller for microhydro power plant.," in *12th IEEE International Conference on Control and Automation (ICCA)*, 2016.

[119] F. P. Demello, R. J. Koessler, J. Agee, P. M. Anderson, J. H. Doudna, J. H. Fish and P. A. L. H. e. al., "Hydraulic-turbine and turbine control-models for system dynamic studies.," *IEEE Transactions on Power Systems,* vol. 7, no. 1, 1992.

[120] M.Hanmandlu and H. Goyal, "Proposing a new advanced control technique for micro hydro power plants," *International Journal of Electrical Power & Energy Systems,* vol. 30, no. 4, p. 272–282, 2008.

[121] S. Doolla and T. S. Bhatti, "Load Frequency Control of an Isolated Small-Hydro Power Plant With Reduced Dump Load," *IEEE Transactions on Power Systems,* vol. 21, no. 4, pp. 1912 - 1919, 2006.

[122] L. G. Scherer, R. F. d. Camargo, H. Pinheiro and C. Rech, "Advances in the Modeling and Control of Micro Hydro Power Stations with Induction Generators," *Energy Conversion Congress and Exposition (ECCE), IEEE,* pp. 997-1004, 2011.

[123] R. Saiju, "Hybrid Power System Modelling-Simulation and Energy Management Unit Development," PhD Thesis, University of Kassel, Kassel, 2008.

[124] A. Suliman, "A test case for implementing feedback control in a micro hydro power plant," Kansas State University, Manhattan, KS, 2010.

[125] R. Gupta, "Automation of Small Hydropower Station," Indian Institute of Technology Roorkee, Roorkee, 2007.

[126] B. Bhandari, "Design and Evaluaion of Tri-Hybrid Renewable Energy System (THRES)," PhD Thesis, Department of Mechanical & Aerospace Engineering, Seoul National University,, Seoul, Korea, 2014.

[127] B. Bhandari, S. R. Poudel, K.-T. Lee and S.-H. Ahn, "Mathematical Modeling of Hybrid Renewable Energy System: A Review on Small Hydro-Solar-Wind Power Generation," *International Journal of Precision Engineering And Manufacturing - Green Technology,* vol. 1, no. 2, pp. 157-173, 2014.

[128] B. Bhandari, S.-H. Ahn and T.-B. Ahn, "Optimization of Hybrid Renewable Energy Power System for Remote Installations: Case Studies for Mountain and," *International Journal of Precision Engineering And Manufacturing,* vol. 17, no. 6, pp. 815-822, 2016.

[129] A. Gupta, "Modelling of Hybrid Energy System," PhD Thesis, Indian Institute of Technology Roorkee, Roorkee, 2010.

[130] L. Olatomiwa, S. Mekhilef, M. S. Ismail and M. Moghavvemi, "Energy management strategies in hybrid renewable energy systems: A review," *Renewable and Sustainable Energy Reviews,* vol. 62, pp. 821-835, 2016.

[131] C. D. Barley and C. B. Winn, "Optimal dispatch strategy in remote hybrid power systems.," *Solar Energy,* vol. 58, no. 4-6 , pp. 165-179, 1996.

[132] C. D. Barley, "Modeling and Optimization of Dispatch Strategies for Remote Hybrid Power Systems," Colorado State University, Fort Collins, CO, 1996.

[133] R. Hunter and G. E. (editors), Wind-Diesel Systems: A guide to the technology and its implementation, Cambridge University Press, 1994.

[134] E. Verploegen, "Energy Assessment Toolkit," D-Lab, MIT, Boston, 2017.

[135] P. S. Jackson and J. C. R. Hunt, "Turbulent wind flow over a low hill," *Quarterly Journal of the Royal Meteorological Society,* vol. 101, no. 430, p. 929–955, 1975.

[136] M. F. Müller, S. E. Thompson and M. N. Kelly, "Bridging the information gap: A webGIS tool for rural electrification in data-scarce regions," *Applied Energy,* vol. 171, p. 277–286, 2016.

[137] NRGSystems, " Li-Cor LI-200R Pyranometer," [Online]. Available: https://www.nrgsystems.com/products/met-sensors/pyranometers/detail/li-cor-li-200r-pyranometer. [Accessed 20 January 2018].

[138] Kipp & Zonen, "CMP6 Pyranometer," [Online]. Available: http://www.kippzonen.com/Product/12/CMP6-Pyranometer. [Accessed 20 January 2018].

[139] K. N. Poudyal, B. K. B. B. Sapkota and B. Kjeldstad, "Estimation of Global Solar Radiation Using Clearness Index and Cloud Transmittance Factor at Trans-Himalayan Region in Nepal," *Energy and Power Engineering,* vol. 4, pp. 415-421, 2012.

[140] V. A. G. Graham and K. G. T. Hollands, "A method to generate synthetic hourly solar radiation globally.," *Solar Energy,* vol. 44, no. 6, pp. 333-341, 1990.

[141] AWS Scientific, Inc., "Wind Resource Assessment Handbook," National Renewable Energy Laboratory, Golden, CO, 1997.

[142] R. Corotis, "Simulation of wind-speed time series for wind-energy conversion analysis.," Department of Energy, 1982.

[143] T. Lambert, *Wind Resource Inputs,* Homer Energy, 2004.

[144] T. Ishihara, A. Yamaguchi and M. W. Sarwar, "A Study of the Normal Turbulence Model in IEC 61400-1," *Wind Engineering,* vol. 36, no. 6, pp. 759-766, 2012.

[145] A. Papoulis and S. U. Pillai, Probability, Random Variables and Stochastic Processes, 4th Edition, McGraw-Hill Europe, 2002.

[146] L. Marshall, D. Nott and A. Sharma, "A comparative study of Markov chain Monte Carlo methods forconceptual rainfall-runoff modeling," *Water Resource Research,* vol. 40, p. W02501, 2004.

[147] I. Kim, "Markov chain Monte Carlo and acceptance–rejection algorithms for synthesising shortterm variations in the generation output of the photovoltaic system," *IET Renewable Power Generation,* vol. 11, no. 6, pp. 878-888, 2017.

[148] G. E. P. Box, G. M. Jenkins, G. C. Reinsel and G. M. Ljung, Time Series Analysis: Forecasting and Control, John Wiley & Sons. Inc., 2016.

[149] N. Metropolis, A. W. Rosenbluth, M. N. Rosenbluth, A. H. Teller and E. Teller, "Equation of state calculations by fast computing machines," *The journal of chemical physics,* vol. 21, no. 6, pp. 1087-1092, 1953.

[150] W. K. Hastings, "Monte Carlo Sampling Methods Using Markov Chains and Their Applications," *Biometrika,* vol. 57, no. 1, pp. 97-109, 1970.

[151] T.-W. Kim and J. B. Valdés, "Synthetic Generation of Hydrologic Time Series Based on Nonparametric Random Generation," *Journal of Hydrologic Engineering,* vol. 10, no. 5, pp. 395-404, 2005.

[152] L. Ljung, System Identification: Theory for the User, Englewood Cliffs, New jersey: Prentice-Hall, Inc, 1987.

[153] Mathworks, "Subreferencing Models," Matlab: System Identification Toolbox, [Online]. Available: https://www.mathworks.com/help/ident/ug/subreferencing-models.html. [Accessed 23 February 2018].

[154] NOAA's National Weather Service, "Hourly Streamflow Data From USGS," [Online]. Available: http://www.nws.noaa.gov/ohd/hrl/dmip/stream_flow.html. [Accessed 10 December 2016].

[155] J. D.Sandstrom, "A method for predicting solar cell current- voltage curve characteristics as a function of incident solar intensity and cell temperature.," NASA; United States, 1967.

[156] N. Blair, A. P. Dobos, J. Freeman, T. Neises, M. Wagner, T. Ferguson, P. Gilman and S. Janzou, "System Advisor Model, SAM 2014.1.14: General Description, NREL/TP-6A20-61019," National Renewable Energy Laboratory, Golden, CO 80401, 2014.

[157] A. P. Dobos and S. M. MacAlpine, "Procedure for Applying IEC-61853 Test Data to a Single Diode Model," in *Photovoltaic Specialist Conference (PVSC)*, Denver, CO, 2014.

[158] P. Gilman, "SAM Photovoltaic Model Technical Reference, NREL/TP-6A20-64102," National Renewable Energy Laboratory, Golden, CO , 2015.

[159] D. King, W. Boyson and J. Kratochvill, "Photovoltaic Array Performance Model, SAND2004-3535," Sandia National Laboratories, Albuquerque, New Mexico, 2004.

[160] Q. Kou, S. A. Klein and W. A. Beckman, "A Method for estimating the long-term performance of direct-coupled pv pumping systems," *Solar Energy,* vol. 64, no. 1–3, p. 33–40, 1998.

[161] J. F. Manwell, *Notes Regarding a Model for PV Panel Performance,* Amherst, 2016.

[162] J. L. Gray, "The Physics of the Solar Cell," in *Handbook of Photovoltaic Science and Engineering, Second Edition*, John Wiley & Sons, Ltd., 2011, pp. 82-129.

[163] E. v. Dyk and E. Meyer, "Analysis of the effect of parasitic resistances on the performance of photovoltaic modules," *Renewable Energy,* vol. 29, p. 333–344, 2004.

[164] IEC, "Photovoltaic (PV) module performance testing and energy rating - Part 1: Irradiance and temperature performance measurements and power rating," International Electrotechnical Commission, 2011.

[165] J. A. Gow and C.D.Manning, "Development of a photovoltaic array model for use in power-electronics simulation studies," *IEE Proceedings-Electric Power Applications,* vol. 146, no. 2, pp. 193-200, 1999.

[166] A. J. Anderson, "Photovoltaic Translation Equations: A New Approach," National Renewable Energy Laboratory, Golden, CO, 1996.

[167] T. Rheinland, W. Herrmann and W. Wiesner, "Current-Voltage Translation Procedure for PV Generators in the German 1,000 Roofs Programme," in *EUROSUN*, Freiburg, Germany, 1996.

[168] K. Ding, X. Bian, H. Liu and T. Peng, "A MATLAB-Simulink-Based PV Module Model and Its Application Under Conditions of Nonuniform Irradiance," *IEEE Transactions on Energy Conversion,* vol. 27, no. 4, pp. 864-872, 2012.

[169] ANSI/ASHRAE Standard 93-2003, Methods of Testing to Determine the Thermal Performance of Solar collectors., Atlanta, GA: ASHRAE, Inc., 2003.

[170] J. P. Holman, Heat Transfer, McGraw-Hill College, 1996.

[171] T. W. Neises, "Development and Validation of a Model to Predict the Temperature of a Photovoltaic Cell," University of Wisconsin – Madison, 2011.

[172] A. Panda, M. K. Pathak and S. P. Srivastava, "A single phase photovoltaic inverter control for grid connected system," *Sadhana,* vol. 41, no. 1, p. 15–30, 2016.

[173] B. Tummers, "DataThief III manual v. 1.1," DataThief, 2006.

[174] J. H. R. Enslin and D. B. Snyman, "Combined low-cost, high-efficient inverter, peak power tracker and regulator for PV applications," *IEEE Transactions on Power Electronics,* vol. 6, no. 1, pp. 73-82, 1991.

[175] Texas Instruments, "Grid-tied Solar Micro Inverter with MPPT," [Online]. Available: http://www.ti.com/tool/TIDM-SOLARUINV. [Accessed 30 July 2018].

[176] Energy Sector Management Assistance Program (ESMAP), "Sustainable Energy for All: Global Tracking Framework," The World Bank, Washington DC , 2013.

[177] S. Z. N. Dar and M. Mufti, "Enhanced load frequency control response with integration of supervisory controlled superconducting magnetic energy storage system in wind-penetrated two-area power system," *Wind Engineering,* vol. 41, no. 5, p. 330–342, 2017.

[178] AEPC, "Baseline for Rural and Renewable Energy Technologies (Till 15th July 2012)," Alternative Energy Promotion Centre (AEPC), Government of Nepal, Lalitpur, Nepal, 2012.

[179] NMB Bank, "Renewable Energy," [Online]. Available: http://nmbbanknepal.com/renewable-energy.html. [Accessed 8 March 2018].

[180] R. Bhandari, L. G. Saptalena and W. Kusch, "Sustainability assessment of a micro hydropower plant in Nepal," *Energy, Sustainability and Society,* vol. 8, no. 3, 2018.

[181] R. A. Cabraal, D. F. Barnes and S. G. Agarwal, "Productive uses of energy for rural development," *Annual Review aof Environmental Resources,* vol. 30, p. 117–44, 2005.

[182] S. Khennas and A. Barnett, "Micro-hydro power: an option for socio-economic development," in *In World Renewable Energy Congress VI*, Brighton, UK, 2000, pp. 1511-1517.

[183] Asian Development Bank, Cost-benefit analysis for development: A practical guide., Mandaluyong City, Philippines: Asian Development Bank, 2013.

[184] Asian Development Bank, Guidelines for the economic analysis of projects., Mandaluyong City, Philippines: Asian Development Bank, 2017.

[185] "The Distributed Wind Cost Taxonomy," National Renewable Energy Lab, Golden, CO, 2017.

[186] H. R. Varian, Microeconomic Analysis, New York: W. W. Norton & Company, Inc., 1992.

[187] A. Elbatran, O.B.Yaakob, Y. M. Ahmed and H. Shabara, "Operation, performance and economic analysis of low head micro-hydropower turbines for rural and remote areas:A review," *Renewable and Sustainable Energy Reviews,* vol. 43, p. 40–50, 2015.

[188] AEPC, "National Rural and Renewable Energy Program, Nepal Program Document," Alternative Energy Promotion Centre (AEPC), Lalitpur, 2012.

[189] B. Mainali and S. Silveira, "Financing off-grid rural electrification: Country case Nepal," *Energy,* vol. 36, pp. 2194-2201, 2011.

[190] Asian Development Bank, "Nepal's Largest Wind-Solar Hybrid Power System Switched On to Connect a Small Village to the World," [Online]. Available: https://www.adb.org/news/nepals-largest-wind-solar-hybrid-power-system-switched-connect-small-village-world. [Accessed 20 March 2018].

[191] N. Kittner, F. Lill and D. M. Kammen, "Energy storage deployment and innovation for the clean energy transition," *Nature Energy,* vol. 2, 2017.

[192] B. K. Sovacool, "The political economy of energy poverty: A review of key challenges," *Energy for Sustainable Development,* vol. 16, no. 3, pp. 272-282, 2012.

[193] S. Dixit, A. Chitnis, D. Wood, B. Jairaj and S. Martin, "10 Questions to Ask About Electricity Tariffs.," World Resources Institute, Washington, D.C., 2014.

[194] International Monetary Fund, "Trading Economics," [Online]. Available: https://tradingeconomics.com/nepal/inflation-end-of-period-imf-data.html. [Accessed 14 March 2018].

[195] World Bank, "Inflation, GDP deflator (annual %)," [Online]. Available: https://data.worldbank.org/indicator/NY.GDP.DEFL.KD.ZG?end=2016&locations=NP&start=1961. [Accessed 14 March 2018].

[196] R. P. Dhital and J. K. Mallik, "Diversity in power," *The Kathmandu Post,* 11 March 2018.

[197] Nepal Energy Forum, "NEA Electricity tariff rates," [Online]. Available: http://www.nepalenergyforum.com/nea-electricity-tariff-rates/. [Accessed 30 July 2018].

[198] Nepal Rastra Bank, "Foreign Exchange Rates," [Online]. Available: https://www.nrb.org.np/. [Accessed 14 March 2018].

[199] J. K. Mallik, "Development of Grid Connection Policy for Micro/Mini Hydro Plants in Nepal," 8 May 2016. [Online]. Available: https://www.linkedin.com/pulse/development-grid-connection-policy-micromini-hydro-plants-mallik/. [Accessed 23 March 2018].

[200] B. Mainali and S. Silveira, "Alternative pathways for providing access to electricity in developing countries," *Renewable Energy,* vol. 57, pp. 299-310, 2013.

[201] G. R. Pokharel, "Promoting Sustainable Development by Creating Enterprises on Renewable Energy Technologies in Nepal:Case Studies Based on Micro Hydropower Projects," PhD Thesis, University of Flensburg, Flensburg, Germany, 2006.

[202] S. Khennas and A. Barnett, "Best Practices for Sustainable Development of Micro Hydro Power in Developing Countries," World Bank,, Washington, DC., 2000.

[203] Climate Investment Funds, "SREP round table [NEPAL]," 6 February 2017. [Online]. Available: https://climateinvestmentfunds.org/sites/default/files/country/srep_nepal.pdf. [Accessed 20 March 2018].